Cranfield University

College of Aeronautics
Structures and Materials Group

PhD Thesis
2001

Ignacio Romero

Dynamic Analysis and Control System Design of a Deployable Space Robotic Manipulator

Supervisor: Dr. R. Vignjevic

January 2001

This thesis is submitted in fulfilment of the requirements
for the degree of Doctor of Philosophy.

Abstract

This thesis presents a dynamic analysis and a control system for a flexible space manipulator, the Deployable Robotic Manipulator or DRM, which has a deployable/retractable link. The link extends (or retracts) from the containing slewing link of the manipulator to change the DRM's length and hence its workspace. This makes the system dynamics time varying and therefore any control strategy has to adapt to this fact. The aim of the control system developed is to slew the manipulator through a predetermined angle given a maximum angular acceleration, to reduce flexural vibrations of the manipulator and to have a certain degree of robustness, all of this while carrying a payload and while the length of the manipulator is changing. The control system consists of a slewing motor that rotates the manipulator using the open-loop assumed torque method and two reaction wheel actuators, one at the base and one at the tip of the manipulator, which are driven by a closed-loop damping control law. Two closed-loop control laws are developed, a linear control law and a Lyapunov based control law. The linear control law is based on collocated output feedback. The Lyapunov control law is developed for each of the actuators using Lyapunov stability theory to produce vibration control that can achieve the objectives stated above for different payloads, while the manipulator is rotating and deploying or retracting. The response of the system is investigated by computer simulation for two-dimensional vibrations of the deployable manipulator. Both the linear and Lyapunov based feedback control laws are found to eliminate vibrations for a range of payloads, and to increase the robustness of the slewing mechanism to deal with uncertain payload characteristics.

Acknowledgements

This thesis would have never been possible without the invaluable help, support, and encouragement of my wife Virginia who always believed that I could do it, even when I did not. My most sincere thanks also go to my supervisors Dr C. Kirk and Dr R. Vignjevic who through their advice and comments have made possible the completion of the research and the coherence of this thesis. Many other people deserve my thanks, in particular my fellow PhD students at Cranfield University for all the laughs and the very interesting coffee break discussions, and my current colleagues at the European Space Operations Centre who have motivated me to continue and never allowed me to give up. Finally a very special thanks to my parents who have always supported my education and allowed me to follow my dreams.

Table of Contents

Acknowledgements iii

Table of Contents iv

Figures viii

Tables xiv

Acronyms xv

Notation xvi

Chapter 1 : Introduction 1

1.1 Background and Literature Survey 1

1.2 Thesis goals and outline 8

Chapter 2 : Dynamic Modelling 10

2.1 Dynamic System Characteristics 11

2.2 Energy Formulation 13

2.2.1 Kinetic Energy 13

2.2.2 Elastic Strain Energy 17

2.3 Eigenvalue Analysis – Hamilton's Principle 21

2.3.1 Application of Hamilton's Principle to a simplified DRM 22

2.3.2 Exact Formulation of Equations of Motion for the P-DRM 24

2.3.3 Exact Determination of Natural Frequencies for the P-DRM 27

2.3.3.1 Characteristic Problem 29

2.3.3.2 Characteristic Problem Solution: P-DRM Natural Frequencies 32

2.3.3.3 Characteristic Problem Solution: P-DRM Mode Shapes 38

2.4 Approximate Dynamic Analysis of Flexible Manipulators 40

2.4.1 Assumed Modes Method 41

2.5 Approximate Equations of Motion for the DRM 43

2.5.1 Approximate Kinetic and Strain Energies 43

2.5.2 Equations of Motion for a Flexible DRM with Time Varying Length 45

2.6 Vibration Analysis of the P-DRM 51

2.7 Vibration Analysis of the Fully Flexible DRM 55

2.8 NASTRAN Analysis Results 58

2.8.1 NASTRAN Bending Natural Frequencies 59

2.8.2 NASTRAN Torsional Natural Frequencies 59

Chapter 3 : DRM Control 63

3.1 Structural flexibility considerations 64

3.2 Open Loop Slew Control 65

3.2.1 Assumed Torque for Rigid DRM 66

3.2.2 Minimum-Time Acceleration Profile and Torque 68

3.2.3 Near Minimum-Time Acceleration Profile 73

3.2.4 Minimum Energy Acceleration Profile 77

3.2.5 Near Minimum-Energy Acceleration Profile 82

3.3 Closed Loop Vibration Control 87

3.4 Linear Closed Loop Control of the DRM 92

3.4.1 Root Linear Feedback Control Law 92

3.4.2 Tip Linear Feedback Control Law 95

3.5 Lyapunov Closed Loop Control 97

3.5.1 Lyapunov Theory 98

3.5.2 Lyapunov Theory Application 99

3.5.3 Lyapunov Control Law Formulation 106

3.5.3.1 Lyapunov Root Actuator Control Law 107

3.5.3.2 Lyapunov Tip Actuator Control Law 108

3.5.4 Lyapunov Control System Observations 109

Chapter 4 : Simulation Results 111

4.1 Program Verification 112

4.1.1 Open-Loop Energy Conservation 113

4.1.2 Comparison to a similar reported system 115

4.2 Open Loop Undamped Results 117

4.2.1 Minimum-Time Assumed Torque Results 117

4.2.2 Near Minimum-Time Assumed Torque Results 123

4.2.3 Minimum-Energy Assumed Torque Results 127

4.2.4 Near Minimum-Energy Assumed Torque Results 130

4.3 Power Consumption of the Main Slew Motor 133

4.4 DRM Extension and Contraction Results 139

4.5 Robustness of the Open Loop Control Laws 143

4.6 Closed Loop Control Results 145

4.6.1 Linear Feedback Control 145

4.6.1.1 Root Actuator Control Results 146

4.6.1.2 Tip Actuator Control Results 149

4.6.1.3 Complete Linear Feedback Control Results 151

4.6.2 Lyapunov-based Feedback Control 157

4.6.2.1 Root Actuator Control Results 157

4.6.2.2 Tip Actuator Control Results 161

4.6.2.3 Complete Lyapunov Control Results 164

Chapter 5 : Comparison and Discussion 172

Chapter 6 : Conclusions 177

6.1 Summary 177

6.2 Closing Remarks 178

6.3 Future Research Direction 179

References 180

Appendix A: Characteristic Problem Coefficients 184

Appendix B: Assumed Mode Method Examples 186

Appendix C: The DRM Approximate Dynamic Model. 196

Appendix D: Computer Programs 201

Appendix E: The NASTRAN Finite Element Results 223

Figures

Figure 1.1: The SRMS carrying a large payload while in orbit, (Skaar and Ruoff, 1994). 2

Figure 1.2: Deployable Robotic Manipulator (DRM) Schematic. 4

Figure 2.1: DRM System Schematic. 14

Figure 2.2: Flexible Link Detailed Schematic. 15

Figure 2.3: DRM elastic deformation. 18

Figure 2.4: First two zero crossings of the eigenvalue problem for the P-DRM with Payload 1. 35

Figure 2.5: First two zero crossings of the eigenvalue problem for the P-DRM with Payload 2. 35

Figure 2.6: First two zero crossings of the eigenvalue problem for the P-DRM with Payload 3. 35

Figure 2.7: First three zero crossings of the eigenvalue problem for the P-DRM with Payload 1. 36

Figure 2.8: First three zero crossings of the eigenvalue problem for the P-DRM with Payload 2. 36

Figure 2.9: First three zero crossings of the eigenvalue problem for the P-DRM with Payload 3. 36

Figure 2.10: P-DRM link 2 mode shapes with Payload1 (200Kg), for two different lengths 'a' 39

Figure 2.11: P-DRM flexible link 2 mode shapes for a = 8 meters and with M_p=0 39

Figure 2.12: DRM Payload grappling modes in NASTRAN analysis 61

Figure 3.1: The DRM Open Loop Control Diagram 66

Figure 3.2: Minimum-Time angular acceleration, velocity and position for a 50° slew 71

Figure 3.3: Minimum-Time Torque profile for a 50° slew of an extending rigid DRM 71

Figure 3.4: Minimum-Time axial deployment acceleration, velocity and position 72

Figure 3.5: Near-Minimum-Time angular acceleration, velocity and position with a smoothing factor, $\varphi = 0.1$ 76

Figure 3.6: Near-Minimum-Time Torque profile for a 50° slew of an extending rigid DRM with a smoothing factor, $\varphi = 0.1$ 76

Figure 3.7: Minimum-Energy angular acceleration, velocity and position 81

Figure 3.8: Minimum-Energy Torque profile for a 50° slew of an extending rigid DRM 81

Figure 3.9: Near-Minimum-Energy angular acceleration, velocity and position with a smoothing factor, $\varphi = 0.1$ 86

Figure 3.10: Near-Minimum-Energy Torque profile for a 50° slew of an extending rigid DRM with a smoothing factor, $\varphi = 0.1$ 86

Figure 3.11: Closed Loop DRM Control Diagram 87

Figure 3.12: DRM Schematic with feedback actuators 88

Figure 3.13: Disturbance torque for a 50° minimum-time slew of an extending DRM with Payload 0 90

Figure 4.1: DRM Total Energy for an initial tip deflection of 2 cm 113

Figure 4.2: DRM Kinetic and Potential Energy conservation for an initial tip deflection of 2 cm 114

Figure 4.3: DRM link deflections for an initial link 2 tip deflection of 2 cm 114

Figure 4.4: Results from Jniffene and Fahim, (1997) open loop slew of a single link flexible manipulator unloaded in (a) and with a tip mass of 0.1 Kg in (b) 116

Figure 4.5: Reproduction of results in Jniffene and Fahim, (1997). Slew of a single link flexible manipulator both unloaded and with a tip mass of 0.1 Kg 116

Figure 4.6: Applied Root Torque and slew angle for a 50° minimum-time slew of a fixed length DRM with Payload 1 119

Figure 4.7: Undamped tip vibrations for a 50° minimum-time slew of a fixed length DRM with no payload 120

Figure 4.8: Undamped tip vibrations for a 50° minimum-time slew of a fixed length DRM with Payload 0 120

Figure 4.9: Undamped tip vibrations for a 50° minimum-time slew of a fixed length DRM with Payload 1 120

Figure 4.10: Applied Root Torque and slew angle time history for a 50° minimum-time slew of an extending DRM with Payload 1 121

Figure 4.11: Deployment Force and exposed length 'a' time history for a 50° minimum-time slew of the DRM with Payload 0 121

Figure 4.12: Undamped tip vibrations for a 50° minimum-time slew of an extending DRM with no payload 122

Figure 4.13: Undamped tip vibrations for a 50° minimum-time slew of an extending DRM with Payload 0 122

Figure 4.14: Undamped tip vibrations for a 50° minimum-time slew of an extending DRM with Payload 1 122

Figure 4.15: Undamped tip vibrations for a 50° minimum-time slew of an extending DRM with Payload 1 with no torque smoothing factor, φ = 0.0 124

Figure 4.16: Tip vibration for a minimum-time slew of an extending DRM with Payload 1 and no torque smoothing factor, φ = 0.0 125

Figure 4.17: Tip vibration for a near minimum-time slew of an extending DRM with Payload 1 and a torque smoothing factor φ = 0.005 125

Figure 4.18: Tip vibration for a near minimum-time slew of an extending DRM with Payload 1 and a torque smoothing factor φ = 0.01 125

Figure 4.19: Tip vibration for a near minimum-time slew of an extending DRM with Payload 1 and a torque smoothing factor φ = 0.05 126

Figure 4.20: Applied Root Torque and slew angle for a 50° near minimum-time slew of an extending DRM with Payload 1 and a torque smoothing factor φ = 0.05 126

Figure 4.21: Tip vibrations, slew Torque and slew angle for a 50° minimum-energy slew of a fixed length DRM with Payload 1. 128

Figure 4.22: Tip vibrations for a 50° minimum-energy slew for an extending DRM without payload 129

Figure 4.23: Tip vibrations for a 50° minimum-energy slew for an extending DRM with Payload0 129

Figure 4.24: Tip vibrations for a 50° minimum-energy slew for an extending DRM with Payload1 129

Figure 4.25: Tip vibrations for a 50° minimum-energy slew for an extending DRM with Payload 1 with no torque smoothing factor, φ = 0.0 131

Figure 4.26: Tip vibration for a near minimum- energy slew of an extending DRM with Payload 1 and a torque smoothing factor, φ = 0.005 131

Figure 4.27: Tip vibration for a near minimum- energy slew of an extending DRM with Payload 1 and a torque smoothing factor, φ = 0.01 131

Figure 4.28: Tip vibration for a near minimum- energy slew of an extending DRM with Payload 1 and a torque smoothing factor, φ = 0.05 132

Figure 4.29: Applied Root Torque and slew angle for a 50° near minimum-energy slew of an extending DRM with Payload 1 and a torque smoothing factor, φ = 0.05 132

Figure 4.30: Torque motor armature circuit 134

Figure 4.31: Minimum-Time Angular acceleration and slew torque for an extending DRM with Payload 1 137

Figure 4.32: Minimum-Energy angular acceleration and slew torque for an extending DRM with Payload 1 137

Figure 4.33: Power curve for a minimum-time slew of an extending DRM with Payload 1 138

Figure 4.34: Power curve for a minimum-energy slew of an extending DRM with Payload 1 138

Figure 4.35: Applied Root Torque and slew angle for a 50° minimum-time slew of an extending DRM with Payload 1 and a set deployment force 141

Figure 4.36: Undamped tip vibrations for a minimum-time slew of an extending DRM with Payload 1 and a 200 N deployment force for link 2 141

Figure 4.37: Undamped tip vibrations, slew torque, slew angle, deployment force and exposed length time histories for a minimum-time slew of a retracting DRM plus Payload 1 142

Figure 4.38: Rotation angle result for a minimum-time slew of the DRM plus Payload 1 with an error of +15% in the payload mass 144

Figure 4.39: Rotation angle result for a minimum-energy slew of the DRM plus Payload 1 with an error of -15% in the payload mass 144

Figure 4.40: Linear Root feedback tip vibration results for a minimum-time slew of an extending DRM plus Payload 1 147

Figure 4.41: Linear Root feedback control torque for a minimum-time slew of an extending DRM plus Payload 1 147

Figure 4.42: Linear Root feedback tip vibration results for a minimum-time slew of an extending DRM plus Payload 1, using large gains 148

Figure 4.43: Linear Root feedback control torque for a minimum-time slew of an extending DRM plus Payload 1, using large gains 148

Figure 4.44: Linear Tip feedback tip vibration results for a minimum-time slew of an extending DRM carrying Payload 1 150

Figure 4.45: Linear Tip feedback control torque for a minimum-time slew of an extending DRM carrying Payload 1 150

Figure 4.46: Linear Tip feedback tip vibration results for a minimum-time slew of an extending DRM carrying Payload 0 150

Figure 4.47: Linear feedback tip vibration results and control torque for a minimum-time slew of an extending DRM carrying Payload 1 154

Figure 4.48: Linear feedback tip vibration results and control torque for a minimum-time slew of an extending DRM carrying Payload 1 with a +15% payload mass error 155

Figure 4.49: Linear feedback slew angle results of an extending DRM carrying Payload 1 with a +15% payload mass error 155

Figure 4.50: Tip vibration and slew angle for a 50° minimum-time slew plus linear feedback control of an extending DRM carrying Payload 3 with a +15% Payload mass error 156

Figure 4.51: Tip vibration and slew angle for a 50° minimum-time slew plus linear feedback control of an extending DRM carrying Payload 3 with a -15% Payload mass error 156

Figure 4.52: Lyapunov Root actuator damped tip vibrations for a 50° minimum-time slew of an extending DRM with Payload 1 159

Figure 4.53: Lyapunov Feedback root actuator torque time history for a 50° minimum-time slew of an extending DRM with Payload 1 159

Figure 4.54: Lyapunov Root actuator damped tip vibrations for a 50° minimum-energy slew of an extending DRM with Payload 1 159

Figure 4.55: Undamped tip vibrations for a 50° minimum-energy slew of a contracting DRM with Payload 1 160

Figure 4.56: Lyapunov Root actuator damped tip vibrations for a 50° minimum-energy slew of a contracting DRM with Payload 1 160

Figure 4.57: Lyapunov Feedback root actuator torque time history for a 50° minimum-energy slew of a contracting DRM with Payload 1 160

Figure 4.58: Lyapunov Feedback tip actuator damped tip vibrations for a 50° minimum-time slew of an extending DRM with Payload 1 162

Figure 4.59: Lyapunov Feedback tip actuator damped tip vibrations for a 50° minimum-time slew of an extending DRM with Payload 0 163

Figure 4.60: Lyapunov Feedback tip actuator damped tip vibrations for a 50° minimum-energy slew of an extending DRM with Payload 1 163

Figure 4.61: Lyapunov Feedback tip actuator torque time history for a 50° minimum-energy slew of an extending DRM with Payload 1 163

Figure 4.62: Lyapunov damped tip vibrations for a 50° minimum-time slew of an extending DRM with Payload 0 167

Figure 4.63: Lyapunov damped tip vibrations for a 50° minimum-time slew of an extending DRM with Payload 1 167

Figure 4.64: Lyapunov damped tip vibrations for a 50° minimum-time slew of an extending DRM with Payload 3 167

Figure 4.65: Control torques (Feedback and Open loop) for a 50° minimum-time slew plus Lyapunov feedback control of an extending DRM with Payload 1 168

Figure 4.66: Slew angle and tip vibration for a 50° minimum-time slew plus Lyapunov feedback control of an extending DRM with Payload 1 with a +15% Payload mass error 169

Figure 4.67: Slew angle and tip vibration for a 50° minimum-time slew plus Lyapunov feedback control of an extending DRM with Payload 3 with a -15% Payload mass error 169

Figure 4.68: Control torques (Lyapunov Feedback and Open loop) for a 50° minimum-time slew of an extending DRM with Payload 1 with a +15% Payload mass error 170

Figure 4.69: Tip vibration for a near minimum-time slew plus Lyapunov feedback control of an extending DRM with Payload 1 and a smoothing factor of φ=0.005 171

Figure 4.70: Tip vibration for a near minimum-energy slew plus Lyapunov feedback control of an extending DRM with Payload 1 and a smoothing factor of φ=0.005 171

Figure 5.1: Undamped tip vibrations for a minimum-time slew of an extending DRM with a 3000Kg Payload 176

Figure 5.2: Linear feedback control tip vibrations for a minimum-time slew of an extending DRM with a 3000Kg Payload 176

Figure 5.3: Lyapunov feedback tip vibrations for a minimum-time slew of an extending DRM with a 3000Kg Payload 176

Figure B.1: Cantilever Euler-Bernoulli Beam with a Tip Point Mass. 191

Figure D.1: The ACSL DRM dynamic simulation environment 222

Figure E.1: The DRM NASTRAN model definition 224

Tables

Table 2-1: SRMS and SSRMS Physical characteristics 12

Table 2-2: DRM Physical characteristics 12

Table 2-3: Payload characteristics 32

Table 2-4: P-DRM Natural Frequencies (in Hz) as Link 2 is deployed 37

Table 2-5: P-DRM Approx. Nat. Freq. (in Hz) for several different values of extended Link 2 52

Table 2-6: P-DRM Nat. Freq. Percent error between exact and approximate methods 53

Table 2-7: New Payload characteristics 54

Table 2-8: P-DRM + Payload 0 Nat. Freq. (Hz) for several different values of extended Link 2 54

Table 2-9: DRM Approximate Nat. Freq. (Hz) for different values of extended Link 2 and Payloads 56

Table 2-10: DRM + Payload 1 Approximate Nat. Freq. (Hz) with different mode shapes and an increasing number of functions 57

Table 2-11: DRM Bending Natural Frequencies by NASTRAN, and Error Comparison to Approx. Values in Table 2-9 59

Table 2-12: DRM Torsional Natural Frequencies by NASTRAN 60

Table 3-1: Feedback actuator characteristics 88

Table 4-1: DRM Slew motor characteristics 136

Table B-1: Natural frequencies errors for an Assumed Mode discretization model of a Cantilever Beam 190

Table B-2: Natural frequencies errors for an Assumed Mode discretization model of a Cantilever Beam with a 100 Kg tip mass 193

Table B-3: Natural Frequencies of Cantilever Beam 195

Table B-4: Natural Frequencies of Cantilever Beam with a tip point mass, M_p=100 kg 195

Acronyms

DRM ..... Deployable Robotic Manipulator
ERA ..... European Robot Arm
EVA ..... Extravehicular Activity
ISSA ..... International Space Station Alpha
JEM-RMS ..... Japanese Experiments Module Remote Manipulator System
MDM ..... Mobile Deployable Manipulator
MTE ..... Mobile Transporter Element
P-DRM ..... Partially Flexible Deployable Robotic Manipulator
SRMS ..... Shuttle Remote Manipulator System
SSRMS ..... Space Station Remote Manipulator System

Notation

ρ_1	Link 1 mass per unit length
ρ_2	Link 2 mass per unit length
L_1	Link 1 length
L_2	Link 2 length
EI_1	Link 1 flexural rigidity
EI_2	Link 2 flexural rigidity
L_p	Payload length
M_p	Payload mass
I_p	Payload mass moment of inertia
I_r	P-DRM rigid section mass moment of inertia
a	Length of Link 2 outside Link 1
b	Length of Link 2 inside Link 1
$\theta, \dot{\theta}, \ddot{\theta}$	DRM slew angle, velocity, acceleration
$\theta_{ref}, \dot{\theta}_{ref}, \ddot{\theta}_{ref}$	DRM Rigid slew angle, velocity, acceleration
$\theta_e, \dot{\theta}_e, \ddot{\theta}_e$	DRM Error slew angle, velocity, acceleration
y_1	Link 1 flexibility
y_2	Link 2 flexibility
P_1	Axial Load for the length of Link 2 inside Link 1
P_2	Axial Load for the length of Link 2 outside Link 1
$A_{a\eta}$	Acceleration along Link 2
T	Kinetic Energy
V	Potential Energy
L	Lagrangian
t	Time

$\mathbf{U}$	Lyapunov function
T_1	Actuator torque of the root feedback actuator
T_2	Actuator torque of the tip feedback actuator

Chapter 1 : Introduction

1.1 Background and Literature Survey

The dynamics and control of flexible manipulators in space have been under continued study over the last few decades, in particular since the conception in the 1970s of the Shuttle Remote Manipulator System (SRMS), Figure 1.1, and its successful implementation to all Shuttle missions during the 1980s and 1990s. This large, teleoperated, flexible manipulator was designed to aid astronauts in Extravehicular Activities (EVAs) and to deploy and retrieve satellites from and to the Shuttle cargo bay. This large flexible robotic structure has been the subject or the inspiration of many researchers in robotics, structural dynamics and in control theory (Kirk and Doengi, 1994), (Junkins, 1990), (Skaar and Ruoff, 1994), etc. This interest has been due to the large number of problems which can be formulated and solved, from possible manoeuvring strategies, the representation of the flexibility of the manipulator's links, the control strategies, etc.

Currently, apart from the existing SRMS a number of other space manipulator systems are being developed and will be deployed in the next few years to the International Space Station Alpha (ISSA), to aid in construction, maintenance and to

help in external experimental work. The manipulators currently planned are the Space Station Remote Manipulator System (SSRMS), the European Robot Arm (ERA) for the Russian segment of the ISSA, and the Japanese Experiments Module Remote Manipulator System (JEM-RMS).

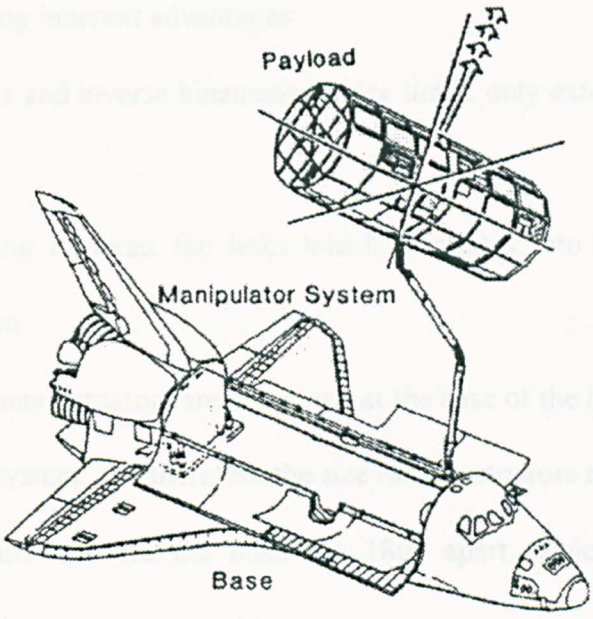

Figure 1.1: The SRMS carrying a large payload while in orbit, (Skaar and Ruoff, 1994).

All of these manipulators are based on a doubly articulated design in which two long links are connected via an elbow connection that can perform rotations, and a shoulder connection of the entire manipulator to the orbiting structure. The inclusion of an elbow connection at the end of the first flexible link introduces the need to have a torque motor at the joint to drive the second link through a slew. This torque motor introduces a large mass at the mid point of the entire extended manipulator which can negatively affect its manoeuvring and vibration dynamics. Having this large mass at the end of the first flexible link increases the moment of inertia of the system and therefore can produce large amplitudes of vibration, which are undesirable due to long settling times and possible component fatigue and failure.

In this thesis, a different class of large manipulator system is proposed for space applications, the Deployable Robotic Manipulator (DRM). This design contains two long links, which are connected to each other via a prismatic or telescopic link and to the supporting orbiting structure by a traditional shoulder revolute joint, Figure 1.2. This design has the following inherent advantages:

- Simpler kinematics and inverse kinematics, since link 2 only extends or retracts from the end of link 1.
- No inertia coupling between the links which translates into simpler equation of motion formulation.
- Slew and deployment actuators are contained at the base of the links which minimises the inertia of the system, and therefore the size of the actuators needed.
- No singular positions, were the links are 180° apart, which could exceed the actuator's capability to manoeuvre the arm.
- Unique configurations that simplify the manoeuvring of the manipulator since there is only one way to reach each particular position or orientation. In traditional manipulators, there is usually more than one way to reach each position and therefore optimisation strategies for manoeuvring have to be devised.
- Linear motion can be achieved easily by the prismatic joint, which extends or retracts link 2 of the DRM. In traditional manipulators linear motion, to approach or release a satellite without inducing any rotations, is achieved by very precise control of the revolute joints, but any miscalculation could send the payload tumbling out of control.

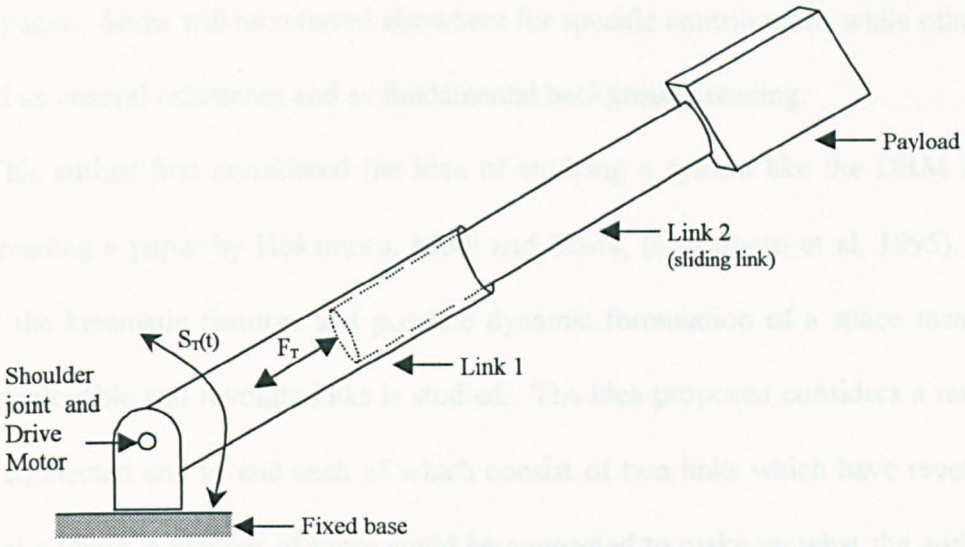

Figure 1.2: Deployable Robotic Manipulator (DRM) Schematic.

The DRM design also has a disadvantage, which is that it cannot reach the workspace area around the base of the manipulator. This disadvantage can be easily overcome by moving the base point of the manipulator using a device similar to the Mobile Transporter Element (MTE) (Skaar and Ruoff, 1994) used by the SSRMS on the ISSA.

The idea to propose and study a system such as the DRM is not an original one, as a few other space researchers have proposed and studied similar systems. It is nonetheless clear that this is a design which has received very limited attention in the literature and in particular in the areas of gross angular motion and vibration control no literature has been found to date. This opened the opportunity to provide a detailed study of the dynamics and control issues associated with this design. The few published studies of systems similar to the DRM concentrate on specific aspects or interactions with other orbiting elements, or they simplify the problem in some crucial way, so that the specific issues addressed in this thesis are not covered elsewhere in the literature. A review of the literature available on systems similar to the DRM is included below. The research works presented have all contributed to prepare and complete the research presented in

these pages. Some will be referred elsewhere for specific contributions while others have served as general references and as fundamental background reading.

This author first considered the idea of studying a system like the DRM in detail after reading a paper by Hokamoto, Modi and Misra, (Hokamoto et al, 1995). In this paper the kinematic features and possible dynamic formulation of a space manipulator with deployable and revolute links is studied. The idea proposed considers a number of units connected end to end each of which consist of two links which have revolute and prismatic joints, a number of these could be connected to make up what the authors call the Mobile Deployable Manipulator (MDM). Link flexibility is considered and the equations of motion in recursive form are derived. Control results are presented for a flexible MDM consisting of 4 links, two with revolute joints and two prismatic, based on direct velocity feedback, but no details, only results are given. This research has been expanded recently in (Hokamoto et al, 1998) to include the differences in behaviour of a rigid and a flexible MDM under the same control strategy and the researchers conclude that some vibration damping needs to be introduced to control the dynamics of the flexible modes, no payloads are simulated in the two aforementioned studies.

One other space application of a deployable manipulator is given in (Marom and Modi, 1993) and the related PhD thesis (Marom, 1993). In these two works, the researchers study the interaction dynamics of a large deployable manipulator attached to an orbiting flexible platform. The links of the manipulator are considered rigid and flexibility is introduced at the joint of the manipulator with the orbiting structure. Motor shaft and gear flexibility are considered, as well as the orbit and attitude dynamics of the entire assembly. A non-linear control strategy based on Feedback Linearisation Technique (FLT) is developed to manoeuvre the manipulator while maintaining the

attitude of the orbiting platform. Another recent study (Pandey and Agrawal, 1997) investigated the path planning of free flying spacecraft containing rigid manipulators with several deployable links.

Outside the area of space applications the study of manipulators with prismatic joints was found (Kim and Gibson, 1991) and the associated PhD thesis (Kim, 1988) where the vibration control of an industrial robot with a sliding link is presented. Only the deployable link is considered flexible and a small point mass payload is simulated at the end of the flexible link. An advanced variable order adaptive controller is developed to handle the shock of the sudden stop of the deployment of the flexible link.

Apart from the studies dealing explicitly with similar systems to the DRM (industrial robots or space manipulators), literature has also been sought on the related fields of dynamics of translating flexible beams, dynamics and control of flexible links, and Lyapunov based control system design. These areas are of direct importance to the study of the dynamics and control of the DRM since they play a part in formulating the equations of motion and in the control system design presented herein.

In the related field of the dynamics of an axially moving flexible cantilever beam an important study is presented in (Tabarrok et al, 1974) where the equations of motion of a beam whose length changes with time are derived. In the publication (Theodore et al, 1996) the modelling of axially moving flexible beams is also studied, equations of motion are developed by using the assumed mode method for the beam's flexibility. Another influential study in this field (Wang and Wei, 1987) which studies vibrations of a flexible moving beam, the authors found that the extending and contracting motions have destabilising and stabilising effects respectively on the vibration response of the beam.

The same subject of axially moving flexible beams but with the added complexity of rotation is studied in (Banerjee and Kane, 1989) where the extrusion of a flexible beam from a rotating base is studied by modelling the flexible beam as a series of rigid links connected with elastic springs. The same problem is also studied in (Yuh and Young, 1991) where a flexible beam having rotational and linear motion is described and its response investigated by computer simulation and experiment. Another approach to the same problem is in (Yüksel and Gürgöze, 1997), where the authors consider gravity effects, rotary inertia and axial force effects to develop the equations of motion and the associated boundary conditions. There is also a non-linear model developed in (Gordaninejad et al, 1991) to study the motion of a planar robot arm consisting of one revolute and one prismatic joint.

In the field of control of flexible space manipulator systems there are many relevant references in the literature both from a structural dynamics perspective and from a purely control theory perspective. On the one hand, the problem of slewing a long flexible beam with a payload at the end presents many interesting control stability problems due to sensor/actuator collocation, due to unmodelled flexible modes, etc. There is also a great deal of interest in this problem from researchers trying more advanced and different control strategies for flexible structures, so it is a very common problem to be used as an example. Due to this, it is impossible to make here a detail analysis of all the literature that could be applicable to the control system design of the DRM, therefore only the literature which was most influential to this author while doing this research is presented.

A very important group of references are (Junkins and Turner, 1986), (Junkins and Kim, 1993), (Oh et al, 1992), (Junkins et al, 1990) and (Junkins and Bang, 1993). As a former student of Prof. Junkins the author was naturally inclined to consult and study

these references. They provide a very solid foundation for flexible structure dynamics and control, for feedback control design and for Lyapunov control system design. In the control of large flexible structures, the following have also been influential: (Kirk and Doengi, 1994), (Kirk and Lee, 1994) and (Scott and Gilbert, 1993), where feedback control of flexible structures on the Space Shuttle are studied. Other references of interest are (Juang et al, 1986) and (Juang et al, 1989), which discuss DC motor modelling in the control of flexible manipulators. For Lyapunov control system design, (Jnifene and Fahim, 1997) and (Choura et al, 1991), which present and discuss control approaches for one-link flexible manipulators. Other references have been included in the text as their specific contributions to this thesis are presented.

1.2 Thesis goals and outline

The aims of this thesis are:

- To present the dynamics and vibration response for the Deployable Robotic Manipulator.
- To develop and validate a simplified dynamic model of the DRM simulating a small number of vibration degrees of freedom.
- To develop a control system for the DRM for large angular motions, for vibration control and to deal with payload uncertainties using both a linear control law and a Lyapunov based control law.

The thesis is divided into five distinct chapters covering each of the topics needed to satisfy the stated aims of this research. This first chapter presents a literature survey to explain how this research fits into the field of flexible robotic studies. Chapter 2 presents the system's energies, which are used, in the first instance for an exact eigenvalue

analysis to find the natural frequencies of vibration of the DRM. The assumed mode discretization method is introduced and applied to the flexible links to produce an approximate set of equations of motion for the DRM. The frequencies of vibration are calculated with the approximate equations of motion and compared to the exact frequencies calculated earlier to validate the approximate flexible model. Chapter 3 presents the open loop control strategy for the DRM based on the assumed torque method with one of four acceleration profiles. The feedback actuators are introduced, a linear control law is presented and a Lyapunov based control law is developed for the DRM. Chapter 4 presents the results of the dynamic simulations of the DRM under open loop and closed loop control. These results show the ability of both of the closed loop control laws to achieve the performance objectives. Chapter 5 presents some closing remarks and discusses some results. Chapter 6 finishes the thesis with conclusions on the research presented and remarks on directions of future research which can be pursued using this thesis as a starting point.

Chapter 2 : Dynamic Modelling

The proposed Deployable Robotic Manipulator (DRM) is a teleoperated system to be used by astronauts in EVA operations or to carry out limited independent operations, such as automatically replacing damaged units, retrieval of external experiments, etc. The majority of the manipulator's operations can be classified as grappling payloads and moving or slewing them with respect to the space station or some other orbiting structure. This thesis investigates the manoeuvring of the manipulator plus payload by analysing a large angle slew while at the same time extending or retracting link 2 of the manipulator. Hence, a dynamical model of the DRM is developed here for use in computer simulations and control law design.

In Section 2.1 the elements of the DRM schematic are presented and discussed. In Section 2.2 the kinetic and strain energies for the flexible manipulator are formulated as the first step in modelling its dynamics. In Section 2.3 the partial differential equations for the dynamics of the flexible manipulator are presented. In addition, in this section the differential eigenvalue problem for a rigid manipulator with a flexible deployable link is solved to find the natural frequencies of vibration of the manipulator, and the mode shapes of the flexible link. In Section 2.4 an approximate method for describing the flexible components of the manipulator is presented. In Section 2.5 the DRM's

approximate equations of motion are derived by discretizing the flexible deflections. These equations are then used in the dynamic simulations in Chapter 4. Sections 2.6 and 2.7 present the approximate natural frequency calculations for the P-DRM and for the flexible DRM, respectively. Finally in Section 2.8 a NASTRAN natural frequency analysis of the DRM is presented, and the results compared with the approximate dynamic model developed.

2.1 Dynamic System Characteristics

The manipulator system is a robotic device that contains both slewing and telescopic links, shown schematically in Figure 1.2. The lower link of the DRM is attached to an orbiting structure via the shoulder joint and the upper link is contained inside the lower one. At the base of the manipulator, there is an electric torque motor operating via a reduction gear for the slewing motion and a linear electro-mechanical actuator for the prescribed deployment of the upper link. This link (link 2) slides in and out of the lower link (link 1) and carries the payload at its tip by means of a grappling device.

The DRM, while in operation in earth orbit, will perform a number of different tasks. Principally it will move payloads by rotating with respect to the shoulder joint and extending or contracting link 2. This is the baseline manoeuvre that will be studied in terms of tip positioning and vibration levels; a slew through a predetermined angle in one plane, no out-of-plane effects and no torsion will be considered in this study. This limitation simplifies the problem so that interactions between the deployment dynamics and the slew dynamics of the DRM can be better understood. Torsion dynamics are not studied here nor included in the dynamic simulations, but the torsion response is presented in Section 2.8 and torsion could be included in an expansion of this work.

To determine the vibration levels expected during the manoeuvre typical physical characteristics of the DRM have to be defined, these are based on the SRMS and the SSRMS values as presented in Table 2-1.

Table 2-1: SRMS and SSRMS Physical characteristics
(Hedley, 1986), (Skaar and Ruoff, 1994)

	SRMS		SSRMS	
	Lower boom	Upper boom	Lower boom	Upper boom
Length	6.4 m	7.06 m	7.11 m	7.11 m
EI	2.82e6 Nm^2	4.2e6 Nm^2	3.8e6 Nm^2	3.8e6 Nm^2
Mass	140.0 Kg	88.0 Kg	315.0 Kg	280.0 Kg

Using the values in Table 2-1 as a reference, the physical characteristics of the DRM are defined as shown in Table 2-2. Which show the DRM is a long and slender manipulator. Link structural flexibility has to be taken into account to model its dynamic behaviour correctly and it is assumed that the stiffness is sufficient to guarantee that the total flexural deformation caused by slewing/extension loads stay within prescribed limits, since too much flexure could degrade the sliding efficiency of link 2 inside link 1.

Table 2-2: DRM Physical characteristics

	DRM	
	Link 1	Link 2
Length	7.0 m	8.0 m
EI	2.5e6 Nm^2	3.0e6 Nm^2
Mass	100.0 Kg	75.0 Kg

For accurate positioning of the end effector or the payload, it is not sufficient just to work out the kinematics of the tip position for particular manoeuvres, as for rigid Earth-based manipulators. For the DRM, the dynamic response of the elastic structure due to different inputs of shoulder torque, $S_T(t)$, and deployment force, $F_T(t)$, is analysed using the equations of motion for the flexible DRM. The control system then attempts to achieve desired manoeuvre accuracy while trying simultaneously to reduce the flexible vibrations caused by the manoeuvre.

2.2 Energy Formulation

The equations of motion for the DRM are derived by Lagrange's equation and thus require expressions for the kinetic and strain energies for the various components of the DRM.

2.2.1 Kinetic Energy

The energy formulation for the DRM starts by identifying the different contributing elements to the energy state of the system. In this case, four distinct sections are considered, from Figure 2.1:

1. Link 1, from the shoulder joint (point O_1) to L_1.
2. The portion of link 2 inside link 1, length b(t), which has the physical characteristics of link 2 but since it is contained inside link 1 it is assumed to have the same deflection as link 1.
3. The portion of link 2 outside of link 1, length a(t).

4. The rigid payload, attached to the free end of the manipulator by a grappling device.

The grappling device of the manipulator is assumed to be part of the payload in terms of its mass and inertia, and it is simulated as representing a rigid connection between the end of link 2 and the payload.

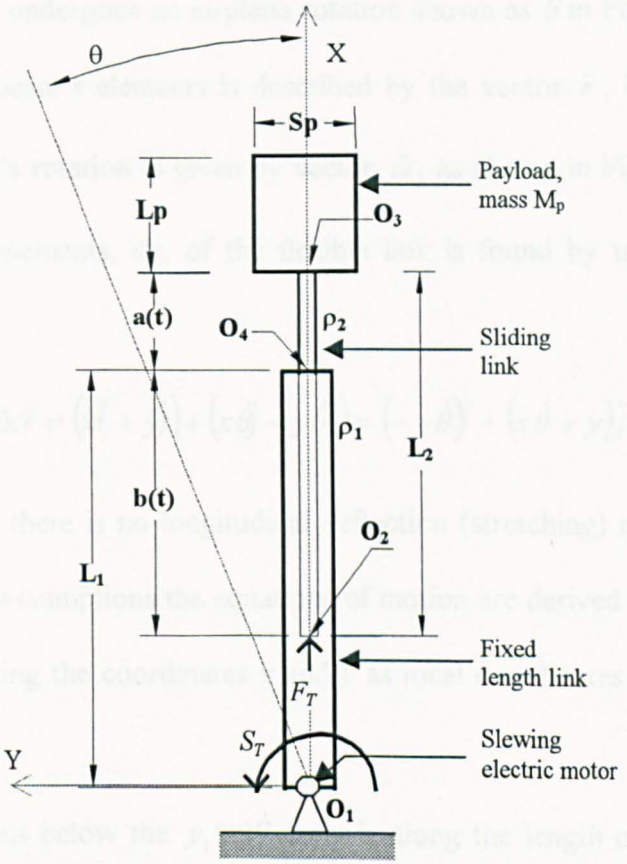

Figure 2.1: DRM System Schematic.

The slew angle θ, shown in Figure 2.3, is the slew angle of the DRM as measured at the root of the manipulator. For a mass element of either link 1 or link 2, the kinetic energy has components parallel and perpendicular to the manipulator, as shown in Figure 2.2.

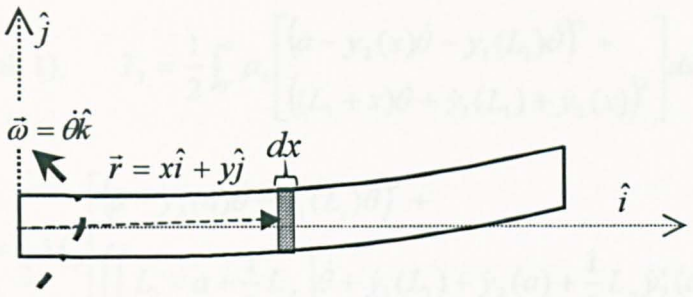

Figure 2.2: Flexible Link Detailed Schematic.

Each of the flexible links undergoes an in-plane rotation shown as θ in Figure 2.1. The position of each of the beam's elements is described by the vector $\vec{r}$, in the rotating frame $\hat{i}, \hat{j}, \hat{k}$. The beam's rotation is given by vector $\vec{\omega}$, as shown in Figure 2.2. The velocity of each of the elements, *dx*, of the flexible link is found by taking the time derivative of vector $\vec{r}$,

$$\frac{d\vec{r}}{dt} = \dot{\vec{r}} + \vec{\omega}x\dot{\vec{r}} = \left(\dot{x}\hat{i} + \dot{y}\hat{j}\right) + \left(x\dot{\theta}\hat{j} - y\dot{\theta}\hat{i}\right) = \left(-y\dot{\theta}\right)\hat{i} + \left(x\dot{\theta} + \dot{y}\right)\hat{j}$$

where it is assumed that there is no longitudinal deflection (stretching) of the beam so that $\dot{x} = 0$. Using these assumptions the equations of motion are derived for each of the sections of the DRM, using the coordinates *x* and *y* as local coordinates within each of the integral limits below.

Thus, in the equations below the $y_1(x)\dot{\theta}$ term is along the length of the arm, and $x\dot{\theta} + \dot{y}_1(x)$ is perpendicular as is shown above. Therefore, if $\dot{a}(t)$ is the instantaneous axial velocity of the manipulator at time *t* we have the following kinetic energy expressions for each of the defined sections:

Link 1, $$T_1 = \frac{1}{2}\int_0^{L_1} \rho_1 \left[\left(-y_1(x)\dot{\theta}\right)^2 + \left(x\dot{\theta} + \dot{y}_1(x)\right)^2\right] dx \qquad (2.2.1)$$

Link 2 (inside link 1), $$T_2 = \frac{1}{2}\int_{L_1-b}^{L_1} \rho_2 \left[\left(\dot{a} - y_1(x)\dot{\theta}\right)^2 + \left(x\dot{\theta} + \dot{y}_1(x)\right)^2\right] dx \qquad (2.2.2)$$

Link 2 (outside link 1), $$T_3 = \frac{1}{2}\int_0^a \rho_2 \left[\begin{array}{l} \left(\dot{a} - y_2(x)\dot{\theta} - y_1(L_1)\dot{\theta}\right)^2 + \\ \left((L_1 + x)\dot{\theta} + \dot{y}_1(L_1) + \dot{y}_2(x)\right)^2 \end{array} \right] dx \qquad (2.2.3)$$

Payload, $$T_4 = \frac{1}{2}M_p \left[\begin{array}{l} \left(\dot{a} - y_2(a)\dot{\theta} - y_1(L_1)\dot{\theta}\right)^2 + \\ \left(\left(L_1 + a + \frac{1}{2}L_p\right)\dot{\theta} + \dot{y}_1(L_1) + \dot{y}_2(a) + \frac{1}{2}L_p\dot{y}_2'(a)\right)^2 \end{array} \right] + \qquad (2.2.4)$$
$$\frac{1}{2}I_p\left(\dot{\theta} + \dot{y}_2'(a)\right)^2$$

It is noted in the above equations that the term $y_1(x)\dot{\theta}$ represents geometric stiffening which is only significant when the slew rate, $\dot{\theta}$, approaches the first natural frequency of vibration of the system, otherwise it can be neglected (Tabarrok et al, 1974), (Theodore et al, 1996), (Yuh and Young, 1991), (Chapnik et al, 1993). It is also noted that in Equation (2.2.3), the upper integration limit, *a*, is the length of link 2 outside link 1 which is time varying, and in Equation (2.2.2) the lower integration limit *b* is the length of link 2 inside link 1, also time varying.

In the above equations, $y_1(x)$ represents the transverse elastic deflection of link 1 and $y_2(x)$ the transverse deflection of link 2 as shown in Figure 2.3. The quantities ρ_1 and ρ_2 are the mass per unit length of link 1 and link 2 respectively. M_p is the payload mass, L_p its length, I_p the mass moment of inertia of the payload with respect to its centre of mass and $\dot{a}(t)$ is the deployment velocity. The overdot notation, $\dot{z}$, denotes time derivation and the prime, z', signifies a partial derivative with respect to the spatial coordinate *x*. The payload is assumed prismatic, as shown in Figure 2.1. The payload undergoes rotational motion not only due to the rigid slew motion, θ_s, but also due to the time varying elastic slope at the tip of link 2, $\dot{y}_2'$.

2.2.2 Elastic Strain Energy

The strain energy of this system comes from the flexure of the links, including the effect of the axial force used to deploy link 2. The elastic deformation of the DRM is shown in Figure 2.3. The strain energy is formulated using the Euler-Bernoulli beam assumptions of negligible shear deformation and rotatory inertia. The prescribed extension or contraction of link 2 occurs at the same time as the slew manoeuvre and is achieved with a bang-bang force profile using a linear actuator at the shoulder joint. The flexible parts of the manipulator are link 1 and link 2, and the payload is assumed to be rigid. A flexible payload such as a long truss for the space station could also be considered, then extra degrees of freedom would need to be included, such an analysis is beyond the scope of the investigation in this thesis.

The strain energies for the DRM are formulated, following the coordinate system definitions in Figure 2.3, for the three flexible sections as:

Link 1,
$$V_1 = \frac{1}{2}\int_0^{L_1} EI_1\left(\frac{\partial^2 y_1}{\partial x^2}\right)^2 dx \tag{2.2.5}$$

Link 2 (inside link 1),
$$V_2 = \frac{1}{2}\int_{L_1-b}^{L_1} EI_2\left(\frac{\partial^2 y_1}{\partial x^2}\right)^2 + P_1(x)\left(\frac{\partial y_1}{\partial x}\right)^2 dx \tag{2.2.6}$$

Link 2 (outside link 1),
$$V_3 = \frac{1}{2}\int_0^{a} EI_2\left(\frac{\partial^2 y_2}{\partial x^2}\right)^2 + P_2(x')\left(\frac{\partial y_2}{\partial x}\right)^2 dx' \tag{2.2.7}$$

Where EI_i represents the flexural rigidity of the beam in the plane of bending and $P_i(x)$ is the axial deployment load at the position x.

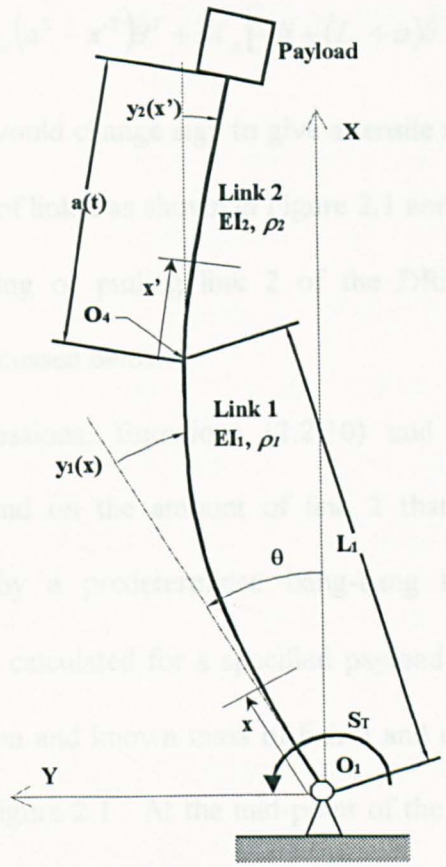

Figure 2.3: DRM elastic deformation.

The axial deployment loads, $P_i(x)$, for every position x along link 2 are formulated as:

$$P_1(x) = \int_x^{L_1} \rho_2 A_{a\eta} d\eta + \int_0^a \rho_2 A_{a\eta} d\eta + M_p A_{a(L_1+a)} \tag{2.2.8}$$

$$P_2(x') = \int_{x'}^{a} \rho_2 A_{a\eta} d\eta + M_p A_{a(L_1+a)} \tag{2.2.9}$$

and may be compressive (extension of link 2) or tensile (retraction of link 2). Thus $A_{a\eta}$ is the absolute acceleration in the axial direction of every mass element along link 2 due to axial acceleration and centrifugal acceleration defined as $A_{a\eta} = -\ddot{a} + \eta\dot{\theta}^2$. Substituting the acceleration and performing the integral in the above equations gives the following axial load expressions:

$$P_1(x) = -\rho_2 \ddot{a}(L_1 - x + a) + \frac{1}{2}\rho_2 \left(L_1^2 - x^2 + a^2\right)\dot{\theta}^2 + M_p\left[-\ddot{a} + (L_1 + a)\dot{\theta}^2\right] \tag{2.2.10}$$

$$P_2(x') = -\rho_2 \ddot{a}(a - x') + \frac{1}{2}\rho_2 (a^2 - x'^2)\dot{\theta}^2 + M_p\left[-\ddot{a} + (L_1 + a)\dot{\theta}^2\right] \qquad (2.2.11)$$

Where for contraction, $\ddot{a}$ would change sign to give a tensile force, P_t. The deployment force is applied at the base of link 2 as shown in Figure 2.1 and is accomplished by means of a linear actuator pushing or pulling link 2 of the DRM using a predetermined deployment schedule as discussed below.

The axial load expressions, Equations (2.2.10) and (2.2.11) depend on the deployment acceleration and on the amount of link 2 that has been deployed. The deployment is achieved by a predetermined bang-bang force time history. The deployment acceleration is calculated for a specified payload mass, M_p, and manoeuvre time. From the acceleration and known mass of link 2 and of the payload the required force is calculated, F_T in Figure 2.1. At the mid-point of the slew manoeuvre, the force is reversed to bring the payload to rest.

The linear actuator providing the deployment and contraction force for the DRM is envisaged as an electrical linear actuator similar to a conventional hydraulic jack but for space use, it is assumed to have a sufficiently wide bandwidth and short time constant to make link 2 of the DRM follow the specified deployment profile exactly (Kim and Gibson, 1991). It provides a force at the base of link 2 of the DRM according to a predetermined control law as will be shown and discussed in Figure 4.11 from the required linear acceleration time history as shown in Figure 3.4. There are two possible modes of operation for this actuator studied in this thesis, for the majority of the simulations the deployment takes place during the time of the slew, both final times are made to coincide by reducing the deployment force to fit the slew. On the other hand the possibility exists, as is highlighted in Figure 3.1, to specify a force for the deployment

actuator. This force is taken as the actuator limit and the deployment takes place following a minimum-time deployment profile.

The contribution of the axial load to the strain energy clearly influences the transverse vibration levels in the manipulator. A compressive axial force (for deployment) will lower the natural frequencies of vibration of the DRM and conversely will raise them when the force is tensile. The effect of the axial load on the DRM's vibrations increases when the linear acceleration, $\ddot{a}$, is high, or if the manipulators' angular velocity, $\dot{\theta}$, is large. When neither $\ddot{a}$ or $\dot{\theta}$ are large the effects of the axial load on the dynamic response have been found to be small, but for completeness it will be included in the dynamic simulations presented in Chapter 4.

In a complete natural frequency analysis of a time varying DRM, the contribution of the deployment force to lower or increase the natural frequencies will of course completely depend on the size of that force. Therefore all of the natural frequencies for the DRM would have to be calculated for different forces, this has been deemed to be a very complicated exercise for very little gain into the understanding of the DRM's vibrations. Therefore, in the natural frequency analysis for the DRM presented in subsequent sections of this thesis the axial deployment is not considered. The natural frequencies of vibration of the DRM will be calculated assuming various fixed lengths.

2.3 Eigenvalue Analysis – Hamilton's Principle

The first few natural frequencies ω_n of the DRM and payload system are of importance in the dynamic analysis and in designing the closed-loop control system. The values of ω_n will depend on:

1. The dimensions and mass of the payload.
2. The instantaneous length of the DRM.

Clearly the ω_n will decrease as the DRM's length increases and will increase during contraction. This section presents an exact eigenvalue analysis for various fixed lengths of the DRM for latter comparison with the approximate simulation model.

The kinetic and strain energies of the DRM have been formulated in the previous section. In which, one discrete and two distributed coordinates have been identified. The discrete coordinate is the slew angle theta, θ. The distributed coordinates, $y_i(x,t)$, representing the link elastic deflections. The two latter coordinates are called distributed coordinates of the system because they are functions of both space and time. The flexible deflections vary along the length of each link as well as in time according to inputs or initial conditions.

Due to the errors introduced in selecting the approximate expressions to describe the elastic deflections, say by the assumed mode method, an exact eigenvalue solution is first considered using Hamilton's principle. These results can then be compared with the simpler approximate model presented in Section 2.5 used to obtain the slewing-deployment dynamic response. In practice, for the approximate model, only the first one

or two modes of vibrations will be of importance in the dynamic analysis, since the modal amplitudes are proportional to $\frac{1}{\omega_n^2}$.

2.3.1 Application of Hamilton's Principle to a simplified DRM

To derive the equations of motion of this continuous distributed parameter system the generalised Hamilton's principle is applied to the energy formulas defined in the previous section. Hamilton's variation principle is given by:

$$\int_{t_1}^{t_2} \delta(T-V)dt + \int_{t_1}^{t_2} \delta W_{nc} dt = 0 \qquad (2.3.1)$$

where T is the kinetic energy, V is the potential energy, δ the variational parameter and W_{nc} is the work done by the non-conservative forces. Equation (2.3.1) presents practical difficulties in its application to multibody problems with distributed coordinates. In particular, the integration by parts required to take the integral over the distributed elements in links 1 and 2. The analysis in this section will be limited to, as mentioned above, a comparative study of the manipulator's natural frequencies with the approximate model developed later. Therefore, to limit the complexity of the mathematical formulation, an infinite dimensional model for a simplified DRM, which has a rigid link 1, and a flexible link 2 is developed. The partially flexible DRM is referred to as the P-DRM. The following analysis will give the natural frequencies of vibration of the P-DRM for fixed lengths with several different payloads. This analysis will then serve to validate the discretized model developed in the next section by comparing the natural frequencies values calculated using the approximate discrete model and the values obtained from the continuous model.

To formulate the continuous equations of motion and the boundary conditions of the P-DRM the distributed coordinate $y_i(x,t)$ associated with the flexibility of link 1, Figure 2.3, is set to zero in the equations (2.2.1) to (2.2.7). A further simplification introduced at this time is to neglect the geometrical stiffness, the $-y_i\dot{\theta}$ velocity terms in the kinetic energy expressions. This velocity term is perpendicular to the transverse deflection and is considered a second order effect for low slew rates, $\dot{\theta}$, which are considered in this thesis. The simplifications of the above energy equations, (2.2.1) through to (2.2.7), produce the following combined energy expressions for the manipulator:

$$T_T = \frac{1}{2}\rho_1\int_0^{L_1}\left(x\dot{\theta}\right)^2 dx + \frac{1}{2}\rho_2\int_{L_1-b}^{L_1}\left(x\dot{\theta}\right)^2 dx + \frac{1}{2}\int_0^a \rho_2\left((L_1+x)\dot{\theta}+\dot{y}_2(x)\right)^2 dx + \frac{1}{2}M_p\left[(L_1+a)\dot{\theta}+\dot{y}_2(a)\right]^2 + \frac{1}{2}I_{yy}\left[\dot{\theta}+\dot{y}_2'(a)\right]^2 + \frac{1}{2}M_pL_p\left((L_1+a)\dot{\theta}+\dot{y}_2(a)\right)\left(\dot{\theta}+\dot{y}_2'(a)\right) \tag{2.3.2}$$

$$V_T = \frac{1}{2}\int_0^a EI_2\left(\frac{\partial^2 y_2}{\partial x^2}\right)^2 dx \tag{2.3.3}$$

The axial deployment velocity term, $\dot{a}$, is not included in the above kinetic energy expression, as it does not contribute significantly to the transverse vibrations of the P-DRM, and it would only serve to further complicate the analysis. Therefore, for the natural frequency analysis the P-DRM will be considered at fixed lengths with no deployments velocity or acceleration.

In Equation (2.3.2), I_{yy} is the mass moment of inertia of the payload with respect to the attachment point to the manipulator. Note that the last term in Equation (2.3.2), is seldom included in the study of manipulators carrying large payloads. This term, takes into account the fact that the payload's centre of mass is a distance of $\frac{L_p}{2}$ from the

attachment point to the link. This effect is usually not included as most of the flexible manipulator studies published concentrate on small payloads or point mass payloads where the term would not exist or would be of little importance (Ata et al, 1996), (Tokhi et al, 1995), (Kim and Gibson, 1991), (Jnifene and Fahim, 1997), etc. In this thesis, the effect of payload length is included as it can have considerable effects in the natural frequency calculations for the system and in the control law formulation. The payloads width is captured in the payload moment of inertia, I_{yy}, in Equation (2.3.2). Furthermore, the payload is assumed to be grappled along its centre of mass axis. Off-axis grappling is not considered in this thesis but could be an interesting extension to this work. These effects are important when dealing with medium or large size payloads at the end of flexible manipulators, as is the case here.

2.3.2 Exact Formulation of Equations of Motion for the P-DRM

The equations of motion are formulated from the energy expressions T and V, Equations (2.3.2) and (2.3.3), above. The rigid degree of freedom, θ, is obtained from the application of Lagrange's equation:

$$\frac{d}{dt}\left(\frac{\partial L}{\partial \dot{\theta}}\right)-\frac{\partial L}{\partial \theta}=S_T(t) \tag{2.3.4}$$

where the Lagrangian is given by:

$$\begin{aligned} L=T_T-V_T=&\frac{1}{2}\rho_1\int_0^{L_1}\left(x\dot{\theta}\right)^2dx+\frac{1}{2}\rho_2\int_{L_1-b}^{L_1}\left(x\dot{\theta}\right)^2dx+\\ &+\frac{1}{2}\int_0^{a}\rho_2\left((L_1+x)\dot{\theta}+\dot{y}_2(x)\right)^2-EI_2\left(\frac{\partial^2 y_2}{\partial x^2}\right)^2dx+\\ &+\frac{1}{2}M_p\left[(L_1+a)\dot{\theta}+\dot{y}_2(a)\right]^2+\frac{1}{2}I_{yy}\left[\dot{\theta}+\dot{y}_2'(a)\right]^2+\\ &+\frac{1}{2}M_pL_p\left((L_1+a)\dot{\theta}+\dot{y}_2(a)\right)\left(\dot{\theta}+\dot{y}_2'(a)\right) \end{aligned} \tag{2.3.5}$$

the Lagrangian can be further simplified from Equation (2.3.5), by performing the first two integrals:

$$L=\frac{1}{6}\rho_1 L_1^3\dot{\theta}^2+\frac{1}{6}\rho_2\left[L_1^3-(L_1-b)^3\right]\dot{\theta}^2+\frac{1}{2}\int_0^a\rho_2\left((L_1+x)\dot{\theta}+\dot{y}_2(x)\right)^2-EI_2\left(\frac{\partial^2 y_2}{\partial x^2}\right)^2dx+$$
$$+\frac{1}{2}M_p\left[(L_1+a)\dot{\theta}+\dot{y}_2(a)\right]^2+\frac{1}{2}I_{yy}\left[\dot{\theta}+\dot{y}_2'(a)\right]^2+\frac{1}{2}M_pL_p\left((L_1+a)\dot{\theta}+\dot{y}_2(a)\right)\left(\dot{\theta}+\dot{y}_2'(a)\right)$$

Applying Lagrange's equation, we find the partial derivatives with respect to $\dot{\theta}$ and θ:

$$\begin{aligned}\frac{\partial L}{\partial\dot{\theta}}&=\frac{1}{3}\rho_1 L_1^3\dot{\theta}+\frac{1}{3}\rho_2\left[L_1^3-(L_1-b)^3\right]\dot{\theta}+\int_0^a\rho_2(L_1+x)\left((L_1+x)\dot{\theta}+\dot{y}_2(x)\right)dx+\\&+M_p(L_1+a)\left[(L_1+a)\dot{\theta}+\dot{y}_2(a)\right]+I_{yy}\left[\dot{\theta}+\dot{y}_2'(a)\right]+M_pL_p(L_1+a)\dot{\theta}+\\&\frac{1}{2}M_pL_p\dot{y}_2(a)+\frac{1}{2}M_pL_p(L_1+a)\dot{y}_2'(a)\\\frac{\partial L}{\partial\theta}&=0\end{aligned}\qquad(2.3.6)$$

Hence from Equation (2.3.6):

$$\begin{aligned}\frac{d}{dt}\left(\frac{\partial L}{\partial\dot{\theta}}\right)&=\frac{1}{3}\rho_1 L_1^3\ddot{\theta}+\frac{1}{3}\rho_2\left[L_1^3-(L_1-b)^3\right]\ddot{\theta}+\\&\int_0^a\rho_2(L_1+x)\left((L_1+x)\ddot{\theta}+\ddot{y}_2(x)\right)dx+\\&+M_p(L_1+a)\left[(L_1+a)\ddot{\theta}+\ddot{y}_2(a)\right]+I_{yy}\left[\ddot{\theta}+\ddot{y}_2'(a)\right]+\\&M_pL_p(L_1+a)\ddot{\theta}+\frac{1}{2}M_pL_p\ddot{y}_2(a)+\frac{1}{2}M_pL_p(L_1+a)\ddot{y}_2'(a)\end{aligned}\qquad(2.3.7)$$

which on collecting the terms and equating to the input torque $S_T(t)$, gives the equation of motion:

$$\begin{aligned}&I_R\ddot{\theta}+I_{yy}\left(\ddot{\theta}+\ddot{y}'(a)\right)+M_p(L_1+a)\left[(L_1+a)\ddot{\theta}+\ddot{y}(a)\right]+\frac{1}{2}M_pL_p\ddot{y}(a)+\\&\frac{1}{2}M_pL_p(L_1+a)\ddot{y}'(a)+\rho_2\int_0^a(L_1+x)\left[(L_1+x)\ddot{\theta}+\ddot{y}\right]dx=S_T(t)\end{aligned}\qquad(2.3.8)$$

where $I_R=\frac{1}{3}\rho_1 L_1^3+\rho_2\left[\frac{L_1^3}{3}-\frac{(L_1-b)^3}{3}\right]+M_pL_p(L_1+a)$, the mass moment of inertia of the rigid section of the manipulator plus the payload, about point $\mathbf{O}_1$, as shown in Figure

2.1. The input $S_T(t)$ is the slew torque at the shoulder joint used to rotate the arm through the desired angle. The equation of free vibration of link 2, is:

$$\rho_2\left[\ddot{y}+(L_1+x)\ddot{\theta}\right]+EI_2\frac{\partial^4 y}{\partial x^4}=0 \tag{2.3.9}$$

The boundary conditions for flexible link 2 involve the shear force and bending moment at the end effector, $x=a$, thus:

$$\begin{aligned}&\text{(a)}\ \ y\big|_{x=0}=0\ ,\quad \text{(c)}\ \ y''\big|_{x=a}=-\frac{I_{yy}}{EI_2}\left(\ddot{\theta}+\ddot{y}'(a)\right)-\frac{M_pL_p}{2EI_2}\left[(L_1+a)\ddot{\theta}+\ddot{y}(a)\right]\\&\text{(b)}\ \ y'\big|_{x=0}=0\ ,\qquad\qquad \text{(d)}\ \ y'''\big|_{x=a}=\frac{M_p}{EI_2}\left[(L_1+a)\ddot{\theta}+\ddot{y}(a)\right]\end{aligned} \tag{2.3.10}$$

These boundary conditions can also be formulated from the variational equations of Hamilton's principle, Equation (2.3.1), which has been done for this general class of systems (pg. 156, Junkins and Kim, 1993), or by inspection of the physical system. The equations of motion together with the boundary conditions define the dynamics of the slew and the vibrations of the P-DRM. Equations (2.3.8) to (2.3.10), are used below to formulate the eigenvalue problem and to find the natural frequencies of vibration of the P-DRM.

The exact equations of motion for the manipulator developed in this section, Equations (2.3.8) and (2.3.9), are not useful for simulating the dynamic response of the P-DRM in real-time as their solution is cumbersome, in terms of complex hyperbolic functions. However, they are used next to obtain the natural frequencies of the P-DRM with different fixed lengths of link 2 extended.

2.3.3 Exact Determination of Natural Frequencies for the P-DRM

In the free vibration analysis of the P-DRM, all external torque inputs are considered to be zero, and the system is studied at fixed lengths, therefore the axial deployment velocity and acceleration, are set to zero.

This section uses the semi-rigid DRM (the P-DRM) with a rigid link1 and flexible link 2 to help develop a better understanding of the exact natural frequencies of both the P-DRM and the fully flexible DRM system. By analysing the exact results of the P-DRM produced in this section, some conclusions can be reached both as to the accuracy of the approximation method used in the next section and as to the natural frequencies of the DRM. This can be done since both the P-DRM and the DRM share all characteristics except the flexibility of link 1, and the latter will have a predictable effect in the natural frequencies of the DRM from basic vibration theory.

To proceed with the natural frequency analysis of the P-DRM a general solution is adopted for the deflection of the flexible link 2, and for the slew angle of the manipulator, θ. These general solutions are then substituted in the equations of motion and the boundary conditions from the previous section, and an eigenvalue problem is formulated.

The general solution for the deflection of flexible link 2 is based on the separation of variables method. It represents the deflection of link 2 as:

$$y(x,t) = A_2 e^{i\omega t} Y(x) \tag{2.3.11}$$

The first part of the solution is the harmonically-varying amplitude and $Y(x)$ is the spatially varying beam deformation shape function. The rigid body angle of the manipulator has the general solution:

$$\theta(t) = A_1 e^{i\omega t} \tag{2.3.12}$$

The natural frequencies of the P-DRM are obtained from the governing equation of motion for $y(x,t)$, Equation (2.3.9). The solution for y also has to satisfy Equations (2.3.8) and (2.3.10). Therefore, the general solutions above are substituted into (2.3.9) to give:

$$\frac{\rho}{EI_2}\left[-\omega^2 A_2 e^{i\omega t} Y(x) + (L_1 + x)\left(-\omega^2 A_1 e^{i\omega t}\right)\right] + A_2 e^{i\omega t} Y^{IV}(x) = 0 \tag{2.3.13}$$

The separation of variables is accomplished in (2.3.13) since the time varying and the spatially dependent portions of the flexible deflections are now independent of each other. Since the time varying portion of the solution can be cancelled out from equation (2.3.13) we are left with the equation for the beam shape function:

$$Y^{IV}(x) - \frac{\omega^2 \rho}{EI_2} Y(x) = \frac{(L_1 + x)\omega^2 A_1 \rho}{A_2 EI_2} \tag{2.3.14}$$

This equation has a solution for $Y(x)$, composed of a general homogeneous solution and a non-homogeneous part due to the non-zero right hand side of the equation, given by:

$$\begin{gathered} Y(x) = -\frac{C_0}{k^4} F(x) + C_1 \sin(kx) + C_2 \cos(kx) + C_3 \sinh(kx) + C_4 \cosh(kx) \\ C_0 = \frac{A_1}{A_2}; \quad k = \sqrt{\frac{\omega}{c}}; \quad c = \sqrt{\frac{EI_2}{\rho}}; \quad F = \frac{(L_1 + x)\omega^2}{c^2} \end{gathered} \tag{2.3.15}$$

where the C_i coefficients are constants which define the shape of the general solution and ω are the natural frequencies of the fixed length system. The general solution for the flexible deflection of link 2 is found by bringing together Equations (2.3.11) and (2.3.15):

$$y(x,t) = A_2 e^{i\omega t}\left(-\frac{C_0}{k^4} F(x) + C_1 \sin(kx) + C_2 \cos(kx) + C_3 \sinh(kx) + C_4 \cosh(kx)\right) \tag{2.3.16}$$

The choice of parameters, C_i and ω, must satisfy Equations (2.3.8), (2.3.9), and (2.3.10).

2.3.3.1 Characteristic Problem

To satisfy the boundary conditions, Equation (2.3.10), the following equations are substituted: Equation (2.3.16), and the general solution for θ, Equation (2.3.12). Substitution into the first boundary condition, Equation (2.3.10)(a):

$$y(0,t) = A_2 e^{i\omega t}\left(-\frac{C_0}{k^4}F(0) + C_1\sin(k0) + C_2\cos(k0) + C_3\sinh(k0) + C_4\cosh(k0)\right) = 0$$

which gives:

$$-C_0 L_1 + C_2 + C_4 = 0 \qquad (2.3.17)$$

Proceeding in the same way for all the boundary conditions and equations of motion of the system an algebraic set of equations is produced which is referred to as the *characteristic problem* (Meirovitch, 1986). Solving this characteristic problem will yield the natural frequencies of vibration of the system. For the second boundary condition, Equation (2.3.10)(b), the slope of the deflection at the cantilevered end must always be zero:

$$y'(0,t) = A_2 e^{i\omega t}\left(-C_0 + kC_1\cos(k0) - kC_2\sin(k0) + kC_3\cosh(k0) + kC_4\sinh(k0)\right) = 0$$

which gives the equation:

$$-C_0 + kC_1 + kC_3 = 0 \qquad (2.3.18)$$

Substituting the general solutions for slew angle and flexible deflection into the bending moment boundary condition at the tip, Equation (2.3.10)(c), yields:

$$y''(a,t) \Rightarrow A_2 e^{i\omega t}\left(-k^2 C_1 \sin(ka) - k^2 C_2 \cos(ka) + k^2 C_3 \sinh(ka) + k^2 C_4 \cosh(ka)\right) =$$

$$= \frac{I_{yy}}{EI_2}\begin{pmatrix} A_1\omega^2 e^{i\omega t} + \\ A_2\omega^2 e^{i\omega t}\left(-C_0 + kC_1\cos(ka) - kC_2\sin(ka) + kC_3\cosh(ka) + kC_4\sinh(ka)\right)\end{pmatrix} +$$

$$\frac{M_p L_p}{2EI_2}\left[\begin{matrix}(L_1 + a)A_1\omega^2 e^{i\omega t} + \\ A_2\omega^2 e^{i\omega t}\left(-\frac{C_0}{k^4}F(a) + C_1\sin(ka) + C_2\cos(ka) + C_3\sinh(ka) + C_4\cosh(ka)\right)\end{matrix}\right]$$

since:

$$\ddot{\theta} = -A_1\omega^2 e^{i\omega t}; \quad \ddot{y}'(a,t) = -A_2\omega^2 e^{i\omega t}Y'(a); \quad \ddot{y}(a,t) = -A_2\omega^2 e^{i\omega t}Y(a);$$

noting that $e^{i\omega t}$ is a common term in the above expression, dividing by A_2 and collecting all the terms on the left hand side gives:

$$EI_2\left[-k^2 C_1\sin(ka) - k^2 C_2\cos(ka) + k^2 C_3\sinh(ka) + k^2 C_4\cosh(ka)\right] -$$
$$I_{yy}\left[\omega^2\left(kC_1\cos(ka) - kC_2\sin(ka) + kC_3\cosh(ka) + kC_4\sinh(ka)\right)\right] -$$
$$\frac{1}{2}M_p L_p\left[\omega^2\left(C_1\sin(ka) + C_2\cos(ka) + C_3\sinh(ka) + C_4\cosh(ka)\right)\right] = 0$$

collecting the C_1, C_2, C_3 and C_4 terms, the expression can be written as:

$$D_1C_1 + D_2C_2 + D_3C_3 + D_4C_4 = 0 \qquad (2.3.19)$$

The D_i coefficients are presented in Appendix A. The last boundary condition for the flexible link is the shear force at the tip, Equation (2.3.10)(d). Substituting the assumed solutions gives:

$$y'''(a,t) \Rightarrow A_2 e^{i\omega t}\left(-k^3 C_1\cos(ka) + k^3 C_2\sin(ka) + k^3 C_3\cosh(ka) + k^3 C_4\sinh(ka)\right) =$$

$$\frac{M_p}{EI_2}\left[\begin{matrix}-(L_1 + a)A_1\omega^2 e^{i\omega t} - \\ A_2\omega^2 e^{i\omega t}\left(-\frac{C_0}{k^4}F(a) + C_1\sin(ka) + C_2\cos(ka) + C_3\sinh(ka) + C_4\cosh(ka)\right)\end{matrix}\right]$$

collecting all the terms on the left hand side of the equation, dividing by A_2 and eliminating common terms gives the expression:

$$E_1C_1 + E_2C_2 + E_3C_3 + E_4C_4 = 0 \qquad (2.3.20)$$

The E_i coefficients of (2.3.20) are presented in Appendix A. Substituting Equations (2.3.12) and (2.3.16) into the θ equation of motion, Equation (2.3.8), considering no external input, $S_T(t) = 0$, produces a long complicated algebraic expression:

$$I_R\omega^2 A_1 e^{i\omega t} + I_{yy}\left(\omega^2 A_1 e^{i\omega t} + \omega^2 A_2 e^{i\omega t} Y'(a)\right) + M_p(L_1 + a)\left[(L_1 + a)\omega^2 A_1 e^{i\omega t} + \omega^2 A_2 e^{i\omega t} Y(a)\right] +$$
$$\frac{1}{2}M_p L_p \omega^2 A_2 e^{i\omega t} Y(a) + \frac{1}{2}M_p L_p (L_1 + a)\omega^2 A_2 e^{i\omega t} Y'(a) +$$
$$\rho_2 \int_0^a (L_1 + x)\left[(L_1 + x)\omega^2 A_1 e^{i\omega t} + \omega^2 A_1 e^{i\omega t} Y(a)\right] dx = 0$$

after substituting the general shape function the expression becomes:

$$I_R\omega^2 A_1 e^{i\omega t} + I_{yy}\left(\omega^2 A_1 e^{i\omega t} + \omega^2 A_2 e^{i\omega t}\begin{pmatrix} -C_0 + kC_1 s\cos(ka) - kC_2\sin(ka) + \\ kC_3\cosh(ka) + kC_4\sinh(ka)\end{pmatrix}\right) +$$
$$+M_p(L_1 + a)\left[(L_1 + a)\omega^2 A_1 e^{i\omega t} + \omega^2 A_2 e^{i\omega t}\begin{pmatrix} -\frac{C_0}{k^4}F + C_1\sin(ka) + C_2\cos(ka) + \\ C_3\sinh(ka) + C_4\cosh(ka)\end{pmatrix}\right] +$$
$$+\frac{1}{2}M_p L_p \omega^2 A_2 e^{i\omega t}\begin{pmatrix} -\frac{C_0}{k^4}F + C_1\sin(ka) + C_2\cos(ka) + \\ C_3\sinh(ka) + C_4\cosh(ka)\end{pmatrix} +$$
$$+\frac{1}{2}M_p L_p (L_1 + a)\omega^2 A_2 e^{i\omega t}\begin{pmatrix} -C_0 + kC_1 s\cos(ka) - kC_2\sin(ka) + \\ kC_3\cosh(ka) + kC_4\sinh(ka)\end{pmatrix} +$$
$$+\rho_2\int_0^a (L_1 + x)\left[(L_1 + x)\omega^2 A_1 e^{i\omega t} + \omega^2 A_1 e^{i\omega t}\begin{pmatrix} -\frac{C_0}{k^4}F + C_1\sin(ka) + C_2\cos(ka) + \\ C_3\sinh(ka) + C_4\cosh(ka)\end{pmatrix}\right] dx = 0$$

which after simplification can be expressed as:

$$F_0C_0 + F_1C_1 + F_2C_2 + F_3C_3 + F_4C_4 = 0 \qquad (2.3.21)$$

Where the F_i coefficients are given in Appendix A. The equations developed above can be written as the following system of algebraic equations:

$$\begin{bmatrix} -L_1 & 0 & 1 & 0 & 1 \\ -1 & k & 0 & k & 0 \\ 0 & D_1 & D_2 & D_3 & D_4 \\ 0 & E_1 & E_2 & E_3 & E_4 \\ F_0 & F_1 & F_2 & F_3 & F_4 \end{bmatrix}\begin{Bmatrix} C_0 \\ C_1 \\ C_2 \\ C_3 \\ C_4 \end{Bmatrix} = \begin{Bmatrix} 0 \\ 0 \\ 0 \\ 0 \\ 0 \end{Bmatrix} \qquad (2.3.22)$$

For this set of homogeneous equations to have a nontrivial solution (non-zero values for the C_i coefficients), the determinant of the matrix must vanish (Kreyzig, 1993). The determinant of the matrix equated to zero with k as the only variable to satisfy the equation is called the characteristic equation. The roots of the characteristic equation are the eigenvalues of the matrix and since the roots give the natural frequencies, $\omega=ck^2$, from Equation (2.3.15). It is clear from looking at the matrix elements of Equation (2.3.22) that the characteristic equation's roots cannot be found explicitly in a closed form solution. Therefore, the roots will be determined using first a graphical method to identify the function's zero crossings and then a numerical method to produce the desired numerical accuracy.

2.3.3.2 Characteristic Problem Solution: P-DRM Natural Frequencies

Many results have been obtained which will not be included here for brevity, since there are many combinations of payload mass, and length, exposed length of link 2, etc. It is of main interest to examine the spectrum of the natural frequencies of the DRM with a selection of payloads. It is also important to obtain the natural frequencies of the DRM as the exposed length of link 2 (length a, from Figure 2.1) is changed. The physical characteristics of the DRM are in Table 2-2 and for the payloads considered in Table 2-3.

Table 2-3: Payload characteristics

	Mass	Length	Width
Payload 1	200 Kg	100 cm	50 cm
Payload 2	350 Kg	150 cm	75 cm
Payload 3	500 Kg	200 cm	100 cm

Due to the complexity of the characteristic equation, the zero crossings are best represented graphically as a first step in their solution. These approximate roots will then be inserted as the first guess in a numerical Newton method to find the roots of the characteristic equation. The commercial program MATHEMATICA was used for this analysis (Wolfram, 1988).

In Figure 2.4 the first two zero crossings of the characteristic equation are shown for the DRM carrying Payload 1 with 4 metres of link 2 deployed. The P-DRM will always have a first eigenvalue of zero associated with the free rotation of the whole manipulator, so the characteristic equation always has a solution at the value of $k=0$. The modes after the zero mode are those associated with the flexibility of link 2 and they are referred to here as mode 1, mode 2, etc. Figure 2.5 and Figure 2.6 show the zero crossings of the characteristic equation for the P-DRM carrying Payloads 2 and 3 with an exposed length of link 2 (length a) of 4 metres. From the figures, it can be seen that as the payload gets larger the frequencies of vibration for mode 1 and mode 2 are reduced. This is in agreement with observations of similar physical systems.

Due to the presence of hyperbolic functions in the characteristic equation finding the zero crossings even graphically can be a difficult task since the characteristic equation behaves in a rapidly divergent, oscillatory fashion. The zero crossings for the eigenvalues are nearly perpendicular for higher and higher eigenvalues. This can start to be appreciated in the figures on page 35, as the values of k are slowly increased the value of the characteristic equation f(k) increases or decreases by very large amounts.

In Figure 2.7 a graph of the first three eigenvalues of the characteristic equation is presented for the partially flexible DRM carrying Payload 1 with link 2 extended 4 meters. Figure 2.8 and Figure 2.9 present the same plot for the P-DRM while carrying

Payloads 2 and 3 respectively. By plotting the function, $\log[1+Abs(\mathrm{f}(k))]$ the characteristic equation solutions can be appreciated as the inflexion points along the upward moving curve (Junkins and Kim, 1993). These inflexion points are then used as the starting points in a numerical Newton method procedure to find the eigenvalues to ten significant digits using the MATHEMATICA command ***FindRoot***, as shown in the subroutine **gensol.ma** in Appendix D, which is used to produce all the results in this section. The values of k which make the characteristic equation zero are then squared, multiplied by $\sqrt{\frac{EI_2}{\rho_2}}$, from its definition in Equation (2.3.15), and divided by 2π to obtain the natural frequencies of vibration, f, in Hertz.

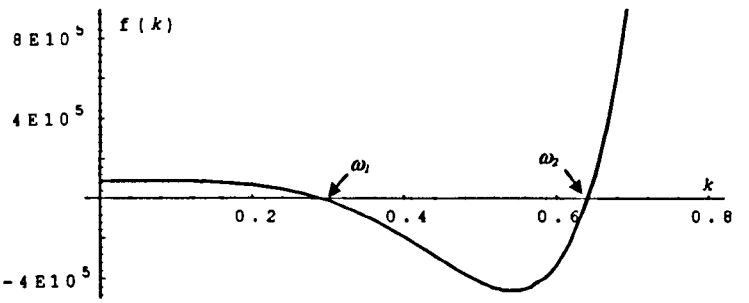

Figure 2.4: First two zero crossings of the eigenvalue problem for the P-DRM with Payload 1.

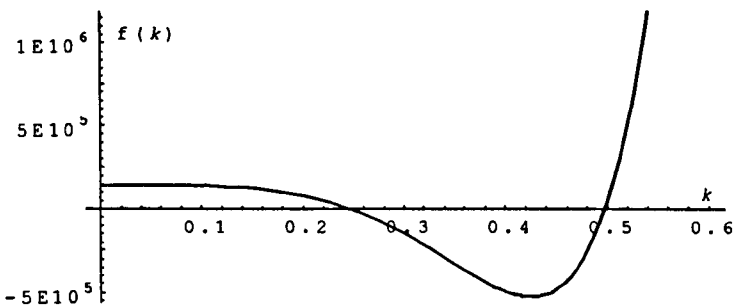

Figure 2.5: First two zero crossings of the eigenvalue problem for the P-DRM with Payload 2.

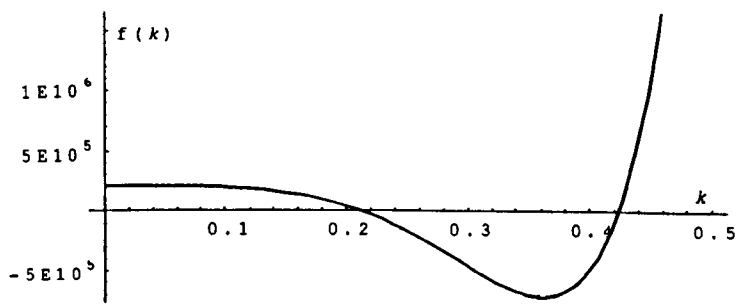

Figure 2.6: First two zero crossings of the eigenvalue problem for the P-DRM with Payload 3.

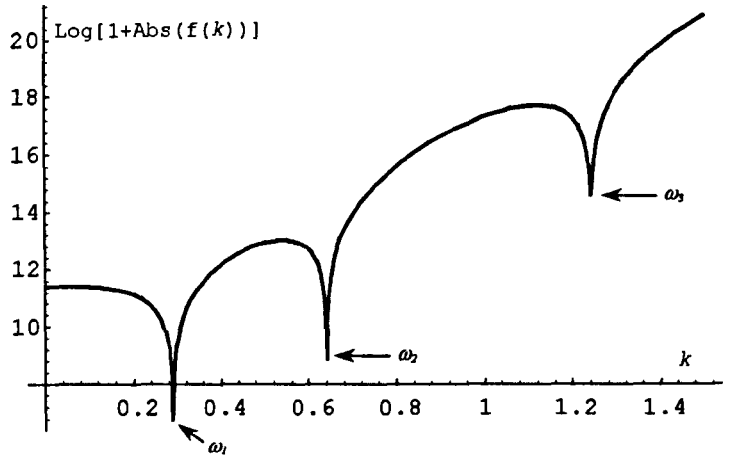

Figure 2.7: First three zero crossings of the eigenvalue problem for the P-DRM with Payload 1.

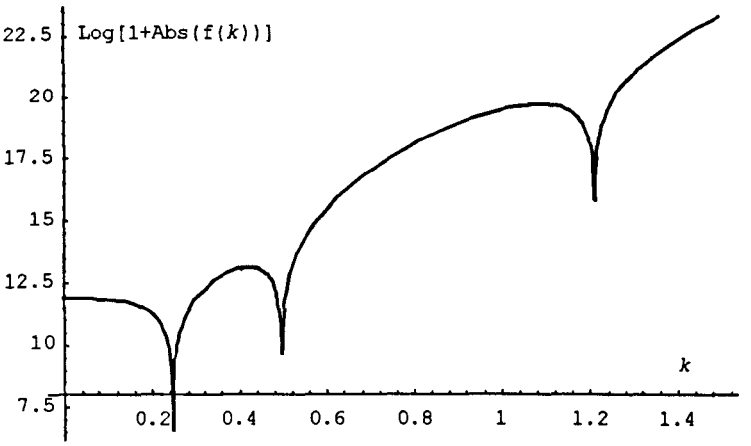

Figure 2.8: First three zero crossings of the eigenvalue problem for the P-DRM with Payload 2.

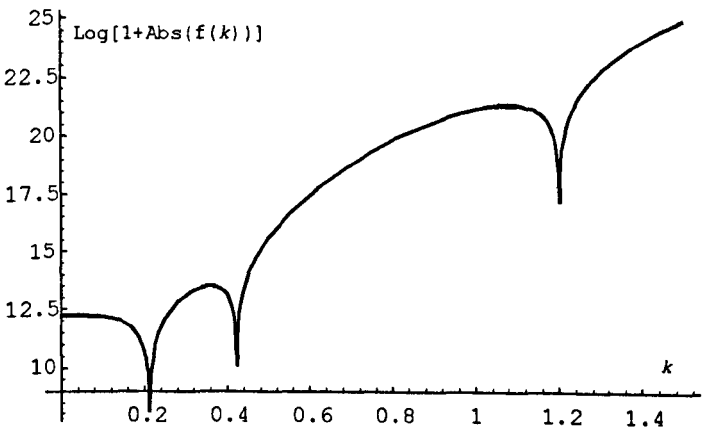

Figure 2.9: First three zero crossings of the eigenvalue problem for the P-DRM with Payload 3.

The first few natural frequencies of the P-DRM are presented in Table 2-4 while carrying no payload and the three payloads of Table 2-3, for eight different values of length a. These results will be compared with the results for the discretized P-DRM developed in the next section to assess the accuracy of the discretized model.

Table 2-4: P-DRM Natural Frequencies (in Hz) as Link 2 is deployed
(Link 1 – rigid; Link 2 – flexible)

	$a = 1.0$	$a = 2.0$	$a = 3.0$	$a = 4.0$	$a = 5.0$	$a = 6.0$	$a = 7.0$	$a = 8.0$
No Payload	f_1=333.1 f_2=2015.	f_1=89.0 f_2=512.4	f_1=42.2 f_2=231.6	f_1=25.4 f_2=132.7	f_1=17.4 f_2=86.6	f_1=13.0 f_2=61.6	f_1=10.4 f_2=46.6	f_1=8.66 f_2=37.1
Payload 1 (200 Kg)	f_1=29.2 f_2=155.9 f_3=2048.	f_1=17.8 f_2=70.9 f_3=523.7	f_1=12.1 f_2=48.2 f_3=239.6	f_1=8.94 f_2=37.6 f_3=140.0	f_1=7.01 f_2=31.0 f_3=94.1	f_1=5.74 f_2=26.2 f_3=69.4	f_1=4.87 f_2=22.5 f_3=54.7	f_1=4.25 f_2=19.4 f_3=45.2
Payload 2 (350 Kg)	f_1=16.2 f_2=119.7 f_3=2036.	f_1=11.1 f_2=49.2 f_3=515.8	f_1=8.22 f_2=30.8 f_3=232.6	f_1=6.44 f_2=23.0 f_3=133.1	f_1=5.23 f_2=18.8 f_3=87.0	f_1=4.38 f_2=16.0 f_3=61.9	f_1=3.76 f_2=14.1 f_3=46.9	f_1=3.30 f_2=12.6 f_3=37.2
Payload 3 (500 Kg)	f_1=10.6 f_2=98.8 f_3=2030.	f_1=7.51 f_2=39.0 f_3=511.6	f_1=5.81 f_2=23.4 f_3=229.6	f_1=4.72 f_2=16.9 f_3=130.5	f_1=3.94 f_2=13.4 f_3=84.5	f_1=3.37 f_2=11.3 f_3=59.5	f_1=2.93 f_2=9.87 f_3=44.4	f_1=2.59 f_2=8.81 f_3=34.6

From the figures on page 36 and from the results on Table 2-4 it can be seen that there is a considerable spacing between the natural frequencies of the P-DRM. The first two natural frequencies are closer together in the frequency spectrum than the third or higher frequencies while carrying a payload. This is important in deciding how many flexible modes to include in the discretized model of the DRM. It can be concluded that the first two natural frequencies would dominate the vibration response of the P-DRM. Mode 3 and higher modes will contribute insignificantly to the amplitude of vibration of the P-DRM since their frequencies are high and their amplitudes small. The effects from those modes will be damped out by the small structural damping in the structure. Therefore, the fully flexible model used for dynamic simulation will include only one flexible mode for each link, thus including mode 1 and mode 2 of the DRM. This will

produce a simple mathematical representation of the DRM, which is one of the aims of this thesis, but still retaining enough accuracy to reproduce the real DRM behaviour. The method used to produce the simplified mathematical dynamical system is presented in Section 2.4.

2.3.3.3 Characteristic Problem Solution: P-DRM Mode Shapes

Given the solution to the characteristic equation shown above, by finding the value of k the characteristic problem can now be completely solved by finding the values of the constants C_i, in Equation (2.3.22), and then plotting the shape of the elastic deformation, Equation (2.3.15), also called the mode shapes. The mode shapes are shown in Figure 2.10, they show the first four mode shapes for the flexible link, link 2, of the P-DRM while carrying Payload 1 from Table 2-3, the 200 Kg payload. It can be seen that having the payload's large inertia at the end of the flexible link limits the tip deflection and curvature at the tip. This can be easily observed when comparing the case when the flexible link is fully extended to 8 meters in the unloaded case, Figure 2.11, and while carrying Payload 1 on the end of the flexible link, Figure 2.10. The payload acts to restrict the tip's motion, as expected.

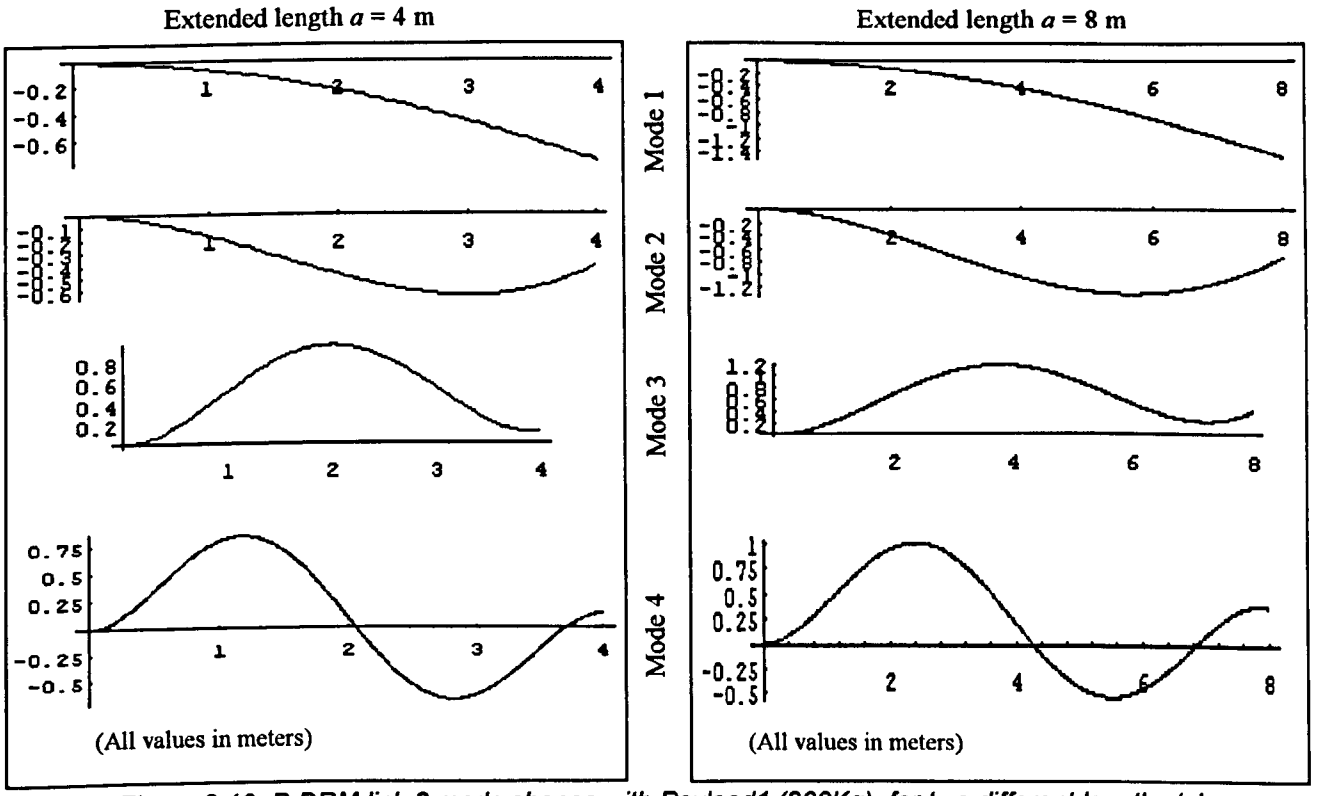

Figure 2.10: P-DRM link 2 mode shapes with Payload1 (200Kg), for two different lengths 'a'

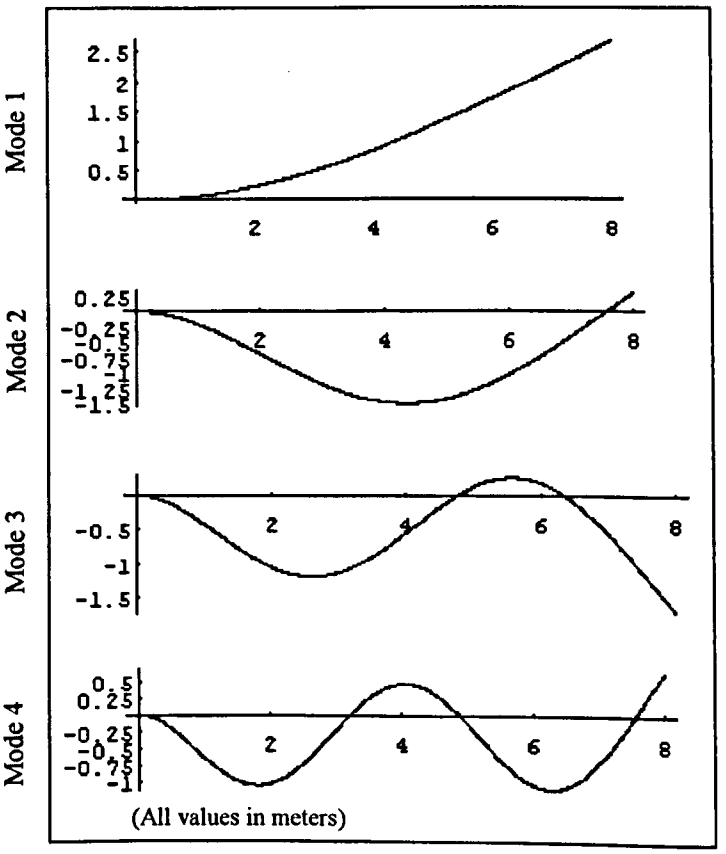

Figure 2.11: P-DRM flexible link 2 mode shapes for a = 8 meters and with M_p=0

2.4 Approximate Dynamic Analysis of Flexible Manipulators

For dynamic and control design purposes of a real robotic manipulator it is more convenient to approximate the deflection of the flexible portion of the arm than attempt to utilise the more rigorous mathematical description of an infinite dimensional analysis. In a general engineering sense, the added complexity introduced with an exact dynamical model of a system is not productive for realistic analysis purposes. The problem is that not all of the actual robot operating conditions are known, or the construction engineering details can be modelled to a high degree of accuracy. Hence approximation techniques are preferred to simplify the dynamic modelling and still retain the most important aspects of the manipulator behaviour.

In the case of a long slender space manipulator, like the DRM, the flexibility effects are important from the point of view of structural design and vibration control law design. Since the manipulator must position objects at specific positions of an orbiting structure, such as the Space Station, the effects of moving the DRM must be understood in terms of the final tip position and any residual vibration. The tip position will be subjected to vibrations due to the flexibility of the links whose amplitude, frequency and damping must be known for the design and operation to be reliable. On the other hand, it is clear that given the inputs necessary to manoeuvre the DRM and the overall working conditions for it, not all of the information from a flexibility analysis is relevant. The high frequencies of vibration in the DRM are not likely to be excited significantly by normal operating procedures. If vibrations of high frequency were excited, the inherent structural damping and the damping in the joints of the DRM would attenuate them, as pointed out in the previous section. Thus, only the first few modes of vibration are

considered important in terms of positioning payload and tracking set trajectories, and only these are retained in the dynamic model of the DRM.

The most common approximate methods for large flexible structures replace the elastic system by a spatially discrete system. These include the Finite Element method, the Galerkin method, the Rayleigh-Ritz method and others as elegantly described in (Dimarogonas, Chapter 10, 1996). Using these approaches leads to linear, finite-dimensional, equations of motion for approximating the dynamic response of a flexible structure. One of the approaches used when the geometry of the system is not very complicated is the *assumed modes method* which is selected for the DRM discretization because it is simple to apply and produces straightforward approximate equations. A brief discussion of the method is presented below. Several different assumed functions are evaluated in a few illustrative examples in Appendix B, and the case is made for the function used in the discretization of the DRM based on the results reported there. The evaluation of the different assumed shapes are performed by comparing the natural frequency values for the different assumed shapes with the exact solutions for two important problems, a cantilevered beam and a cantilevered beam plus a point mass payload at its tip.

2.4.1 Assumed Modes Method

The *assumed modes method* for the approximation of the deflection of elastic structures replaces the exact modal deflection, as shown in Figure 2.3, by a finite series of space dependent functions (shape functions) that are multiplied by specified time dependent functions (generalised coordinates), Equation (2.4.1). The shape functions do not satisfy the equations of motion and the boundary conditions exactly, for if they did

they would be the exact solution for the flexural response. However, they provide what is hoped to be a good approximation, chosen based on physical considerations of the beam and payload system. Therefore, in the finite series describing the link's flexibility, the time dependent functions become generalised coordinates of the system.

The space dependent functions should be selected to satisfy at least the geometric boundary conditions of the system, and be differentiable at least half as many times as the order of the system. These are the most common types of functions used with this method and they are referred to as *admissible functions*. There is another group of functions which is a subset of the first in which the functions are selected to satisfy both geometric (deflection and slope) and physical boundary conditions (bending moment and shear force) and are differentiable as many times as the order of the system. This second set is referred to as *comparison functions* (Junkins and Kim, 1993). In general using *comparison functions* will generate more accurate results than *admissible functions*. Whether the assumed function is an admissible or comparison function, there will be some numerical examples conducted to justify the choice of function for this class of problem (see Appendix B).

Having chosen a suitable space dependent function for the approximation of the deflection of the flexible members we generate an n degree of freedom approximate differential equation model for the continuous system. The displacement of the flexible members is substituted by a linear combination of prescribed functions, which are then used to approximate the system's normal modes of vibration. The flexible deformation is approximated by,

$$y(x,t)=\sum_{i=1}^{n} q_i(t)\phi_i(x) \qquad (2.4.1)$$

where $\phi_i(x)$ denotes the space dependent assumed mode or shape function, $q_i(t)$ denotes the ith generalised coordinate for the system and n is the number of functions retained in the approximation. Substituting Equation (2.4.1) into the kinetic and potential energy expressions for a particular system and using Lagrange's equation,

$$\frac{d}{dt}\left(\frac{\partial L}{\partial \dot{q}_i}\right) - \frac{\partial L}{\partial q_i} = Q_i, \qquad i = 1,2,3,...,n \tag{2.4.2}$$

where L, the Lagrangian, is defined as the kinetic energy minus the potential energy (T-V), q_i are the generalised coordinates of the system and Q_i are the system inputs.

2.5 Approximate Equations of Motion for the DRM

The equations of motion for the DRM to be used for dynamic simulations are based on approximate kinetic and strain energy functions by discretizing the distributed coordinates of the DRM using the assumed modes method and then applying Lagrange's equation.

2.5.1 Approximate Kinetic and Strain Energies

Four distinct sections of the DRM have been identified for the energy formulation as presented in Section 2.2 and in Figure 2.3. The energy formulations are presented in Equations (2.2.1) to (2.2.7) for the kinetic and potential energies. Bringing all of these together, we have the total kinetic and strain energies as,

$$
\begin{aligned}
\mathbf{T_T} &= \frac{1}{2}\int_0^{L_1}\rho_1\left[\left(-y_1(x)\dot{\theta}\right)^2+\left(x\dot{\theta}+\dot{y}_1(x)\right)^2\right]dx+\\
&+\frac{1}{2}\int_{L_1-b}^{L_1}\rho_2\left[\left(\dot{a}-y_1(x)\dot{\theta}\right)^2+\left(x\dot{\theta}+\dot{y}_1(x)\right)^2\right]dx+\\
&+\frac{1}{2}\int_0^{a}\rho_2\left[\left(\dot{a}-y_2(x)\dot{\theta}-y_1(L_1)\dot{\theta}\right)^2+\left((L_1+x)\dot{\theta}+\dot{y}_1(L_1)+\dot{y}_2(x)\right)^2\right]dx+\\
&+\frac{1}{2}M_p\left[\begin{array}{l}\left(\dot{a}-y_2(a)\dot{\theta}-y_1(L_1)\dot{\theta}\right)^2+\\ \left(\left(L_1+a+\frac{1}{2}L_p\right)\dot{\theta}+\dot{y}_1(L_1)+\dot{y}_2(a)+\frac{1}{2}L_p\dot{y}_2'(a)\right)^2\end{array}\right]+\\
&+\frac{1}{2}I_p\left(\dot{\theta}+\dot{y}_2'(a)\right)^2
\end{aligned}
\qquad (2.5.1)
$$

$$
\begin{aligned}
\mathbf{V_T} &= \frac{1}{2}EI_1\int_0^{L_1}\left(\frac{\partial^2 y_1}{\partial x^2}\right)^2dx+\frac{1}{2}EI_2\int_{L_1-b}^{L_1}\left(\frac{\partial^2 y_1}{\partial x^2}\right)^2+P_1(x)\left(\frac{\partial y_1}{\partial x}\right)^2dx+\\
&\frac{1}{2}EI_2\int_0^{a}\left(\frac{\partial^2 y_2}{\partial x^2}\right)^2+P_2(x)\left(\frac{\partial y_2}{\partial x}\right)^2dx
\end{aligned}
\qquad (2.5.2)
$$

The kinetic energy equation includes all of the components in the velocity vectors for all of the mass elements along the DRM, but there are several common simplifying assumptions that can be made at this point. First, it can be seen that if the elastic deflection of the links is small and $\dot{\theta}$ is small then the geometrical stiffness terms, $y_i\dot{\theta}$, can be ignored throughout Equation (2.5.1). These velocity components are parallel to the DRM longitudinal axis and can be considered of second order importance for slew manoeuvres with small $\dot{\theta}$, as previously explained in page 16.

The deployment and retraction dynamics are predetermined, as stated in Section 2.3, so that *a(t)* in Equations (2.5.1) and (2.5.2) is not a generalised coordinate of the system. Therefore, since the deployment is predetermined no equation of motion is developed for the deployment dynamics, and the velocity component $\dot{a}$ can be removed from the kinetic energy expression since it is the only remaining velocity component parallel to the DRM and it doesn't contribute to the in-plane vibrations under study (Wang and Wei, 1987),

(Kim and Gibson, 1991). It is worth noting here that the time varying length a is still present in the kinetic energy expression in the form of the integration limits, which include both lengths a and b, the latter being the portion of link 2 still contained inside link 1, Figure 2.1. The extended length of link 2, length a, is also included in the expressions for the kinetic energy via the shape function used to approximate y_2, as will be shown in the next few pages.

Once the simplifications explained above are completed the strain energy equation remains unchanged, from Equation (2.5.2), and the kinetic energy becomes,

$$\begin{aligned} T_T = & \frac{1}{2}\int_0^{L_1} \rho_1 \left[\left(x\dot{\theta} + \dot{y}_1(x)\right)^2\right] dx + \frac{1}{2}\int_{L_1-b}^{L_1} \rho_2 \left[\left(x\dot{\theta} + \dot{y}_1(x)\right)^2\right] dx + \\ & + \frac{1}{2}\int_0^a \rho_2 \left[\left((L_1 + x)\dot{\theta} + \dot{y}_1(L_1) + \dot{y}_2(x)\right)^2\right] dx + \\ & + \frac{1}{2} M_p \left[\left(\left(L_1 + a + \frac{1}{2}L_p\right)\dot{\theta} + \dot{y}_1(L_1) + \dot{y}_2(a) + \frac{1}{2}L_p \dot{y}_2'(a)\right)^2\right] + \\ & + \frac{1}{2} I_p \left(\dot{\theta} + \dot{y}_2'(a)\right)^2 \end{aligned} \tag{2.5.3}$$

We now have the kinetic energy with the flexural velocity components perpendicular to the arm, which will describe the DRM's slew and flexible vibration, and which also contains the effects of the time-varying changes of the DRM's length.

2.5.2 Equations of Motion for a Flexible DRM with Time Varying Length

The elastic deflections of the two links is represented by a finite number of assumed mode shapes, as follows:

$$y_1(x,t) = \sum_{i=1}^{n} \alpha_i(t)\phi_i(x) \tag{2.5.4}$$

$$y_2(x,t) = \sum_{v=1}^{m} \beta_v(t)\varphi_v(x) \tag{2.5.5}$$

where α_i and β_v denote generalised coordinates for the system and $\phi_i(x)$ and $\varphi_v(x)$ are assumed mode shape functions, which can be chosen to be the same for the discretization of both elastic deflections or they could easily be represented by two different shape functions (more on the assumed functions in Appendix B). Finally, n and m denote the number of functions retained in the approximation for each of the elastic deflections. It is worth noting here that link 1 is essentially a pinned-free beam whereas link 2 is a cantilever beam at the end of link 1 but is largely influenced as shown in Section 2.3.3.3 by the payload at its free end. Therefore, link 1 can be expected to be simpler to approximate than the flexible deflections of link 2.

Substituting Equations (2.5.4) and (2.5.5) into Equations (2.5.2) and (2.5.3) gives us the approximated energies of the system. Constructing the Lagrangian as, $L = \mathbf{T_T} - \mathbf{V_T}$, and then applying Lagrange's equation, Equation (2.4.2), for the discrete coordinates $\mathbf{q} = \{\theta, \alpha_1, \alpha_2, ..., \alpha_n, \beta_1, \beta_2, ..., \beta_m\}$ we get the general approximate discrete continuous equations of motion. This can be done for n and m equal to 1, therefore approximating the first two flexible modes of the DRM.

The approximate energy expressions following the discretization of the flexible deflections are:

$$\begin{aligned}\mathbf{T_T} = {} & \frac{1}{2}\int_0^{L_1} \rho_1 \left[\left(x\dot{\theta} + \dot{\alpha}(t)\phi(x)\right)^2\right] dx + \frac{1}{2}\int_{L_1-b}^{L_1} \rho_2 \left[\left(x\dot{\theta} + \dot{\alpha}(t)\phi(x)\right)^2\right] dx + \\ & + \frac{1}{2}\int_0^a \rho_2 \left[\left((L_1 + x)\dot{\theta} + \dot{\alpha}(t)\phi(L_1) + \frac{d}{dt}\{\beta(t)\varphi(x)\}\right)^2\right] dx + \\ & + \frac{1}{2}M_p \left[\left(\left(L_1 + a + \frac{1}{2}L_p\right)\dot{\theta} + \dot{\alpha}(t)\phi(L_1) + \frac{d}{dt}\{\beta(t)\varphi(a)\} + \frac{1}{2}L_p \frac{d}{dt}\{\beta(t)\varphi'(a)\}\right)^2\right] + \\ & + \frac{1}{2}I_p\left(\dot{\theta} + \dot{\beta}(t)\dot{\varphi}'(a)\right)^2\end{aligned}$$

$$\mathbf{V_T} = \frac{1}{2}EI_1\int_0^{L_1}(\alpha(t)\phi''(x))^2\,dx + \frac{1}{2}EI_2\int_{L_1-b}^{L_1}(\alpha(t)\phi''(x))^2 + P_1(x)(\alpha(t)\phi'(x))^2\,dx +$$
$$\frac{1}{2}EI_2\int_0^a(\beta(t)\varphi''(x))^2 + P_2(x)(\beta(t)\varphi'(x))^2\,dx$$

where the subscripts for flexible deflection functions have been omitted for simplicity. The Lagrangian is formulated as:

$$\mathbf{L_T} = \frac{1}{2}\int_0^{L_1}\rho_1\left[\left(x\dot{\theta}+\dot{\alpha}(t)\phi(x)\right)^2\right]dx + \frac{1}{2}\int_{L_1-b}^{L_1}\rho_2\left[\left(x\dot{\theta}+\dot{\alpha}(t)\phi(x)\right)^2\right]dx +$$
$$+\frac{1}{2}\int_0^a\rho_2\left[\left((L_1+x)\dot{\theta}+\dot{\alpha}(t)\phi(L_1)+\frac{d}{dt}\{\beta(t)\varphi(x)\}\right)^2\right]dx +$$
$$+\frac{1}{2}M_p\left[\left(\left(L_1+a+\frac{1}{2}L_p\right)\dot{\theta}+\dot{\alpha}(t)\phi(L_1)+\frac{d}{dt}\{\beta(t)\varphi(a)\}+\frac{1}{2}L_p\frac{d}{dt}\{\beta(t)\varphi'(a)\}\right)^2\right]+$$
$$+\frac{1}{2}I_p\left(\dot{\theta}+\frac{d}{dt}\{\beta(t)\varphi'(a)\}\right)^2 - \frac{1}{2}EI_1\int_0^{L_1}(\alpha(t)\phi''(x))^2\,dx - \frac{1}{2}EI_2\int_{L_1-b}^{L_1}(\alpha(t)\phi''(x))^2 -$$
$$P_1(x)(\alpha(t)\phi'(x))^2\,dx - \frac{1}{2}EI_2\int_0^a(\beta(t)\varphi''(x))^2 - P_2(x)(\beta(t)\varphi'(x))^2\,dx$$

It must be noted that the time derivative of the flexible deflection of link 2 is left unresolved at this point since from Equation (2.6.8) it will be shown that the deflection of link 2 is approximated by:

$$y_2 = \beta(t)\left[3\left(\frac{x}{a(t)}\right)^2 - \left(\frac{x}{a(t)}\right)^3\right]$$

the assumed shape φ for link 2 depends on $a(t)$, the extended length of link 2, which is time varying. Therefore, the time derivative cannot be explicitly written until the assumed shape substitution is made. Substituting the selected assumed shape, as shown above, for the flexible link deflection and the axial load expressions, Equations (2.2.10) and (2.2.11), the Lagrangian becomes:

$$\mathbf{L_T} = \frac{1}{2}\int_0^{L_1}\rho_1\left[\left(x\dot{\theta}+\dot{\alpha}(t)\left\{3\left(\frac{x}{L_1}\right)^2-\left(\frac{x}{L_1}\right)^3\right\}\right)^2\right]dx+\frac{1}{2}\int_{L_1-b}^{L_1}\rho_2\left[\left(x\dot{\theta}+\dot{\alpha}(t)\left\{3\left(\frac{x}{L_1}\right)^2-\left(\frac{x}{L_1}\right)^3\right\}\right)^2\right]dx+$$

$$+\frac{1}{2}\int_0^{a}\rho_2\left[\left((L_1+x)\dot{\theta}+2\dot{\alpha}(t)+\left\{\dot{\beta}(t)\left[\frac{3x^2}{a^2}-\frac{x^3}{a^3}\right]+\beta(t)\left[\frac{3\dot{a}x^3}{a^4}-\frac{6\dot{a}x^2}{a^3}\right]\right\}\right)^2\right]dx+$$

$$+\frac{1}{2}M_p\left[\left(\left(L_1+a+\frac{1}{2}L_p\right)\dot{\theta}+2\dot{\alpha}(t)+2\dot{\beta}(t)+\frac{3L_p}{2}\left\{\frac{a\dot{\beta}(t)-\dot{a}\beta(t)}{a^2}\right\}\right)^2\right]+$$

$$+\frac{1}{2}I_p\left(\dot{\theta}+3\left\{\frac{a\dot{\beta}(t)-\dot{a}\beta(t)}{a^2}\right\}\right)^2-\frac{1}{2}EI_1\int_0^{L_1}\left(\alpha(t)\left\{\frac{6}{L_1^2}-\frac{6x}{L_1^3}\right\}\right)^2dx-$$

$$\frac{1}{2}EI_2\int_{L_1-b}^{L_1}\left(\alpha(t)\left\{\frac{6}{L_1^2}-\frac{6x}{L_1^3}\right\}\right)^2-\left(\begin{matrix}-\rho_2\ddot{a}(L_1-x+a)+M_p\left[-\ddot{a}+(L_1+a)\dot{\theta}^2\right]\\+\frac{1}{2}\rho_2\left(L_1^2-x^2+a^2\right)\dot{\theta}^2\end{matrix}\right)\left(\alpha(t)\left\{6\left(\frac{x}{L_1^2}\right)-3\left(\frac{x^2}{L_1^3}\right)\right\}\right)^2dx-$$

$$\frac{1}{2}EI_2\int_0^{a}\left(\beta(t)\left\{\frac{6}{a^2}-\frac{6x}{a^3}\right\}\right)^2-\left(\begin{matrix}-\rho_2\ddot{a}(a-x)+\frac{1}{2}\rho_2\left(a^2-x^2\right)\dot{\theta}^2\\+M_p\left[-\ddot{a}+(L_1+a)\dot{\theta}^2\right]\end{matrix}\right)\left(\beta(t)\left\{6\left(\frac{x}{a^2}\right)-3\left(\frac{x^2}{a^3}\right)\right\}\right)^2dx$$

Applying Lagrange's equation, Equation (2.4.2), for each of the coordinates, $\{\theta, \alpha_l, \beta_l\}$ produces the approximate equations of motion. For θ, the results of applying Lagrange's equation is the non-linear equation of motion:

$$\frac{d}{dt}\left(\frac{\partial L_T}{\partial\dot{\theta}}\right)=\left\{\begin{matrix}I_p+\frac{L_1^3\rho_1}{3}+\frac{a^3\rho_2}{3}+L_1a^2\rho_2+L_1^2a\rho_2+\frac{L_1^3\rho_2}{3}-\frac{(L_1-b)^3\rho_2}{3}+\\\frac{aL_pM_p}{2}+\frac{L_pL_1M_p}{2}+a(L_1+a)M_p+\frac{L_p(L_1+a)M_p}{2}+L_1(L_1+a)M_p+\\\left\{\begin{matrix}-2.4\frac{a^2\rho_2}{L_1}-1.16L_1\rho_2+\frac{6a^2(L_1-b)^3\rho_2}{L_1^4}+\frac{6(L_1-b)^3\rho_2}{L_1^2}-\frac{4.5a^2(L_1-b)^4\rho_2}{L_1^5}-\\\frac{4.5(L_1-b)^4\rho_2}{L_1^3}+\frac{0.9a^2(L_1-b)^5\rho_2}{L_1^6}-\frac{2.7(L_1-b)^5\rho_2}{L_1^4}+\frac{3(L_1-b)^6\rho_2}{L_1^5}-\\\frac{0.643(L_1-b)^7\rho_2}{L_1^6}-\frac{24}{5}M_p-\frac{24aM_p}{5L_1}+\frac{12a(L_1-b)^3M_p}{L_1^4}+\frac{12(L_1-b)^3M_p}{L_1^3}-\\\frac{9a(L_1-b)^4M_p}{L_1^5}-\frac{9(L_1-b)^4M_p}{L_1^4}+\frac{9a(L_1-b)^5M_p}{5L_1^6}+\frac{9(L_1-b)^5M_p}{5L_1^5}\end{matrix}\right\}\alpha^2+\\\left\{-1.16a\rho_2-\frac{24M_p}{5}-\frac{24L_1M_p}{5a}\right\}\beta^2\end{matrix}\right\}\ddot{\theta}+$$

$$+\left\{\begin{array}{l}\frac{11L_1^2\rho_1}{20}+a^2\rho_2+2aL_1\rho_2+\frac{11L_1^2\rho_2}{20}-\frac{3(L_1-b)^4\rho_2}{4L_1^2}+\frac{(L_1-b)^5\rho_2}{5L_1^3}+\\ 2aM_p+L_pM_p+2L_1M_p\end{array}\right\}\ddot{\alpha}+$$

$$+\left\{\frac{3I_p}{a}+\frac{11a^2\rho_2}{20}+\frac{3aL_1\rho_2}{4}+2aM_p+\frac{5L_pM_p}{2}+2L_1M_p+\frac{3L_pL_1M_p}{2a}\right\}\ddot{\beta}+$$

$$+\left\{2a\dot{a}\rho_2+2\dot{a}L_1\rho_2+\frac{3\dot{b}(L_1-b)^3\rho_2}{L_1^2}-\frac{\dot{b}(L_1-b)^4\rho_2}{L_1^3}+2\dot{a}M_p\right\}\dot{\alpha}+$$

$$+\left\{\begin{array}{l}\frac{6\dot{a}^2I_p}{a^3}-\frac{3\ddot{a}I_p}{a^2}-\frac{9\dot{a}^2\rho_2}{10}-\frac{9a\ddot{a}\rho_2}{10}-\frac{5\ddot{a}L_1\rho_2}{4}+\frac{3\dot{a}^2L_pM_p}{2a^2}-\frac{3\ddot{a}L_pM_p}{2a}+\\ \frac{3\dot{a}^2L_pL_1M_p}{a^3}-\frac{3\ddot{a}L_pL_1M_p}{2a^2}\end{array}\right\}\beta+$$

$$+\left\{\frac{-6\dot{a}I_p}{a^2}+\frac{a\dot{a}\rho_2}{5}-\frac{\dot{a}L_1\rho_2}{2}+2\dot{a}M_p-\frac{3\dot{a}L_pM_p}{2a}-\frac{3\dot{a}L_1L_pM_p}{a^2}\right\}\dot{\beta}+$$

$$+\left\{\begin{array}{l}a^2\dot{a}\rho_2+2a\dot{a}L_1\rho_2+\dot{a}L_1^2\rho_2+\dot{b}(L_1-b)^2\rho_2+a\dot{a}M_p+\dot{a}L_pM_p+\dot{a}L_1M_p\\ +\dot{a}(L_1+a)M_p+\left(-1.16\dot{a}\rho_2+\frac{24\dot{a}L_1M_p}{5a^2}\right)\beta^2-\left(2.3a\rho_2+\frac{48M_p}{5}+\frac{48L_1M_p}{5a}\right)\beta\dot{\beta}\end{array}\right\}\dot{\theta}+$$

$$+\left\{\left(\begin{array}{l}-4.8\frac{a^2\rho_2}{L_1}-2.3L_1\rho_2+\frac{12a^2(L_1-b)^3\rho_2}{L_1^4}+\frac{12(L_1-b)^3\rho_2}{L_1^2}-\\ \frac{9a^2(L_1-b)^4\rho_2}{L_1^5}-\frac{9(L_1-b)^4\rho_2}{L_1^3}+\frac{1.8a^2(L_1-b)^5\rho_2}{L_1^6}-\frac{5.4(L_1-b)^5\rho_2}{L_1^4}+\\ \frac{6(L_1-b)^6\rho_2}{L_1^5}-\frac{1.3(L_1-b)^7\rho_2}{L_1^6}-\frac{48}{5}M_p-\frac{48}{5L_1}aM_p+\frac{24a(L_1-b)^3M_p}{L_1^4}+\\ \frac{24(L_1-b)^3M_p}{L_1^3}-\frac{18a(L_1-b)^4M_p}{L_1^5}-\frac{18(L_1-b)^4M_p}{L_1^4}+\frac{18a(L_1-b)^5M_p}{5L_1^6}+\\ \frac{18(L_1-b)^5M_p}{5L_1^5}\end{array}\right)\alpha\dot{\alpha}\right\}\dot{\theta}+$$

$$+\left\{\left(\begin{array}{l}
-4.8a\dot{a}\frac{\rho_2}{L_1}-\frac{18a^2\dot{b}(L_1-b)^2\rho_2}{L_1^4}-\frac{18\dot{b}(L_1-b)^2\rho_2}{L_1^2}+\frac{18a^2\dot{b}(L_1-b)^3\rho_2}{L_1^5}+ \\
\frac{12a\dot{a}(L_1-b)^3\rho_2}{L_1^4}+\frac{18\dot{b}(L_1-b)^3\rho_2}{L_1^3}-\frac{4.5a^2\dot{b}(L_1-b)^4\rho_2}{L_1^6}-\frac{9a\dot{a}(L_1-b)^4\rho_2}{L_1^5}+ \\
\frac{13.5\dot{b}(L_1-b)^4\rho_2}{L_1^4}+\frac{1.8a\dot{a}(L_1-b)^5\rho_2}{L_1^6}-\frac{18\dot{b}(L_1-b)^5\rho_2}{L_1^5}+\frac{4.5\dot{b}(L_1-b)^6\rho_2}{L_1^6}- \\
\frac{24\dot{a}M_p}{5L_1}-\frac{36a\dot{b}(L_1-b)^2M_p}{L_1^4}-\frac{36\dot{b}(L_1-b)^2M_p}{L_1^3}+\frac{36a\dot{b}(L_1-b)^3M_p}{L_1^5}+ \\
\frac{12\dot{a}(L_1-b)^3M_p}{L_1^4}+\frac{36\dot{b}(L_1-b)^3M_p}{L_1^4}-\frac{9a\dot{b}(L_1-b)^4M_p}{L_1^6}-\frac{9\dot{a}(L_1-b)^4M_p}{L_1^5}- \\
\frac{9\dot{b}(L_1-b)^4M_p}{L_1^5}+\frac{9\dot{a}(L_1-b)^5M_p}{5L_1^6}
\end{array}\right)\alpha^2\right\}\dot{\theta}$$

$$\frac{\partial L_T}{\partial \theta}=0$$

For clarity in the flow of the text the results for α and β are not presented here but included in Appendix C. Bringing the above expressions together and equating them to the system's inputs produce the equations of motion for each one of the discrete coordinates. The expressions can be represented in matrix form as:

$$\begin{bmatrix} M_{\theta\theta} & M_{\theta\alpha} & M_{\theta\beta} \\ M_{\theta\alpha}^T & M_{\alpha\alpha} & M_{\alpha\beta} \\ M_{\theta\beta}^T & M_{\alpha\beta}^T & M_{\beta\beta} \end{bmatrix}\begin{bmatrix} \ddot{\theta} \\ \ddot{\alpha} \\ \ddot{\beta} \end{bmatrix}+\begin{bmatrix} C_{\theta\theta} & C_{\theta\alpha} & C_{\theta\beta} \\ C_{\theta\alpha} & C_{\alpha\alpha} & C_{\alpha\beta} \\ C_{\theta\beta} & C_{\alpha\beta} & C_{\beta\beta} \end{bmatrix}\begin{bmatrix} \dot{\theta} \\ \dot{\alpha} \\ \dot{\beta} \end{bmatrix}+\begin{bmatrix} 0 & 0 & K_{\theta\beta} \\ 0 & K_{\alpha\alpha} & K_{\alpha\beta} \\ 0 & 0 & K_{\beta\beta} \end{bmatrix}\begin{bmatrix} \theta \\ \alpha \\ \beta \end{bmatrix}=\begin{bmatrix} S_T(t) \\ 0 \\ 0 \end{bmatrix} \quad (2.5.6)$$

where the matrix elements are given in Appendix C. The above equations can also be written as,

$$[\mathbf{M}]\ddot{x}+[\mathbf{C}]\dot{x}+[\mathbf{K}]x=[\mathbf{D}]u \quad (2.5.7)$$

where **[M]**, **[C]** and **[K]** are in general time varying matrices non-linear due to the axial load inclusion, and where the state vector, x, and the control input, u, and the vector D are defined as,

$$x=\begin{Bmatrix} \theta \\ \alpha \\ \beta \end{Bmatrix}, \qquad u=S_T(t), \qquad \mathbf{D}=\begin{bmatrix} 1 \\ 0 \\ 0 \end{bmatrix}$$

at this point the control vector includes only the slew torque applied by the main DRM actuator, the complete control vector will include the feedback actuator inputs which will be introduced in Chapter 3.

In these equations the terms proportional to the velocities are in matrix **C**, and as can be seen in Appendix C they are damping like terms which come from the deployment velocity and acceleration of link 2. The off-diagonal terms in the stiffness matrix **K** are also proportional to the deployment velocity and acceleration. When there is deployment or contraction of link 2 the dynamics of the DRM are affected by the time varying damping and stiffness matrices, apart from the predictable effect of having a time varying inertia matrix, **[M]**. In Equation (2.5.6) the right hand side of the equation is composed of the driving torque applied to the shoulder joint for the slew manoeuvre, $S_T(t)$, which is the time-varying torque necessary to achieve a particular rotation angle given a predetermined maximum angular acceleration, whether the DRM is contracting or deploying throughout the manoeuvre, or if the DRM is fixed at a particular length. Its details are discussed in Section 3.2.

Now that the approximate equations of motion for the partially flexible DRM and the flexible DRM are formulated, the calculation of the natural frequencies of vibration is performed. In the calculations in the following two sections below the values are found by assuming no external inputs to the system.

2.6 Vibration Analysis of the P-DRM

Using the following assumed shape function in Equations (2.5.1) and (2.5.2) (Function (B.8) from Appendix B, (Timoshenko, 1937)):

$$\phi_i = (i+2)\left(\frac{x}{L}\right)^{i+1} - i\left(\frac{x}{L}\right)^{i+2} \qquad (2.6.8)$$

for link 2 of the P-DRM the natural frequencies can be calculated for fixed lengths of link 2. This function has been shown in Appendix B to be the best shape function of those used to approximate a beam plus payload system. The number of functions used, n, in the approximation, in Equation (2.4.1), has been selected as 2. Therefore, the first two modes of vibration of the y_2 deflection, shown in Figure 2.3, can be calculated. The numerical results are shown in Table 2-5. Clearly for this problem mode 0 is the rigid body rotation (the slew angle, θ) which has zero frequency, $\omega_\theta = 0$, as stated in Section 2.3.3.

Table 2-5: P-DRM Approx. Nat. Freq. (in Hz) for several different values of extended Link 2
(Link 1 – rigid; Link 2 – flexible)

	a =1.0 m	a =2.0 m	a =3.0 m	a =4.0 m	a =5.0 m	a =6.0 m	a =7.0 m	a =8.0 m
No Payload	f_1=334. f_2=2034.	f_1=89.0 f_2=517.	f_1=42.2 f_2=234.	f_1=25.4 f_2=134.1	f_1=17.4 f_2=87.6	f_1=13.0 f_2=62.4	f_1=10.4 f_2=47.3	f_1=8.7 f_2=37.7
Payload 1 (M_p=200 Kg)	f_1=39.1 f_2=283.6	f_1=20.5 f_2=133.2	f_1=13.5 f_2=86.0	f_1=9.8 f_2=61.1	f_1=7.7 f_2=46.7	f_1=6.33 f_2=36.0	f_1=5.3 f_2=28.5	f_1=4.74 f_2=24.0
Payload 2 (M_p=350 Kg)	f_1=27.2 f_2=231.4	f_1=16.1 f_2=100.5	f_1=11.2 f_2=64.1	f_1=8.50 f_2=46.7	f_1=6.8 f_2=36.3	f_1=5.7 f_2=29.3	f_1=4.90 f_2=24.3	f_1=4.34 f_2=20.8
Payload 3 (M_p=500 Kg)	f_1=20.1 f_2=201.	f_1=12.8 f_2=82.7	f_1=9.4 f_2=51.4	f_1=7.4 f_2=37.4	f_1=6.1 f_2=29.3	f_1=5.15 f_2=24.2	f_1=4.5 f_2=20.5	f_1=4.00 f_2=17.8

The results in Table 2-5 are calculated for the P-DRM with no payload and for the three payloads of Table 2-3, they were produced with the function **drmnac3.m,** found in Appendix D, written for the program MATLAB (Shahian and Hassul, 1993). The results, when compared to the exact values of Table 2-4 follow the theory stated by Lord Raleigh that any approximate method to calculate the natural frequencies of vibration of

a system will predict frequencies of vibration higher than the exact solutions. The results in Table 2-5 are well spaced from mode 1 to mode 2, following the pattern pointed out in Section 2.3.3, and the first natural frequency of the system will dominate the vibrations of the P-DRM in slewing operations.

Comparing the exact values from Table 2-4 with the approximate values of Table 2-5, as shown in Table 2-6 in percent of error. It can be seen from Table 2-6 that the approximate method calculates the frequencies for the P-DRM with no payload extremely well. It can be said that the approximation chosen for the flexible deflection works very well for an unloaded P-DRM. This conclusion led this author to be confident that a very high quality model could be programmed for the DRM + Payload simulations by using the selected assumed function.

Table 2-6: P-DRM Nat. Freq. Percent error between exact and approximate methods

(Link 1 – rigid; Link 2 – flexible)

	a =1.0 m	a =2.0 m	a =3.0 m	a =4.0 m	a =5.0 m	a =6.0 m	a =7.0 m	a =8.0 m
No Payload	f_1=0.27% f_2=0.93%	f_1=0% f_2=0.89%	F_1=0% f_2=1%	f_1=0% f_2=1.04%	f_1=0% f_2=1.14%	f_1=0% f_2=1.30%	f_1=0% f_2=1.50%	f_1=0.46% f_2=1.60%
Payload 1 (M_p=200 Kg)	f_1=34% f_2=81.9%	f_1=15.2% f_2=89.7%	f_1=12.5% f_2=79.2%	f_1=9.6% f_2=62.5%	f_1=10% f_2=50.6%	f_1=11% f_2=38.5%	f_1=8.8% f_2=26.7%	f_1=11.8% f_2=23.7%
Payload 2 (M_p=350 Kg)	f_1=68% f_2=92.5%	f_1=45% f_2=104%	f_1=36.6% f_2=108%	f_1=32% f_2=103%	f_1=30% f_2=93%	f_1=29.5% f_2=83%	f_1=29.2% f_2=70.9%	f_1=16.5% f_2=65%
Payload 3 (M_p=500 Kg)	f_1=89.6% f_2=103%	f_1=71% f_2=112%	f_1=62% f_2=121%	f_1=57% f_2=120%	f_1=54.8% f_2=123%	f_1=52.8% f_2=114%	f_1=53% f_2=107%	f_1=54% f_2=102%

Unfortunately, the difficulty comes when payloads of medium to large size are considered. As can be seen when comparing the values of the approximate frequencies to the exact frequencies the errors range from 10% for Payload 1 to 100% for Payload 3, depending on the amount of link2 extended. The frequencies predicted for the DRM

plus one of these medium size payloads by the assumed mode method are too high compared with the exact frequencies. On the other hand, the approximation for the DRM does work well for small point mass payloads. Due to this, a new payload is introduced, Payload 0 which is a 50 Kg point mass at the end of the DRM. Therefore, the new payload is included in Table 2-7, below, the new payload definition table.

Table 2-7: New Payload characteristics

	Mass	Length	Width
Payload 0	50 Kg	10 cm	10 cm
Payload 1	200 Kg	100 cm	50 cm
Payload 2	350 Kg	150 cm	75 cm
Payload 3	500 Kg	200 cm	100 cm

For Payload 0, the natural frequencies calculation using the exact method from Section 2.3.3 and the approximate method from this section are as follows.

Table 2-8: P-DRM + Payload 0 Nat. Freq. (Hz) for several different values of extended Link 2

(Link 1 – rigid; Link 2 – flexible)

M_p = 50kg	a =1.0 m	a =2.0 m	a =3.0 m	a =4.0 m	a =5.0 m	a =6.0 m	a =7.0 m	a =8.0 m
Exact Method	f_1=91.1 f_2=986.9	f_1=35.4 f_2=344.6	f_1=20.2 f_2=164.8	f_1=13.7 f_2=96.8	f_1=10.29 f_2=64.4	f_1=8.192 f_2=46.6	f_1=6.840 f_2=35.8	f_1=5.919 f_2=28.9
Assumed Modes Method	f_1=93.5 f_2=1246.	f_1=35.9 f_2=351.7	f_1=20.2 f_2=164.9	f_1=13.7 f_2=96.9	f_1=10.3 f_2=64.5	f_1=8.204 f_2=46.7	f_1=6.844 f_2=35.9	f_1=5.922 f_2=29.1

The errors using the approximation method for the flexible link of P-DRM can be seen from Table 2-8 in the natural frequency calculations. The calculations using the

exact method and the approximate method yield very similar results. The discrepancies are for all extended lengths of link 2 are less than 3%. The approximation for the P-DRM with Payload 0 can therefore be considered adequate from a general engineering point of view. Dynamic simulations using the assumed mode method approximate model will be run in Chapter 4 for the DRM using an unloaded manipulator and also carrying the two smallest payloads of Table 2-7, the 50 Kg and the 200 Kg payloads, since those are the configurations that approximate the real system behaviour most accurately.

2.7 Vibration Analysis of the Fully Flexible DRM

Calculations can now be performed with the approximate model developed to estimate the natural frequencies of vibration of the fully flexible DRM. The frequencies of vibration of the fully flexible system are determined for a non-deploying DRM, as for the cases before, the length a is frozen at a particular value and $\dot{a}$ and $\ddot{a}$ are set to zero. This reduces the overall complexity of Equation (2.5.6), by eliminating the off diagonal terms of the **K** matrix, the **C** matrix, and simplifying many of the terms in the inertia matrix, **M**. The solution of the natural frequency problem is the solution of the characteristic problem of Equation (2.5.6), as simplified by assuming no linear deployment velocity and acceleration:

$$\begin{bmatrix} M_{\theta\theta} & M_{\theta\alpha} & M_{\theta\beta} \\ M_{\theta\alpha}^T & M_{\alpha\alpha} & M_{\alpha\beta} \\ M_{\theta\beta}^T & M_{\alpha\beta}^T & M_{\beta\beta} \end{bmatrix} \begin{bmatrix} \ddot{\theta} \\ \ddot{\alpha} \\ \ddot{\beta} \end{bmatrix} + \begin{bmatrix} 0 & 0 & 0 \\ 0 & K_{\alpha\alpha} & 0 \\ 0 & 0 & K_{\beta\beta} \end{bmatrix} \begin{bmatrix} \theta \\ \alpha \\ \beta \end{bmatrix} = \begin{bmatrix} 0 \\ 0 \\ 0 \end{bmatrix}$$

The elements are as shown in Appendix A. The right hand side is now set to zero as the frequency analysis is for a system without any inputs. Solving the eigenvalue problem

with the matrices **M** and **K** give the eigenvalues of the system which are the natural frequencies of vibration of the DRM.

Table 2-9: DRM Approximate Nat. Freq. (Hz) for different values of extended Link 2 and Payloads
(Link 1 – flexible; Link 2 – flexible)

	a =2.0 m	a =3.0 m	a =4.0 m	a =5.0 m	a =6.0 m	a =7.0 m	a =8.0 m
Payload 0 (M_p=50 Kg)	f_1=22.8 f_2=38.1	f_1=14.9 f_2=31.6	f_1=10.2 f_2=30.8	f_1=7.71 f_2=30.6	f_1=6.23 f_2=29.4	f_1=5.35 f_2=27.7	f_1=4.82 f_2=27.2
Payload 1 (M_p=200 Kg)	f_1=16.3 f_2=31.9	f_1=10.6 f_2=30.2	f_1=7.64 f_2=30.0	f_1=5.97 f_2=29.7	f_1=4.97 f_2=28.5	f_1=4.35 f_2=26.7	f_1=3.97 f_2=26.3

The results in Table 2-9 are for the fully flexible DRM approximate model using a single shape function, Equation (2.6.8), per link, as in the simulation model. The results are produced using the function **flexnac3.m**, as found in Appendix D, for the program MATLAB. As has been discussed above, this limits the payloads that can be modelled since, as shown in Section 2.3.3.3, link 2 is affected by the payload at its free end, and using one function is not enough to properly predict the vibration characteristics of the system. The decision was taken to reduce the payload sizes simulated, rather than to increase the number of approximating functions due to the available computer resources at the time, and to keep the overall complexity of the approximate model down. With respect to the computer resources it was found that the time necessary to perform simulations, and plot results increased from about 10 minutes to almost 5 hours and therefore the attempt was abandoned. The reason for such disparity in simulation times comes from the limitations of the computer hardware, such as processor speed, memory availability, hard disk speed, etc. It also comes from the fact that to simulate a higher order system the integration step size has to be reduced considerably to capture the

higher frequency dynamics of vibration, this greatly increases the time to complete each simulation run.

To cross check the frequency results in Table 2-9, other assumed functions and an increasing number of functions have been used to approximate the natural frequencies of DRM plus payload. Table 2-10 shows that the results for the first two natural frequencies are close enough for practical purposes, and in particular the frequency for the first mode, which will dominate the dynamic response in each case. The results are produced using the function **flexnac2.m**, **flexnac3.m**, and **flexasm.m** as found in Appendix D, for the program MATLAB.

Table 2-10: DRM + Payload 1 Approximate Nat. Freq. (Hz) with different mode shapes and an increasing number of functions

(Link 1 – flexible; Link 2 – flexible)

Assumed Shape	$a = 2.0$ $n=m= 5$	$a = 4.0$ $n=m= 5$	$a = 4.0$ $n=m= 10$	$a = 6.0$ $n=m= 5$	$a = 6.0$ $n=m= 10$	$a = 8.0$ $n=m= 5$	$a = 8.0$ $n=m= 10$
Equation (2.6.8)	ω_1=14.2 ω_2=22.2	ω_1=7.13 ω_2=21.9	ω_1=7.12 ω_2=21.7	ω_1=4.87 ω_2=20.3	ω_1=4.88 ω_2=20.2	ω_1=3.92 ω_2=19.9	ω_1=3.91 ω_2=19.9
Equation (B.9)	ω_1=14.4 ω_2=22.6	ω_1=7.10 ω_2=21.0	ω_1=7.05 ω_2=20.7	ω_1=4.87 ω_2=20.4	ω_1=4.87 ω_2=20.2	ω_1=3.92 ω_2=20.0	ω_1=3.91 ω_2=19.9
Equation (B.7)	ω_1=15.8 ω_2=22.3	ω_1=7.48 ω_2=22.5	ω_1=7.23 ω_2=21.8	ω_1=5.10 ω_2=20.6	ω_1=4.94 ω_2=20.3	ω_1=4.05 ω_2=20.1	ω_1=3.95 ω_2=20.1

It has to be mentioned here, as remarked also in Appendix B, that due to the nature of assumed shapes functions (2.6.8) and (B.7), they produce ill-conditioned mass matrices in the numerical resolution of this problem, in particular when more than 5 functions are used. This can produce incorrect results as the eigenvalues calculations break down for ill-conditioned matrices. On the other hand assumed shape (B.9) produces better matrices for which the eigenvalue solutions are well defined. In a

situation were a large number of assumed functions would need to be used the selection of functions is therefore very important for the correct solution to the problem.

In this Chapter so far the flexible DRM dynamical model has been developed as it will be used in computer simulations to find out the open loop and closed loop DRM responses in Chapter 4. First, though, the following section presents natural frequency results calculated for the DRM using a commercial finite elements program. The control inputs to drive the DRM are developed in the next chapter.

2.8 NASTRAN Analysis Results

As an independent source of natural frequency information the commercial programs NASTRAN has been utilised to provide the exact fundamental vibration modes for the DRM under several different configurations. The dynamic model developed above is an approximation created to study the complex dynamics of the system and for the purpose of testing and validating a novel control approach. With this purpose in mind the model sacrifices complexity in the flexible mode approximation for simplicity in the formulation. The simpler formulation is needed, as remarked above, to keep run times to reasonable levels and more importantly to gain a clear insight into the dynamic interactions taking place, which a more complex and accurate flexible model may obscure with very complicated mathematical expressions. The exact natural frequency results in this section have been included to more clearly gage the validity of the approximations made in the flexibility model and to highlight where the model needs to be refined in any extension to this research.

2.8.1 NASTRAN Bending Natural Frequencies

The complete NASTRAN results together with the details of the model simulated are shown in Appendix E. Table 2-11 shows the bending natural frequencies of the DRM at different lengths of extended link 2 while carrying some of the payloads of Table 2-7, plus the difference of those values with the ones reported in Table 2-9 obtained with the approximate model.

Table 2-11: DRM Bending Natural Frequencies by NASTRAN, and Error Comparison to Approx. Values in Table 2-9
(Link 1 – flexible; Link 2 – flexible)

	a =6.0 m		a =8.0 m	
		% diff		*% diff*
Payload 0 (M_p=50 Kg)	f_1= 5.02	16	f_1= 3.55	25
	f_2= 18.9	35	f_2= 12.6	51
	f_3= 44.3	-	f_3= 27.4	-
	f_4= 73.0	-	f_4= 47.8	-
		% diff		*% diff*
Payload 1 (M_p=200 Kg)	f_1= 4.08	18	f_1= 3.10	22
	f_2= 16.4	41	f_2= 11.2	55
	f_3= 32.3	-	f_3= 23.5	-
	f_4= 59.3	-	f_4= 38.7	-

While there are errors in the natural frequencies calculated by the assumed modes model with respect to those generated by NASTRAN, the approximate model represents a first approximation of the flexibility in the DRM links. For the purposes of studying the main characteristics of the dynamic response of the DRM in terms of gross angular motion as well as in vibration, and also to use as a test bed for the proposed control systems, the approximate model used in this thesis serves its purpose. On the other hand it is important to investigate and present the limitations of any approximate model.

2.8.2 NASTRAN Torsional Natural Frequencies

It is also very much of interest with this NASTRAN analysis to find out the torsional modes of the DRM while carrying a payload. The assumption made in this research is

that only in-plane bending modes are important when studying the basic slew problem. This is standard practice for the dynamic study of long and slender structures such as the DRM (Skaar and Ruoff, 1994), (Hyochoong, 1992), (Huang and Yang, 1988), etc. Nonetheless it is important for the direction of future research, and for completeness in this thesis, to include a look at the torsional modes of the DRM while carrying a payload. The torsional modes are presented in Table 2-12 and complete results and further discussion can be found in Appendix E.

Table 2-12: DRM Torsional Natural Frequencies by NASTRAN
(Link 1 – flexible; Link 2 – flexible)

	a =6.0 m	a =8.0 m
Payload 0 (M_p=50 Kg)	*Not found in the first 10 modes of the system (up to 73 Hz)*	*Not found in the first 10 modes of the system (up to 48 Hz)*
Payload 1 (M_p=200 Kg)	t_1=24.3 Hz	t_1=19.1 Hz
Offset Payload 0 (M_p=50 Kg)	*Not simulated*	*Not found in the first 10 modes of the system (up to 48 Hz)*
Offset Payload 1 (M_p=200 Kg)	*Not simulated*	t_1=13.3 Hz
Rotate + Offset Payload 1 (M_p=200 Kg)	*Not simulated*	t_1=6.72 Hz

For the cases shown in Table 2-12 while the DRM is carrying the 50 Kg payload no torsional mode can be found in the first 10 normal modes of the system, in any configuration, the payload's mass moment of inertia is too small to induce torsional vibrations. For the DRM plus the 200 kg payload the first torsional mode is situated outside the first two bending modes therefore confirming that the assumption of not taking it into account for the in-plane study is correct. On the other hand, the frequency

of vibration for the first torsional mode is close enough to the first two bending modes that in a future expansion of this work it should probably be simulated to find the exact effects on the dynamic response of the DRM while conducting a slew plus length extension manoeuvre. Two offset cases of the 200 Kg payload have been also included in the NASTRAN analysis and are shown in Table 2-12. By offsetting the Payload away from the regular neutral grappling point changes the mass moment of inertia of the payload with respect to the DRM and reduces the frequency of torsional vibration. For the extreme case of rotation and offsetting of the 200 Kg payload the first torsional mode is in between the first and second frequencies of vibration.

The neutral grappling point referred to above is the standard way the payload is attached to the DRM throughout this thesis, and corresponds to grappling at the centre of the side facing the DRM with the long axis of the payload along the long axis of the DRM. The *Offset* and the *Rotate + Offset* grappling modes of the payload are best described in Figure 2.12.

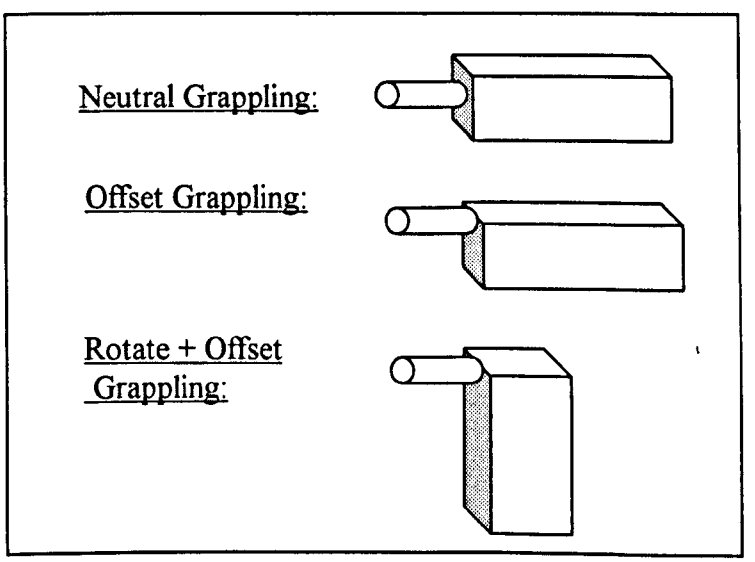

Figure 2.12: DRM Payload grappling modes in NASTRAN analysis

These different grappling modes for the payload change considerably the mass moment of inertia along the long axis of the DRM and therefore change considerably the torsional frequency modes as has been shown in Table 2-12.

Having completed the development of the approximate dynamical model and the study of the flexibility the following chapter presents the development of the control laws for the DRM.

Chapter 3 : DRM Control

The main purpose of a space robotic manipulator is to move objects (construction elements, external experiments, replacement units, etc) with respect to other structures in orbit. This thesis focuses on the analysis of the dynamics and control system design for slew of a DRM through a specified angle. Together with the slew a predetermined length change of the manipulator is performed, as discussed in Chapter 2. Therefore, this involves controlling the rotational manoeuvre (slew) of the manipulator payload in one plane through a predefined angle, with a simultaneous predetermined length change, $a(t)$, due to sliding in or out of link 2. This manoeuvre has an obvious complications since length changes influence the inertia and stiffness properties. The control system must hence adapt in some way to be able to slew the manipulator and payload through a given angle. There are also Coriolis type interactions between the angular velocity, $\dot{\theta}$, and the deployment velocity, $\dot{a}$ which contribute to the time varying stiffness and damping terms during the manoeuvre.

To accurately control the DRM through the slew, transient vibrations will have to be damped out during the manoeuvre to ensure correct slew manoeuvring and to prevent long settling times at the end of it. Vibrations of the DRM occur due to stop/start angular acceleration/deceleration operations. It is important to damp out these

vibrations while manoeuvring, so as to prevent fatigue of mechanical components, such as the slew drive gear trains. In addition, vibrations could be transmitted to the supporting space structure, which could affect micro-gravity experiments on board, or transmitted to the payload damaging sensitive components.

In this Chapter, the control aspects of the DRM are discussed and several controllers are designed which are later compared by computer simulations, in Chapter 4. In Section 3.1 the importance of the structural flexibility of the DRM to the controller design is discussed. In Section 3.2 the open-loop slewing strategy for the DRM is presented, which is a control law based on the inverse dynamics of the rigid DRM, also angular acceleration profile from minimum-time and minimum-energy solutions are developed. In Section 3.3 the need for a closed loop control law is presented and closed loop control actuators independent of the slewing actuator are proposed. Section 3.4 presents a linear feedback control law based on the outputs of the system, this is a very simple control law which will be shown by simulations to produce good results. Finally, in Section 3.5 a non-linear output feedback control law is derived using the Lyapunov direct method to guarantee the stability of the control law. This control law supplements the open-loop slew control law, it adds robustness to the large angle slew of the DRM, and reduces the transient vibrations of the manipulator both during and after a slew.

3.1 Structural flexibility considerations

In almost every mechanical system, there is some degree of structural flexibility as part of the nature of the design and the material from which it is constructed. Mechanical systems such as the DRM have high flexibility and very low structural damping due to the design and construction materials, and due to their low mass, which minimises costs

to orbit. If the requirements for manoeuvring the DRM are such that the structural flexibility induces no position errors, then the system may be considered as perfectly rigid for controller design and operation.

The latter is the case with most robotic applications on Earth where industrial manipulators are designed to be very bulky to provide high rigidity. Thus they are almost always treated as perfectly rigid systems and flexibility is mostly ignored. In space manipulators, however, the same rigidity cannot be provided since the manipulators must have orders of magnitude larger workspace and be designed with mass-to-orbit costs in mind. Therefore a space manipulator is in general long and slender, including the DRM proposed in this thesis. Furthermore, space robots may have to manipulate very large payloads, say 30,000 kg, as shown in Figure 1.1, with high mass moments of inertia, which will lower their frequencies of vibration, as has been shown in Chapter 2. This will make most controllers based on a perfectly rigid system unable to satisfy the manoeuvring requirements for a range of payloads. This is the case for the DRM and, as will be shown by simulations in Chapter 4, the repositioning of the DRM by a slew manoeuvre will induce tip vibrations which could affect the DRM's overall performance or damage sensitive components in the DRM itself or in the payload.

3.2 Open Loop Slew Control

An open loop control law is developed to drive the manipulator through a slew angle using only the slew actuator at the DRM's attachment point, as shown in Figure 1.2. In some cases of control of dynamical systems open loop control is favoured to closed loop control because it is simpler to implement and safer since the commands to the actuators are completely predetermined. Open loop control laws for manipulators generally use

the *Assumed Torque Method.* This method treats the manipulator plus payload as a rigid body, and solves the inverse dynamic problem to find the necessary torque to be applied by the actuator to manoeuvre the system, as required.

Figure 3.1 illustrates the open loop control of the DRM. The maximum angular acceleration, and the final slew angle will be specified to the system, the deployment/contraction force for link 2 may also be specified, if the force is not specified then the length change will be carried out during the manoeuvre and will be coincident in time with the slew.

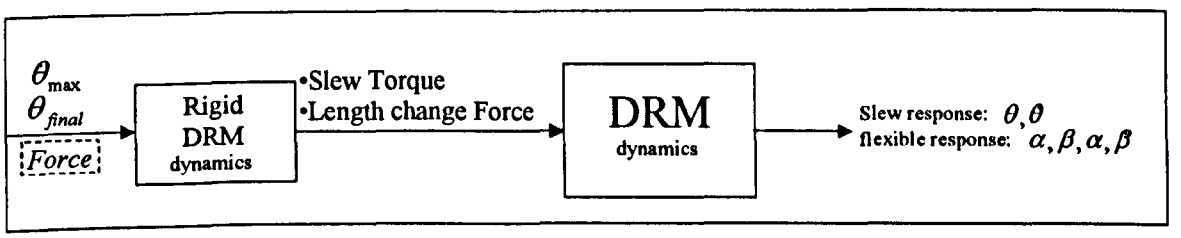

Figure 3.1: The DRM Open Loop Control Diagram

3.2.1 Assumed Torque for Rigid DRM

To achieve the slew of the rigid manipulator through a certain rotation angle, θ_{final}, a torque motor is used at point $\mathbf{O}_1$ of the system (Figure 2.1). This torque motor is the main actuator of the DRM. To reach the specified slew angle while the length of the manipulator, and therefore its inertia are changing, the assumed torque method is used. This method is based on solving the inverse dynamics of a rigid manipulator either on-line or before the manoeuvre begins. The rigid dynamic equations of motion are found from the kinetic energy of the DRM, Equation (2.5.1):

$$T_T = \frac{1}{2}\int_0^{L_1} \rho_1 \left[\left(-y_1(x)\dot{\theta}\right)^2 + \left(x\dot{\theta} + \dot{y}_1(x)\right)^2\right]dx + \frac{1}{2}\int_{L_1-b}^{L_1} \rho_2 \left[\left(\dot{a} - y_1(x)\dot{\theta}\right)^2 + \left(x\dot{\theta} + \dot{y}_1(x)\right)^2\right]dx +$$
$$+\frac{1}{2}\int_0^a \rho_2 \left[\left(\dot{a} - y_2(x)\dot{\theta} - y_1(L_1)\dot{\theta}\right)^2 + \left((L_1 + x)\dot{\theta} + \dot{y}_1(L_1) + \dot{y}_2(x)\right)^2\right]dx +$$
$$+\frac{1}{2}M_p\left[\begin{array}{l}\left(\dot{a} - y_2(a)\dot{\theta} - y_1(L_1)\dot{\theta}\right)^2 + \\ \left(\left(\left(L_1 + a + \frac{1}{2}L_p\right)\dot{\theta} + \dot{y}_1(L_1) + \dot{y}_2(a) + \frac{1}{2}L_p\dot{y}_2'(a)\right)^2\right]\end{array}\right] +$$
$$+\frac{1}{2}I_p\left(\dot{\theta} + \dot{y}_2'(a)\right)^2$$

Assuming in this equation the elastic y_i components as zero, the equation becomes the total energy of the rigid DRM:

$$E_R = \frac{1}{2}\rho_1\int_0^{L_1}\left(x\dot{\theta}\right)^2 dx + \frac{1}{2}\rho_2\int_{L_1-b}^{L_1}\left(x\dot{\theta}\right)^2 dx + \frac{1}{2}\int_0^a \rho_2\left((L_1 + x)\dot{\theta}\right)^2 dx +$$
$$\frac{1}{2}M_p\left[(L_1 + a)\dot{\theta}\right]^2 + \frac{1}{2}I_{yy}\dot{\theta}^2 + \frac{1}{2}M_pL_p\left((L_1 + a)\dot{\theta}^2\right)$$

where $a = a(t)$ and applying Lagrange's equation, Equation (2.4.2):

$$\frac{d}{dt}\left(\frac{\partial E_R}{\partial\dot{\theta}}\right) - \frac{\partial E_R}{\partial\theta} = S_T(t)$$

for the discrete coordinate θ, the rigid equation of motion is formulated, with the torque S_T as the only external input. The rigid equation of motion is therefore:

$$\left[a^2\dot{a}\rho_2 + 2a\dot{a}L_1\rho_2 + \dot{a}L_1^2\rho_2 + \dot{b}(L_1 - b)^2\rho_2 + \dot{a}L_pM_p + 2\dot{a}(L_1 + a)M_p\right]\dot{\theta} +$$
$$\left[\begin{array}{l}\frac{1}{3}L_1^3\rho_1 + \frac{1}{3}a^3\rho_2 + \frac{1}{3}L_1^3\rho_2 + a^2L_1\rho_2 + aL_1^2\rho_2 - \frac{1}{3}(L_1 - b)^3\rho_2 + \\ I_{yy} + L_p(L_1 + a)M_p + (L_1 + a)^2M_p\end{array}\right]\ddot{\theta} = S_T(t) \qquad (3.2.1)$$

where $a = a(t)$, the time varying length of link 2 extended beyond the tip of link 1, $b(t)$ is the length of link 2 contained inside link 1, ρ_1 and ρ_2 are the mass per unit lengths of link 1 and link 2 respectively, M_p is the payload mass and I_{yy} is the payload mass moment of inertia with respect to the attachment point of the DRM.

Equation (3.2.1) gives the torque necessary for the torque motor to drive the DRM through a predetermined slew angle, θ. The quantities $\dot{\theta}$ and $\ddot{\theta}$ are pre-determined for a given slew angle from either the minimum-time or minimum-energy solutions for the slew, which are discussed in the subsequent sections.

The open loop control torque, Equation (3.2.1), is the exact solution to rotate the rigid DRM through a slew if the size, mass and inertia of the payload are exactly known. In the case of applying Equation (3.2.1) to the flexible system, some position error will occur as the flexible modes of the DRM are excited and cause small vibration perturbations in the slew angle. In applying Equation (3.2.1) to drive the DRM with a different payload than expected (incorrect size or mass) then the applied torque, $S(t)$, will be either insufficient to slew the DRM through to the predetermined angle or will overshoot it. Either of these effects is undesirable as it would most probably require another slew to correct the position, wasting operating time in space which is expensive. This shortcoming of the open loop control approach will be addressed in the closed loop control section.

3.2.2 Minimum-Time Acceleration Profile and Torque

The problem of finding the velocity and acceleration profiles to drive the rigid DRM is the well known case of the rotation of a rigid body constrained to rotate about a fixed axis with bounded controls. The requirements on the solution to the problem are that the system reaches a predetermined final state as quickly as possible and that it is a rest-to-rest manoeuvre. The rest-to-rest imposition on the solution of the acceleration profile is fundamental in the application of optimal control theory to space manipulators. The DRM must not rely on the brakes to slow down or stop once the final state has been

reached, since braking would create further undesirable transient oscillations, thus the slew actuator must control the complete manoeuvre. If the brake system at the attachment joint was applied to stop the DRM when the desired slew angle was reached, the DRM would become rigidly attached to the orbiting platform and the vibrations due to the sudden stop would propagate throughout the entire combined structure. This effect could have detrimental effects to on-board experiments, mechanical systems, sun pointing ability of the supporting structure, etc.

It is not intended to give a detailed derivation of the minimum-time rest-to-rest solution to the manoeuvre of a rigid body with bound controls, as this has been solved many times in the literature. The solution is a bang-bang control law which saturates positively during the first half of the manoeuvre and then saturates negatively during the last half of the manoeuvre (Kirk, 1970), (Bryson & Ho, 1975), (Junkins and Turner, 1986). Since the slewing torque in this case, is bound to a maximum positive and negative of control effort this minimum-time solution applied to a simple rigid body implies that the slew actuator must always be at the boundary of the control region.

For the DRM, the problem is slightly changed. The torque to be applied can no longer be considered constant during the manoeuvre, as has been shown in Equation (3.2.1). The minimum time control is changed and instead of having bound controls as for the classical solution, the DRM control constraint is to have bound angular acceleration,

$$\left|\ddot{\theta}\right| \leq \ddot{\theta}_{\max}$$

Given this slightly different constraint, the minimum-time solution for a rest-to-rest manoeuvre of the DRM requires the angular acceleration to saturate for the first part of

the manoeuvre and then reverse itself in the second half to bring the system to a stop at the desired final state. The bang-bang character of the angular acceleration solution can be appreciated in Figure 3.2. The velocity and position plots are also shown in Figure 3.2, as can be seen the angular position reaches the final desired state, in this case 50° (0.87 rad) smoothly and with zero residual velocity and acceleration. To accomplish this manoeuvre while the DRM is extending link 2, Equation (3.2.1) is used to calculate the required torque. The torque profile is shown in Figure 3.3, and can be seen to adapt to the DRM's changing inertia as the manipulator's length is changing to maintain the minimum-time acceleration profile.

The length of the DRM during this slew manoeuvre is extended from 1 to 8 meters, as shown in Figure 3.4 below. The figure shows the deployment acceleration and velocity which are calculated to make the deployment manoeuvre coincide in time with the bang-bang slew profile. For all of the manoeuvres presented in this section, the deployment of link 2 follows the profile of Figure 3.4 unless otherwise stated.

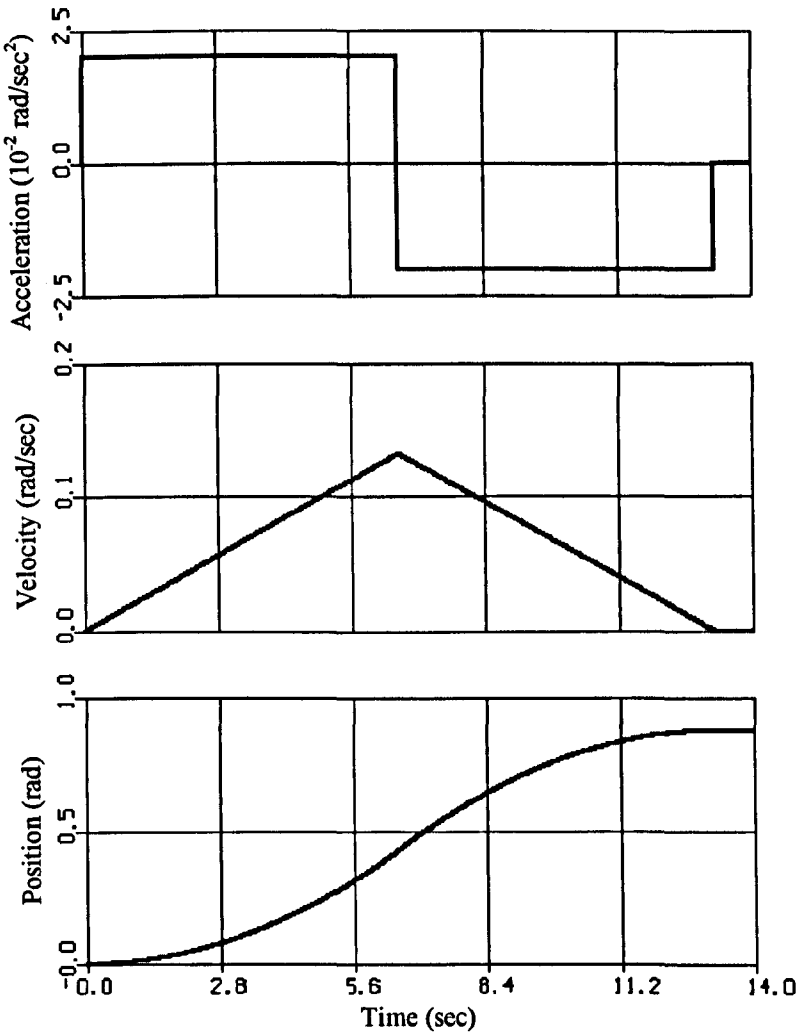

Figure 3.2: Minimum-Time angular acceleration, velocity and position for a 50° slew

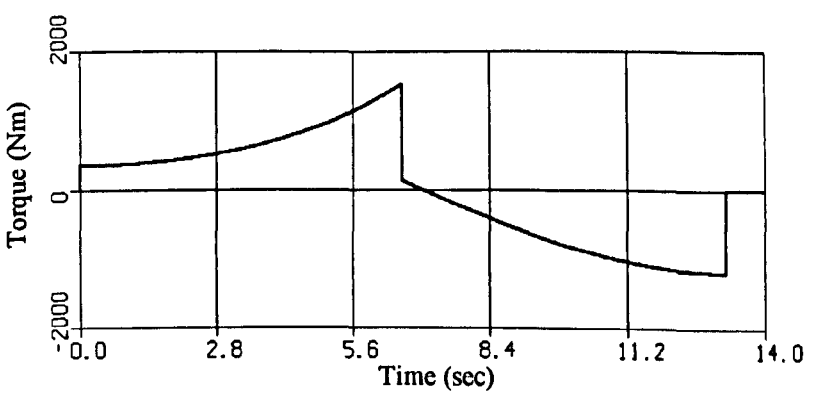

Figure 3.3: Minimum-Time Torque profile for a 50° slew of an extending rigid DRM

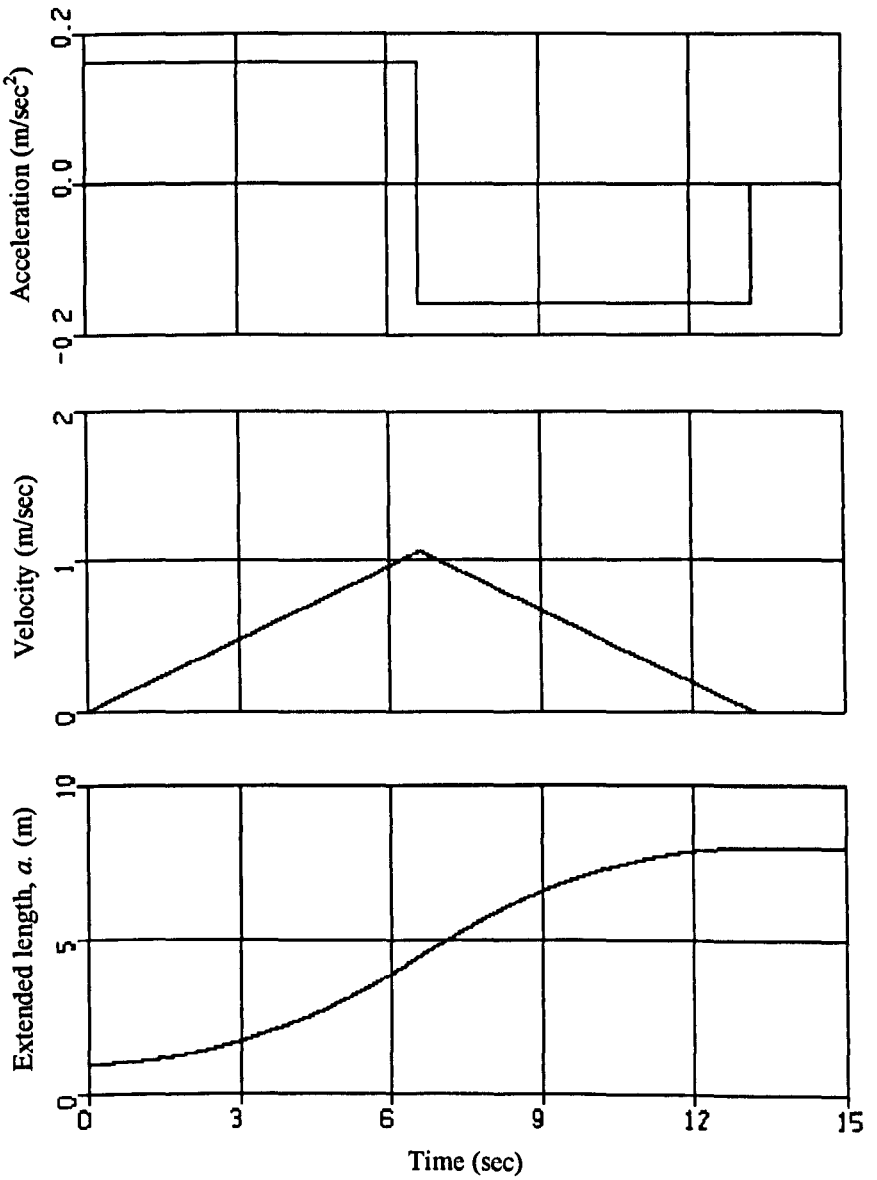

Figure 3.4: Minimum-Time axial deployment acceleration, velocity and position

3.2.3 Near Minimum-Time Acceleration Profile

The bang-bang solution to the minimum-time problem presents implementation problems in terms of real hardware since there is no actuator which can provide the step function required to achieve a truly bang-bang profile. It is also not recommended for a flexible manipulator to manoeuvre the system using sharp torque applications, since they will certainly excite many frequencies of vibration of the structure. Therefore, many references (Tokhi and Azad, 1995), (Junkins et al, 1990), (Choura et al, 1991) provide smoothing techniques to the bang-bang solution. Smoothing of the sharp switches in the bang-bang slew inevitably extend the manoeuvre final time and so the solution is no longer truly minimum-time and is often referred to as '*near-minimum-time*' as referred to in this section.

One way to provide smoothing of the bang-bang torque is by the use of polynomials to carry out the transitions required. This approach produces a smooth continuous approximation that is easier to implement and excites less vibration. To proceed with the near minimum-time formulation, the bang-bang acceleration profile in Figure 3.2 is first divided into five sections over which distinct polynomials are fitted. The duration of each section is controlled by the use of a smoothing parameter, φ. The five sections and their duration periods are:

1. From zero to maximum acceleration, when $0 \le t \le \varphi t_{final}$.
2. Maximum acceleration, when $\varphi t_{final} \le t \le \frac{t_{final}}{2} - \varphi t_{final}$.
3. Switch from maximum to minimum, when $\frac{t_{final}}{2} - \varphi t_{final} \le t \le \frac{t_{final}}{2} + \varphi t_{final}$.
4. Minimum acceleration, when $\frac{t_{final}}{2} + \varphi t_{final} \le t \le t_{final} - \varphi t_{final}$.

5. From minimum acceleration to zero, when $t_{final} - \varphi t_{final} \le t \le t_{final}$.

Over sections 1, 3 and 5 a cubic spline polynomial is fitted to approximate the transitions. Over sections, 2 and 4 the angular acceleration is at its boundary so no cubic polynomial is needed. For section 1 the polynomial is formulated as a general cubic spline, with the associated boundary conditions:

$$\ddot{\theta}(t) = \left(a_1 t^3 + a_2 t^2 + a_3 t + a_4\right)\ddot{\theta}_{\max}$$

$$\ddot{\theta}(0) = \frac{d}{dt}\left(\ddot{\theta}\right)(0) = 0, \quad \ddot{\theta}(\varphi t_{final}) = \ddot{\theta}_{\max}, \quad \frac{d}{dt}\left(\ddot{\theta}\right)(\varphi t_{final}) = 0$$

The boundary conditions show that the value of the function for $\ddot{\theta}(t)$ has to be zero at time equal zero and maximum at φt_{final}, and the function's time derivative must be zero at time equal zero and at φt_{final}. Using the boundary conditions, with the polynomial function for the angular acceleration the values for the coefficients, a_i, can be easily found. The same is done for the cubic splines of sections, 3 and 5 which results in the following expression for the near-minimum-time angular acceleration:

$$\ddot{\theta}(t) = \ddot{\theta}_{\max}\begin{cases} \left(\frac{t}{\varphi t_f}\right)\left(3 - 2\left(\frac{t}{\varphi t_f}\right)\right) & 0 \le t \le \varphi t_{final} \equiv t_a \\ 1 & t_a \le t \le \frac{t_{final}}{2} - t_a \equiv t_1 \\ 1 - 2\left(\frac{t - t_1}{2t_a}\right)^2\left(3 - 2\left(\frac{t - t_1}{2t_a}\right)\right) & t_1 \le t \le \frac{t_{final}}{2} + t_a \equiv t_2 \\ -1 & t_2 \le t \le t_{final} - t_a \equiv t_3 \\ -1 + \left(\frac{t - t_3}{t_a}\right)^2\left(3 - 2\left(\frac{t - t_3}{t_a}\right)\right) & t_3 \le t \le t_{final} \end{cases} \tag{3.2.2}$$

This angular acceleration formula (Junkins, Rahman and Bang, 1990) gives the following equation for the final time,

$$t_f = \sqrt{\left[\frac{\theta_f}{\ddot{\theta}_{\max}}\left(\frac{1}{0.25 - 0.5\varphi + 0.1\varphi^2}\right)\right]} \qquad (3.2.3)$$

where clearly the minimum-time final time formula is recovered when the smoothing factor φ is set to zero.

Using Equation (3.2.2), and its first two integrals over the manoeuvre time gives the angular acceleration, velocity and position shown in Figure 3.5. The necessary slew torque for the DRM to accomplish such profiles is presented in Figure 3.6 for a standard slew while carrying a payload and extending link 2 from 1 to 8 meters, with a smoothing factor $\varphi = 0.1$. In comparison with Figure 3.3 the torque in the near minimum-time case has no sharp switches. It will be shown in the next chapter that because of this it drives the DRM more smoothly, without exciting as many flexible vibrations as the minimum-time slew torque.

The length of the DRM during these simulations is increasing due to the deployment of link 2 following the profiles shown in Figure 3.4.

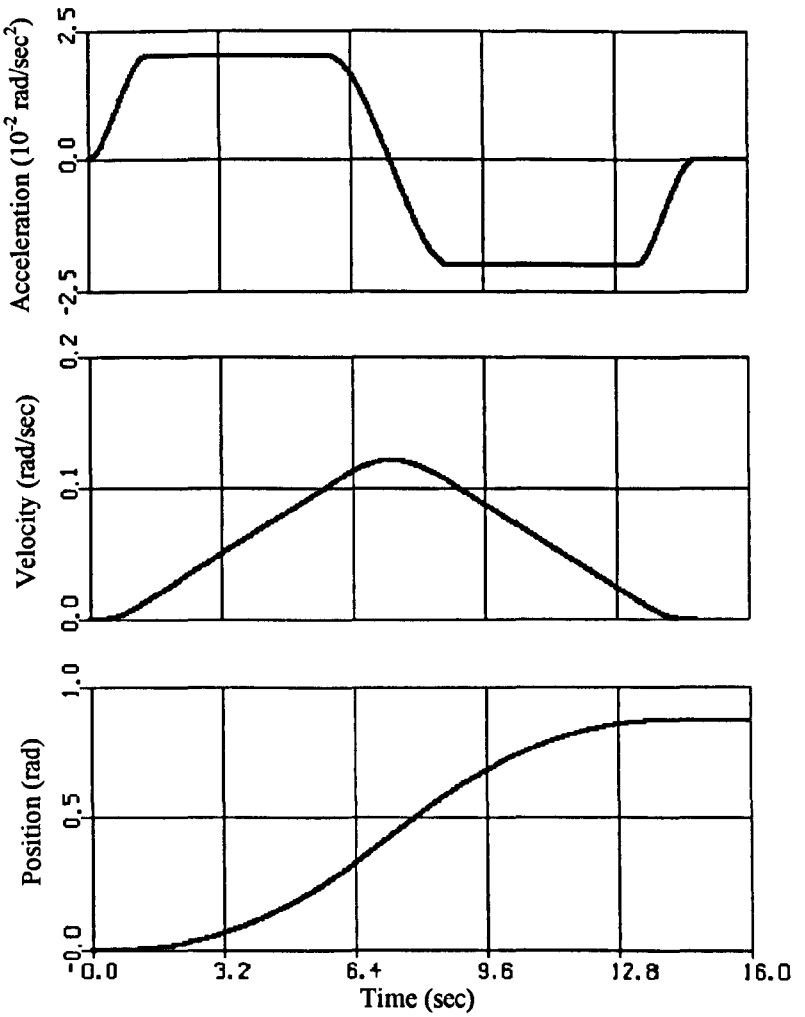

Figure 3.5: Near-Minimum-Time angular acceleration, velocity and position with a smoothing factor, $\varphi = 0.1$

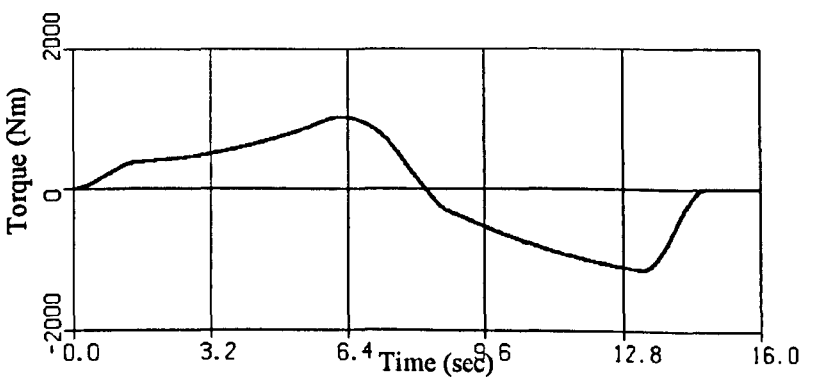

Figure 3.6: Near-Minimum-Time Torque profile for a 50° slew of an extending rigid DRM with a smoothing factor, $\varphi = 0.1$

3.2.4 Minimum Energy Acceleration Profile

The minimum-energy acceleration formulation for the open loop slew strategy requires minimising the energy expenditure (electrical current in this case) of the slew motor at the base of the DRM. The solution to minimum-energy problems is well known and presented in many optimal control references (Kirk, 1970), (Junkins and Turner, 1986) so only a brief development is given here.

The slew torque motor being an electrical device requires that the performance functional to be minimised is:

$$J = \frac{1}{2}\int_0^{t_f} u^2(t)dt \tag{3.2.4}$$

where *u(t)* is the control torque and, in this case it could be interpreted as the current supplied to the slew torque motor to produce a specific torque. Using this performance index together with the equations of motion for a single axis rotation of a rigid body, we have:

$\ddot{\theta} = u$, which is represented as the state equations: $\begin{cases} \dot{x}_1 = x_2 \\ \dot{x}_2 = u \end{cases}$

where the variable substitution has been made ($x_1 = \theta$, $x_2 = \dot{\theta}$). The Hamiltonian can be formed using the Lagrange multipliers, λ_i, (Kirk, 1970), (Junkins and Turner, 1986):

$$H = \frac{1}{2}u^2 + \lambda_1 x_2 + \lambda_2 u \tag{3.2.5}$$

applying the necessary conditions for optimality, $\frac{\partial H}{\partial u} = 0$ and $-\frac{\partial H}{\partial x_i} = \dot{\lambda}_i$ gives the state and co-state equations for this optimal control problem, with four constants, c_i, to be determined from the boundary conditions. Hence from (3.2.5):

$$
\begin{aligned}
-\frac{\partial H}{\partial x_1} = \dot{\lambda}_1 \Rightarrow \dot{\lambda}_1 = 0 \quad & or \quad & \lambda_1 = c_1 \\
-\frac{\partial H}{\partial x_2} = \dot{\lambda}_2 \Rightarrow \dot{\lambda}_2 = -\lambda_1 \quad & or \quad & \lambda_2 = -c_1 t + c_2 \\
\frac{\partial H}{\partial u} = 0 \Rightarrow u = -\lambda_2 \quad & or \quad & \boxed{u = c_1 t - c_2} \\
\dot{x}_2 = u \quad & or \quad & x_2 = \frac{1}{2} c_1 t^2 - c_2 t + c_3 \\
\dot{x}_1 = x_2 \quad & or \quad & x_1 = \frac{1}{6} c_1 t^3 - \frac{1}{2} c_2 t^2 + c_3 t + c_4 = \theta(t)
\end{aligned}
\tag{3.2.6}
$$

In the control input equation, outlined by the rectangle above, the well-known ramp solution to the minimum energy problems is shown.

The application of the minimum-energy solution to the DRM open loop control problem requires that the ramp solution be applied to the DRM's angular acceleration, and not as it is normally done to the slew torque. The slew torque, *S(t)*, will be calculated from the specified angular acceleration profile by the assumed torque method from Equation (3.2.1). The ramp solution still requires finding the values for the c_i constants, which come from the boundary conditions specified for the problem. In this case the manoeuvre has to be a rest-to-rest slew reaching the specified slew angle in the final time: $\theta(0) = 0$, $\dot{\theta}(0) = 0$, $\theta(t_f) = \theta_{final}$ and $\dot{\theta}(t_f) = 0$.

Using the boundary conditions and applying them to the above equations, we can get the following results:

Since $\theta(0) = 0$, then $x_1(0) = 0 - 0 + 0 + c_4 = 0$, therefore $c_4 = 0$.

Since $\dot{\theta}(0) = 0$, then $x_2(0) = 0 - 0 + c_3 = 0$, therefore $c_3 = 0$.

Since $\dot{\theta}(t_f) = 0$, then $x_2(t_f) = \frac{1}{2} c_1 t_f^2 - c_2 t_f = 0$, and since $\theta(t_f) = \theta_f$, then $x_1(t_f) = \frac{1}{6} c_1 t_f^3 - \frac{1}{2} c_2 t_f^2 = \theta_f$. With these two equations and two unknowns constants

they are easily found to be $c_1 = -\frac{12}{t_f^3}\theta_f$, $c_2 = -\frac{6}{t_f^2}\theta_f$. Therefore the angular acceleration solution to the minimum-energy problem is:

$$\ddot{\theta} = -\frac{12}{t_f^3}\theta_f t + \frac{6}{t_f^2}\theta_f = \frac{6\theta_f}{t_f^2}\left[1 - \frac{2}{t_f}t\right] \tag{3.2.7}$$

It is clear from Equation (3.2.7) that either the final time is specified to calculate the maximum and minimum angular accelerations, or the angular acceleration limits are set and the final time is found by solving for it. The angular acceleration limits, either specified or as bound by the final time have to be known before hand to ensure that the torque limits of the slew actuator will not be exceeded while carrying the different payloads.

To calculate the final time, t_f, the angular acceleration has to be bound, as for the minimum-time case above, or the final time could be specified and the angular acceleration maximum and minimum calculated. In this thesis, the maximum angular acceleration is predefined for the minimum-energy solution, as for the minimum-time solution. Once the angular acceleration limits are set, the final time is calculated from Equation (3.2.7) by finding the points for t when the equation gives the angular accelerations limits. These limits occur when the square bracket part of the equation is either 1 or –1, when t is 0 or t_f, so that:

$$\ddot{\theta}_{\max}(0) = \frac{6}{t_f^2}\theta_f \quad \therefore \quad t_f = \sqrt{\frac{6\theta_f}{\ddot{\theta}_{\max}}} \tag{3.2.8}$$

Using these equations the final time is found and the slew acceleration, velocity and rotation angle are as shown in Figure 3.7.

The torque required to slew the DRM while carrying a payload and deploying link 2 is shown in Figure 3.8. The strange shape is due to the extension of link 2. In the first section of the slew (while the required angular acceleration is positive) the torque level is kept almost constant since the inertia of the DRM is increasing then the angular acceleration is indeed decreasing as expected. At the point when the required angular acceleration is negative, the torque changes to slow down the DRM.

The length of the DRM during these simulations is increasing due to the deployment of link 2 following the profiles shown in Figure 3.4.

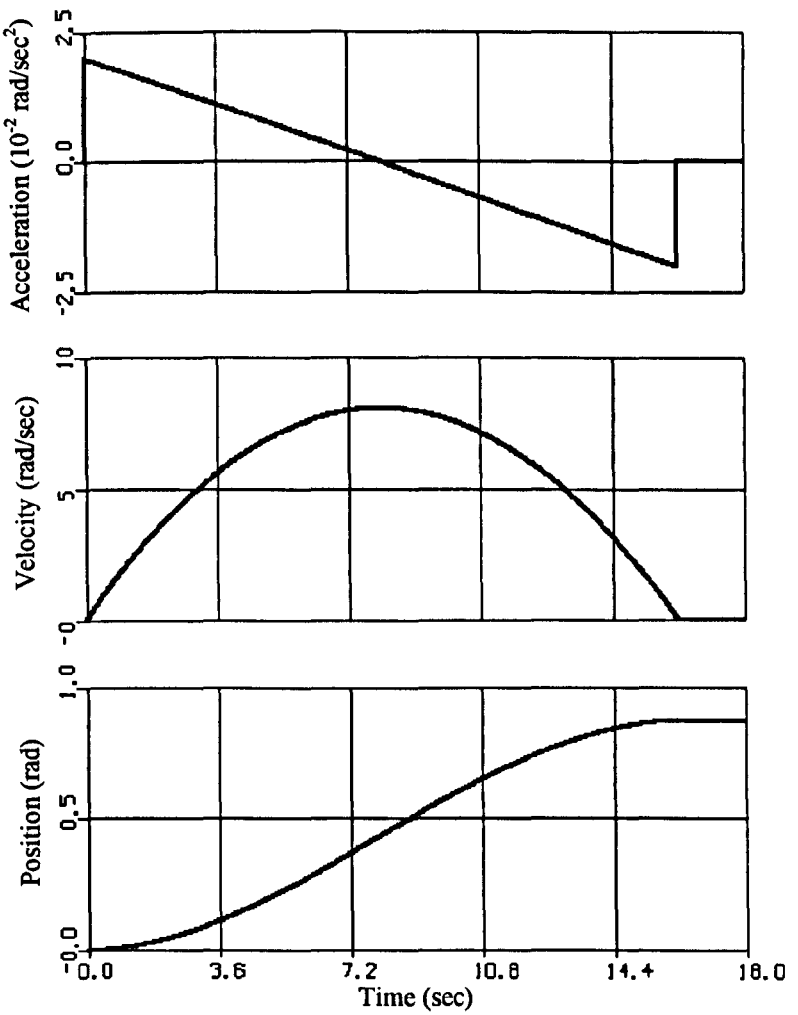

Figure 3.7: Minimum-Energy angular acceleration, velocity and position

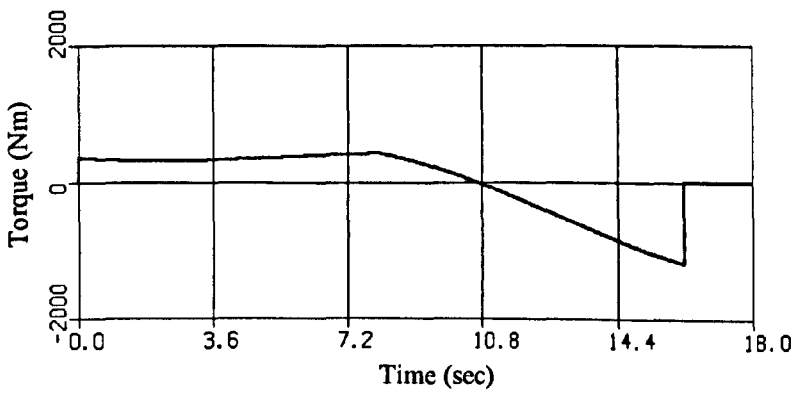

Figure 3.8: Minimum-Energy Torque profile for a 50° slew of an extending rigid DRM

3.2.5 Near Minimum-Energy Acceleration Profile

The application of the minimum-energy torque profile, Figure 3.8, described in the previous section can introduce vibrations due to the sharp switches at the beginning and at the end of the slew. To reduce the vibrations the minimum-energy solution can be smoothed using a polynomial approximation to slightly extended the initial and final torque switches so that they do not represent instantaneous switches.

The acceleration profile in Figure 3.7 is smoothed using a polynomial fitting at the beginning and at the end of the manoeuvre, as for the near minimum-time approach using a smoothing factor, φ. The following sections of the acceleration profile and their duration are identified, from Figure 3.7:

1. From zero to maximum acceleration, when $0 \le t \le \varphi t_{final}$.
2. Ramp acceleration, when $\varphi t_{final} \le t \le \frac{t_{final}}{2} - \varphi t_{final}$.
3. From minimum acceleration to zero, when $t_{final} - \varphi t_{final} \le t \le t_{final}$.

The duration of the sections can be controlled by the smoothing parameter, α. Therefore, the system returns to a minimum-energy solution as φ tends to zero. Fitting a cubic function in sections 1 and 3 from the list above changes the angular acceleration from a minimum-energy ramp solution to the following angular acceleration schedule:

$$\ddot{\theta}(t) = \ddot{\theta}_{\max} \begin{cases} \left(\frac{t}{t_a}\right)^2 \left(3 - 2\frac{t}{t_a}\right) & 0 \le t \le \varphi t_{final} \equiv t_a \\ 1 - 2\left(\frac{t - t_a}{t_1 - t_a}\right) & t_a \le t \le t_{final} - t_a \equiv t_1 \\ -1 + \left(\frac{t - t_1}{t_a}\right)^2 \left(3 - 2\frac{t - t_1}{t_a}\right) & t_1 \le t \le t_{final} \end{cases} \tag{3.2.9}$$

where $\ddot{\theta}_{\max}$ is prescribed and the final time is calculated using the following formula:

$$t_f = \sqrt{\frac{60\theta_f}{(10 - 10\varphi - 2\varphi^2)\ddot{\theta}_{\max}}} \tag{3.2.10}$$

which reduces back to the equation for the final time shown in the previous section, Equation (3.2.8), as α approaches zero.

The formula for the final time of the near-minimum-energy acceleration profile, Equation (3.2.10), is developed as follows: Given the equation for $\ddot{\theta}$ that goes through $\frac{t_f}{2}$, from Equation (3.2.9):

$$\ddot{\theta} = \ddot{\theta}_{\max}\left[1 - 2\left(\frac{t - t_a}{t_1 - t_a}\right)\right] = \ddot{\theta}_{\max}\left[1 - 2\left(\frac{t - \varphi t_{final}}{t_{final} - 2\varphi t_{final}}\right)\right]$$

integrating in time to find $\dot{\theta}$ and θ:

$$\dot{\theta} = \ddot{\theta}_{\max}\left[\frac{t(t - t_{final})}{t_{final}(2\varphi - 1)} + c_1\right], \text{ therefore: } \theta = \ddot{\theta}_{\max}\left[\frac{t\left(\frac{1}{3}t^2 - \frac{1}{2}t t_{final}\right)}{t_{final}(2\varphi - 1)} + c_1 t + c_2\right] \tag{3.2.11}$$

the integration constants c_i are found by matching the boundary conditions of the complete $\ddot{\theta}$ function as given by Equation (3.2.9). For the first section of the angular acceleration, from *0* to φt_{final} the angular acceleration is as follows:

$$\ddot{\theta} = \ddot{\theta}_{\max}\left(\frac{t}{\varphi t_{final}}\right)^2\left(3 - 2\frac{t}{\varphi t_{final}}\right)$$

which integrating gives:

$$\dot{\theta} = \ddot{\theta}_{\max}\left(\frac{t^3}{\varphi^2 t_{final}^2} - \frac{t^4}{2\varphi^3 t_{final}^3}\right) + b_1, \text{ and } \theta = \ddot{\theta}_{\max}\left[\frac{t^4}{4\varphi^2 t_{final}^2} - \frac{t^5}{10\varphi^3 t_{final}^3}\right] + b_1 t + b_2 \tag{3.2.12}$$

and given the boundary conditions at $t = 0$, $\dot{\theta} = 0$, $\theta = 0$, resolves the constants b_i and finds them all to be zero, $b_1 = 0$ and $b_2 = 0$. Therefore matching the value of $\dot{\theta}$ at $t = \varphi t_{final}$ from expressions (3.2.11) and (3.2.12):

$$\dot{\theta}(\varphi t_{final}) \rightarrow \ddot{\theta}_{\max}\left(\frac{(\varphi t_{final})^3}{\varphi^2 t_{final}^2} - \frac{(\varphi t_{final})^4}{2\varphi^3 t_{final}^3}\right) = \ddot{\theta}_{\max}\left[\frac{\varphi t_{final}(\varphi t_{final} - t_{final})}{t_{final}(2\varphi - 1)} + c_1\right]$$

which gives the value for the constant c_1:

$$c_1 = \frac{\varphi t_{final}}{4\varphi - 2}$$

following a similar procedure equating the θ equations from expressions (3.2.11) and (3.2.12), above. The equation to be solved for c_2 is:

$$\theta(\varphi t_{final}) \rightarrow$$
$$\ddot{\theta}_{\max}\left[\frac{(\varphi t_{final})\left(\frac{1}{3}(\varphi t_{final})^2 - \frac{1}{2}(\varphi t_{final})t_{final}\right)}{t_{final}(2\varphi - 1)} + \left(\frac{\varphi t_{final}}{4\varphi - 2}\right)\varphi t_{final} + c_2\right] = \ddot{\theta}_{\max}\left[\frac{(\varphi t_{final})^4}{4\varphi^2 t_{final}^2} - \frac{(\varphi t_{final})^5}{10\varphi^3 t_{final}^3}\right]$$

which gives the value for the constant c_2:

$$c_2 = \frac{(\varphi t_{final})^2(2\varphi + 9t_{final})}{60(1 - 2\varphi)}$$

given c_1 and c_2 the equation for θ in expression (3.2.11) is now complete and can be equated to its known value, $\frac{\theta_{final}}{2}$ at $\frac{t_{final}}{2}$:

$$\frac{\theta_{final}}{2} = \ddot{\theta}_{\max}\left[\frac{\frac{t_{final}}{2}\left(\frac{1}{3}\left(\frac{t_{final}}{2}\right)^2 - \frac{1}{2}\left(\frac{t_{final}}{2}\right)t_{final}\right)}{t_{final}(2\varphi - 1)} + \frac{\varphi t_{final}}{4\varphi - 2}\left(\frac{t_{final}}{2}\right) + \frac{(\varphi t_{final})^2(2\varphi + 9t_{final})}{60(1 - 2\varphi)}\right]$$

which solving for t_{final} gives the expression for the final time in Equation (3.2.10), since θ_{final} is prescribed. The angular acceleration, velocity and position for the near

minimum-time solution are presented in Figure 3.9, with a smoothing factor, $\varphi = 0.1$. The character of the functions can be seen to be very similar to Figure 3.7, but with a longer time to completion, and smoother transitions. The torque derived using these quantities is shown in Figure 3.10, for a standard DRM slew plus length extension.

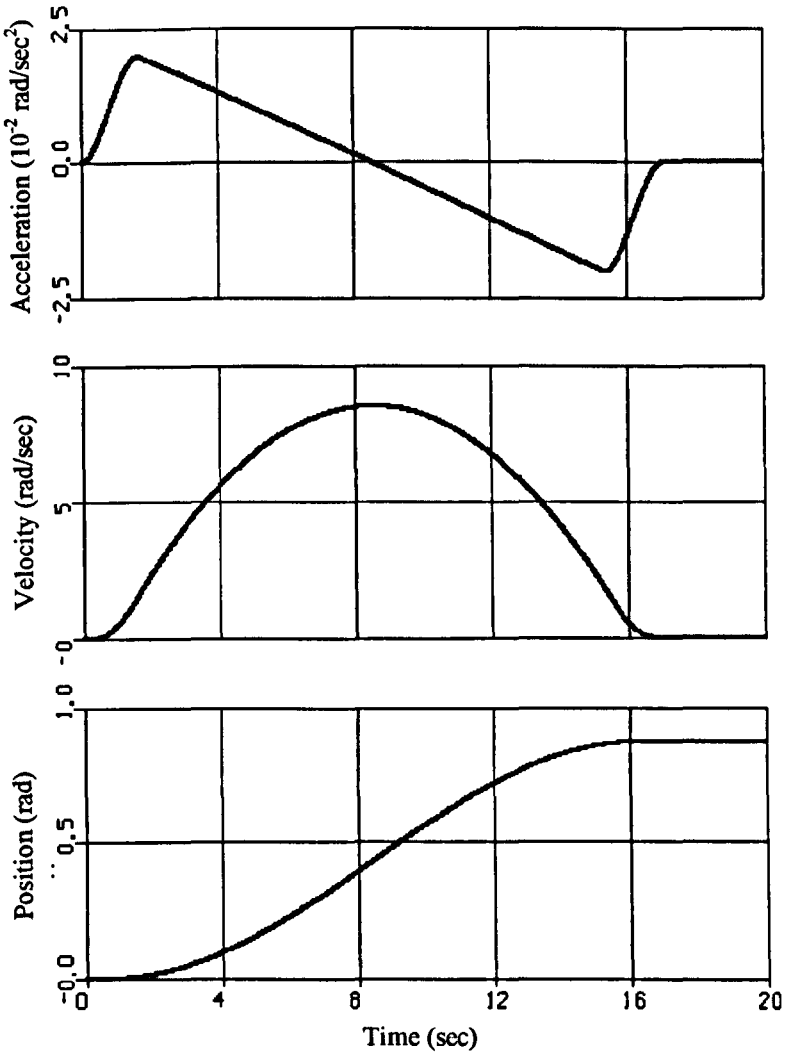

Figure 3.9: Near-Minimum-Energy angular acceleration, velocity and position with a smoothing factor, $\varphi = 0.1$

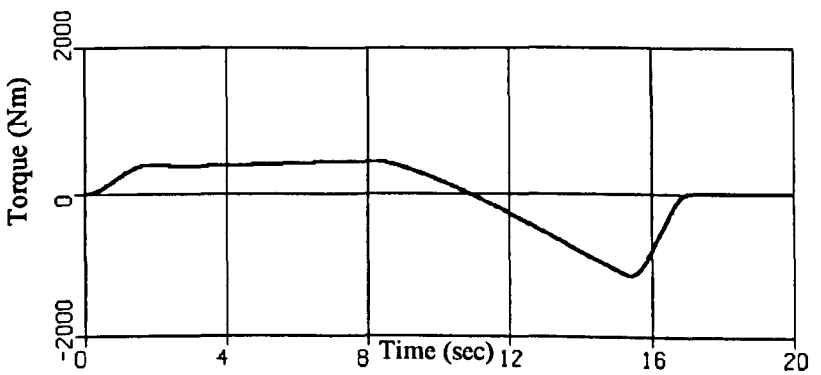

Figure 3.10: Near-Minimum-Energy Torque profile for a 50° slew of an extending rigid DRM with a smoothing factor, $\varphi = 0.1$

3.3 Closed Loop Vibration Control

The near optimal open loop slew control laws presented in the previous section can excite the vibration modes of the DRM when used as the sole control inputs to the manipulator (as shown in Section 4.2). The idea in the sections below is to design a velocity feedback control law to damp out DRM vibrations. This feedback damping can be accomplished using the existing slew actuator on the DRM, Figure 1.2, or by a different set of actuators independent of the large slew torque motor. The latter approach is proposed in this thesis, since the large slew motor is ill-suited to follow a feedback control torque that will require constant torque changes. This is especially important if the slew motor drives the DRM through a high reduction ratio gear box which could have non-linearities and backlash.

The velocity measurements will be provided to the control system via strain gages, accelerometers or piezo-ceramic sensors placed on the tip of link 2. These will sense the overall flexural vibration of the tip of the manipulator for feedback via the closed loop actuators. A diagram of the overall system is given in Figure 3.11.

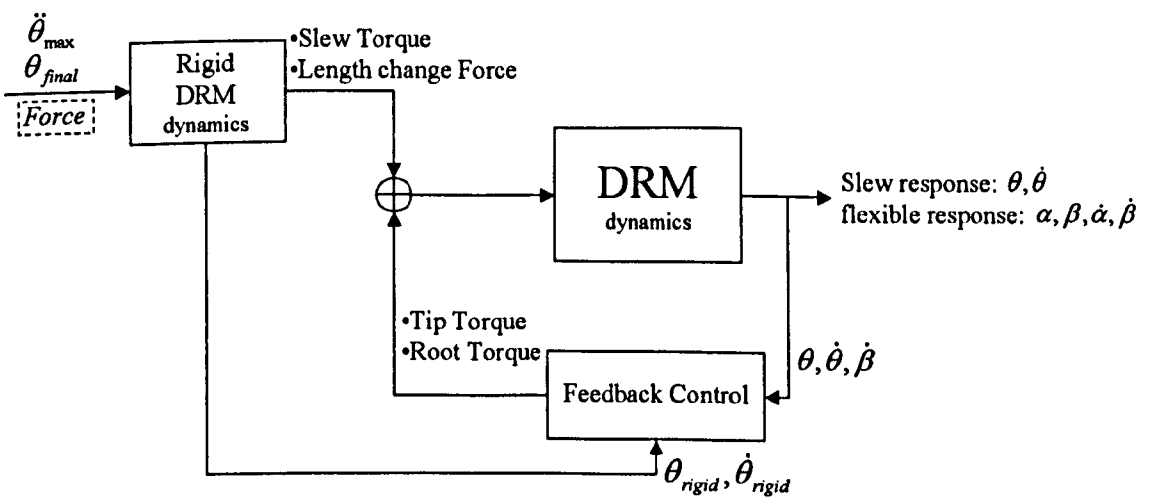

Figure 3.11: Closed Loop DRM Control Diagram

To apply the feedback control torques (Tip and Root torques as shown in Figure 3.11, above) it is proposed to use two reaction wheel actuators located one at the root, collocated with the large slew motor, and another at the tip of the DRM. These reaction wheels will have zero bias and will also have maximum torque values, as shown in Table 3-1.

Table 3-1: Feedback actuator characteristics

	Position	Torque input	Mass
Root actuator	DRM base	±100 Nm	50 Kg
Tip actuator	DRM tip	±10 Nm	10 Kg

The actuator characteristics of Table 3-1 have been chosen to provide effective damping in a reasonable amount of time for the range of payloads selected for the simulations in this thesis (Table 2-7). Their approximate positions are shown in Figure 3.12, the root feedback actuator is shown displaced from the shoulder joint for clarity only.

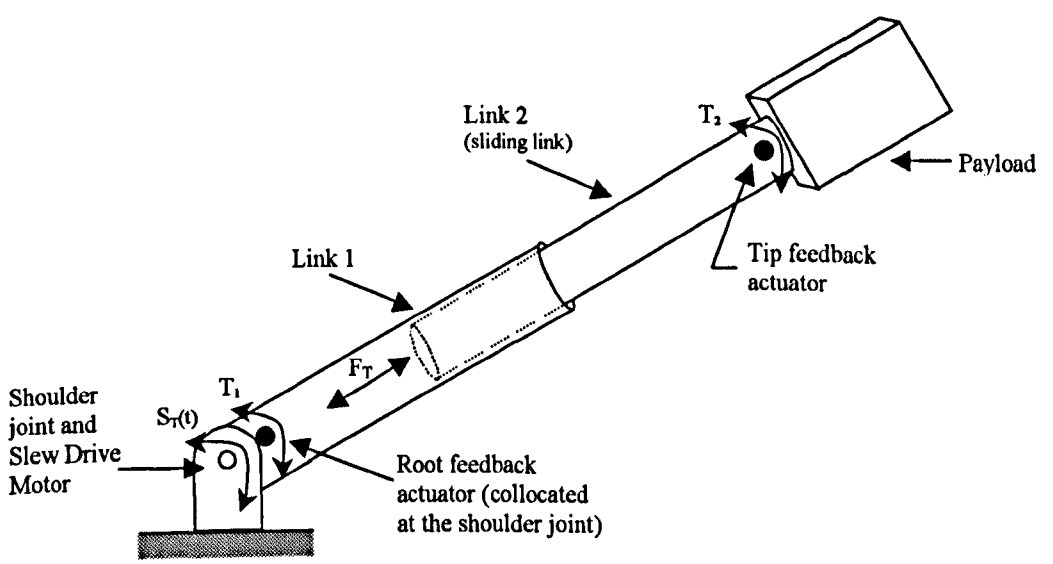

Figure 3.12: DRM Schematic with feedback actuators

The feedback torque input levels, shown in Table 3-1, have been derived from looking at the inverse dynamics equation for the flexible DRM model and subtracting the rigid driving torque. It therefore involves the first equation of Equation (2.5.6):

$$\begin{bmatrix} M_{\theta\theta} & M_{\theta\alpha} & M_{\theta\beta} \end{bmatrix} \begin{bmatrix} \ddot{\theta} \\ \ddot{\alpha} \\ \ddot{\beta} \end{bmatrix} + \begin{bmatrix} C_{\theta\theta} & C_{\theta\alpha} & C_{\theta\beta} \end{bmatrix} \begin{bmatrix} \dot{\theta} \\ \dot{\alpha} \\ \dot{\beta} \end{bmatrix} + \begin{bmatrix} 0 & 0 & K_{\theta\beta} \end{bmatrix} \begin{bmatrix} \theta \\ \alpha \\ \beta \end{bmatrix} = S(t)$$

minus the rigid inverse dynamics, Equation (3.2.1):

$$\begin{bmatrix} a^2\dot{a}\rho_2 + 2a\dot{a}L_1\rho_2 + \dot{a}L_1^2\rho_2 + \dot{b}(L_1 - b)^2\rho_2 + \dot{a}L_pM_p + 2\dot{a}(L_1 + a)M_p \end{bmatrix} \dot{\theta}_r + \\ \begin{bmatrix} \frac{1}{3}L_1^3\rho_1 + \frac{1}{3}a^3\rho_2 + \frac{1}{3}L_1^3\rho_2 + a^2L_1\rho_2 + aL_1^2\rho_2 - \frac{1}{3}(L_1 - b)^3\rho_2 + \\ I_{yy} + L_p(L_1 + a)M_p + (L_1 + a)^2M_p \end{bmatrix} \ddot{\theta}_r = S(t)$$

in the latter equation θ_r refers to the rigid slew motion of the DRM, and in the former equation θ contains the rigid slew motion plus the flexible response. By subtracting the two equations it is this flexible component of the DRM's response which is isolated:

$$\begin{bmatrix} M_{\theta\theta} & M_{\theta\alpha} & M_{\theta\beta} \end{bmatrix} \begin{bmatrix} \ddot{\theta}_e \\ \ddot{\alpha} \\ \ddot{\beta} \end{bmatrix} + \begin{bmatrix} C_{\theta\theta} & C_{\theta\alpha} & C_{\theta\beta} \end{bmatrix} \begin{bmatrix} \dot{\theta}_e \\ \dot{\alpha} \\ \dot{\beta} \end{bmatrix} + \begin{bmatrix} 0 & 0 & K_{\theta\beta} \end{bmatrix} \begin{bmatrix} \theta_e \\ \alpha \\ \beta \end{bmatrix} = D(t) \quad (3.3.1)$$

It is assumed in the preceding development that the terms multiplying $\ddot{\theta}$ and $\dot{\theta}$ are the same. This can be checked with the values of $C_{\theta\theta}$ and $M_{\theta\theta}$ as presented in Appendix C, where they are explicitly shown and $C_{\theta\theta}$ is exactly the same. The value of $M_{\theta\theta}$ is almost completely the same except for two very small terms depending on α and β which appear due to the consideration of the axial force, and they can effectively be ignored when compared to the other terms. Equation (3.3.1) also shows the term $D(t)$ which represents the disturbance torque which comes from the flexibility in the DRM.

The value $D(t)$ has been plotted in Figure 3.13 for a DRM 50° slew manoeuvre (minimum-time, length extending from 1 to 8 meters) while carrying Payload 0 from Table 2-7. The plot shows that the disturbance torque is quite considerable, especially after the mid-manoeuvre switch when more of the DRM is extended. Since $D(t)$, as shown in Figure 3.13, is most of the time close to or even under 100 Nm that is why that value was chosen as the root control torque limit. The tip actuator limit is nominally set as a 10% of the root value.

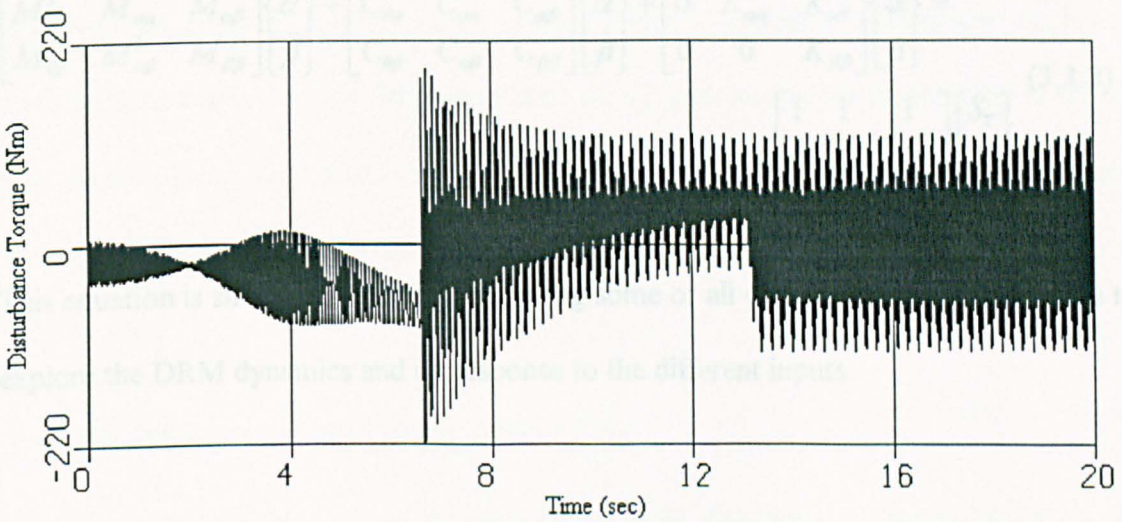

Figure 3.13: Disturbance torque for a 50° minimum-time slew of an extending DRM with Payload 0

With the feedback actuators' size and locations selected, in Figure 3.12, their inputs must be included in the DRM equations of motion, Equation (2.5.6). The root actuator torque can be simply added to the open loop torque since it acts through the degree of freedom θ, so it is added to the right hand side of the θ equation of motion.

On the other hand, the contribution to the DRM dynamics of the tip torque is through the slope of the DRM at the tip, it also has to recognised that the tip input torque has an effect on the rotation angle, θ. Given a DRM at rest and since the shoulder joint is free to rotate then a torque input at the tip would have the obvious

effect on the tip, as it would start to vibrate, and as the vibrations are propagated through the DRM to the shoulder joint the angle θ would also rotate about its original position. This can be appreciated by inspection for a simple problem such as this one or by following the principle of virtual work to find the generalised input vector, Q for Equation (2.4.2), as done in (Junkins and Kim, 1993), among others.

The general equation of motion for the DRM with feedback control becomes:

$$\begin{bmatrix} M_{\theta\theta} & M_{\theta\alpha} & M_{\theta\beta} \\ M_{\theta\alpha}^T & M_{\alpha\alpha} & M_{\alpha\beta} \\ M_{\theta\beta}^T & M_{\alpha\beta}^T & M_{\beta\beta} \end{bmatrix} \begin{Bmatrix} \ddot{\theta} \\ \ddot{\alpha} \\ \ddot{\beta} \end{Bmatrix} + \begin{bmatrix} C_{\theta\theta} & C_{\theta\alpha} & C_{\theta\beta} \\ C_{\theta\alpha} & C_{\alpha\alpha} & C_{\alpha\beta} \\ C_{\theta\beta} & C_{\alpha\beta} & C_{\beta\beta} \end{bmatrix} \begin{Bmatrix} \dot{\theta} \\ \dot{\alpha} \\ \dot{\beta} \end{Bmatrix} + \begin{bmatrix} 0 & 0 & K_{\theta\beta} \\ 0 & K_{\alpha\alpha} & K_{\alpha\beta} \\ 0 & 0 & K_{\beta\beta} \end{bmatrix} \begin{Bmatrix} \theta \\ \alpha \\ \beta \end{Bmatrix} = \begin{bmatrix} 1 & 1 & 1 \\ 0 & 0 & 0 \\ 0 & 0 & \varphi'(a) \end{bmatrix} \begin{Bmatrix} S_T \\ T_1 \\ T_2 \end{Bmatrix} \tag{3.3.2}$$

This equation is simulated in Chapter 4, using some or all of the right hand side inputs to explore the DRM dynamics and its response to the different inputs.

3.4 Linear Closed Loop Control of the DRM

Vibrations can sometimes be avoided by the use of a control law with very small driving accelerations or by the shaped torques as shown in Sections 3.2.2 and 3.2.4. These shaped torques can produce long manoeuvre times, which are undesirable and inefficient in space construction. Vibrations can also be reduced passively, either by the choice of construction materials, or by the introduction of passive dampers at the joints. Finally, as proposed in Section 3.3, a closed loop vibration damping mechanism could be introduced to safely operate the manipulator with higher accelerations and thus speed up manoeuvre times. This section will introduce the feedback control law for the actuators proposed in the previous section based on linear velocity and displacement feedback control theory.

3.4.1 Root Linear Feedback Control Law

For the linear root actuator a feedback control law has been developed based on the linear combination of the states that can be measured. The velocities considered are the elastic reaction of the slew angle due to the vibrations, $\dot{\theta}_e$, this is the slew velocity as measured at the root, $\dot{\theta}$, (by a tachometer for example) with the reference rigid motion, $\dot{\theta}_r$, subtracted. The root feedback control law will also include θ_e, the difference between the actual slew angle at every point in time during a manoeuvre and the expected reference slew angle given from integrating the rigid inverse dynamics equation, Equation (3.2.1). Therefore the feedback quantities are,

$$\theta_e = \theta - \theta_r$$

$$\dot{\theta}_e = \dot{\theta} - \dot{\theta}_r$$

The root feedback control law is formulated as follows,

$$T_1 = K_1\dot{\theta}_e + K_2\theta_e \quad where, \quad K_1 \leq 0 \quad K_2 \leq 0 \tag{3.4.1}$$

The terms K_i are the tuneable damping and stiffness gains used. Selecting these gains can be a matter of simple trial and error to ensure that the vibrations are damped and the actuator is not constantly saturated. On the other hand a large set of linear control methods can be used to determine the optimum gains to provide a certain level of damping. These methods are well known in control theory and they include methods such as pole placement, LQR, LQG, etc.

Various sets of gains K_i have been tried in closed loop simulations to evaluate obtain the most satisfactory damped response. It has been found that gains cannot be optimised during the whole slew + length change manoeuvres. Since the inertia of the system is changing with time, the DRM has to be frozen at a particular length to use the traditional linear control techniques. For a particular length the gains can be found using one of the standard linear control techniques, and then tested by simulation for the whole manoeuvre, as the DRM slews and extends. This is clearly a sub-optimal application of linear control theory since whatever performance measure the gains are supposed to provide, is only given for one length of the DRM. One possible solution to this problem is to analyse the system for several different lengths and change gains throughout the manoeuvre in a step like manner, or to construct a time varying set of gains which depend explicitly on the extended length of link 2, length a.

Another consideration is the payload and again linear control methods can control accurately any system with a known set of parameters. For the DRM perhaps the most important parameter is the payload, its size and mass, and therefore its inertia, which can change considerably from task to task, from a set of replacement solar panels to a new

space telescope. It is thus impossible to simply prescribe a set of gains and expect them to work for each payload. A set of payloads would have to be analysed using the linear methods discussed above, to obtain appropriate gains for each case, for example a low payload inertia case, a medium case and a large case. At the time of operating a DRM the astronaut would decide where each payload fits, based on observations and construction data from the manufacturer, and would select that family of gains for the DRM feedback control. On the other hand a function could be formulated for each of the gains which includes not only the time varying length a, as mentioned above, but also the payload's mass and inertia. This last solution would create a function from fitting a polynomial curve, for example, to approximate the gains calculated by the linear control method for each DRM length and possible payload.

It was concluded that approaches such as step changes of the gains or complicated gain fitting functions while plausible are not very satisfactory for several reasons. First, changing the gains in a step manner during a manoeuvre could prove to be counter productive in its application since it could represent a sudden shock input to the system as the transition is made from one to another. Second, while the complete range of DRM length changes can be easily anticipated and studied, since it's a simple linear motion, the number of possible payloads is hard to predict and therefore the feedback control system would be limited to a set of payloads, for any other payload it could only provide approximate damping, not being able to guarantee the requirements that the control system were designed to (settling time, etc). Third, with a set of constantly changing feedback gains the task of ensuring the stability of the system could be affected. It is assumed that since the gains would be developed using proven linear techniques that the stability of the DRM control system would never be compromised but since we are

applying it to a time varying system it is possible that some configuration leads to problems, mathematical certainty that none of the possible inputs of the feedback controllers will produce problems is not complete.

Following the arguments above, a limited amount of space will be devoted to linear feedback control methods. Only one example of linear feedback control of the DRM is presented in this thesis, and it must be clear that it is not intended to be a comprehensive application of linear control theory, but the example presented should serve as a comparison to the second control method proposed, given in the next section. This is the Lyapunov derived feedback control law method.

3.4.2 Tip Linear Feedback Control Law

The linear feedback tip control law is developed based on the feedback of the velocity of vibration at the tip. The vibration can be measured by integrating the output of an accelerometer for example. Having the actuator and sensor collocated on the DRM is important to minimise reaction time between sensing the vibration and applying the control torque.

The proposed damping control law is based on the tip velocity of the DRM:

$$T_2 = J\dot{y}_2(a,t) \quad where, \quad J \leq 0 \tag{3.4.2}$$

J is a tuneable gain, the selection of which is based on preventing excessive continuous saturation of the actuator based on simulation results. In other words ensuring that the feedback torque is within the limits as stated in Table 3-1, this clearly limits the speed of response of the control system since the damping control torque is limited.

Continuing the discussion from the previous section the gain for the tip feedback controller should be selected for each payload and DRM length. To provide similar

levels of damping with the tip controller for a range of payloads the gain J would have to change. In this case the time varying length $a(t)$ would have little effect on the tip control law, the actuator is trying to damp out tip vibrations, so as long as the vibration speed is measured correctly and fed back with the right phase the vibrations will be reduced. The fact that the DRM may be fully extended or not is not important, the vibrations will be damped out regardless of the DRM length, within the capabilities of the actuator.

Since the tip actuator is bound, and control input limited, as shown in Table 3-1, it must be accepted that it will not be able to provide the same level of damping for every payload. Therefore, the fixed gain J will be based on not saturating the actuator for a fully extended DRM while carrying a medium size payload. The implementation of this control law is presented in Section 4.6.1, below.

It is important to comment here on the fact that feeding the tip velocity as shown in Equation (3.4.2) could potentially feed energy into the high vibration modes of the system, the ones not properly modelled. This could have the effect of increasing instead of reducing the tip vibrations which would be very detrimental for DRM operations. Therefore a filter should be included to make sure the tip actuator doesn't feedback unwanted torques.

3.5 Lyapunov Closed Loop Control

Lyapunov stability theory has been used to produce stable control laws mainly for non-linear dynamical systems as shown in the references by Slotine and Li, (1991), Juang, Yang and Huang, (1989), Junkins and Kim, (1993). The DRM dynamic formulation has been linearised for the most part in Chapter 2 when the linear deployment dynamics were separated from the slewing dynamics, by not considering the influence of the geometric stiffness term, $y_i\dot{\theta}$, in the direction of the deployment of link 2. It is not immediately apparent why a traditionally non-linear control design method such as Lyapunov stability theory is being applied. The DRM is a time-varying dynamical system and, as can be seen from the linear control section, to maintain the same level of performance from a linear controller throughout a slew manoeuvre while deploying link 2, the feedback damping gains have to be actively changed during the manoeuvre. More importantly, the damping gains have to be changed considerably from one payload to another even when no deployment of link 2 occurs, so a database of possible gains would have to be kept for all the different payload possibilities. This seems like a satisfactory option when there are only a few payloads and their mass and size is well known. In the case of the proposed manipulator, it would be used for space construction, launching satellites, replacing solar panels, etc the payload's mass and dimensions may not be exactly known and there will be many different payloads. It would then be very useful to have a vibration control system with fixed gains that works for different payloads and has a certain amount of robustness to deal with erroneous or approximate payload information.

Lyapunov stability theory is used in this section to produce a stable, robust closed loop control law. This control law can cope with the time varying nature of the

manipulator dynamics, with different size payloads and with payload mass errors. The control law can also accomplish the desired slew with the minimum of vibrations throughout the manoeuvre and reach the desired slew angle with no residual vibrations.

3.5.1 Lyapunov Theory

The basic fundamental principle of Lyapunov's direct method is the observation that if the total disturbance (error) energy of a system is continuously dissipated, then the system must eventually settle down to rest or to an equilibrium point (Slotine and Li, 1991). The method proceeds by formulating an energy-like function, $\mathbf{U}(x)$, for the dynamical system, called the Lyapunov function, where x is the vector of states of the system. Through $\mathbf{U}(x)$, the control laws for the actuators can be formulated guaranteeing that the system will be asymptotically stable. For stability, the following conditions must hold for the Lyapunov function at all times:

$$\begin{aligned} &\mathbf{U}(x) > 0 \qquad x \neq x_t \\ &\mathbf{U}(x_t) = 0 \\ &\dot{\mathbf{U}}(x) < 0 \qquad x \neq x_t \end{aligned} \tag{3.5.1}$$

The vector x_t represent the system states desirable for the system, or Target State. The objective is to differentiate the Lyapunov function, $\mathbf{U}(x)$, with respect to time, substitute the equations of motion and the boundary conditions of the system and ensure that the control inputs make $\dot{\mathbf{U}}(x)$ as negative as possible and thus move every initial state to the target state as fast as possible.

The Lyapunov function is an energy-like expression containing the dynamical system's energies to be controlled. The control system designer decides how much or how little information goes into the Lyapunov function. If all of the energy information goes into the function, its mathematical complexity may become a severe problem when

the time derivative has to be calculated. A complex Lyapunov function, $\mathbf{U}(x)$, could also produce a very complicated feedback control law that would be very hard to implement. On the other hand, a function that is too simple will not capture all of the important elements of the disturbance energy necessary to control the dynamical system. Therefore the first step in using the Lyapunov method for control law design is to decide how much or how little energy information to include in the Lyapunov function. The application of this method to the DRM feedback control law formulation is given below.

3.5.2 Lyapunov Theory Application

As described above this method is a '*brute force*' mathematical method. If enough energy information is provided about any system, no matter how non-linear or time varying the system is, a stabilising control law can be found. The clear drawback to this is that too much information in $\mathbf{U}(x)$ can make the result very difficult to obtain mathematically or impossible to implement due to its complexity. Too little information in $\mathbf{U}(x)$ could produce an unsatisfactory control law that cannot control the real system correctly. The control system designer therefore has to select what to include in the Lyapunov function.

For the application of the Lyapunov direct method to the design of a control law for the DRM the system is simplified. This corresponds to assuming that the actual system to be controlled has less degrees of freedom than it actually has, the Lyapunov direct method is applied and a feedback control law is found. The feedback control law found will control the vibrations of the simplified system exactly as it is expected. That feedback control law based of the simplified dynamical system is then applied to the real

system to ensure that it can be controlled within the specified vibration response criteria, if it does then the control law is validated.

The feedback control law developed in this section is based on the output information and not in a full state feedback, since all of the states cannot be easily measured. The outputs that can be measured are assumed to be the slew angle, slew rate, tip vibration amplitude and tip vibration rate, θ, $\dot{\theta}$, $y_2(a)$, $\dot{y}_2(a)$. The use of only these quantities in the feedback control law means that no information on the flexible deflection of link 1 shall be included in the Lyapunov function. This means that the simplified Lyapunov system used to formulate the control law is a DRM with link 1 considered rigid like the P-DRM defined in Section 2.3.

The proposed Lyapunov energy function, **U**(x), comes from the energy expressions in Section 2.2, which are simplified to reduce the mathematical complexity of the Lyapunov function, the simplifications are as follows:

1. The Kinetic Energy is taken from the expressions formulated in Equations (2.2.1), (2.2.2), (2.2.3) and (2.2.4) with y_1 set equal to zero (link 1 is assumed rigid).
2. The quantity $y_2\dot{\theta}$ is not considered in the formulation since its perpendicular to the slew direction and it is a small contribution to the transverse vibrations of the DRM for small values of $\dot{\theta}$, the slew rate.
3. The kinetic energy contributions due to the velocity term $\dot{a}(t)$, are not included in the Lyapunov function, since the deployment is predetermined, therefore $\dot{a}(t) = 0$ in this development. As in the developments in Chapter 2, the change in length of link 2 is not a degree of freedom of the system and cannot be used as a control input.

4. The length, $L_p/2$ is assumed small in Equation (2.2.4), and the elastic slope term, $\frac{1}{2}L_p\dot{y}_2'(a)$ is not considered. This assumes a small payload overhang, compared to the overall length of the manipulator, at the end of the DRM consistent with the findings of Section 2.5 which limit the size of payload that can be correctly modelled with the assumed modes model.
5. The Potential Energy of the P-DRM is included in the Lyapunov function by considering only the bending energy of link 2 from Equation (2.2.7).

The simplified system is a partly flexible DRM, with only the sliding link considered flexible, that is composed of the following kinetic and potential energy expressions:

$$T_T = \frac{1}{2}\rho_1\int_0^{L_1}\left(x\dot{\theta}\right)^2 dx + \frac{1}{2}\rho_2\int_{L_1-b}^{L_1}\left(x\dot{\theta}\right)^2 dx + \frac{1}{2}\int_0^a \rho_2\left((L_1+x)\dot{\theta}+\dot{y}_2(x)\right)^2 dx + \frac{1}{2}M_p\left[(L_1+a)\dot{\theta}+\dot{y}_2(a)\right]^2 + \frac{1}{2}I_{yy}\left[\dot{\theta}+\dot{y}_2'(a)\right]^2 \tag{3.5.2}$$

$$V_T = \frac{1}{2}\int_0^a EI_2\left(\frac{\partial^2 y_2}{\partial x^2}\right)^2 dx \tag{3.5.3}$$

where, a and b are the portions of link 2 outside and inside link 1 respectively, as shown in Figure 2.1, which for this development are assumed fixed so that their time derivatives will be zero. The feedback control law derived by this method will still be applicable to the time varying DRM. This is so, since the quantities a and b are contained in the formulation they will be fed into the control laws as link 2 is extended or contracted thus adjusting the level of feedback automatically. The introduction of these simplifications will clearly produce a less effective solution for the problem than can otherwise be found, but it enables the control laws produced to retain the most important elements of the dynamic response of the DRM.

The P-DRM system has the following rigid-body equation of motion for the slew angle θ_{ref}, the reference slew angle equation:

$$I_r\ddot{\theta}_{ref} = S_T - \left\{ I_{yy}\ddot{\theta}_{ref} + M_p(L_1+a)^2\ddot{\theta}_{ref} + \int_0^a \rho_2(L_1+x)^2\ddot{\theta}_{ref}dx \right\} \tag{3.5.4}$$

where:

$$I_r = \left[\frac{1}{3}\rho_1 L_1^3 + \frac{1}{3}\rho_2\left[L_1^3 - (L_1-b)^3\right]\right] \tag{3.5.5}$$

is the rigid moment of inertia of link 1 and the portion of link 2 contained inside link 1. The driving torque $S_T(t)$ is calculated using the assumed torque method of Section 3.2.

The reduced equations of motion for the flexible P-DRM consist of the slew angle equation of motion, θ, and the flexible beam equation for y_2:

$$I_r\ddot{\theta} = (S_T + T_1) - \left\{ \begin{matrix} I_{yy}\left(\ddot{\theta} + \ddot{y}_2'(a)\right) + M_p(L_1+a)\left[(L_1+a)\ddot{\theta} + \ddot{y}_2(a)\right] + \\ \int_0^a \rho_2(L_1+x)\left[(L_1+x)\ddot{\theta} + \ddot{y}_2\right]dx \end{matrix} \right\} \tag{3.5.6}$$

$$\rho_2\ddot{y}_2 + \rho_2(L_1+x)\ddot{\theta} + EI_2\frac{\partial^4 y_2}{\partial x^4} = 0 \tag{3.5.7}$$

these equations were formulated from the energies defined above, in Equations (3.5.2) and (3.5.3). The four boundary conditions for this simplified problem can be formulated as:

$$\begin{aligned} y|_{x=0} = 0 \quad , \quad y''|_{x=a} &= -\frac{T_2}{EI_2} - \frac{I_{yy}}{EI_2}\left(\ddot{\theta} + \ddot{y}'(a)\right) \quad \text{(Tip Bending Moment)} \\ y'|_{x=0} = 0 \quad , \quad y'''|_{x=a} &= \frac{M_p}{EI_2}\left[(L_1+a)\ddot{\theta} + \ddot{y}_2(a)\right] \quad \text{(Tip Shear Force)} \end{aligned} \tag{3.5.8}$$

The actuator torque at the tip, T_2, is included for completeness.

The Lyapunov function, U(x), is formulated as the error energy between the rigid body DRM, which would follow the reference trajectory defined by Equation (3.5.4), and the P-DRM motion as defined by Equation (3.5.6) and Equation (3.5.7). U(x) is

therefore given by Equation (3.5.2) plus Equation (3.5.3) minus Equation (3.5.2) with the terms involving y_2 set to zero:

$$\mathbf{U}(x) = A_1 \frac{1}{2}\int_0^{L_1} \left\{\rho_1 \left(x\dot{\theta}_e\right)^2\right\} dx + A_1 \frac{1}{2}\int_{L_1-b}^{L_1} \left\{\rho_1 \left(x\dot{\theta}_e\right)^2\right\} dx + A_3\theta_e^2$$
$$A_2\left[\begin{array}{l} \int_0^a \left\{\frac{1}{2}\rho_2\left((L_1+x)\dot{\theta}_e + \dot{y}_2(x)\right)^2 + EI_2\left(\frac{\partial^2 y_2}{\partial x^2}\right)^2\right\} dx + \\ \frac{1}{2}M_p\left[(L_1+a)\dot{\theta}_e + \dot{y}_2(a)\right]^2 + \frac{1}{2}I_{yy}\left(\dot{\theta}_e + \dot{y}_2'(a)\right)^2 \end{array}\right] \qquad (3.5.9)$$

where $\theta_e = \theta - \theta_{ref}$ and $\dot{\theta}_e = \dot{\theta} - \dot{\theta}_{ref}$ are the errors detected during a slew manoeuvre in the rigid degree of freedom position and velocity. The measured quantity during a manoeuvre is θ, and θ_{ref} is the reference quantity calculated either on-line or before the manoeuvre, from the manipulator's rigid model, Equation (3.5.4). The values A_i are positive coefficients to place emphasis on certain sections of the energy. The last term involving, θ_e^2, is a pseudo-energy term to track and correct the rigid rotation angle error during the manoeuvre and to make its equilibrium point the prescribed rotation angle (Junkins and Kim, 1993). The equilibrium point for the system, or desired Target State is:

$$\left(\theta_e, \dot{\theta}_e, y_2, \dot{y}_2\right) = (0,0,0,0) \qquad (3.5.10)$$

Any deviation from the Target State will guarantee that $\mathbf{U}(x) > 0$ and the target state guarantees that $\mathbf{U}(x_t) = 0$ as specified in equation (3.5.1). The time derivative, $\dot{\mathbf{U}}(x)$, has to be calculated from equation (3.5.9), and in the next section the control laws are formulated which guarantee that $\dot{\mathbf{U}}(x)$ is negative.

The time derivative of the Lyapunov function, neglecting $\dot{a}(t)$ and $\dot{b}(t)$ as discussed above, is given by:

$$\dot{U}(x) = \dot{\theta}_e \begin{Bmatrix} A_1 I_r \ddot{\theta}_e + A_3 \theta_e + A_2 \int_0^a \rho_2 (L_1 + x)\left[(L_1 + x)\ddot{\theta}_e + \ddot{y}_2\right] dx \\ A_2 I_{yy}\left(\ddot{\theta}_e + \ddot{y}_2'(a)\right) + A_2 M_p (L_1 + a)\left[(L_1 + a)\ddot{\theta}_e + \ddot{y}_2(a)\right] \end{Bmatrix} +$$
$$A_2 \begin{bmatrix} \int_0^a \dot{y}_2 \rho_2 \left[(L_1 + x)\ddot{\theta}_e + \ddot{y}_2\right] dx + I_{yy}\dot{y}_2'(a)\left(\ddot{\theta}_e + \ddot{y}_2'(a)\right) \\ M_p \dot{y}_2(a)\left[(L_1 + a)\ddot{\theta}_e + \ddot{y}_2(a)\right] \end{bmatrix} + \tag{3.5.11}$$
$$\frac{d}{dt}\left[A_2 \int_0^a EI_2 \left(\frac{\partial^2 y_2}{\partial x^2}\right)^2 dx \right]$$

where I_r is the moment of inertia of the rigid section of the manipulator. The last term above is:

$$\frac{d}{dt}\left[A_2 \int_0^a EI_2 \left(\frac{\partial^2 y_2}{\partial x^2}\right)^2 dx \right] = A_2 EI_2 \frac{d}{dt}\left[\int_0^a \left(\frac{\partial^2 y_2}{\partial x^2}\right)\left(\frac{\partial^2 y_2}{\partial x^2}\right) dx \right] \tag{3.5.12}$$

integrating by parts with $u = \left(\frac{\partial^2 y_2}{\partial x^2}\right) = y_2''$ and $dv = \left(\frac{\partial^2 y_2}{\partial x^2}\right) = y_2''$ gives the following result, where for simplicity the notation of the partial derivative of y_2 with respect to x has been changed to the prime operator, $(\,)'$. The result of the integral is:

$$A_2 EI_2 \frac{d}{dt}\left[y_2'' y_2' \Big|_0^a - \int_0^a y_2' y_2''' dx \right] \tag{3.5.13}$$

integrating the remaining integral by parts with $u = y_2'''$ and $dv = y'$ gives the following expression:

$$A_2 EI_2 \frac{d}{dt}\left[y_2'' y_2' \Big|_0^a - y_2''' y_2 \Big|_0^a + \int_0^a y_2 y_2^{IV} dx \right] \tag{3.5.14}$$

which on expansion gives:

$$A_2 EI_2 \frac{d}{dt}\left[\left(y_2''(a) y_2'(a) - y_2''(0) y_2'(0)\right) - \left(y_2'''(a) y_2(a) - y_2'''(0) y_2(0)\right) + \int_0^a y_2 y_2^{IV} dx \right] \tag{3.5.15}$$

the boundary conditions of the P-DRM, Equation (3.5.8), can now be substituted into equation (3.5.15). Substituting the boundary conditions for $x=0$ into the expression is simplified, since $y_2(0)$ and $y_2'(0)$ must be zero, hence equation (3.5.15) becomes:

$$A_2EI_2\frac{d}{dt}\left[y_2''(a)y_2'(a)-y_2'''(a)y_2(a)+\int_0^a y_2y_2^{IV}dx\right] \tag{3.5.16}$$

having a time derivative given by:

$$A_2EI_2\left[\begin{array}{l}\left(\dot{y}_2''(a)y_2'(a)+y_2''(a)\dot{y}_2'(a)\right)-\left(\dot{y}_2'''(a)y_2(a)+y_2'''(a)\dot{y}_2(a)\right)+\\ \int_0^a\left(\dot{y}_2y_2^{IV}+y_2\dot{y}_2^{IV}\right)dx\end{array}\right] \tag{3.5.17}$$

where the terms $\dot{y}_2''(a)$, $\dot{y}_2'''(a)$ and $\dot{y}_2^{IV}(a)$ are of second order and hence can be neglected. This simplification implies that the time rate of change of the curvature of the tip, and the higher partial derivatives, are small when compared to the time rate of change of the slope of the flexible link at the tip, $\dot{y}_2'(a)$, and of the velocity, $\dot{y}_2(a)$. This is a reasonable assumption for small acceleration manoeuvres which will not induce a significant curvature at the tip of link 2. Using this simplification, equation (3.5.17) reduces to:

$$A_2EI_2\left[y_2''(a)\dot{y}_2'(a)-y_2'''(a)\dot{y}_2(a)+\int_0^a\dot{y}_2y_2^{IV}dx\right] \tag{3.5.18}$$

Which on substituting equation (3.5.8), gives:

$$A_2EI_2\left\{\begin{array}{l}\left[-\frac{T_2}{EI_2}-\frac{I_{yy}}{EI_2}\left(\ddot{\theta}+\ddot{y}'(a)\right)\right]\dot{y}_2'(a)-\\ \left[\frac{M_p}{EI_2}\left[(L_1+a)\ddot{\theta}+\ddot{y}_2(a)\right]\right]\dot{y}_2(a)+\int_0^a\dot{y}_2y_2^{IV}dx\end{array}\right\} \tag{3.5.19}$$

which can be substituted back into the Lyapunov time derivative, equation (3.5.11), and collecting common terms gives the following result:

$$\dot{U}(x) = \dot{\theta}_e \left\{ \begin{matrix} A_1 I_r \ddot{\theta}_e + A_3 \theta_e + A_2 \int_0^a \rho_2 (L_1 + x)\left[(L_1 + x)\ddot{\theta}_e + \ddot{y}_2\right] dx \\ A_2 I_{yy}\left(\ddot{\theta}_e + \ddot{y}_2'(a)\right) + A_2 M_p (L_1 + a)\left[(L_1 + a)\ddot{\theta}_e + \ddot{y}_2(a)\right] \end{matrix} \right\} +$$
$$A_2 \int_0^a \dot{y}_2 \left\{ \rho_2 \left[(L_1 + x)\ddot{\theta}_e + \ddot{y}_2\right] + EI_2 y_2^{IV} \right\} dx + \qquad (3.5.20)$$
$$A_2 \left[I_{yy} \dot{y}_2'(a)\left(\ddot{\theta}_e + \ddot{y}_2'(a)\right) - I_{yy} \dot{y}_2'(a)\left(\ddot{\theta} + \ddot{y}_2'(a)\right) - \dot{y}_2'(a) T_2 \right] +$$
$$A_2 \left\{ M_p \dot{y}_2(a)\left[(L_1 + a)\ddot{\theta}_e + \ddot{y}_2(a)\right] - M_p \dot{y}_2(a)\left[(L_1 + a)\ddot{\theta} + \ddot{y}_2(a)\right] \right\}$$

clearly the last two brackets simplify further by subtracting the similar terms, identifying that by definition, $\ddot{\theta}_e = \ddot{\theta} - \ddot{\theta}_{ref}$. The final expression for the Lyapunov function time derivative then becomes:

$$\dot{U}(x) = \dot{\theta}_e \left\{ \begin{matrix} A_1 I_r \ddot{\theta}_e + A_3 \theta_e + A_2 \int_0^a \rho_2 (L_1 + x)\left[(L_1 + x)\ddot{\theta}_e + \ddot{y}_2\right] dx \\ A_2 I_{yy}\left(\ddot{\theta}_e + \ddot{y}_2'(a)\right) + A_2 M_p (L_1 + a)\left[(L_1 + a)\ddot{\theta}_e + \ddot{y}_2(a)\right] \end{matrix} \right\} +$$
$$A_2 \int_0^a \dot{y}_2 \left\{ \rho_2 \left[(L_1 + x)\ddot{\theta}_e + \ddot{y}_2\right] + EI_2 y_2^{IV} \right\} dx + \qquad (3.5.21)$$
$$A_2 \left[- I_{yy} \dot{y}_2'(a)\ddot{\theta}_{ref} - \dot{y}_2'(a) T_2 \right] + A_2 \left\{ - M_p \dot{y}_2(a)(L_1 + a)\ddot{\theta}_{ref} \right\}$$

Equation (3.5.21) has to be made negative to guarantee that the control system will drive the DRM to the equilibrium point as required by equation (3.5.10). Through the boundary condition substitutions, performed above, the tip control input T_2 was introduced for completeness. The DRM simulation cases, with and without tip control, will be presented and discussed in the next section and results for both cases will be shown in Chapter 4.

3.5.3 Lyapunov Control Law Formulation

The closed loop control laws, for the root and tip actuators, are obtained from Equation (3.5.21). The next step is to introduce the root control input of the DRM into Equation (3.5.21) to ensure that it is negative at all times, and thus make the closed loop control system stable. This is done by identifying the structure of the known dynamic

equations for the DRM, Equations (3.5.4) to (3.5.7) in Equation (3.5.21) and substituting for them to introduce the actuator control input, T_1.

3.5.3.1 Lyapunov Root Actuator Control Law

Substituting Equations (3.5.4) and (3.5.6) into the $\dot{\theta}_e$ bracket of equation (3.5.21), and Equation (3.5.7) into the integral term, which makes the term zero, gives the new expression for the time derivative of the Lyapunov function:

$$\begin{aligned}\dot{U}(x) = \dot{\theta}_e \left\{ \begin{array}{l} A_1 T_1 + A_4 \theta_e + (A_2 - A_1)\int_0^a \rho_2 (L_1 + x)\left[(L_1 + x)\ddot{\theta}_e + \ddot{y}_2\right] dx \\ (A_3 - A_1) I_{yy}\left(\ddot{\theta}_e + \ddot{y}_2'(a)\right) + (A_2 - A_1) M_p (L_1 + a)\left[(L_1 + a)\ddot{\theta}_e + \ddot{y}_2(a)\right] \end{array} \right\} + \\ A_2 \int_0^a \dot{y}_2 \left\{ -\rho_2 (L_1 + x)\ddot{\theta}_{ref} \right\} dx + \\ A_2 \left[-I_{yy}\dot{y}_2'(a)\ddot{\theta}_{ref} - \dot{y}_2'(a) T_2 \right] + A_2 \left\{ -M_p \dot{y}_2(a)(L_1 + a)\ddot{\theta}_{ref} \right\}\end{aligned} \tag{3.5.22}$$

which now includes the control inputs T_1, the actuator torque at the base, and T_2, the actuator torque at the tip. If the $\dot{\theta}_e$ bracket is now set equal to $-A_5\dot{\theta}_e$ then as long as $A_5 > 0$, that section of $\dot{U}(x)$ is guaranteed to be negative. The result, when solved for the control input T_1, gives:

$$\begin{aligned}T_1 = -\frac{A_5}{A_1}\dot{\theta}_e - \frac{A_3}{A_1}\theta_e - \frac{(A_2 - A_1)}{A_1}\int_0^a \rho_2 (L_1 + x)\left[(L_1 + x)\ddot{\theta}_e + \ddot{y}_2\right] dx - \\ \frac{(A_2 - A_1)}{A_1} I_{yy}\left(\ddot{\theta}_e + \ddot{y}_2'(a)\right) - \frac{(A_2 - A_1)}{A_1} M_p (L_1 + a)\left[(L_1 + a)\ddot{\theta}_e + \ddot{y}_2(a)\right]\end{aligned} \tag{3.5.23}$$

this equation can be simplified by substituting the ratio of positive coefficients A_i by another set of coefficients J_i that must satisfy the rules shown below:

$$\begin{aligned}T_1 = -J_1\dot{\theta}_e - J_2\theta_e - J_3\int_0^a \rho_2 (L_1 + x)\left[(L_1 + x)\ddot{\theta}_e + \ddot{y}_2\right] dx - J_3 I_{yy}\left(\ddot{\theta}_e + \ddot{y}_2'(a)\right) - \\ J_3 M_p (L_1 + a)\left[(L_1 + a)\ddot{\theta}_e + \ddot{y}_2(a)\right] \\ J_1 \geq 0 \quad J_2 \geq 0 \quad J_3 > -1\end{aligned} \tag{3.5.24}$$

This substitution from the A_i coefficients to the J_i is done only for convenience. The J_i coefficients now become the tuneable gains for the closed loop control law, and they will be selected to prevent excessive saturation of the feedback control actuator. The gains are related to the original A_i gains used to place emphasis on different sections of the energy in the Lyapunov function by simple arithmetic relationships. The control law developed for T_1 in equation (3.5.24) is not dependent on the discretization method used for y_2, or on how many terms are retained in the approximation, it is a general, stabilising closed loop control law.

3.5.3.2 Lyapunov Tip Actuator Control Law

The next step in the development requires finding a control law for the tip actuator, which together with Equation (3.5.24) ensures that Equation (3.5.22) is negative at all times. Substituting Equation (3.5.24) into (3.5.22) produces the following expression for the Lyapunov function time derivative:

$$\dot{U}(x) = -A_5\dot{\theta}_e^2 - A_2\left[\begin{array}{l}\int_0^a \dot{y}_2\left\{\rho_2(L_1+x)\ddot{\theta}_{ref}\right\}dx + I_{yy}\dot{y}_2'(a)\ddot{\theta}_{ref} + \\ \dot{y}_2'(a)T_2 + M_p\dot{y}_2(a)(L_1+a)\ddot{\theta}_{ref}\end{array}\right] \qquad (3.5.25)$$

The first term of Equation (3.5.25) is clearly always negative or zero. The rest of the terms in the equation must be guaranteed negative, or at least zero. Following the latter idea the bracket of equation (24), containing T_2 is equated to zero:

$$\int_0^a \dot{y}_2\left\{\rho_2(L_1+x)\ddot{\theta}_{ref}\right\}dx + I_{yy}\dot{y}_2'(a)\ddot{\theta}_{ref} + \dot{y}_2'(a)T_2 + M_p\dot{y}_2(a)(L_1+a)\ddot{\theta}_{ref} = 0 \qquad (3.5.26)$$

A control law for T_2 is now chosen based on this equation. Through many simulations of the DRM, the use of many different tip control laws and some basic logic rather than strict mathematical rules a tip control law has been found inspired on Equation (3.5.26).

The basic change to make to Equation (3.5.26) is to assume that the T_2 multiplier is $\ddot{\theta}_{ref}$ and not $\dot{y}_2'(a)$ as it is shown. This development can only be justified by the results shown in Chapter 4, as it provides better overall control than any other formulation tried. The velocity control law for the tip reaction wheel finally becomes:

$$T_2 = -\int_0^a \dot{y}_2 \{\rho_2(L_1 + x)\}dx - I_{yy}\dot{y}_2'(a) - M_p\dot{y}_2(a)(L_1 + a) \qquad (3.5.27)$$

where a is time varying. Essentially this expression takes $\ddot{\theta}_{ref}$ out from equation (3.5.26), as if it was a common term. This tip control law for the reaction wheel is implemented together with equation (3.5.24) as the non-linear feedback control law for the DRM. Only the mathematical formulation of these expressions is included here, its implementation and a short discussion on its realisation is included in the DRM simulations is shown in Section 4.6.2.2, below. It is also noted explicitly here that the tip control law is not strictly Lyapunov, but rather "pseudo-Lyapunov" and its response characteristics is given by simulation in the following chapter.

3.5.4 Lyapunov Control System Observations

A few observations with respect to the application of the derived control laws, Equations (3.5.24) and (3.5.27). First, the open loop slew control law and the Lyapunov closed loop control laws presented may at some times work against each other and some times in co-operation when slewing a payload. This is, of course, a result of the robustness requirement on the control system and adds a certain amount of redundancy. Second, the control laws contain the acceleration rates of the error in the slew angle and of the tip vibration. These acceleration rates have been estimated in the simulations by using the measured output rates, assuming a linear variation over a small time interval,

and calculating the accelerations by the finite difference method. The equations are simply:

$$\ddot{y}_2 = \frac{\dot{y}_2}{t_s}, \qquad \ddot{\theta}_e = \frac{\dot{\theta}_e}{t_s}$$

where t_s is the sampling time, the time between measurements of the output, which is an order of magnitude larger than the integration time step in the simulation. Through different simulation attempts it has been found that for this problem the sampling time of 2×10^{-3} seconds and an integration step time of 5×10^{-4} of seconds adequately capture the DRM behaviour. Smaller quantities delay the simulation execution considerably and with larger time steps the higher frequency dynamics of the DRM are not properly captured.

Chapter 4 : Simulation Results

This Chapter presents the computed results for the DRM slew manoeuvre. The approximate equations of motion from Section 2.5.2 were integrated using the simulation program ACSL (MGA Software, 1995) on a personal computer, using Runge-Kutta fourth order with a fixed time step of $5x10^{-4}$ seconds (as shown in Appendix D). The state variables of the system were recorded at every time step. The results give the manipulator vibrations superimposed on the mean instantaneous position of the DRM at the payload end. Other data may also be presented if considered relevant to illustrate particular points in the discussion.

Section 4.1, presents and discusses the formulation programming and verification, which checks the DRM simulation program for accuracy. The latter is fundamental to establish if the computer simulations are correct and if the program is working correctly. Section 4.2 gives the results for the open loop slews using the torque profiles from Section 3.2. Section 4.3 presents power consumption results for the main slew motor of the DRM using the different open loop slew acceleration profiles. Section 4.4 presents the dynamic response of the DRM undergoing extension and retraction of link 2. Section 4.5 presents the robustness of the open loop control law, the slew results to manoeuvre a payload with the incorrect information. Section 4.6 presents slew

manoeuvre results together with the closed loop control laws developed in sections 3.4 and 3.5. Finally in Section 0 the closed loop results and compared and discussed.

4.1 Program Verification

In modelling a two-body flexible system, such as the DRM, a question concerning the validity of the dynamic modelling formulation and the computer code arises. For the former, a certain amount of validation of the formulation has been performed in Section 2.6, where the natural frequency analysis using the approximate formulation was compared with the exact solutions. For the computer code validity, the assessment of its accuracy presents a challenging task since it cannot be compared directly to any other existing code, as it is a one off program. In addition, the internal inaccuracies of the computer processor, the program compiler and the operating system could play a role in introducing certain biases or miscalculations.

The simplest way of checking both formulation accuracy and code validity would be the comparison with a formulation for the same system, obtained independently by another researcher and reported in the open literature. This has not been found to date and therefore a different way of assessment has to be used. To validate the computer code the two following tasks will be performed:

1. To monitor the system total energy to assure its conservation.
2. To compare other published results with the formulation in this thesis.

The first task can be easily done for any DRM configuration, given a set of initial conditions the system total kinetic and strain energies can be compared to ensure that the energy is conserved. The second task involves using the simulation code to reproduce results in the open literature.

4.1.1 Open-Loop Energy Conservation

It is important to check whether the system's total energy is conserved in the formulation programmed. This is confirmed by running a simulation in which no deployment or slew of the DRM is carried out but with non-zero initial conditions. The initial conditions are a fully deployed DRM carrying Payload 1 of Table 2-7 and an initial deflection at the tip of link 2 of 2 cm. The computer simulation is started with those initial conditions and the total energy, the kinetic and strain energy levels over a given time period with no feedback damping are plotted in Figure 4.1, and Figure 4.2 respectively.

The results shown in the figures confirm that the energy is conserved through the simulation. While the test is very simple it is important to establish whether the formulation programmed is stable and that no 'bugs' have crept into the code. The potential and kinetic energies are exactly 180 degrees out of phase as expected. At $t=0$ the initial condition is a deflection of link 2 of 2 cm and since there is no structural or feedback damping introduced into the dynamic formulation of the DRM the vibrations are continued in time as shown in Figure 4.3. The deflection of the tip periodically returns to its maximum value of 2 cm as expected. The superposition of the two frequencies of vibration for the 2 degree of freedom model can be seen from the result figures.

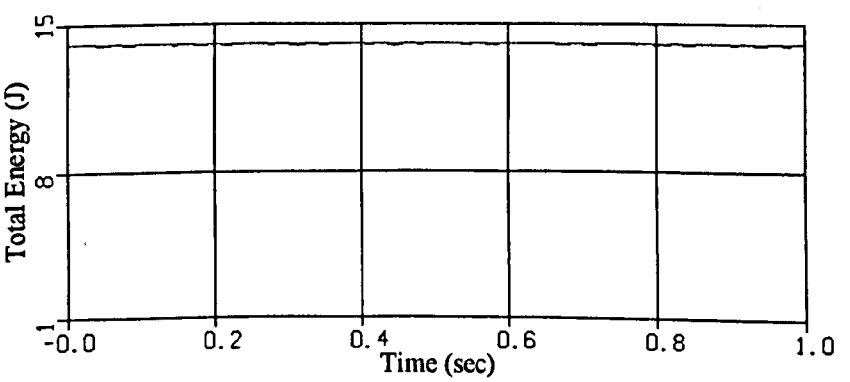

Figure 4.1: DRM Total Energy for an initial tip deflection of 2 cm

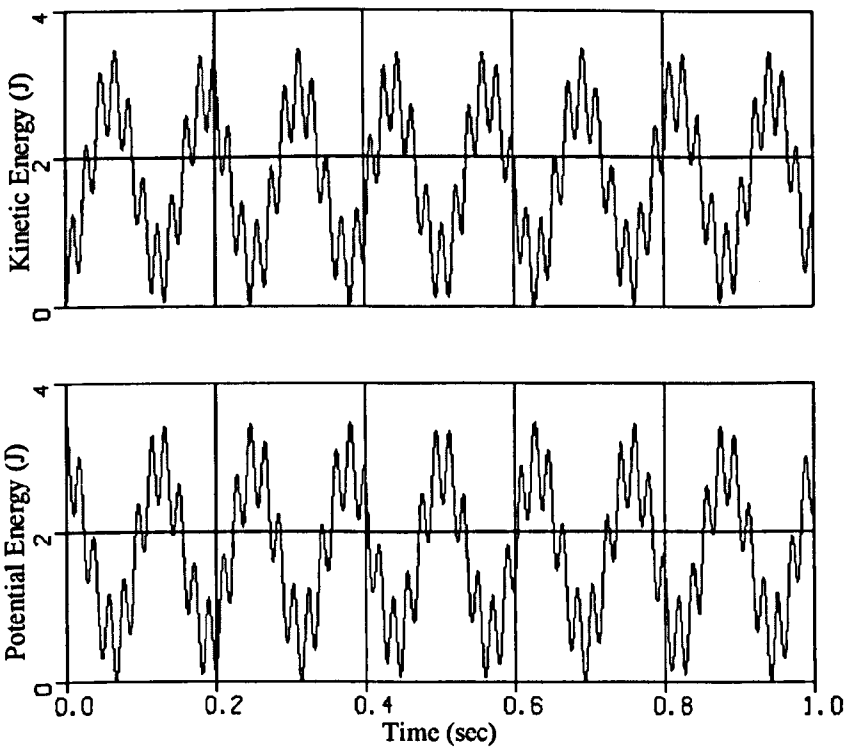

Figure 4.2: DRM Kinetic and Potential Energy conservation for an initial tip deflection of 2 cm

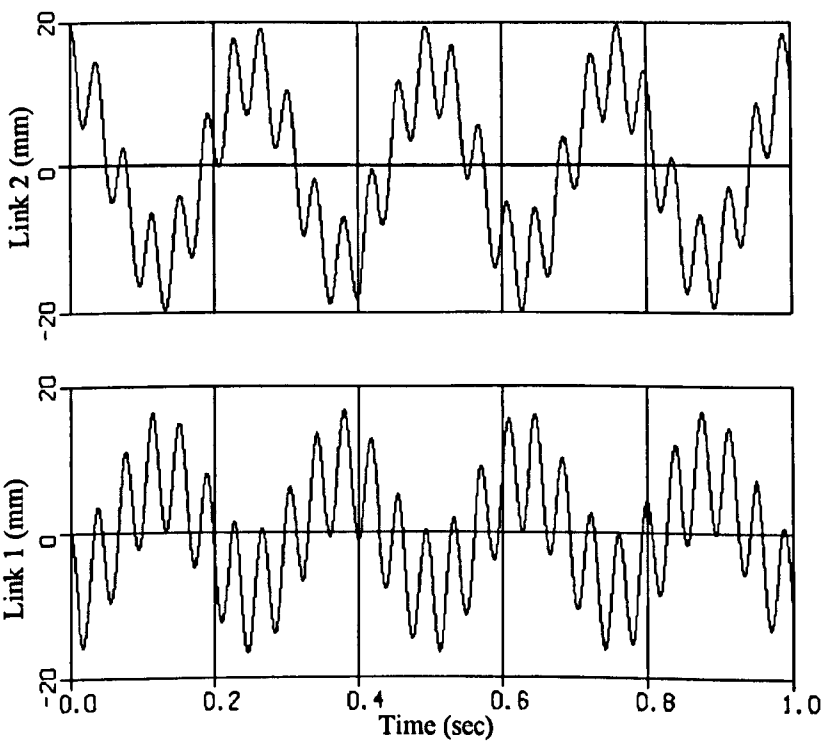

Figure 4.3: DRM link deflections for an initial link 2 tip deflection of 2 cm

4.1.2 Comparison to a similar reported system

The DRM dynamic modelling and computer simulation can be validated by attempting to reproduce the results from an independent researcher and reported in the open literature. Since no exact match to the DRM is reported elsewhere, the formulation and code for the DRM are used to reproduce the results of a similar system. The system to be simulated should have similar characteristics to the DRM, such as a long flexible system of some kind so that only a few parameters will have to be changed to reproduce the test system, no modifications to the code will be necessary.

The simplest candidate to reproduce with the DRM code is the single link fixed length flexible manipulator, which has been frequently studied in the open literature (Jnifene and Fahim, 1997), (Tohki and Azad, 1995 and 1996), (Choura et al., 1991), (Pun and Semercigil, 1997), (Bayo, 1987), (Wang and Vidyasagar, 1992), etc. In the simulation model built for the DRM the length, mass and EI are set to zero for link 1, so that link 2 becomes the single link of the system. The deployment of link 2 is not active during the simulation. The physical characteristics of link 2 are matched to those described in the referenced publication and the input torque to the system is replicated.

The results to be compared are in a paper by Jnifene and Fahim, (1997). This paper presents a time delay approach to the tip control of a single-link flexible manipulator. The results from Figure 4.4 are taken from the publication, which shows the tip vibrations with zero structural damping performing slew manoeuvre without considering geometric stiffness effects. Figure 4.5 shows the results obtained with the programmed DRM simulator. The results agree exactly showing that the DRM formulation programmed is, at least partially, verified.

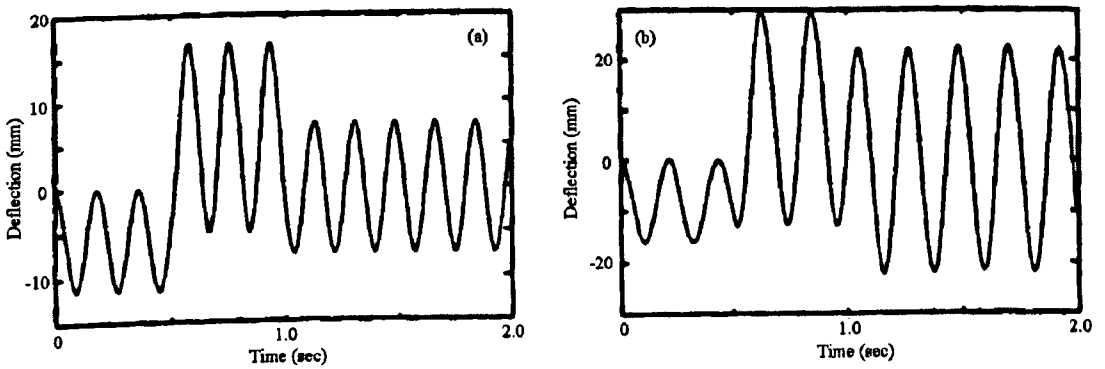

Figure 4.4: Results from Jniffene and Fahim, (1997) open loop slew of a single link flexible manipulator unloaded in (a) and with a tip mass of 0.1 Kg in (b)

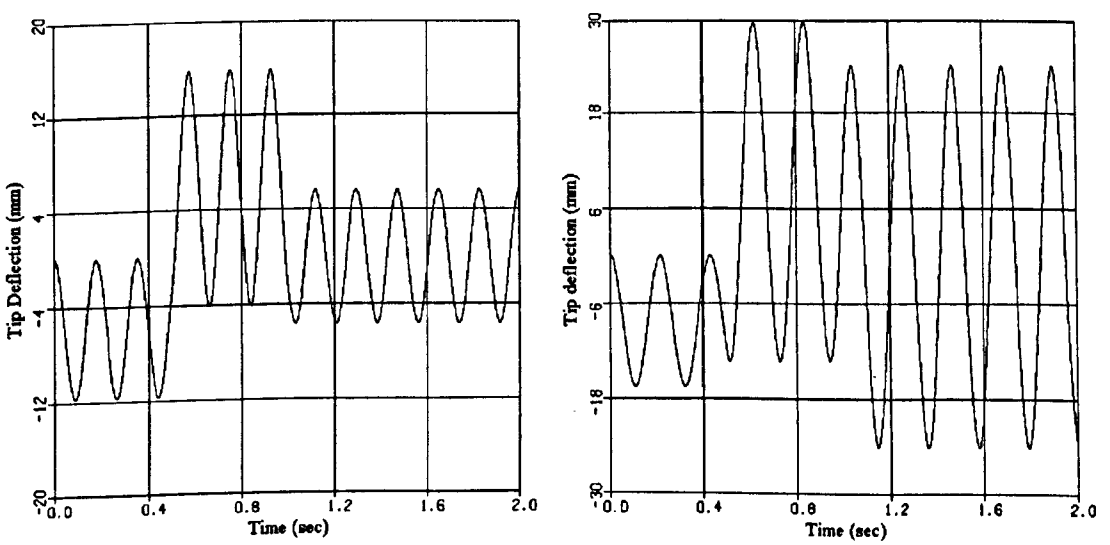

Figure 4.5: Reproduction of results in Jniffene and Fahim, (1997). Slew of a single link flexible manipulator both unloaded and with a tip mass of 0.1 Kg

4.2 Open Loop Undamped Results

The open loop slew results come from applying an assumed torque solution to the DRM with one of the angular acceleration profiles of Section 3.2. In this section the open loop torques are applied to the fully flexible DRM to observe the results both in terms of the gross angular motion and the flexible vibrations. The slew torque actuator, as shown in Figure 1.2, uses the assumed torque solution, via the inverse dynamics of the rigid DRM as explained in Section 3.2.1. No feedback or damping of any kind is included in the results in this section. It is intended to show the behaviour of the system under different open loop inputs.

4.2.1 Minimum-Time Assumed Torque Results

The minimum time assumed solution as explained above in Section 3.2.2 involves driving the manipulator to a predetermined slew angle in the least time possible. For the DRM, with its time varying length, this is accomplished by enforcing a bang-bang acceleration profile.

The first simulation results are given in Figure 4.6. The figure shows the slew angle and the applied root torque for a 50 degree slew while carrying no payload, with a fixed total length of 11 metres, and with the angular acceleration limit set at 0.02 rad/sec^2 (which will be the angular acceleration limit, $\ddot{\theta}_{max}$ for all the simulations in this thesis unless otherwise stated). This angular acceleration limit will give the manoeuvre final time depending on which open loop strategy is chosen (minimum-time, near minimum-energy, etc), as discussed in Section 3.2, above. The figures on page 120 show the tip vibrations for the unloaded case and carrying Payload 0 and Payload 1 of Table 2-7 using

a minimum-time acceleration profile. For this fixed length case it can be seen that there are vibrations throughout the manoeuvre and residual vibrations after the predetermined slew angle has been reached. It can be seen that the interaction between the torque switch and the vibrations is very strong. Once the manoeuvre has started, and depending at what moment, the torque switches are applied, the induced vibrations are different, as they depend on the conditions of deflection at the time of the switch. That is why the residual vibrations in Figure 4.9 are small compared to vibrations throughout the manoeuvre, but larger in Figure 4.7 and Figure 4.8.

Figure 4.10, Figure 4.12, Figure 4.13, and Figure 4.14 show the same results as for the fixed length simulations but for the DRM undergoing a deployment of link 2 from 1 to 8 metres. The deployment of link 2 is predetermined and follows a bang-bang linear force profile, where the applied force is calculated to coincide with the slewing torque, so that the switches in torque and force occur at the same time, Figure 4.11. Comparing the results from the fixed length and the deploying DRM the interaction of the deployment dynamics with the rotational dynamics can be appreciated. As shown in Equation (2.5.6), the linear deployment velocity terms combine with the rotational velocity terms and contribute some Coriolis damping-like terms to the dynamics of the manipulator. In the first section of the manoeuvre, the vibrations are reduced while the deployment and slewing accelerations are positive. At the mid-point of the manoeuvre, the torque switch is applied to retard both the slewing and the deployment. This switch excites large amplitudes of vibration since the exposed length of link 2 of the DRM is 4 metres at that time. The vibrations, and the static flexible deflection (deviation from the zero deflection line), are therefore affected by the deployment of link 2.

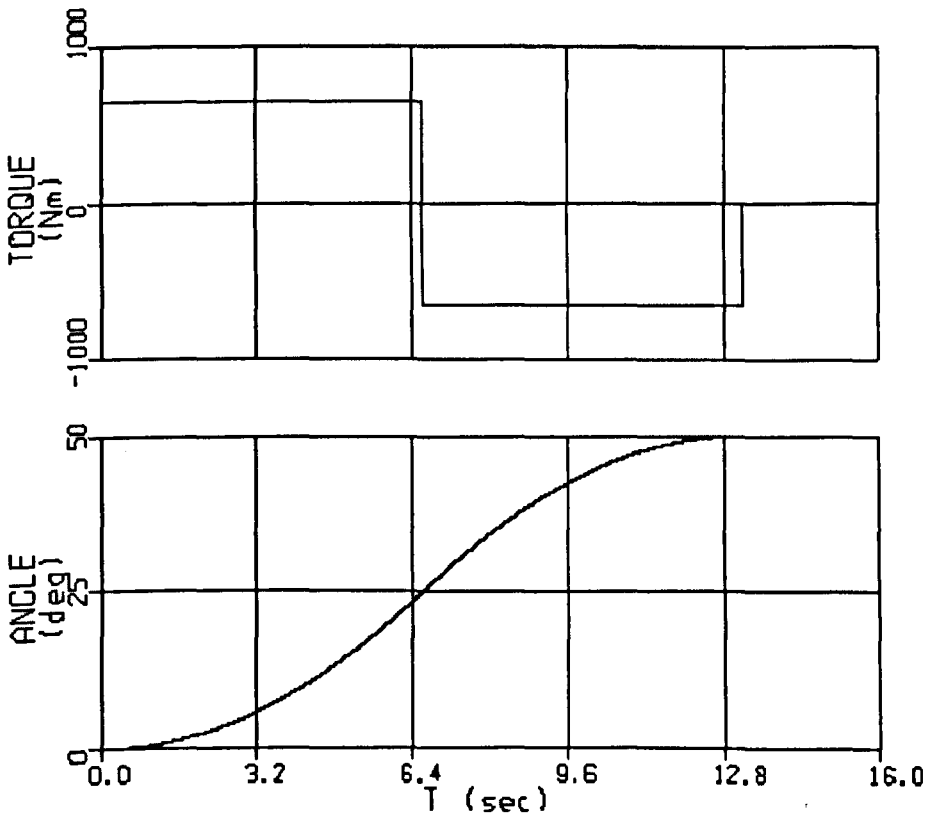

Figure 4.6: Applied Root Torque and slew angle for a 50° minimum-time slew of a fixed length DRM with Payload 1

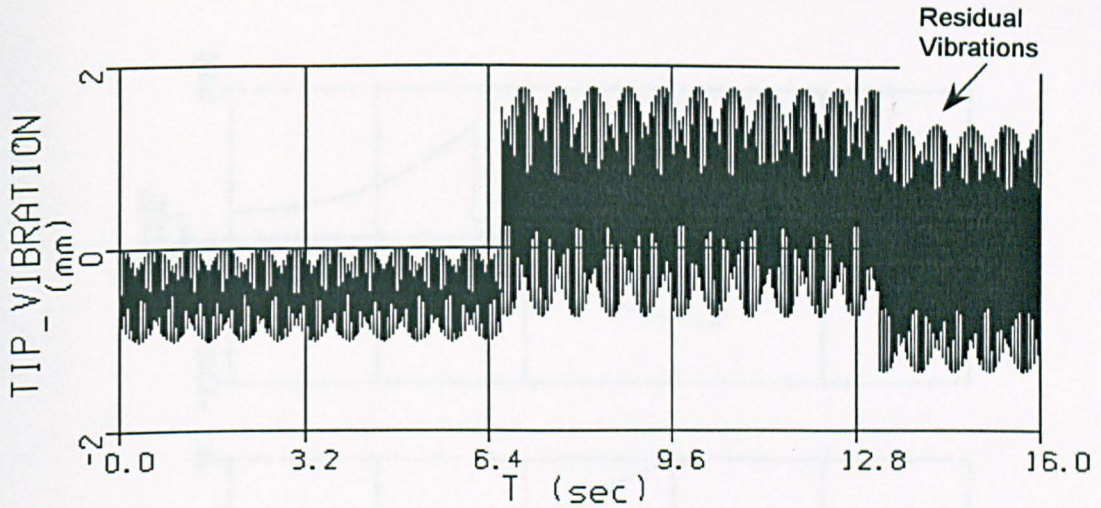

Figure 4.7: Undamped tip vibrations for a 50° minimum-time slew of a fixed length DRM with no payload

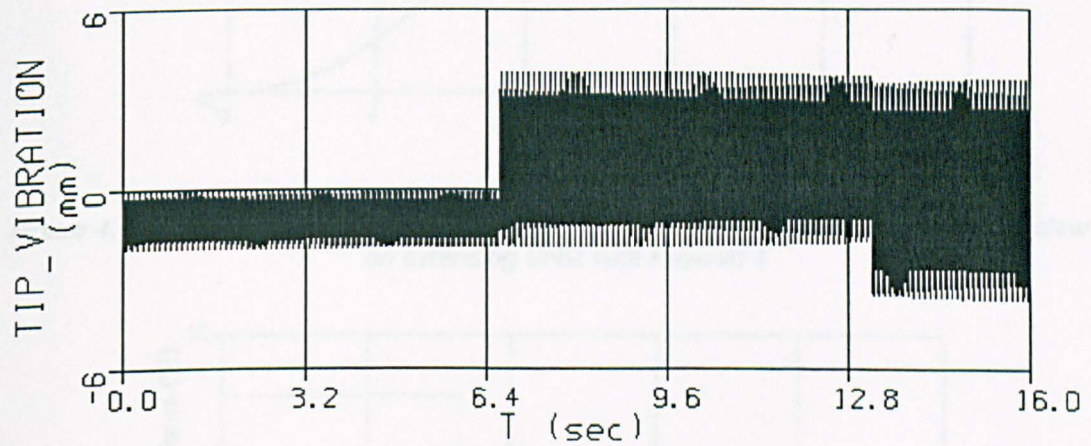

Figure 4.8: Undamped tip vibrations for a 50° minimum-time slew of a fixed length DRM with Payload 0

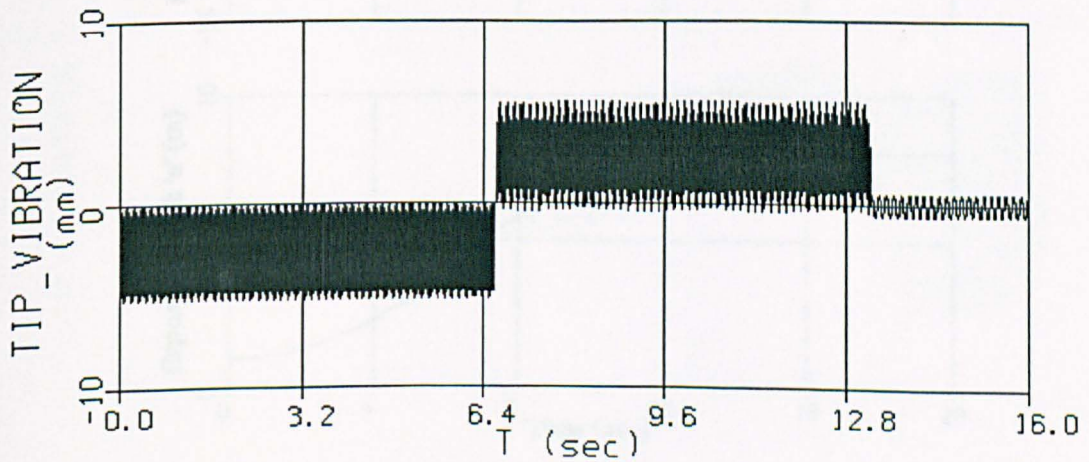

Figure 4.9: Undamped tip vibrations for a 50° minimum-time slew of a fixed length DRM with Payload 1

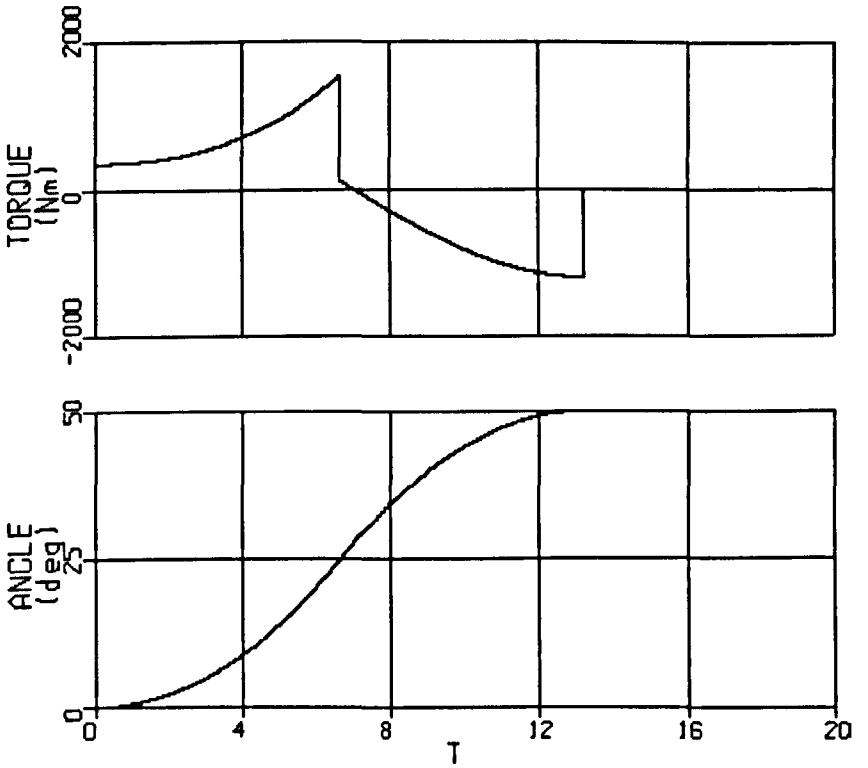

Figure 4.10: Applied Root Torque and slew angle time history for a 50° minimum-time slew of an extending DRM with Payload 1

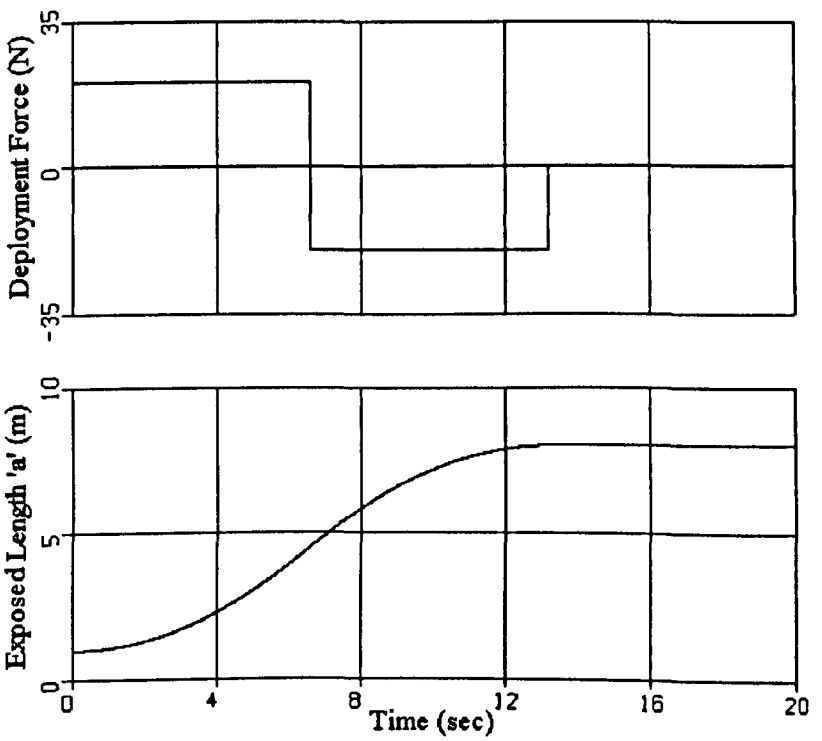

Figure 4.11: Deployment Force and exposed length 'a' time history for a 50° minimum-time slew of the DRM with Payload 0

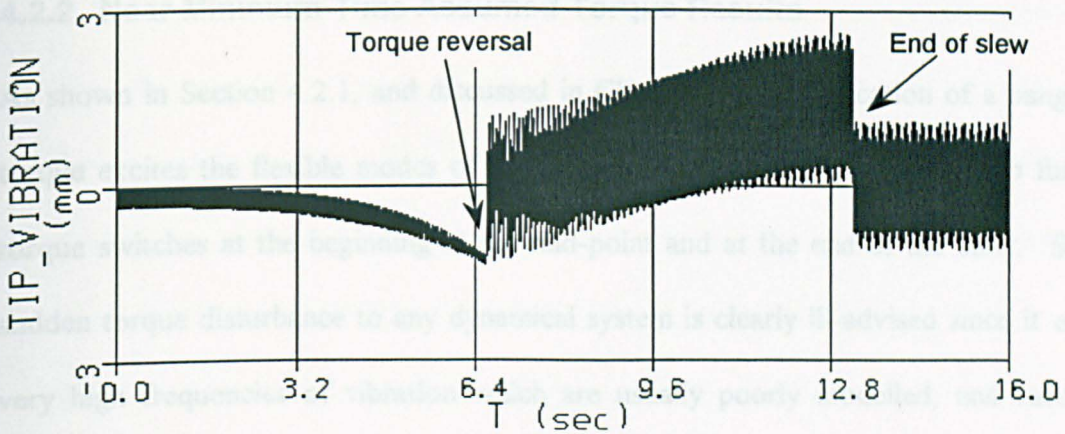

Figure 4.12: Undamped tip vibrations for a 50° minimum-time slew of an extending DRM with no payload

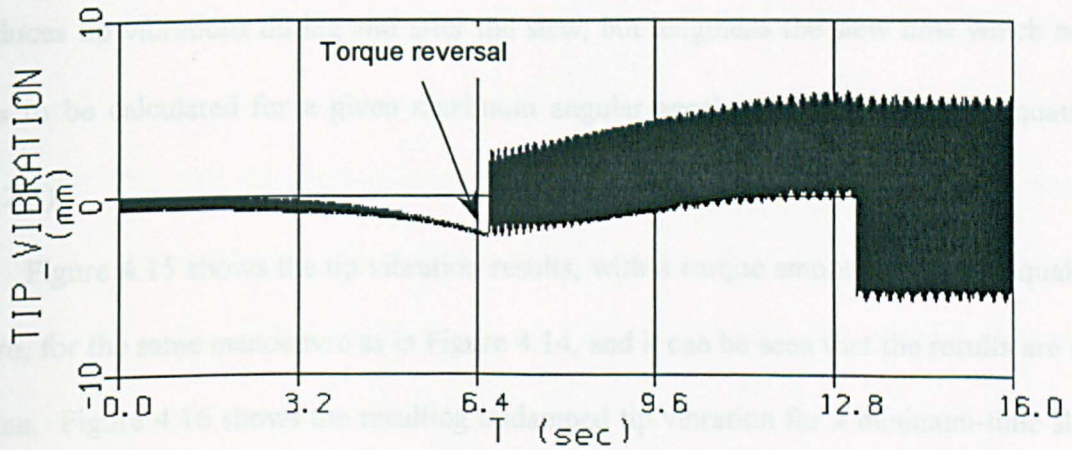

Figure 4.13: Undamped tip vibrations for a 50° minimum-time slew of an extending DRM with Payload 0

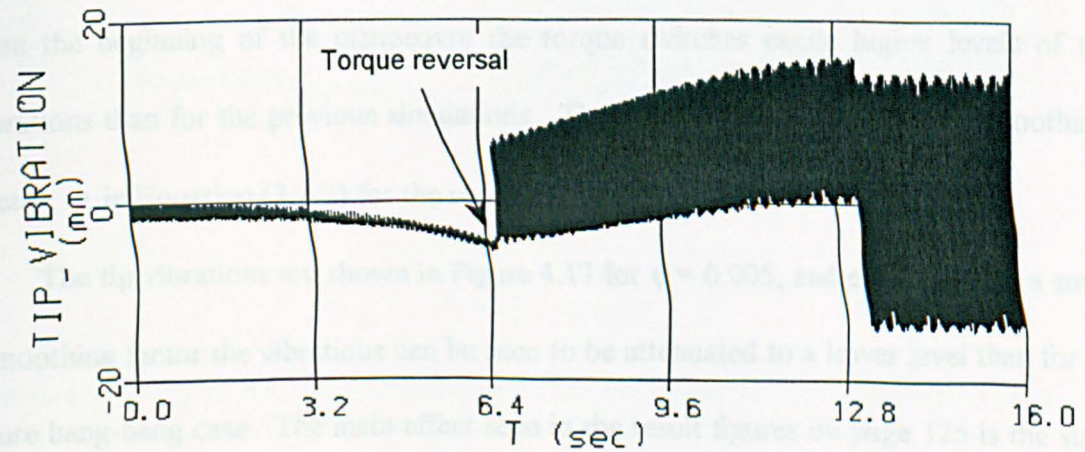

Figure 4.14: Undamped tip vibrations for a 50° minimum-time slew of an extending DRM with Payload 1

4.2.2 Near Minimum-Time Assumed Torque Results

As shown in Section 4.2.1, and discussed in Chapter 3, the application of a bang-bang torque excites the flexible modes of the manipulator. This is due to the step function torque switches at the beginning at the mid-point and at the end of the slew. Such a sudden torque disturbance to any dynamical system is clearly ill-advised since it excites very high frequencies of vibration which are usually poorly modelled, and harder to control. Therefore, the minimum-time acceleration profile (bang-bang) is smoothed as described in Section 3.2.3 by the use of cubic splines. This smoothes out the torque, and reduces tip vibrations during and after the slew, but lengthens the slew time which now has to be calculated for a given maximum angular acceleration, $\ddot{\theta}_{max}$, using Equation (3.2.3).

Figure 4.15 shows the tip vibration results, with a torque smoothing factor equal to zero, for the same manoeuvre as in Figure 4.14, and it can be seen that the results are the same. Figure 4.16 shows the resulting undamped tip vibration for a minimum-time slew manoeuvre with an angular acceleration limit of 0.04 rad/sec^2 and while extending link 2 from 4 to 8 metres. The only difference is that since there is more of the DRM extended from the beginning of the manoeuvre the torque switches excite higher levels of tip vibrations than for the previous simulations. The next step is to increase the smoothing factor, φ, in Equation (3.2.2) for the case shown in Figure 4.16.

The tip vibrations are shown in Figure 4.17 for $\varphi = 0.005$, and even for such a small smoothing factor the vibrations can be seen to be attenuated to a lower level than for the pure bang-bang case. The main effect seen in the result figures on page 125 is the static deflection inherent in slewing a long flexible beam, which disappears at the end of the

slew. The tip vibration levels of the DRM can be reduced further as shown in Figure 4.18 by using $\varphi = 0.01$. For this level of bang-bang smoothing the vibration levels are clearly reduced to the single unit millimetre level. For a system such as the DRM such small vibration levels can probably be considered zero, since the low material and structural damping of the DRM would quickly damp out those vibrations.

Figure 4.19 gives the vibration levels for $\varphi = 0.05$. For that value of smoothing the vibration level is almost zero and rigid body rotation θ dominates. An insert of the tip motion after the slew is completed is included in Figure 4.19. Where it is seen that the residual vibration is of the order of 0.1 mm. These vibrations are not significant for a large manipulator. The results however show that smoothing of the acceleration profile to follow, and thus the applied torque, will reduce the vibrations to very small levels. Figure 4.20 shows the smoothed torque applied to the DRM with $\varphi = 0.05$ to slew it through 50°. The shaped torque drives the DRM perfectly to the desired slew angle while inducing no perceptible vibrations.

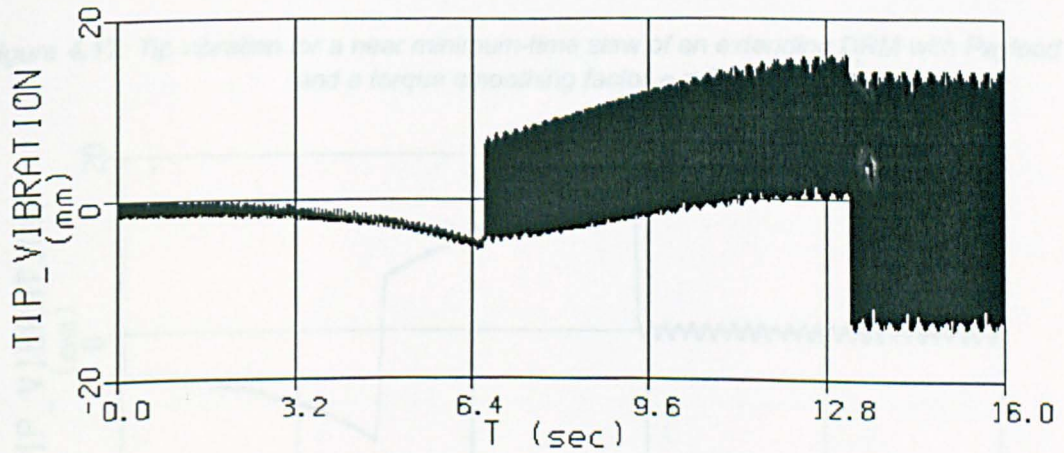

Figure 4.15: Undamped tip vibrations for a 50° minimum-time slew of an extending DRM with Payload 1 with no torque smoothing factor, $\varphi = 0.0$

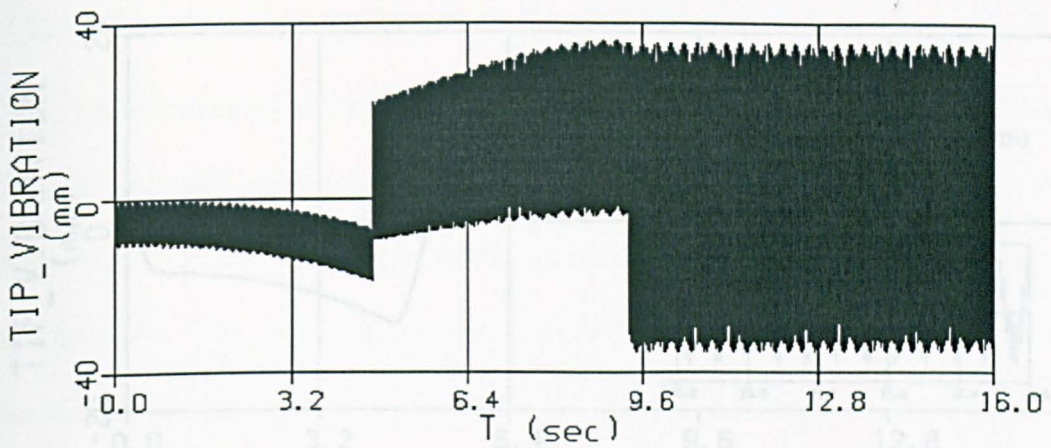

Figure 4.16: Tip vibration for a minimum-time slew of an extending DRM with Payload 1 and no torque smoothing factor, $\varphi = 0.0$

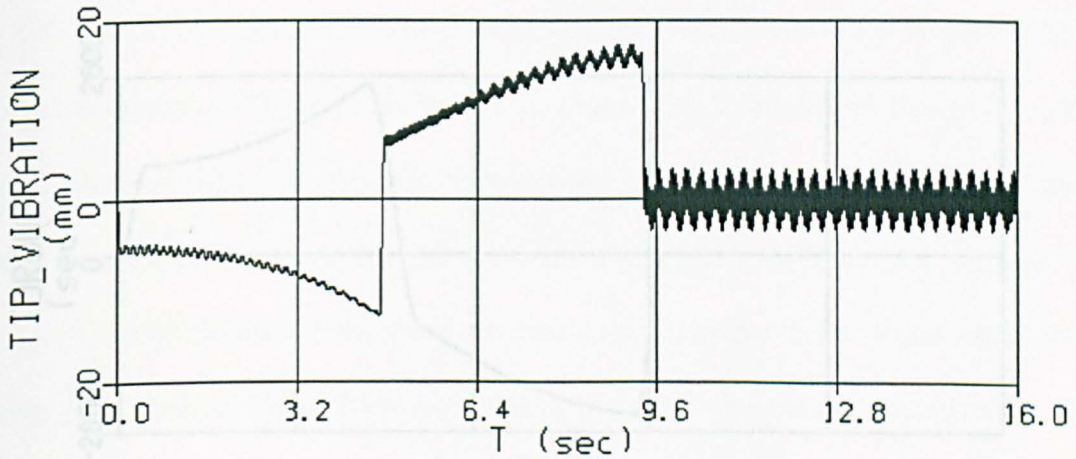

Figure 4.17: Tip vibration for a near minimum-time slew of an extending DRM with Payload 1 and a torque smoothing factor $\varphi = 0.005$

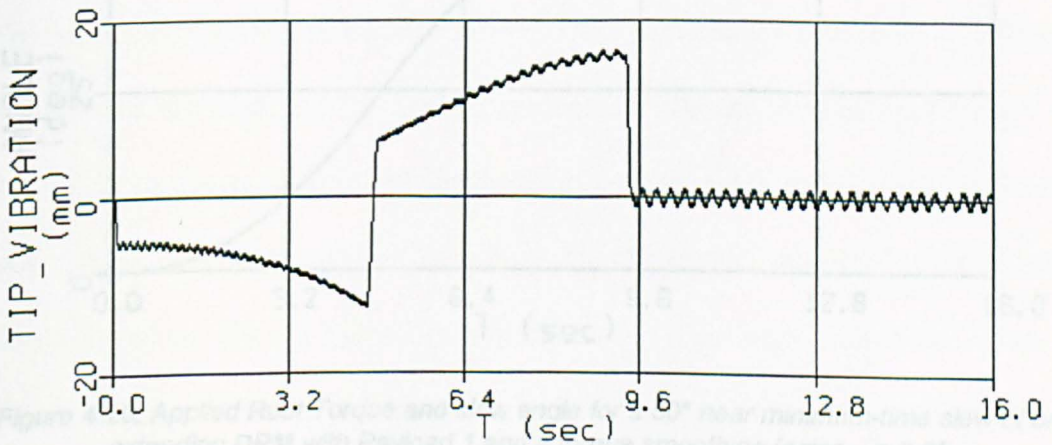

Figure 4.18: Tip vibration for a near minimum-time slew of an extending DRM with Payload 1 and a torque smoothing factor $\varphi = 0.01$

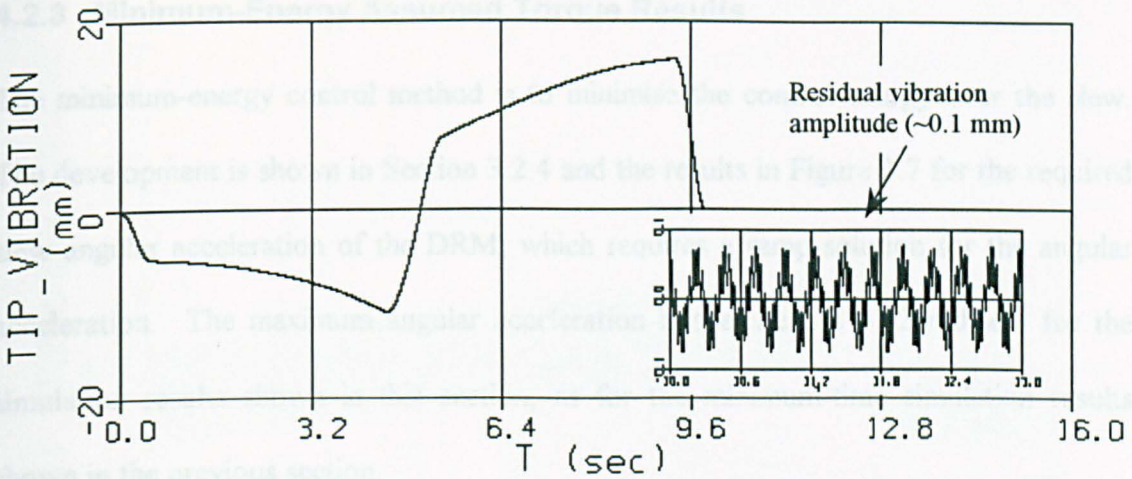

Figure 4.19: Tip vibration for a near minimum-time slew of an extending DRM with Payload 1 and a torque smoothing factor $\varphi = 0.05$

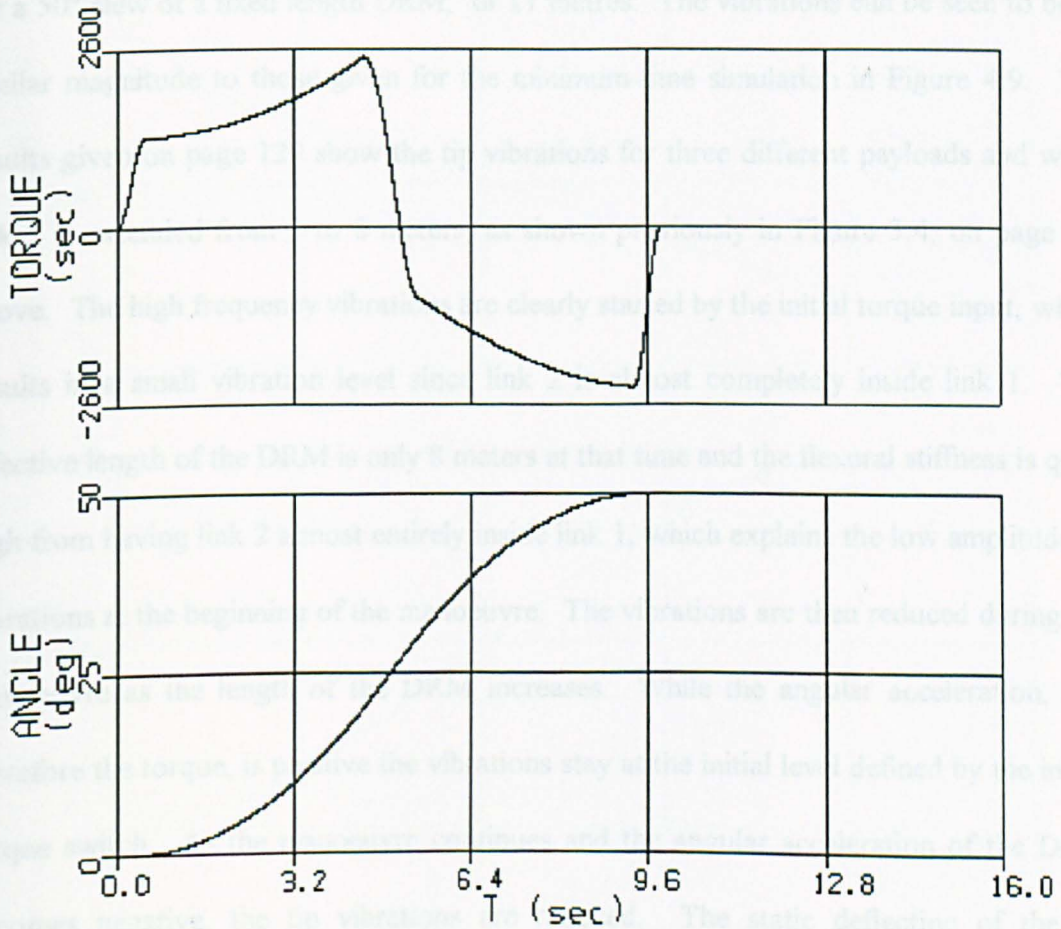

Figure 4.20: Applied Root Torque and slew angle for a 50° near minimum-time slew of an extending DRM with Payload 1 and a torque smoothing factor $\varphi = 0.05$

4.2.3 Minimum-Energy Assumed Torque Results

The minimum-energy control method is to minimise the control energy over the slew. The development is shown in Section 3.2.4 and the results in Figure 3.7 for the required slew angular acceleration of the DRM, which requires a ramp solution for the angular acceleration. The maximum angular acceleration is specified as 0.02 rad/sec^2 for the simulation results shown in this section, as for the minimum-time simulation results shown in the previous section.

Figure 4.21 shows time histories of tip vibration, applied torque and rotation angle for a 50° slew of a fixed length DRM, of 11 metres. The vibrations can be seen to be of similar magnitude to those given for the minimum-time simulation in Figure 4.9. The results given on page 129 show the tip vibrations for three different payloads and while link 2 is extended from 1 to 8 meters, as shown previously in Figure 3.4, on page 72, above. The high frequency vibrations are clearly started by the initial torque input, which results in a small vibration level since link 2 is almost completely inside link 1. The effective length of the DRM is only 8 meters at that time and the flexural stiffness is quite high from having link 2 almost entirely inside link 1, which explains the low amplitude of vibrations at the beginning of the manoeuvre. The vibrations are then reduced during the manoeuvre as the length of the DRM increases. While the angular acceleration, and therefore the torque, is positive the vibrations stay at the initial level defined by the initial torque switch. As the manoeuvre continues and the angular acceleration of the DRM becomes negative, the tip vibrations are reduced. The static deflection of the tip increases at that time, which creates the conditions for large residual vibrations at the end of the manoeuvre.

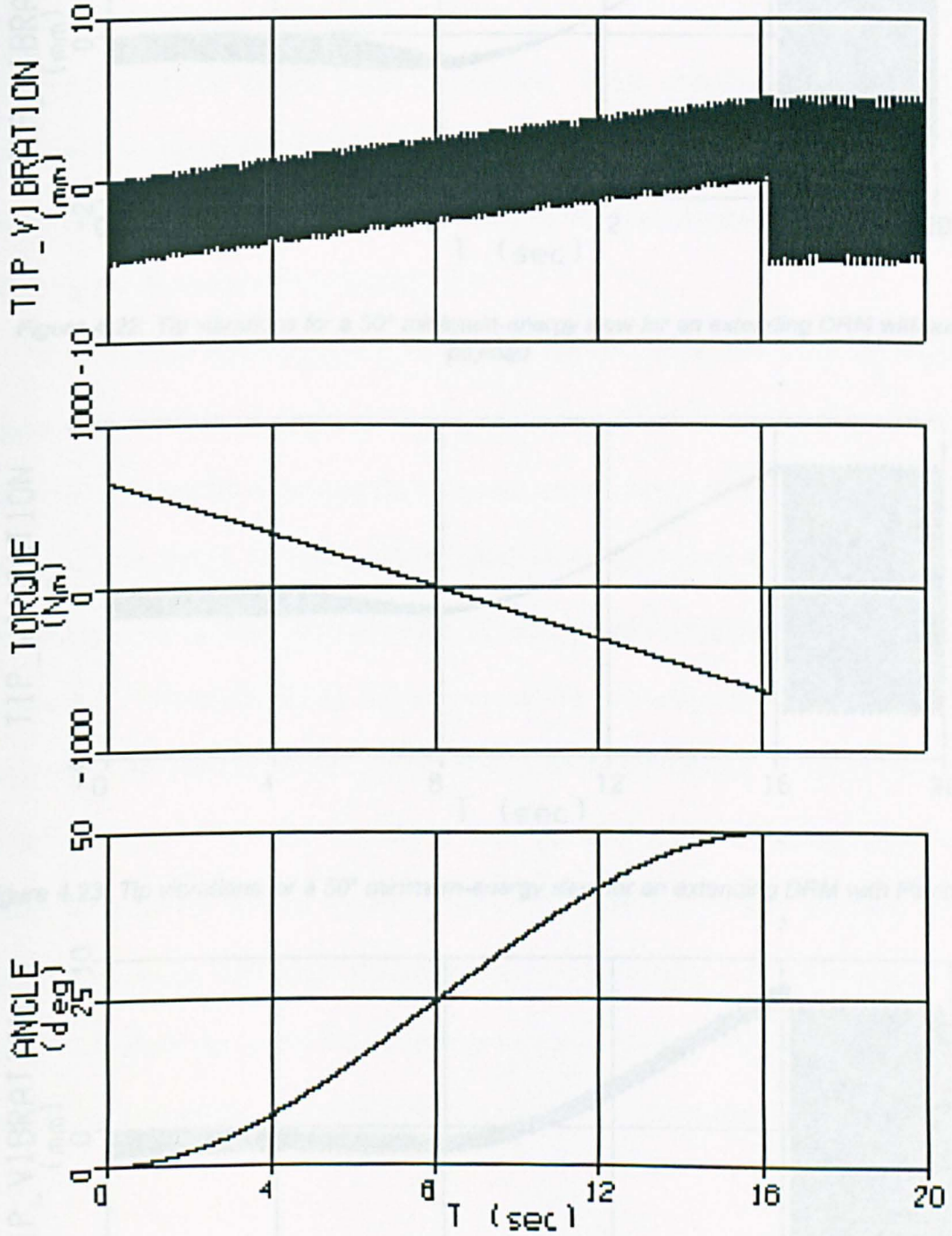

Figure 4.21: Tip vibrations, slew Torque and slew angle for a 50° minimum-energy slew of a fixed length DRM with Payload 1.

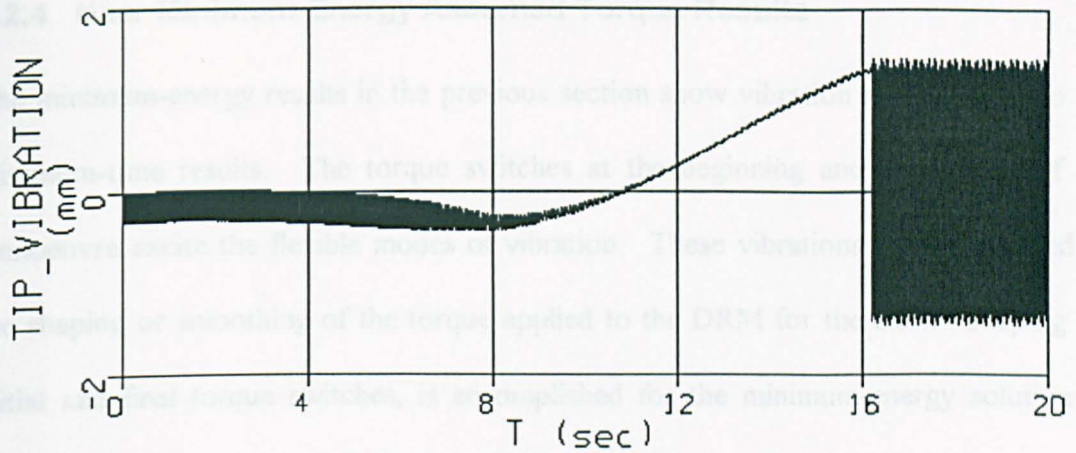

Figure 4.22: Tip vibrations for a 50° minimum-energy slew for an extending DRM without payload

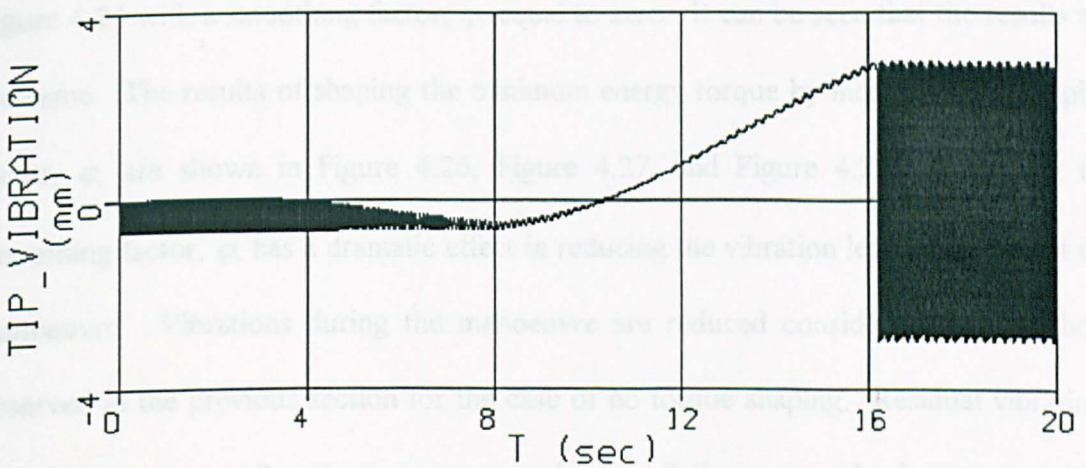

Figure 4.23: Tip vibrations for a 50° minimum-energy slew for an extending DRM with Payload0

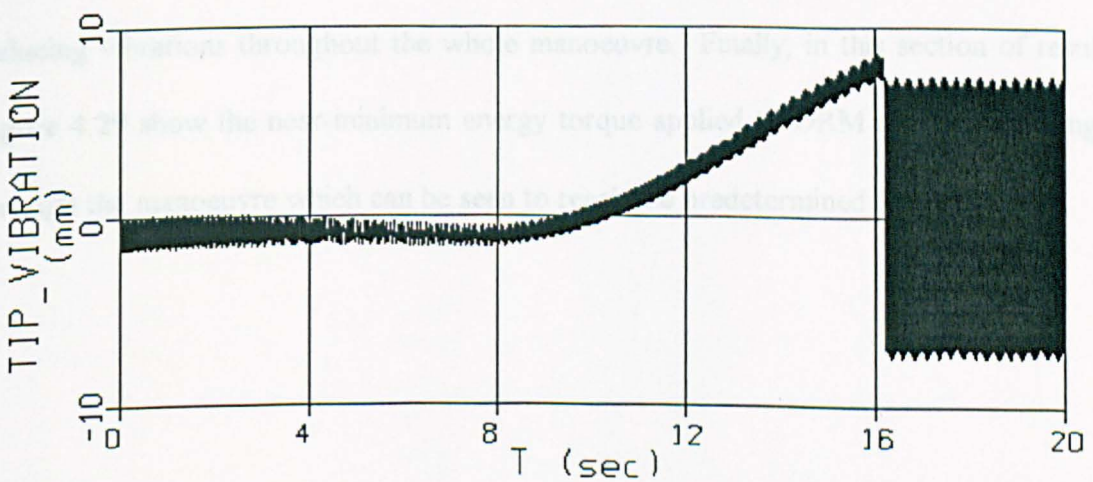

Figure 4.24: Tip vibrations for a 50° minimum-energy slew for an extending DRM with Payload1

4.2.4 Near Minimum-Energy Assumed Torque Results

The minimum-energy results in the previous section show vibration levels similar to the minimum-time results. The torque switches at the beginning and at the end of the manoeuvre excite the flexible modes of vibration. These vibrations can be reduced by the shaping or smoothing of the torque applied to the DRM for the slew. Shaping the initial and final torque switches, is accomplished for the minimum-energy solution by following the developments in Section 3.2.5.

The first result shown in Figure 4.25 are for the same conditions as for the results in Figure 4.24 with a smoothing factor, φ, equal to zero. It can be seen that the results are the same. The results of shaping the minimum energy torque by increasing the shaping factor, φ, are shown in Figure 4.26, Figure 4.27, and Figure 4.28. Increasing the smoothing factor, φ, has a dramatic effect in reducing the vibration levels throughout the manoeuvre. Vibrations during the manoeuvre are reduced considerably below those observed in the previous section for the case of no torque shaping. Residual vibrations nonetheless remain after the manoeuvre ends, for all the torque shaping cases, which makes the case for velocity feedback vibration control as the most effective way of reducing vibrations throughout the whole manoeuvre. Finally, in this section of results Figure 4.29 show the near-minimum energy torque applied to DRM and the slew angle through the manoeuvre which can be seen to reach the predetermined 50°.

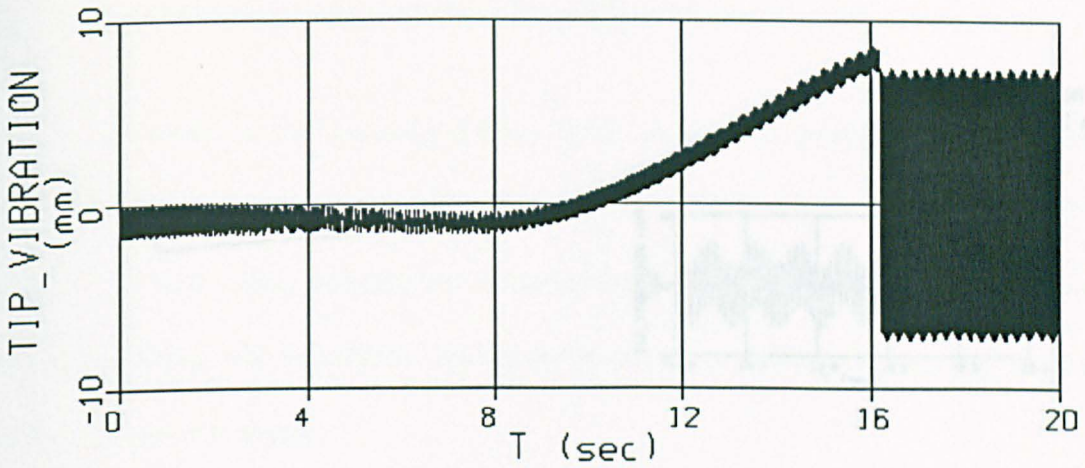

Figure 4.25: Tip vibrations for a 50° minimum-energy slew for an extending DRM with Payload 1 with no torque smoothing factor, $\varphi = 0.0$

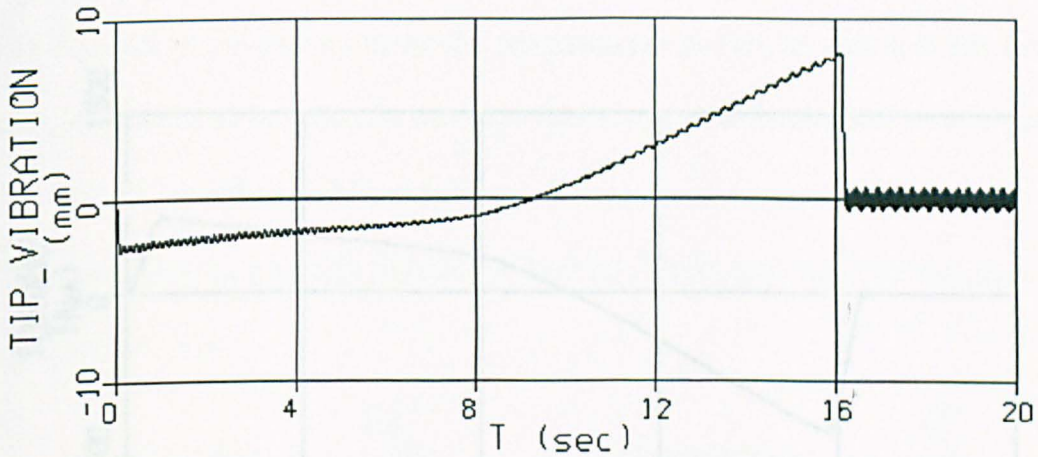

Figure 4.26: Tip vibration for a near minimum- energy slew of an extending DRM with Payload 1 and a torque smoothing factor, $\varphi = 0.005$

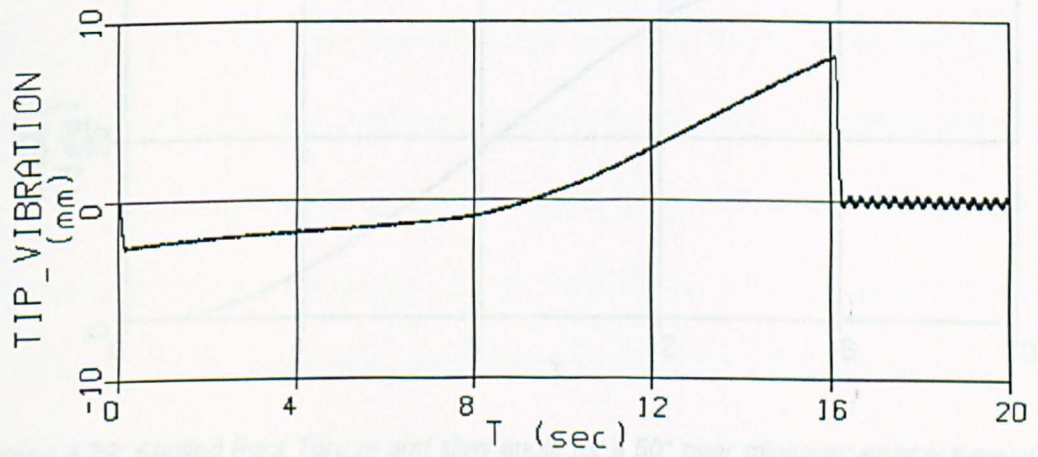

Figure 4.27: Tip vibration for a near minimum- energy slew of an extending DRM with Payload 1 and a torque smoothing factor, $\varphi = 0.01$

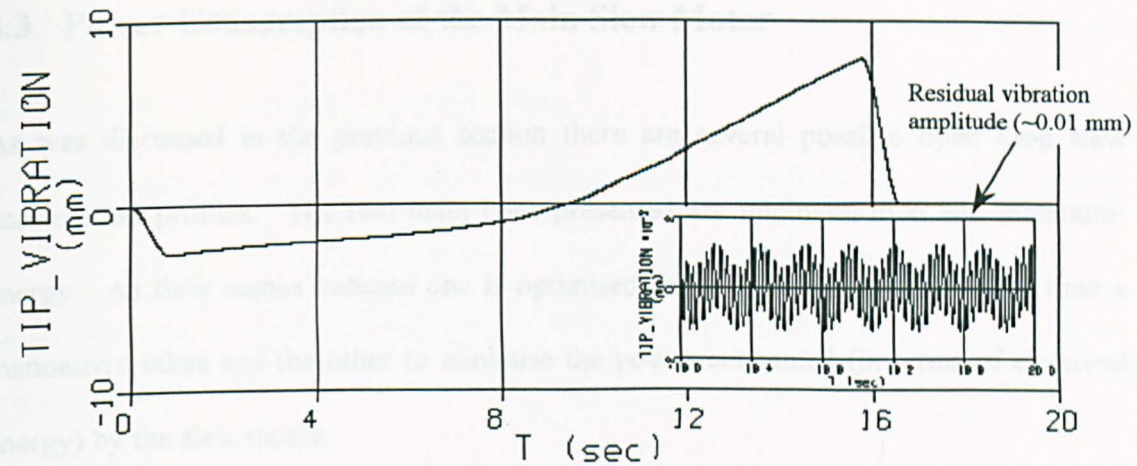

Figure 4.28: Tip vibration for a near minimum- energy slew of an extending DRM with Payload 1 and a torque smoothing factor, φ = 0.05

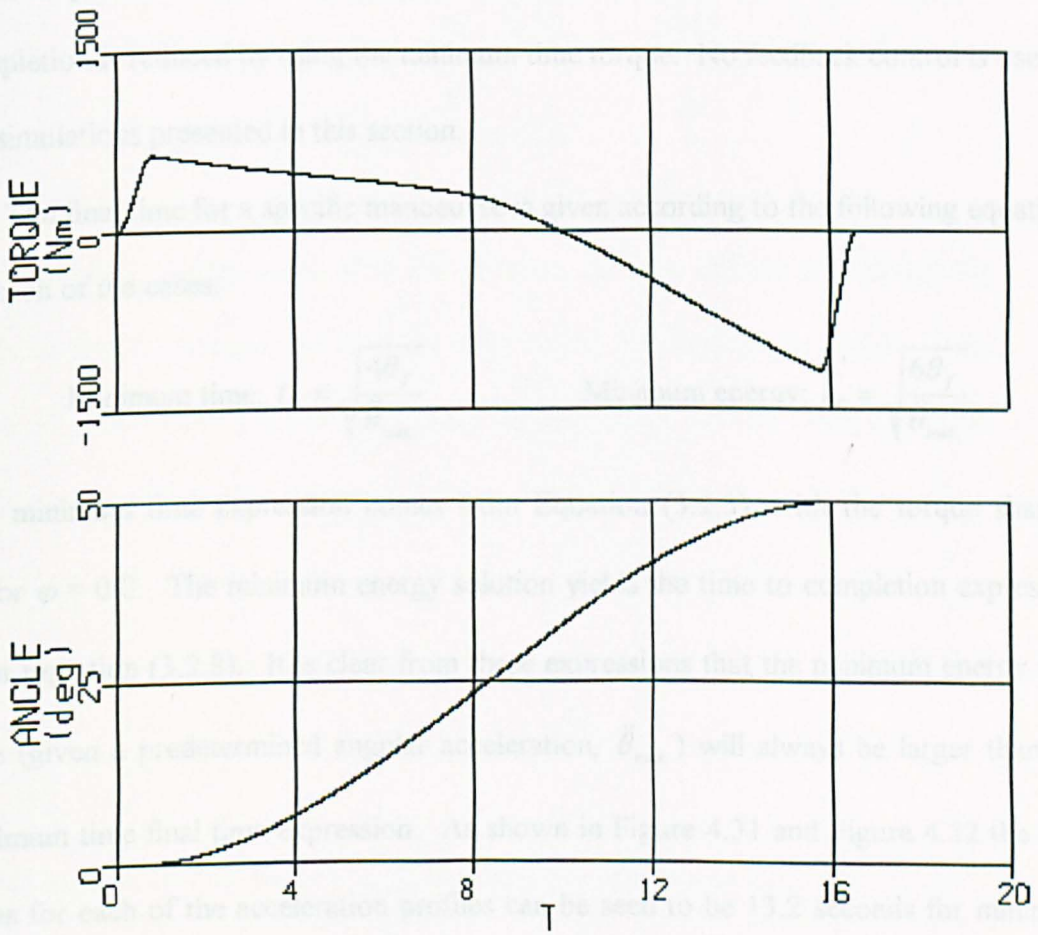

Figure 4.29: Applied Root Torque and slew angle for a 50° near minimum-energy slew of an extending DRM with Payload 1 and a torque smoothing factor, φ = 0.05

4.3 Power Consumption of the Main Slew Motor

As was discussed in the previous section there are several possible open loop slew acceleration profiles. The two main ones presented are minimum-time and minimum-energy. As their names indicate one is optimised for shortening the amount of time a manoeuvre takes and the other to minimise the power consumed (in terms of electrical energy) by the slew motor.

To highlight these two cases this section presents the results for a standard slew manoeuvre while extending link 2 with the 200 Kg Payload 1. The aim is to show how the total power is reduced by using the minimum-energy torque, and how the time to completion is reduced by using the minimum time torque. No feedback control is used in the simulations presented in this section.

The final time for a specific manoeuvre is given according to the following equations for each of the cases:

$$\text{Minimum time: } t_f = \sqrt{\frac{4\theta_f}{\ddot{\theta}_{max}}} \qquad \text{Minimum energy: } t_f = \sqrt{\frac{6\theta_f}{\ddot{\theta}_{max}}}$$

The minimum time expression comes from Equation (3.2.3), with the torque shaping factor $\varphi = 0.0$. The minimum energy solution yields the time to completion expression from Equation (3.2.8). It is clear from these expressions that the minimum energy final time (given a predetermined angular acceleration, $\ddot{\theta}_{max}$) will always be larger than the minimum time final time expression. As shown in Figure 4.31 and Figure 4.32 the final times for each of the acceleration profiles can be seen to be 13.2 seconds for minimum time and 16.2 seconds for minimum energy, for the same 50 degree (0.87 radians) slew

with a $\ddot{\theta}_{max} = 0.02 \ rad/\sec^2$. Therefore it is clear that the minimum time profile will always produce the shortest manoeuvre time.

To evaluate the power used by the torque motor using both of these acceleration profiles a formula has to be developed. Considering the torque motor as an armature circuit (Juang et al, 1986), (Franklin et al, 1994), (Marion and Hornyak, 1984), as shown in Figure 4.30:

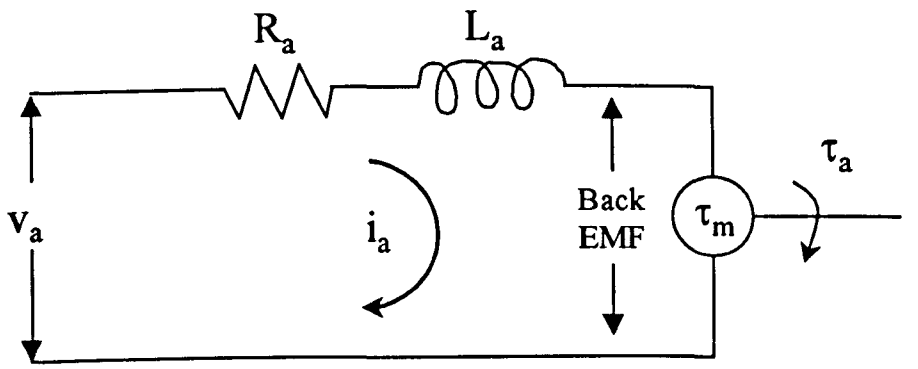

Figure 4.30: Torque motor armature circuit

Where v_a is the voltage supplied to the armature circuit, i_a the current through the circuit, R_a the circuit's resistance and L_a is the inductance. The back EMF, electro motive force, constant is k_b. Using basic circuit theory the expression for the voltage, v_a from Figure 4.30 is:

$$v_a = R_a i_a + L_a \dot{i}_a + k_b \dot{\theta}_m \tag{4.3.1}$$

solving for the current gives:

$$i_a = \frac{v_a}{R_a} - \frac{L_a \dot{i}_a}{R_a} - \frac{k_b \dot{\theta}_m}{R_a} \tag{4.3.2}$$

In this expression the quantity L_a/R_a has units of seconds and is commonly referred to as the motor time constant. Taking as reference the motor time constant for the SSRMS (Skaar and Ruoff, Chapter14, 1994), which is given as 0.00114 seconds, the quantity in

equation (4.3.2) involving the armature inductance, L_a, is not considered further in this development as it is such a small contribution to the circuit's current.

The armature torque generated at the drive axle is τ_a, this is connected to the DRM via a gear box with a gear ratio of N_g, to give the drive torque $S_T(t)$, Figure 2.1. The armature torque itself, τ_a, is due to the internal motor torque, τ_m, which is proportional to the applied current, after it overcomes the drive axle inertia and the viscous drag of the gear train. The gear ratio also relates the rotation angle of the drive axle and the DRM. All of this is summarised in the following expressions (Juang et al, 1986):

Drive Torque: $S_T(t) = N_g \tau_a$ (a)

Motor torque: $\tau_m = k_t i_a = \tau_a + c_v \dot{\theta}_m + I_m \ddot{\theta}_m$ (b) (4.3.3)

Back EMF: $EMF = k_b \dot{\theta}_m$ (c)

Rotation Angle relations: $\theta_m = N_g \theta \therefore \dot{\theta}_m = N_g \dot{\theta} \therefore \ddot{\theta}_m = N_g \ddot{\theta}$ (d)

Where k_t is the torque motor constant, c_v is the viscous drag coefficient, I_m is the motor and gear-train inertia, θ_m is the rotation angle of the motor and θ the slew angle of the DRM. Using equations (4.3.1) and (4.3.3)(a) into equation (4.3.3)(b) gives the following expression for the current used by the slew motor for a given torque applied to the DRM:

$$i_a = \frac{S_T(t)}{k_t N_g} + \frac{c_v}{k_t} N_g \dot{\theta} + \frac{I_m}{k_t} N_g \ddot{\theta} \qquad (4.3.4)$$

The values of the motor and drive-train constants are in Table 4-1, taken from (Skaar and Ruoff, Chapter14, 1994), making the assumption that the slew motor are as those defined for the SSRMS. The viscous drag coefficient is due to the losses in the contact

between the gears and is normally determined experimentally, for the DRM it has been set as 2% of the back EMF term in Equation (4.3.2), above.

Table 4-1: DRM Slew motor characteristics

	DRM Slew motor values
Motor inertia, I_m	2.67×10^{-4} kgm^2
Motor Resistance, R_a	5.16 Ω
Gear ratio, N_g	1845
Torque motor constant, k_t	0.318 Nm/A
Back EMF constant, k_b	0.318 V/rad/s

Using the expression to calculate power: $P = i_a^2 R_a$, the power used at every integration time step can be found, as shown in Figure 4.33 and Figure 4.34, so therefore the energy used (the work done) can be easily found by finding the area under those curves. The latter is done in the simulation program by adding each small contribution at every integration time step. The results give that the minimum-time slew approach uses 185.5 Joules and the minimum-energy uses 85.9 Joules. The difference in energy consumption is quite significant, but has to be weighted against the time to completion, above, to make a decision as to which slew approach is more convenient in each circumstance.

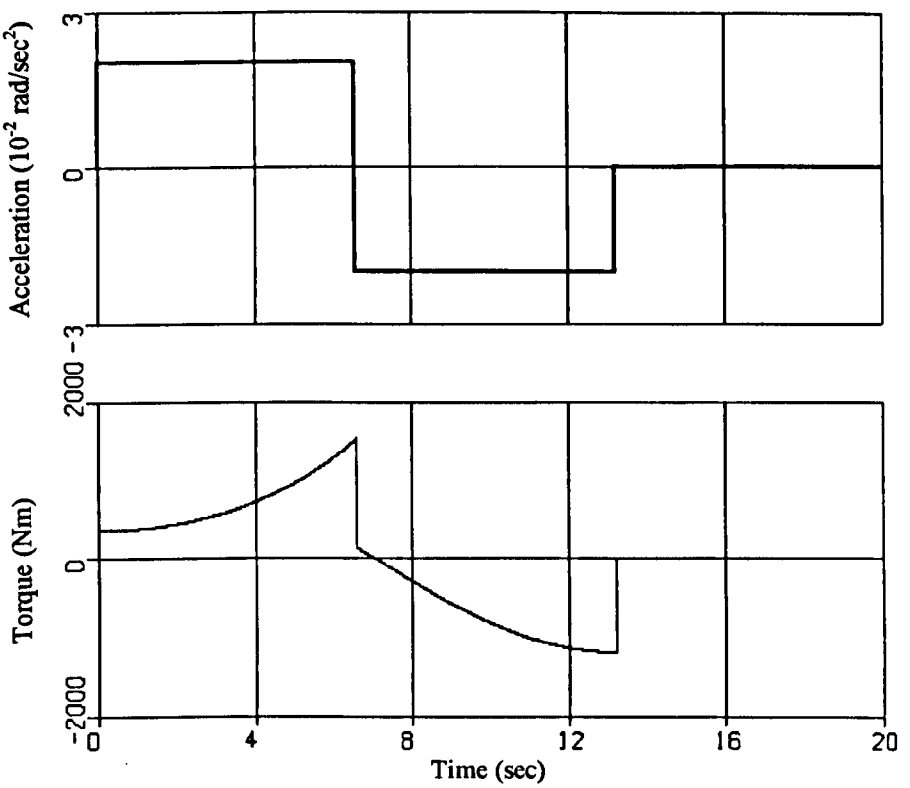

Figure 4.31: Minimum-Time Angular acceleration and slew torque for an extending DRM with Payload 1

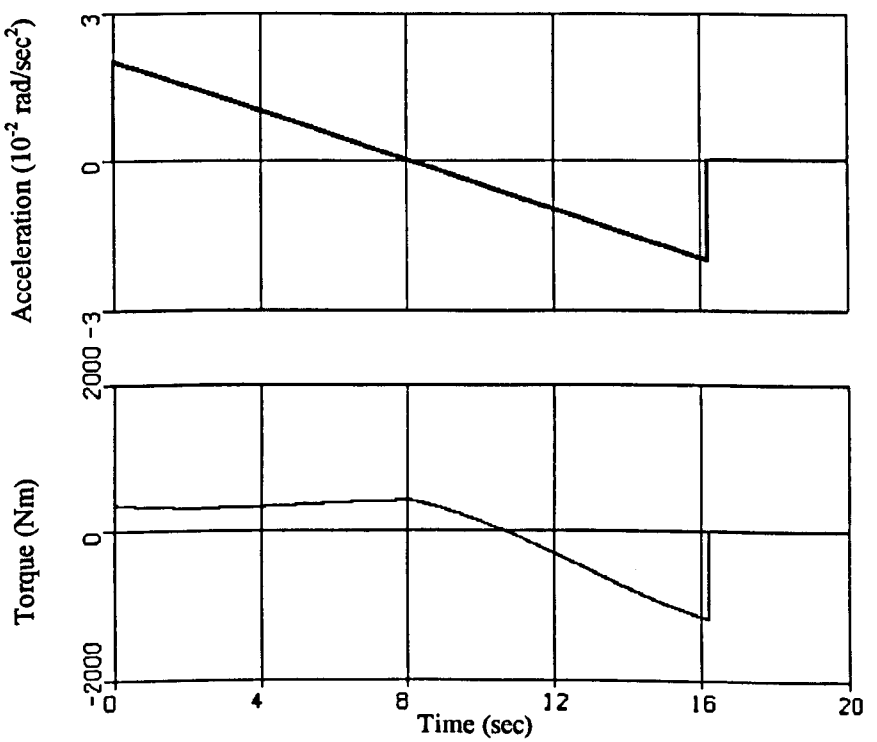

Figure 4.32: Minimum-Energy angular acceleration and slew torque for an extending DRM with Payload 1

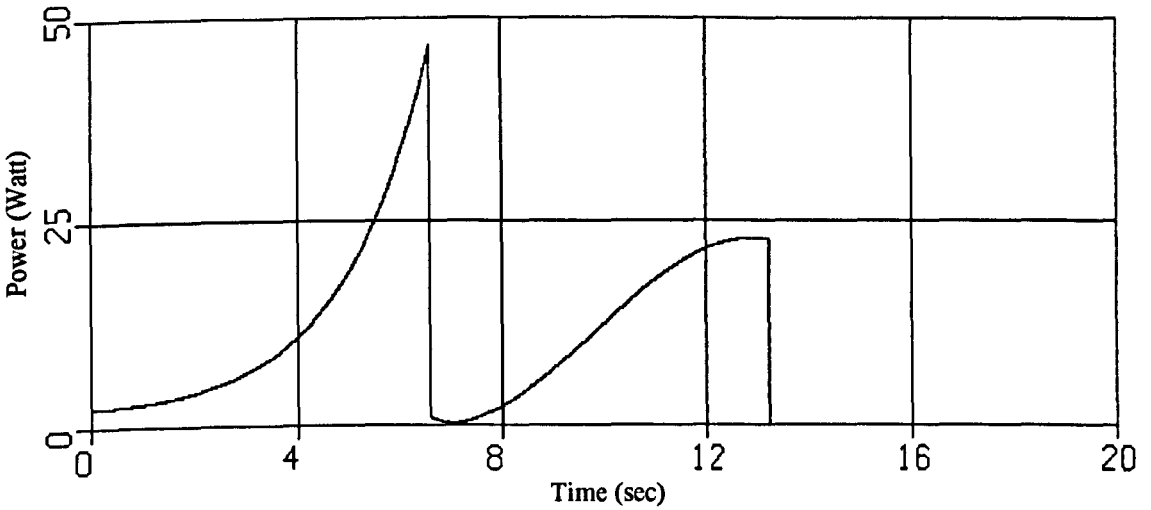

Figure 4.33: Power curve for a minimum-time slew of an extending DRM with Payload 1

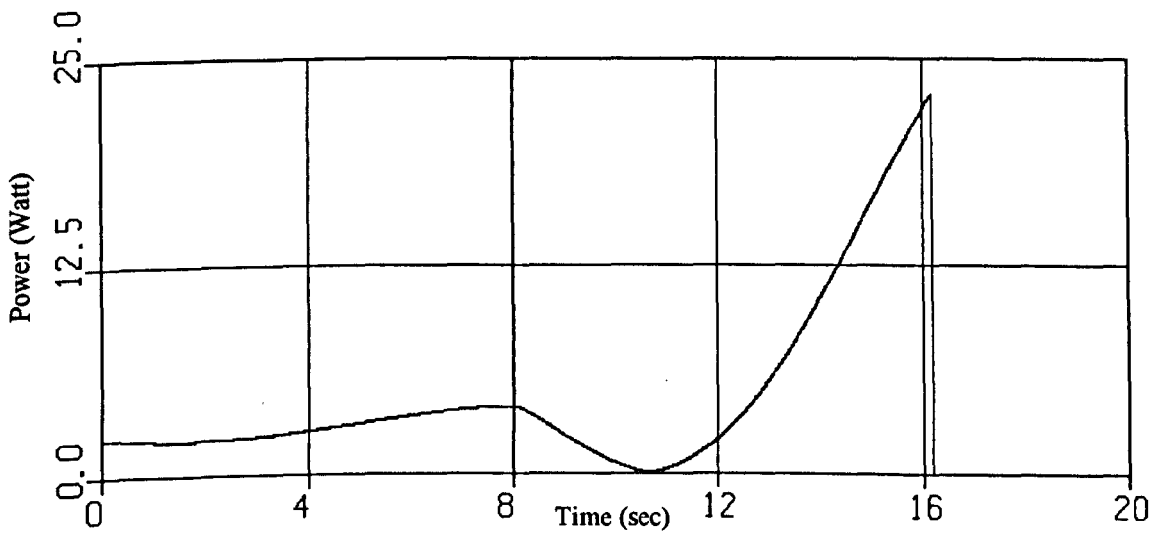

Figure 4.34: Power curve for a minimum-energy slew of an extending DRM with Payload 1

4.4 DRM Extension and Contraction Results

In this section the effect of extending and contracting link 2 on the tip vibrations are presented. The result sections above have dealt with cases of either a fixed length DRM (i.e. Figure 4.7, etc) or an extending DRM, deploying link 2 from 1 to 8 meters (i.e. Figure 4.12, etc).

The linear motion of link 2, which changes the effective length of the DRM increases or decreases the accessible working space for the manipulator and allows it to manoeuvre in confined spaces where a traditional double-jointed manipulator could not operate. The dynamics of the linear motion have been considered as predetermined, which defines the deployment velocity and accelerations, hence no equations of motion have been determined for the deployment. The axial friction effects on the deployment have been neglected in this analysis, assuming both that static and dynamic friction of the sliding link are very small and that they remain small throughout the manoeuvre. The slew dynamics are nonetheless affected by the deployment of link 2 as has been shown in the DRM equations of motion which contain the exposed length of link 2, the linear deployment velocity and acceleration, seen in equation (2.5.6).

The effects on the tip vibrations of the different link 2 motion is shown in the figures in the following pages. In the DRM simulations in this thesis the linear motion of link 2 is based on a minimum-time motion to a predetermined length, as shown in Figure 3.4, with the switch time made to coincide with the minimum-time slew torque. The effects of having non-coincident switch times for the deployment and the slew is shown in Figure 4.35 and Figure 4.36, for the slew torque and the tip vibrations respectively. In these figures a deployment force is specified, 200 Newtons, and the deployment is

executed in minimum-time, maximising the deployment force for the two distinct phases of the deployment, accelerating the link plus payload and then decelerating them. The slew happens concurrently but given the maximum angular acceleration, $\ddot{\theta}_{max}$, of 0.02 rad/sec^2 the slew manoeuvre takes much longer than the deployment. This can be easily appreciated in the slew torque plot in Figure 4.35. The torque applied to maintain a minimum-time acceleration profile is quite complicated for the first half of the manoeuvre in which the length of the DRM is changing rapidly, but once the deployment has stopped the problem is reduced to the slew of a fixed length system, where the torque follows the traditional bang-bang profile.

Another important effect worth simulating is that of retracting link 2, taking the DRM from maximum length, for example, and reduce its length while performing a slew. This has the effect of increasing the natural frequency of the system, as shown in Table 2-9 from about 4 Hz to 16 Hz, which in turn reduces the amplitude of the vibrations. The results for a slew manoeuvre plus length retraction of link 2 from 8 to 1 meter are shown in Figure 4.37, the undamped vibration results can be seen to start off relatively large and they reduce as the length of the DRM is reduced.

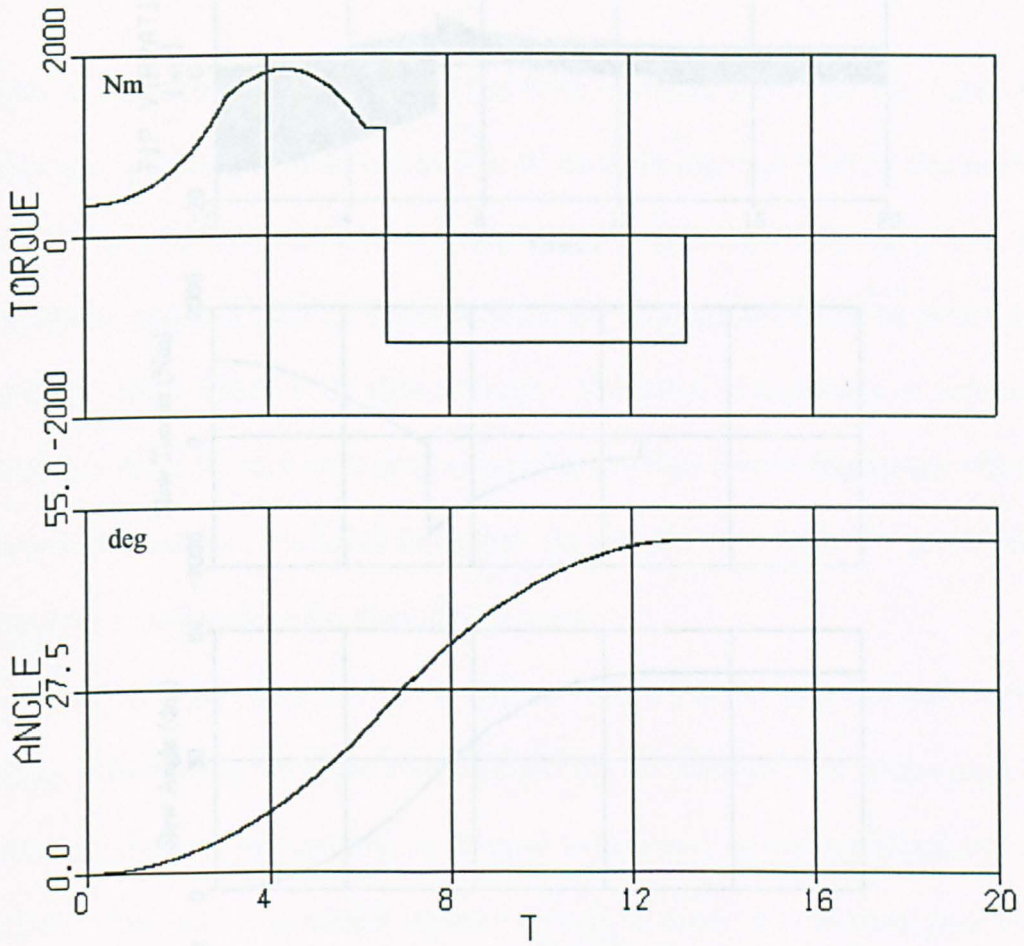

Figure 4.35: Applied Root Torque and slew angle for a 50° minimum-time slew of an extending DRM with Payload 1 and a set deployment force

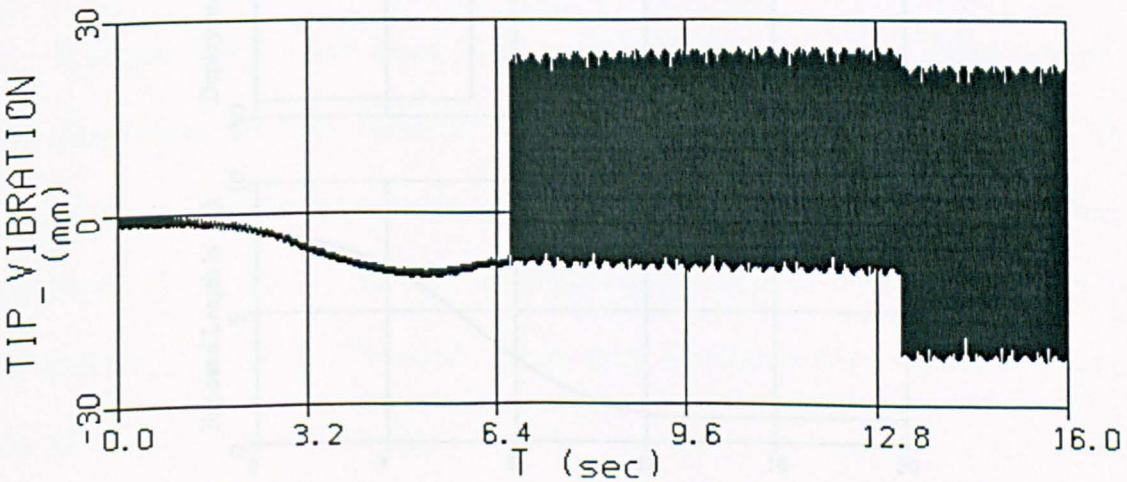

Figure 4.36: Undamped tip vibrations for a minimum-time slew of an extending DRM with Payload 1 and a 200 N deployment force for link 2

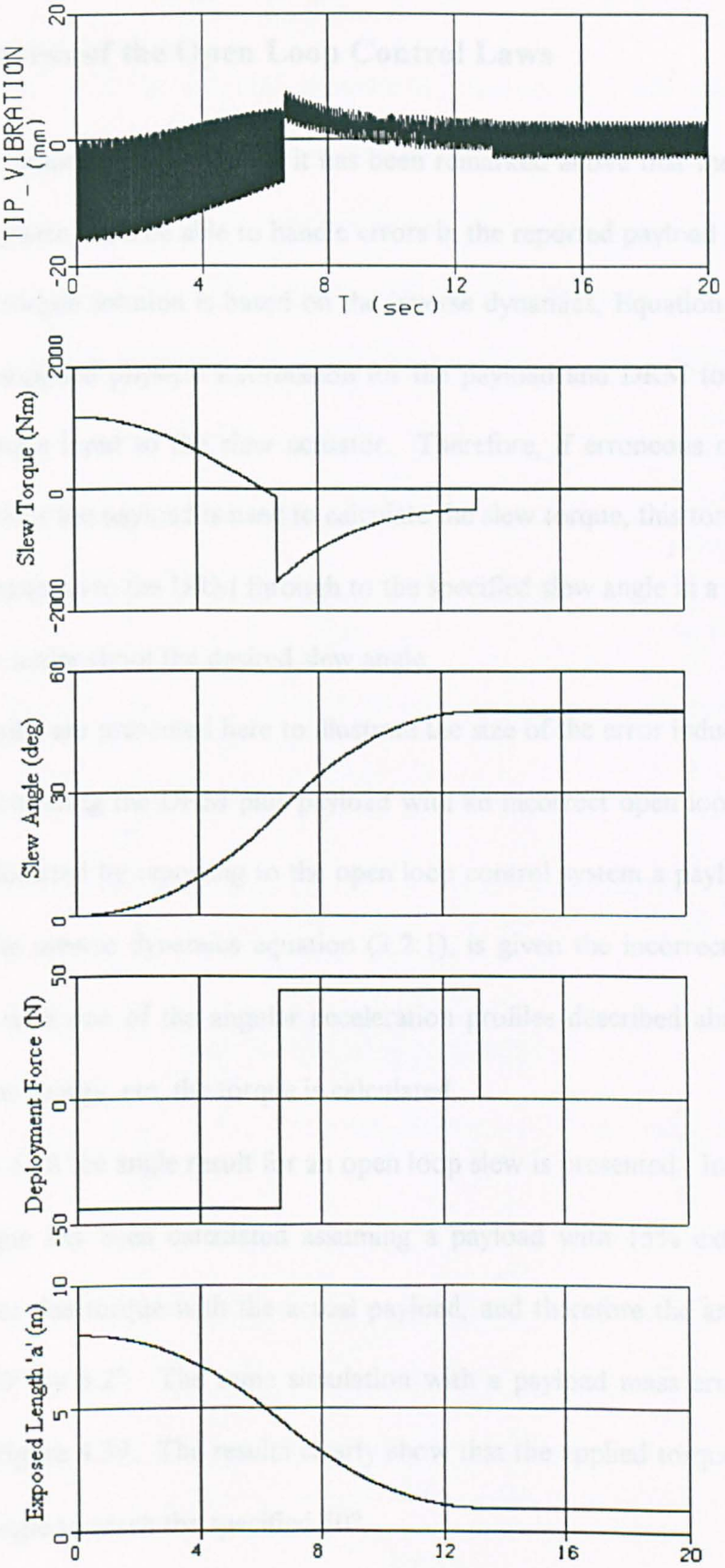

Figure 4.37: Undamped tip vibrations, slew torque, slew angle, deployment force and exposed length time histories for a minimum-time slew of a retracting DRM plus Payload 1

4.5 Robustness of the Open Loop Control Laws

As part of the control system design, it has been remarked above that the vibration and slew control system must be able to handle errors in the reported payload characteristics. The assumed torque solution is based on the inverse dynamics, Equation (3.2.1), which relies on the supplied physical information for the payload and DRM to determine the open loop torque input to the slew actuator. Therefore, if erroneous or approximate information about the payload is used to calculate the slew torque, this torque will not be adequate to manoeuvre the DRM through to the specified slew angle in a given time and it may over or under shoot the desired slew angle.

Some results are presented here to illustrate the size of the error induced in the slew angle by manoeuvring the DRM plus payload with an incorrect open loop torque. The results are calculated by reporting to the open loop control system a payload mass error of ±15%. The inverse dynamics equation (3.2.1), is given the incorrect payload mass and together with one of the angular acceleration profiles described above, minimum-time, minimum-energy, etc, the torque is calculated.

In Figure 4.38 the angle result for an open loop slew is presented. In this simulation the slew torque has been calculated assuming a payload with 15% extra mass. The simulation uses this torque with the actual payload, and therefore the angle overshoots the goal of 50° by 6.2°. The same simulation with a payload mass error of –15%, is presented in Figure 4.39. The results clearly show that the applied torque is not enough for the slew angle to reach the specified 50°.

In both of these cases, it has been shown that the open loop control laws need some enhancement to cover the specified robustness requirement. The enhanced control system must allow the DRM to slew through the specified angle in more than just the perfect case, when every quantity is known a priori to a high degree of accuracy. The closed loop control section of this thesis will address this issue of making the final control system for the DRM more robust to model changes, together with vibration suppression.

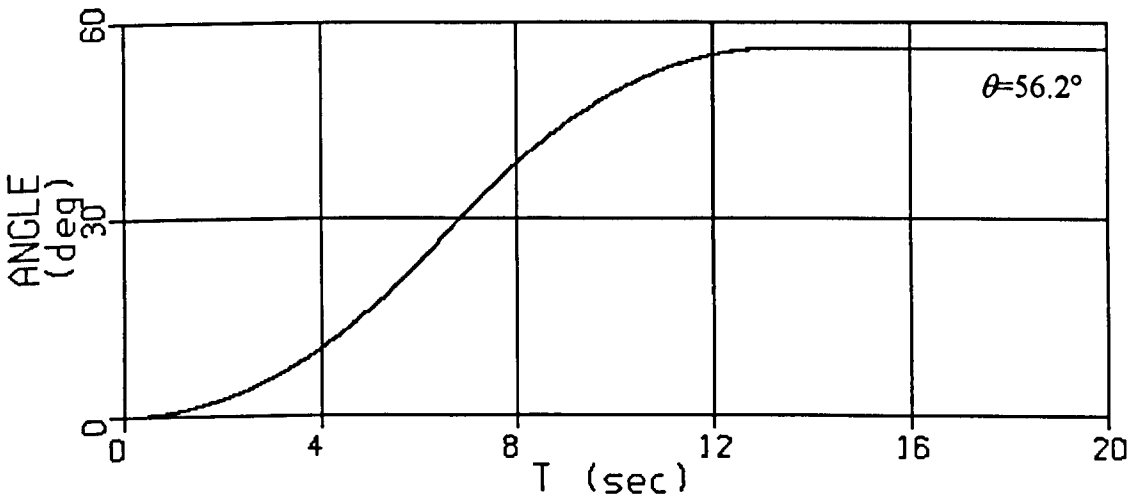

Figure 4.38: Rotation angle result for a minimum-time slew of the DRM plus Payload 1 with an error of +15% in the payload mass

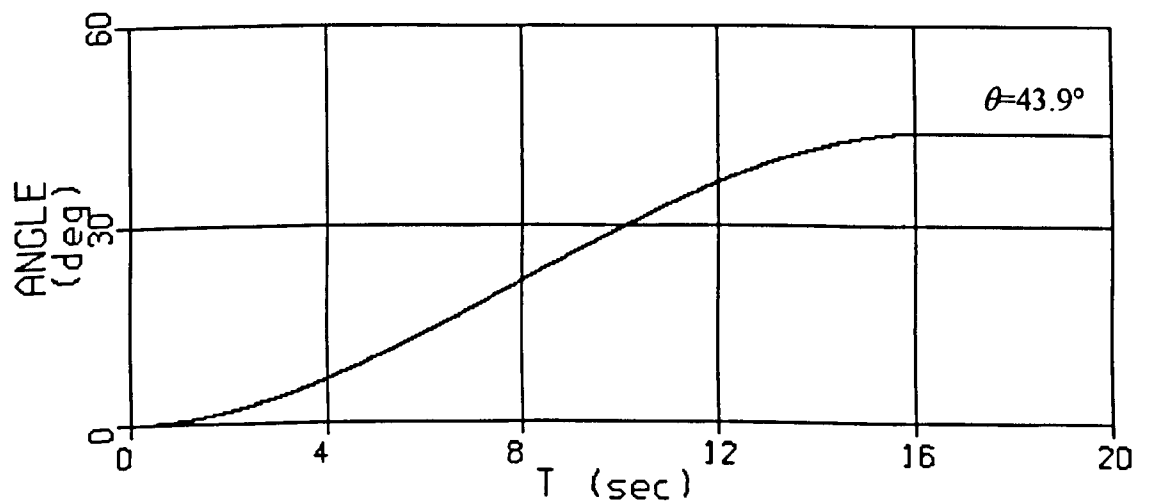

Figure 4.39: Rotation angle result for a minimum-energy slew of the DRM plus Payload 1 with an error of -15% in the payload mass

4.6 Closed Loop Control Results

The results given here show simulations of a slew manoeuvre and length change with feedback control. The slew uses the open-loop torque above, based on the rigid inverse dynamics. The actuator is a large torque motor situated at the shoulder of the DRM. The feedback control is also applied at the root and at the tip by a pair of reaction wheel actuators, as described in Section 3.3. The complete control system consists of a pair of small closed loop torque actuators and a large torque motor driven by one of the open loop control laws described in Section 3.2.

Formulation of the different closed loop control laws tested in this section is shown in Section 3.4 for the linear control laws and in Section 3.5 for the Lyapunov control laws. The closed loop control laws are applied to the DRM while being manoeuvred through to a specified angle. The root and tip closed loop actuators are included in the simulations at different times to demonstrate the effect each has on the overall motion and vibration response of the DRM during a slew. The final results using both closed loop control approaches (Linear and Lyapunov) show the complete control system, for a specified slew angle while carrying a payload and extending or contracting link 2.

4.6.1 Linear Feedback Control

This section shows the effect of using the closed loop actuators with a linear output feedback control law while slewing the DRM. The goals of the closed loop implementation are to reduce tip vibrations during and after the slew, and to increase the overall control system tolerance to model errors. The results presented show the performance of the linear closed loop control laws formulated in Section 3.4.

4.6.1.1 Root Actuator Control Results

The first part of the implementation of the linear feedback control involves using the linear feedback control in Equation (3.4.1). The feedback gains, K_i in Equation (3.4.1) are selected so as not to saturate the actuators in excess. The initial values chosen are:

$$K_1 = -8.0x10^4$$
$$K_2 = -8.0x10^3$$

Figure 4.40 presents the tip vibration results for a standard DRM slew manoeuvre plus length extension (as shown in Figure 3.4) carrying Payload 1, the 200 Kg payload. The feedback root control torque applied by the actuator is shown in Figure 4.41. It can be seen that the residual vibrations are not completely damped out until 20 seconds after the manoeuvre start. As a matter of comparison the gains have been changed and new results produced, the new gains:

$$K_1 = -8.0x10^6$$
$$K_2 = -8.0x10^4$$

produce the results in Figure 4.42, it can be seen that increasing the gains actually produces worse results. This is due to the fact that the actuator is bound, therefore if the feedback gains are too large the actuator will be at its maximum almost all of the time, even when the system outputs are very small, $\dot{\theta}$ and θ. This tends to overwhelm the actuator, as shown in Figure 4.44, and no effective damping for the tip vibrations is produced, as seen in Figure 4.42, the tip vibrations continue even after 30 seconds. The initial values above are thus used for the implementation of the linear feedback root control law.

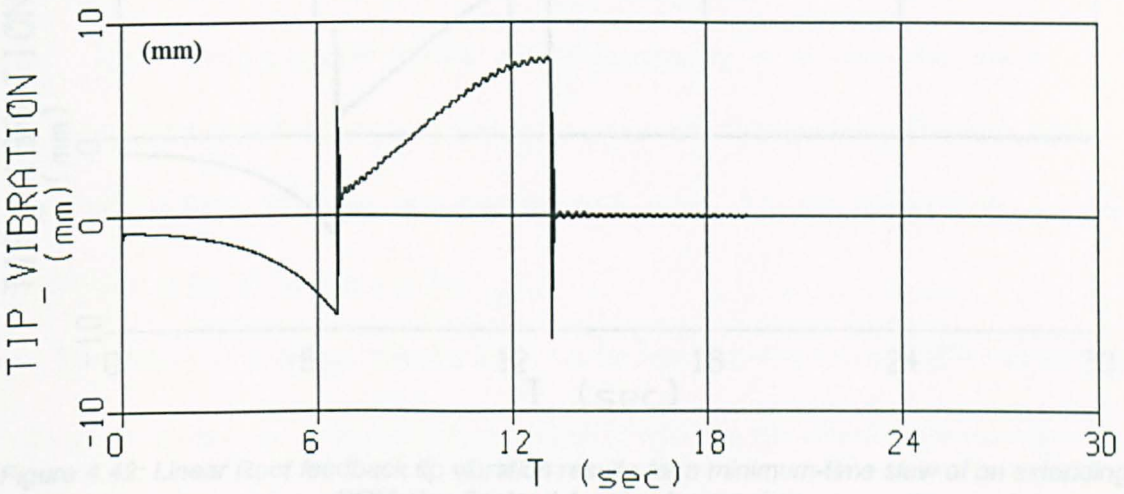

Figure 4.40: Linear Root feedback tip vibration results for a minimum-time slew of an extending DRM plus Payload 1

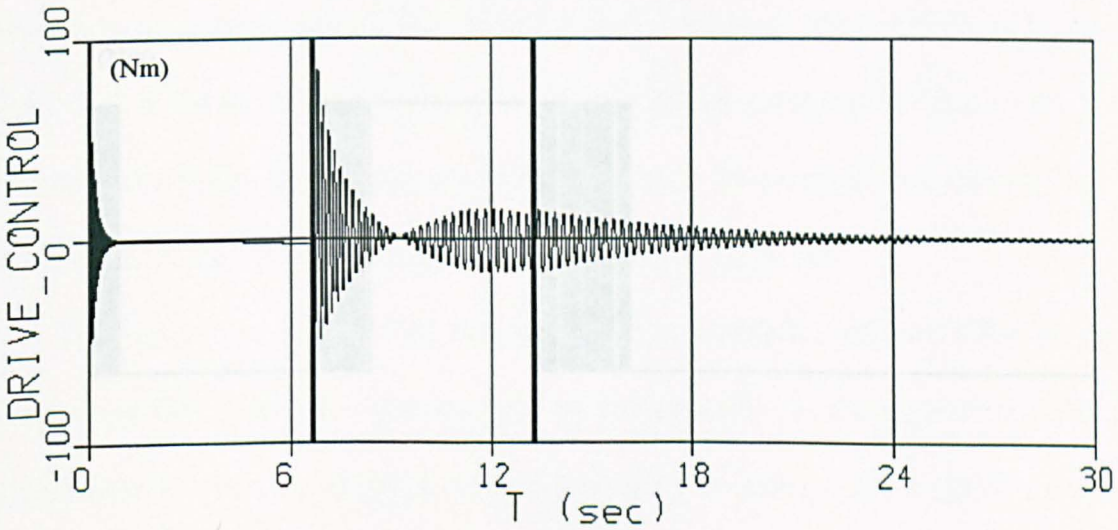

Figure 4.41: Linear Root feedback control torque for a minimum-time slew of an extending DRM plus Payload 1

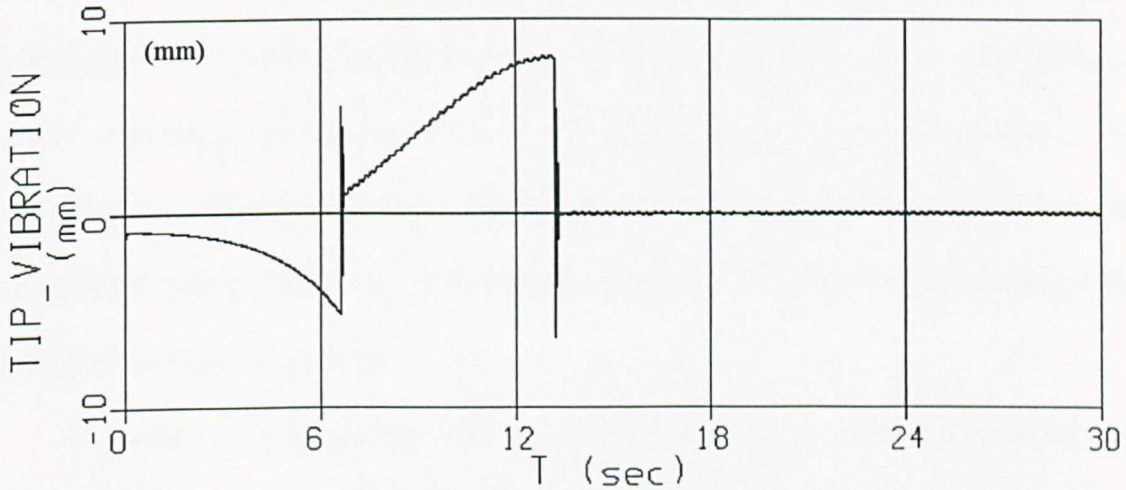

Figure 4.42: Linear Root feedback tip vibration results for a minimum-time slew of an extending DRM plus Payload 1, using large gains

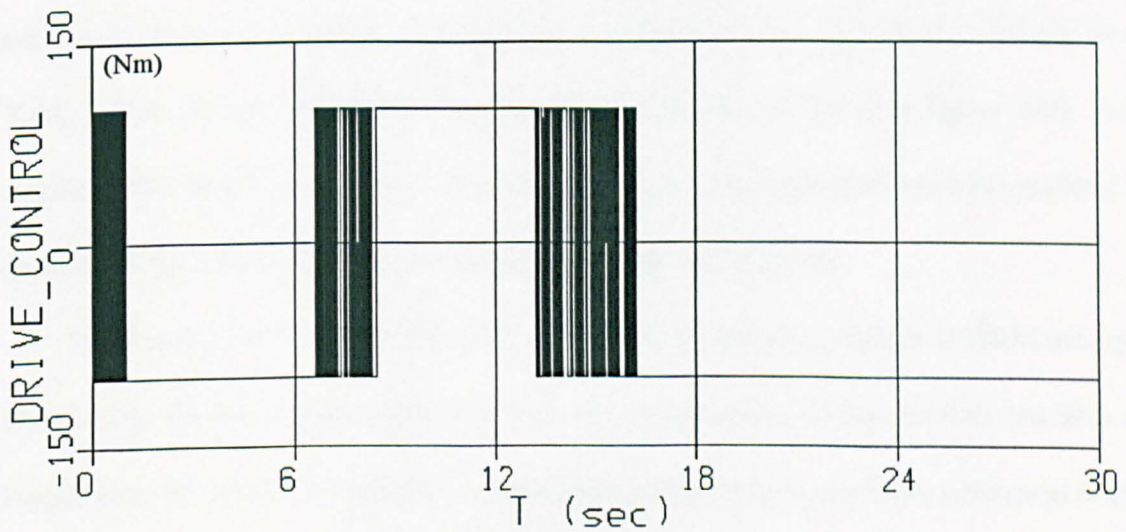

Figure 4.43: Linear Root feedback control torque for a minimum-time slew of an extending DRM plus Payload 1, using large gains

4.6.1.2 Tip Actuator Control Results

The linear velocity feedback tip control, Equation (3.4.2) is applied to the tip actuator with a gain J = -500.0, which produces for Payload 1 the tip vibration result in Figure 4.44. The vibrations results are for a slew manoeuvre of an extending DRM. The vibrations are damped throughout the manoeuvre and the residual vibrations are also completely reduced after the slew manoeuvre is over. The tip torque applied to the manipulator is shown in Figure 4.45.

The results of applying only the linear tip feedback control to the DRM can be seen to be good, even with a very limited controller of ±10 Nm the vibrations are damped out in a reasonable amount of time. This is of course to be expected as the tip actuator is acting at the point of maximum slope at the tip of the manipulator, and hence gives the maximum energy dissipation. Considering a smaller payload, Payload 0 of 50 Kg from Table 2-7, at the end of the DRM the tip vibration results are shown in Figure 4.46. The results in this figure show better vibration results as to be expected since the payload is smaller the tip vibration velocity is smaller and easier to damp out.

The J gain is set at –500.0 by trial an error from simulating different DRM set-ups. Decreasing the tip feedback gain can lead to less saturation of the actuator but also to longer time for vibration damping, whereas increasing the gain produces saturation of the actuator for a longer time and very little vibration damping improvement.

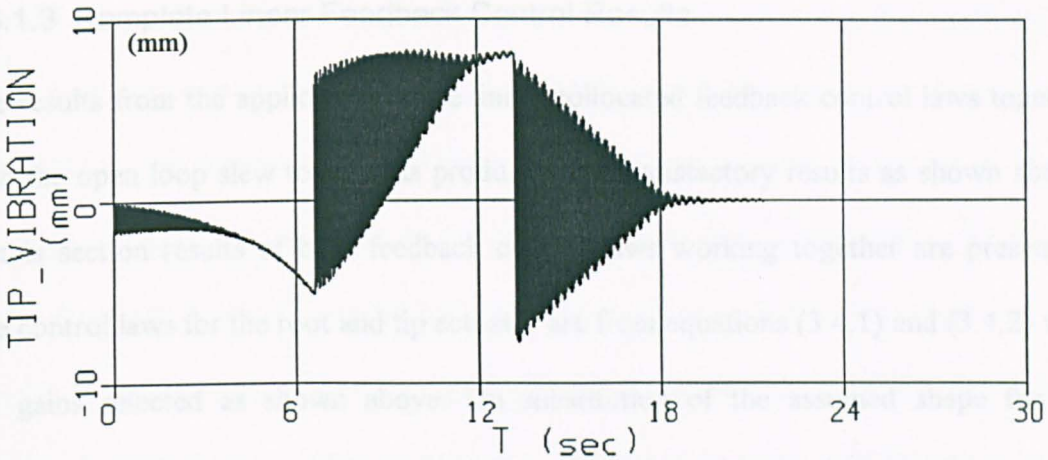

Figure 4.44: Linear Tip feedback tip vibration results for a minimum-time slew of an extending DRM carrying Payload 1

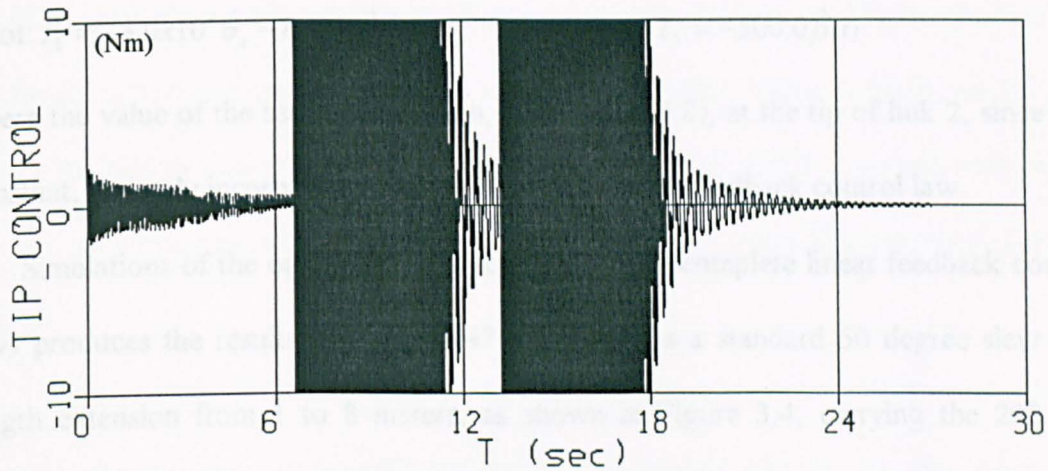

Figure 4.45: Linear Tip feedback control torque for a minimum-time slew of an extending DRM carrying Payload 1

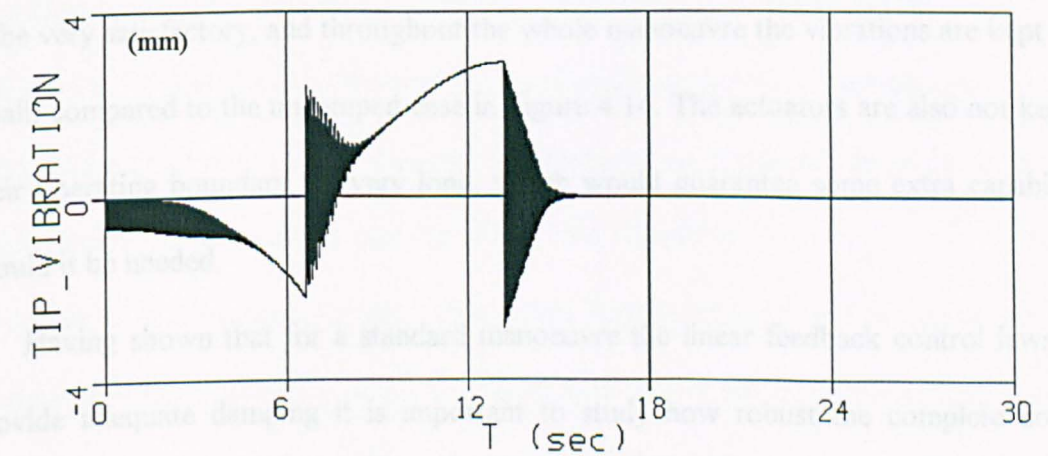

Figure 4.46: Linear Tip feedback tip vibration results for a minimum-time slew of an extending DRM carrying Payload 0

4.6.1.3 Complete Linear Feedback Control Results

The results from the application of the linear collocated feedback control laws together with the open loop slew torque has produced very satisfactory results as shown above. In this section results of both feedback control laws working together are presented. The control laws for the root and tip actuator are from equations (3.4.1) and (3.4.2) with the gains selected as shown above. On substitution of the assumed shape for the deflection of link 2 gives the implementation of these two feedback control laws in the simulation environment developed for the DRM:

Root: $T_1 = -8.0x10^4\dot{\theta}_e - 8.0x10^3\theta_e$ Tip: $T_2 = -500.0\dot{\beta}(t)$

where the value of the assumed function, equation (2.6.8), at the tip of link 2, since it is constant, is simply incorporated into the J gain of the tip feedback control law.

Simulations of the open loop slew torque plus the complete linear feedback control laws produces the results in Figure 4.47 which shows a standard 50 degree slew plus length extension from 1 to 8 meters, as shown in Figure 3.4, carrying the 200 Kg, Payload 1. The plots are of the tip vibrations throughout the slew, and the feedback control torques applied at the tip and at the root of the manipulator. The results are seen to be very satisfactory, and throughout the whole manoeuvre the vibrations are kept very small, compared to the undamped case in Figure 4.14. The actuators are also not kept at their operating boundary for very long, which would guarantee some extra capabilities should it be needed.

Having shown that for a standard manoeuvre the linear feedback control laws can provide adequate damping it is important to study how robust the complete control system is to modelling errors. In the first case the complete control system (open and

closed loop parts) are given a payload mass which is incorrect by +15%, so the torque motor thinks it has to slew a payload 15 % larger than it actually is. If only vibration damping control was applied the DRM it would reach an incorrect slew angle, as shown in Figure 4.38, of 56.2 degrees or 6.2 degrees above the desired angle. The linear feedback control law implemented here feeds back the error in the slew angle and slew rate as the manipulator is moving and so when the actual motion of the manipulator starts to deviate from the reference motion, as calculated from the rigid DRM model, the root feedback control law will react to try to compensate and keep the motion of the DRM as close as possible to the desired motion. Figure 4.48 shows the tip vibration and the feedback torques applied by the tip and root actuators. Figure 4.49 shows the slew angle time history throughout the manoeuvre, it can be seen that it is smooth and reaches the desired 50 degrees with no overshoot or settling time, almost like a critically damped system.

The final set of results presented in this section are of the DRM with a larger payload, the actual dynamic response may not be exactly correct, but the results still validate the control system as the vibrations are damped out correctly. The DRM is simulated as carrying the 500 Kg, Payload 3, from Table 2-7. It has already been pointed out that the current simulation model cannot reproduce the frequencies of vibration while the DRM carries such a large payload, its inertia is not modelled correctly in terms of mode shape approximation and therefore the vibration response is not accurate. However it can be used to see what could happen even if the vibration response calculated is not correctly modelled. Figure 4.50 shows the tip vibration and the slew angle for Payload 3 with a 15% mass error, the vibrations are completely damped out and there is a small amount of overshoot in the slew angle, but in the end it reaches the

desired 50 degrees. Figure 4.51 shows the same results but for a −15% payload mass error, the slew angle reaches the correct value and the vibrations are completely damped out.

For the payloads selected the results of the linear feedback control system are therefore quite good, the feedback control system complements the open loop slew strategy by providing feedback which damps out the flexible vibrations and corrects slew errors from the nominal motion.

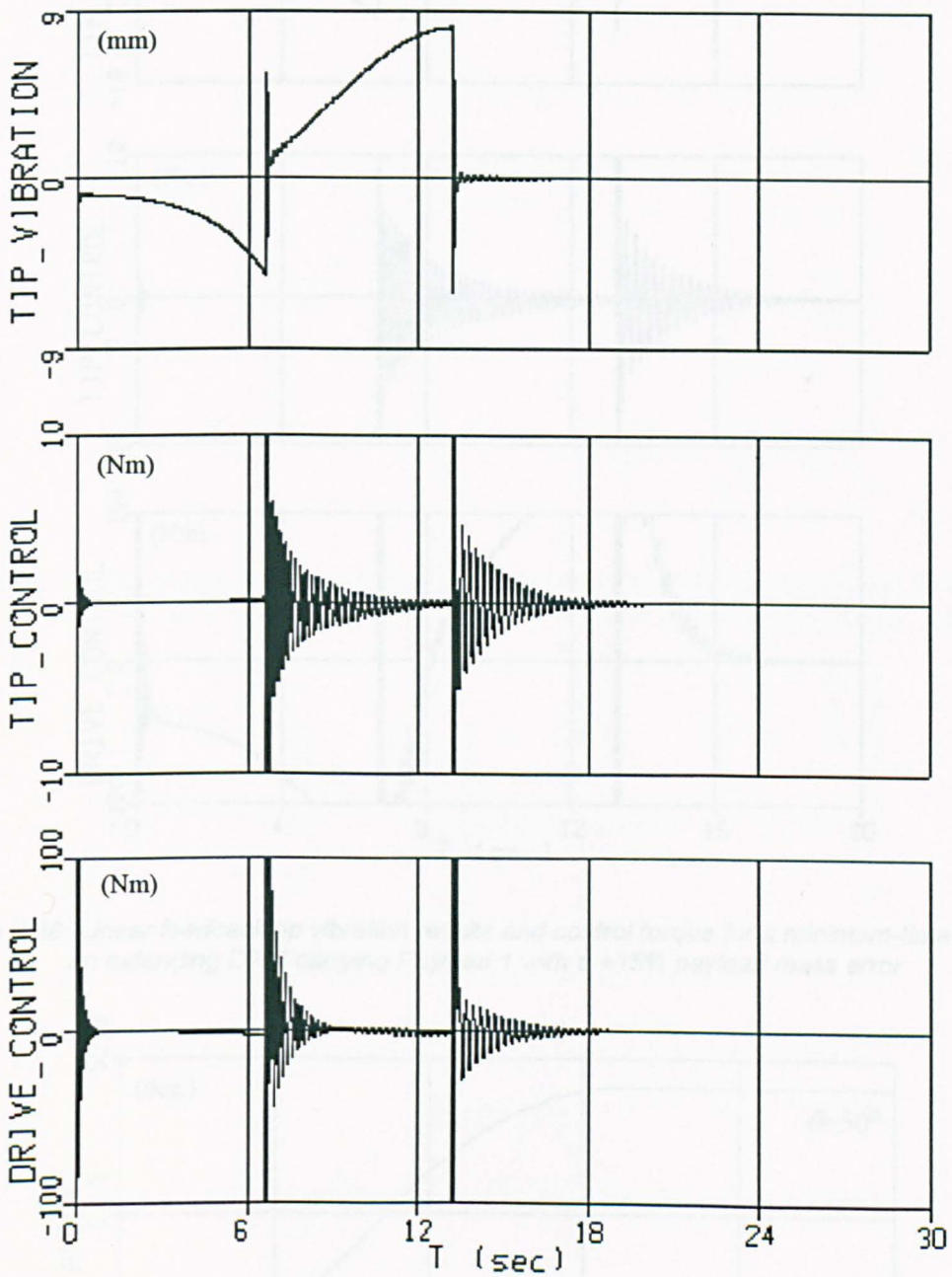

Figure 4.47: Linear feedback tip vibration results and control torque for a minimum-time slew of an extending DRM carrying Payload 1

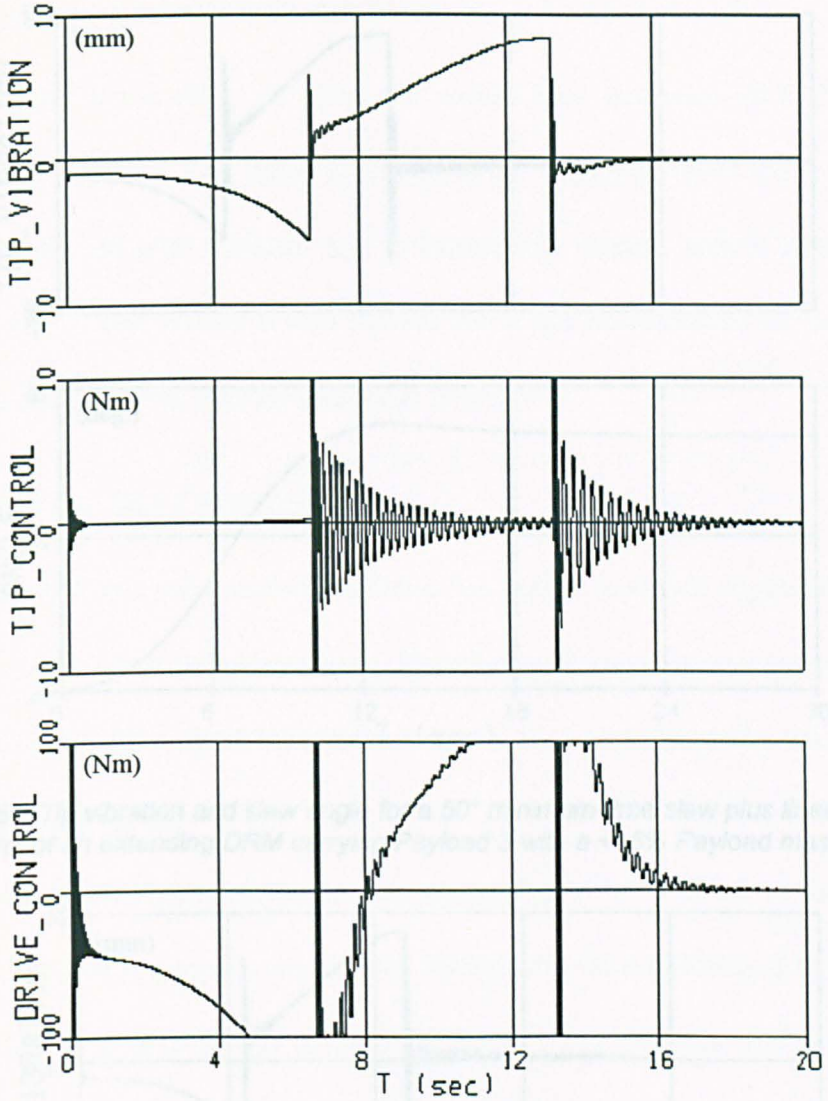

Figure 4.48: Linear feedback tip vibration results and control torque for a minimum-time slew of an extending DRM carrying Payload 1 with a +15% payload mass error

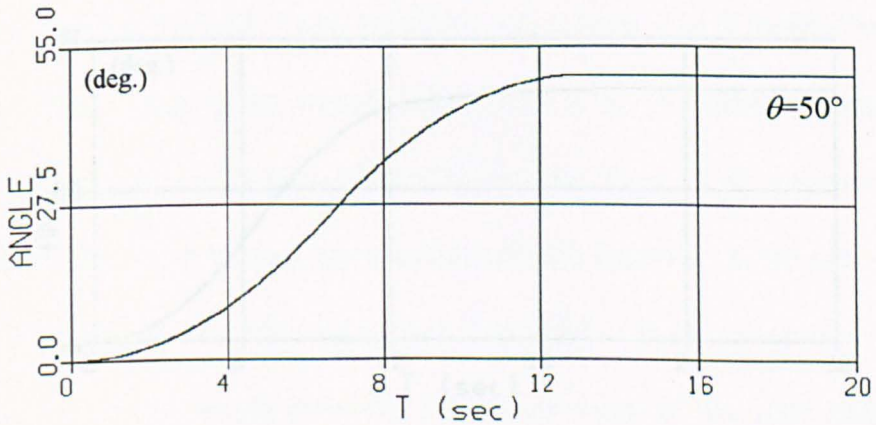

Figure 4.49: Linear feedback slew angle results of an extending DRM carrying Payload 1 with a +15% payload mass error

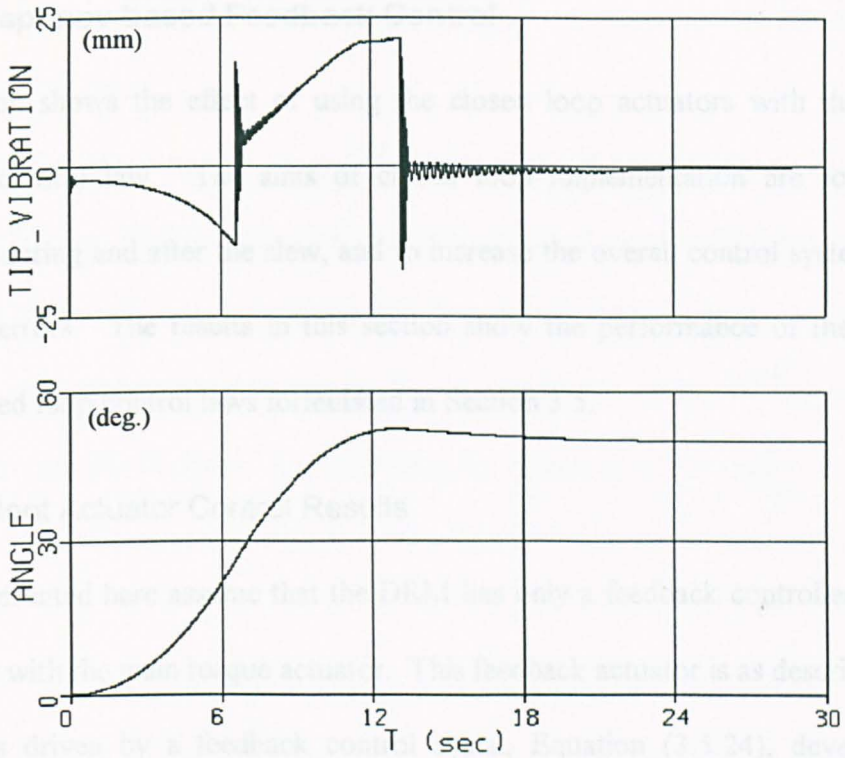

Figure 4.50: Tip vibration and slew angle for a 50° minimum-time slew plus linear feedback control of an extending DRM carrying Payload 3 with a +15% Payload mass error

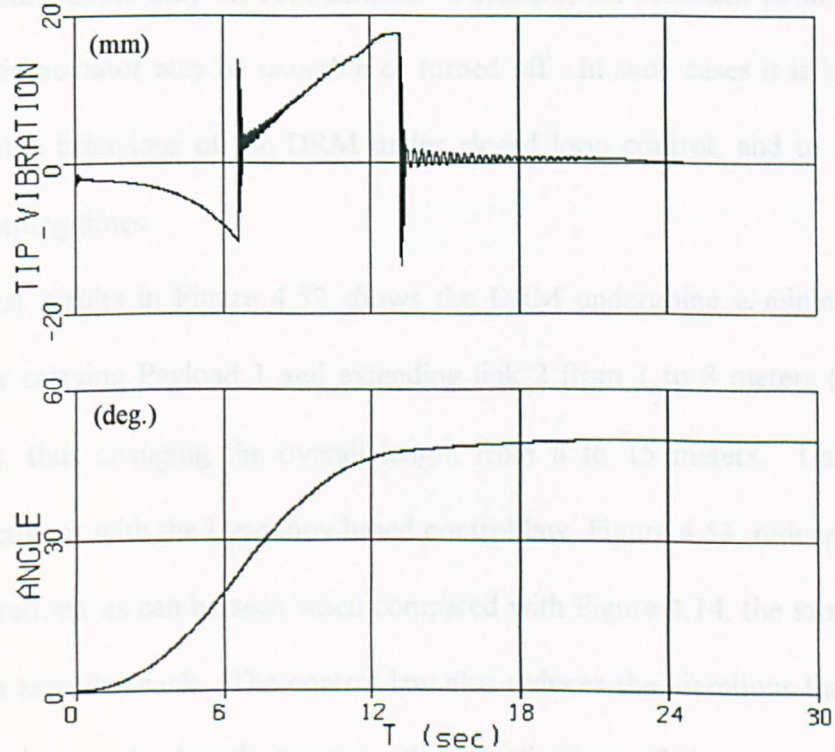

Figure 4.51: Tip vibration and slew angle for a 50° minimum-time slew plus linear feedback control of an extending DRM carrying Payload 3 with a -15% Payload mass error

4.6.2 Lyapunov-based Feedback Control

This section shows the effect of using the closed loop actuators with the Lyapunov feedback control law. The aims of closed loop implementation are to reduce tip vibrations during and after the slew, and to increase the overall control system tolerance to model errors. The results in this section show the performance of the Lyapunov-based closed loop control laws formulated in Section 3.5.

4.6.2.1 Root Actuator Control Results

Results presented here assume that the DRM has only a feedback controller at its base, collocated with the main torque actuator. This feedback actuator is as described in Table 3-1. It is driven by a feedback control signal, Equation (3.5.24), developed using Lyapunov stability theory.

It is assumed that only the root actuator is available for feedback to simulate a case where the tip actuator may be unusable or turned off. In such cases it is interesting to investigate the behaviour of the DRM under closed loop control, and to evaluate the vibration settling times.

The first results in Figure 4.52 shows the DRM undergoing a minimum-time 50 degree slew carrying Payload 1 and extending link 2 from 1 to 8 meters (as shown in Figure 3.4), thus changing the overall length from 8 to 15 meters. Using the root feedback actuator with the Lyapunov based control law, Figure 4.53, reduces the overall level of vibrations, as can be seen when compared with Figure 4.14, the same simulation results with zero feedback. The control law also reduces the vibrations throughout the manoeuvre, but as the length increases the effectiveness of the root control law is

reduced and the actuator cannot reduce the residual tip vibrations quickly, since it needs a longer settling time.

A large number of permutations and combinations of open loop control laws, torque smoothing factors and extension or contraction of link 2 can be simulated together with this feedback control law, but only a few are presented here. Figure 4.54 shows the Lyapunov root feedback control law applied to a minimum-energy 50 degree slew of the DRM while carrying Payload 1 and extending link 2 from 1 to 8 meters.

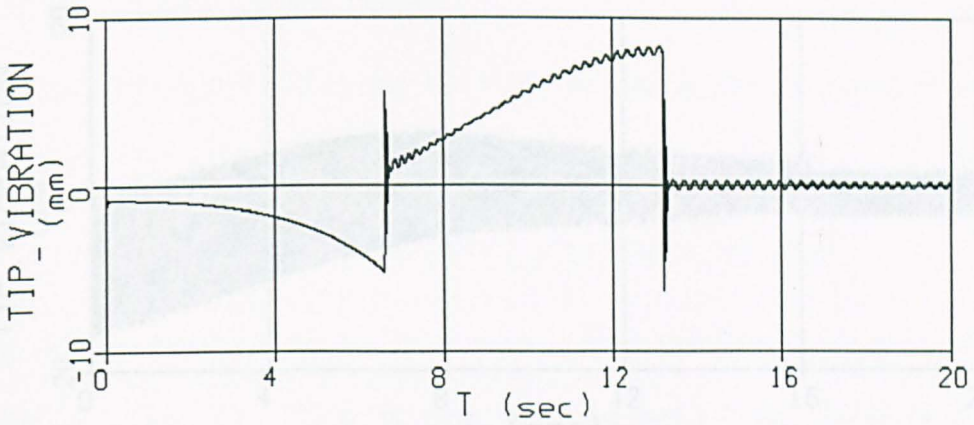

Figure 4.52: Lyapunov Root actuator damped tip vibrations for a 50° minimum-time slew of an extending DRM with Payload 1

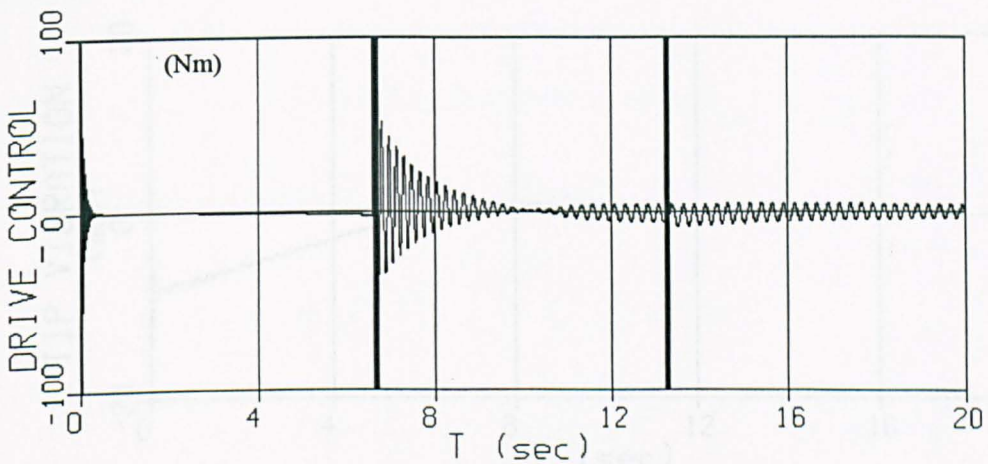

Figure 4.53: Lyapunov Feedback root actuator torque time history for a 50° minimum-time slew of an extending DRM with Payload 1

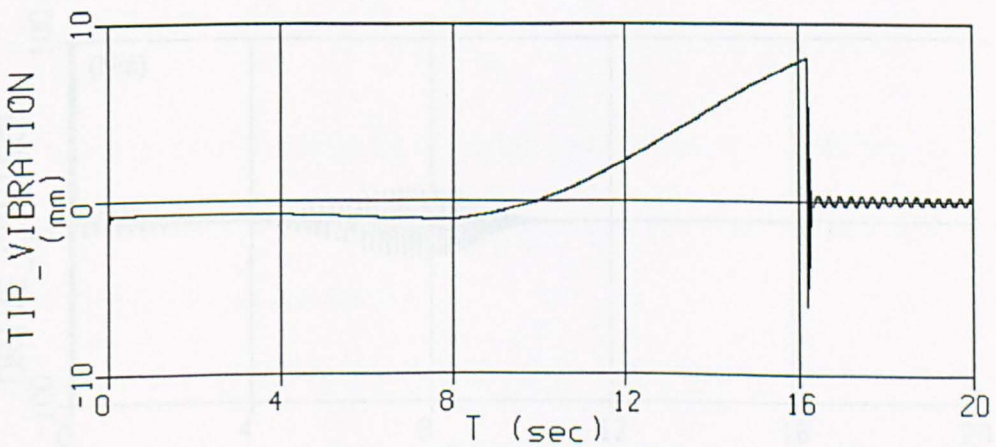

Figure 4.54: Lyapunov Root actuator damped tip vibrations for a 50° minimum-energy slew of an extending DRM with Payload 1

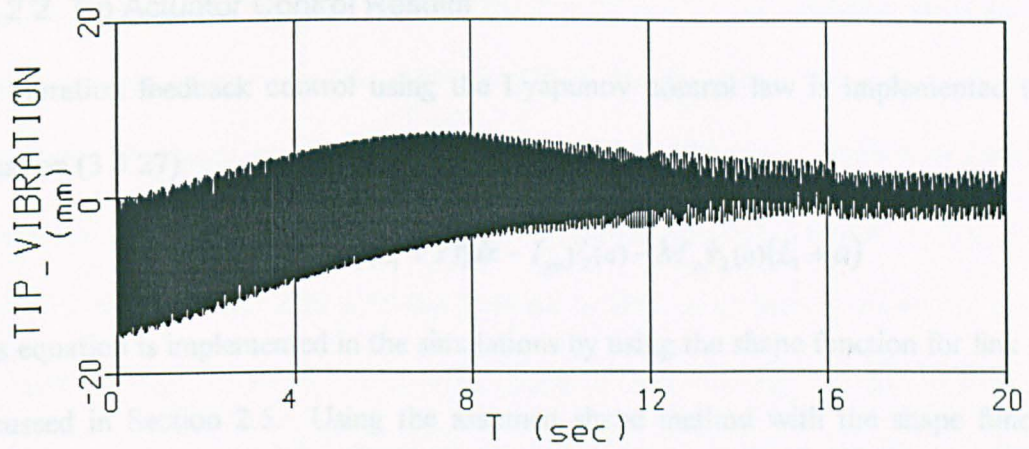

Figure 4.55: Undamped tip vibrations for a 50° minimum-energy slew of a contracting DRM with Payload 1

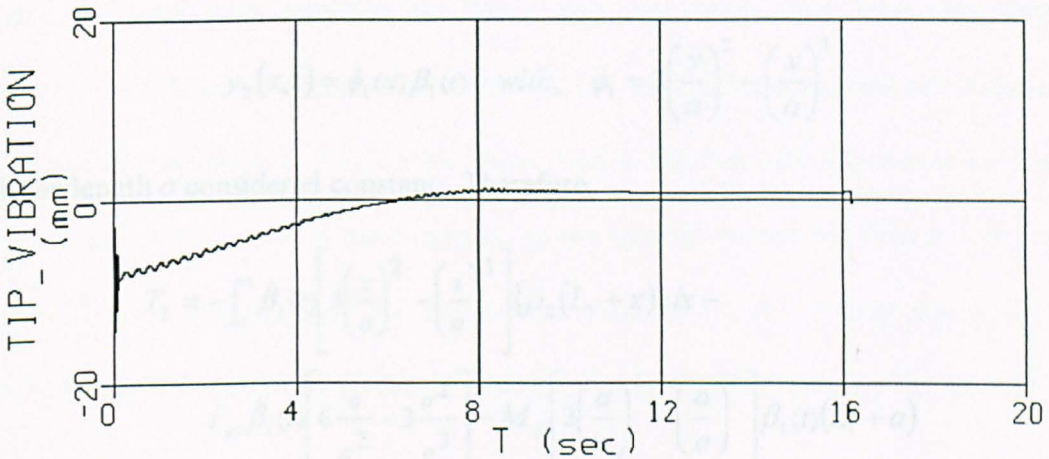

Figure 4.56: Lyapunov Root actuator damped tip vibrations for a 50° minimum-energy slew of a contracting DRM with Payload 1

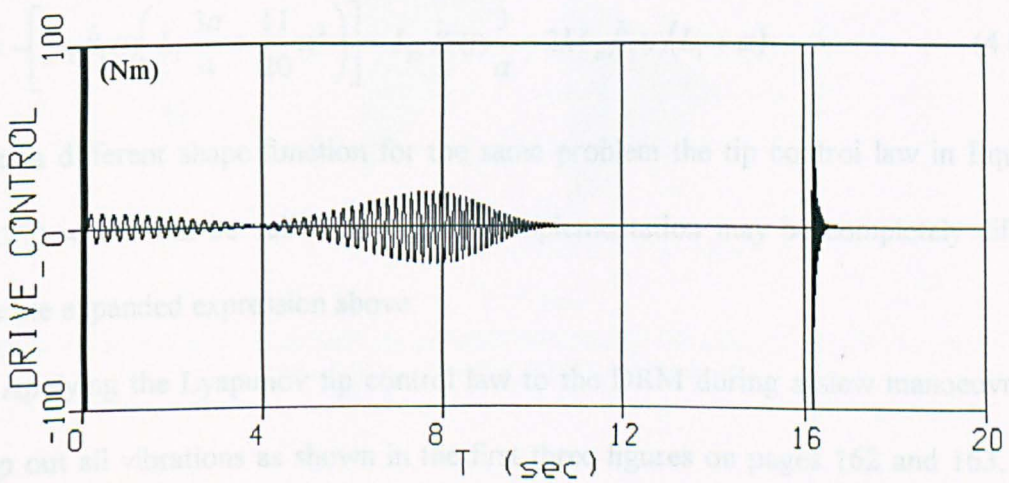

Figure 4.57: Lyapunov Feedback root actuator torque time history for a 50° minimum-energy slew of a contracting DRM with Payload 1

4.6.2.2 Tip Actuator Control Results

Tip vibration feedback control using the Lyapunov control law is implemented using Equation (3.5.27):

$$T_2 = -\int_0^a \dot{y}_2 \{\rho_2 (L_1 + x)\} dx - I_{yy} \dot{y}_2'(a) - M_p \dot{y}_2(a)(L_1 + a)$$

This equation is implemented in the simulations by using the shape function for link 2, as discussed in Section 2.5. Using the assumed shape method with the shape function, Equation (2.6.8), and performing the integrals above gives the following tip control law for this application:

$$y_2(x,t) = \phi_1(x)\beta_1(t) \quad with, \quad \phi_1 = 3\left(\frac{x}{a}\right)^2 - \left(\frac{x}{a}\right)^3$$

with the length a considered constant. Therefore,

$$T_2 = -\int_0^a \dot{\beta}_1(t)\left[3\left(\frac{x}{a}\right)^2 - \left(\frac{x}{a}\right)^3\right]\{\rho_2 (L_1 + x)\} dx -$$

$$I_{yy}\dot{\beta}_1(t)\left[6\frac{a}{a^2} - 3\frac{a^2}{a^3}\right] - M_p\left[3\left(\frac{a}{a}\right)^2 - \left(\frac{a}{a}\right)^3\right]\dot{\beta}_1(t)(L_1 + a)$$

which simplifying gives the Lyapunov tip actuator control torque implemented,

$$T_2 = -\left[\rho_2 \dot{\beta}_1(t)\left(L_1 \frac{3a}{4} + \frac{11}{20}a^2\right)\right] - I_{yy}\dot{\beta}_1(t)\frac{3}{a} - 2M_p\dot{\beta}_1(t)(L_1 + a) \qquad (4.6.1)$$

Given a different shape function for the same problem the tip control law in Equation (3.5.27) would still be valid but its actual implementation may be completely different from the expanded expression above.

Applying the Lyapunov tip control law to the DRM during a slew manoeuvre will damp out all vibrations as shown in the first three figures on pages 162 and 163. This after all is expected since Equation (4.6.1) is an enhanced tip velocity feedback control

law. What is remarkable is the fact that the control law has no tuneable gains, and that regardless what payload is carried with the DRM, the tip control law will damp out the vibrations. The latter can be appreciated from Figure 4.58 and Figure 4.59 which are exactly the same DRM manoeuvre but with different payloads, the first with a 200 Kg payload and the second with a 50 Kg payload, in both cases the vibrations are damped out, with the clear difference that it takes longer to damp out the residual vibrations with the larger payload since the vibrations are larger. Figure 4.60 shows the tip vibration results for a minimum-energy DRM manoeuvre while extending link 2 from 1 to 8 meters, this result highlights the fact that a minimum-energy open loop slew strategy produces less vibrations during the manoeuvre, but almost the same level of vibrations at the end of the manoeuvre. The control input used in this last case is presented in Figure 4.61, the actuator is used in the beginning as the slew is started but then it is not used very much until after the slew is complete and it damps out the residual vibrations, this activity keeps the actuator at its limits until the vibrations are completely damped out.

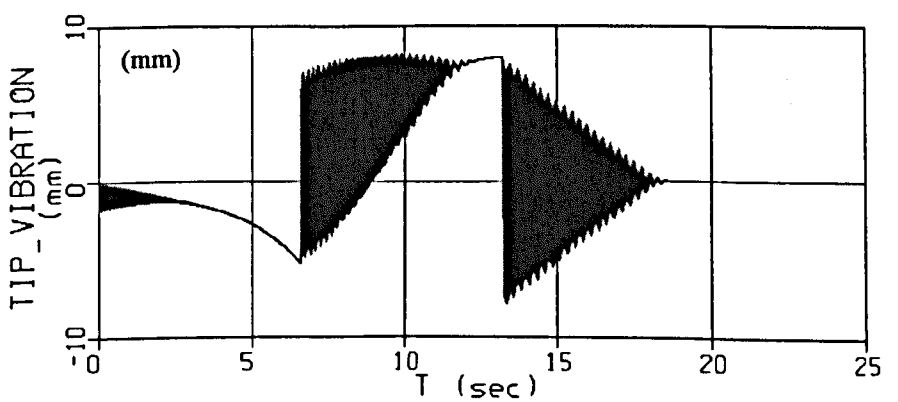

Figure 4.58: Lyapunov Feedback tip actuator damped tip vibrations for a 50° minimum-time slew of an extending DRM with Payload 1

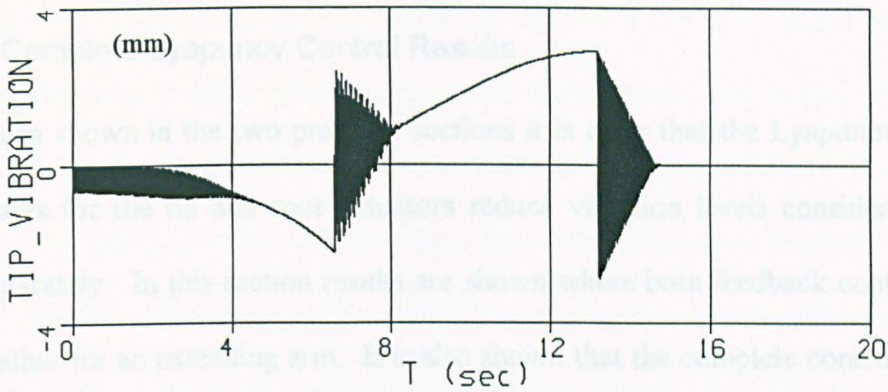

Figure 4.59: Lyapunov Feedback tip actuator damped tip vibrations for a 50° minimum-time slew of an extending DRM with Payload 0

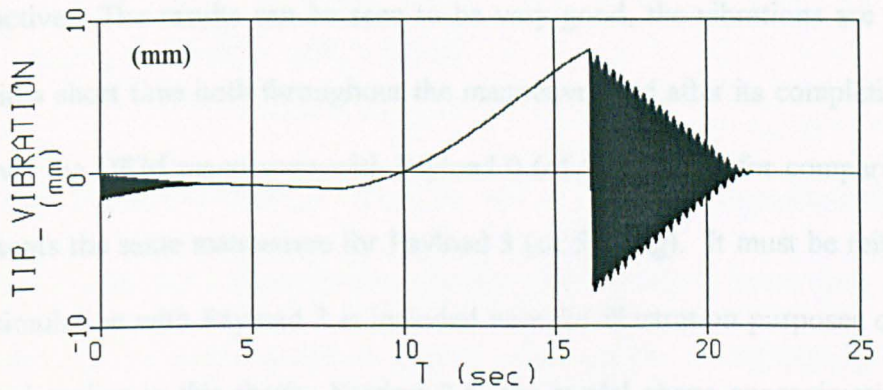

Figure 4.60: Lyapunov Feedback tip actuator damped tip vibrations for a 50° minimum-energy slew of an extending DRM with Payload 1

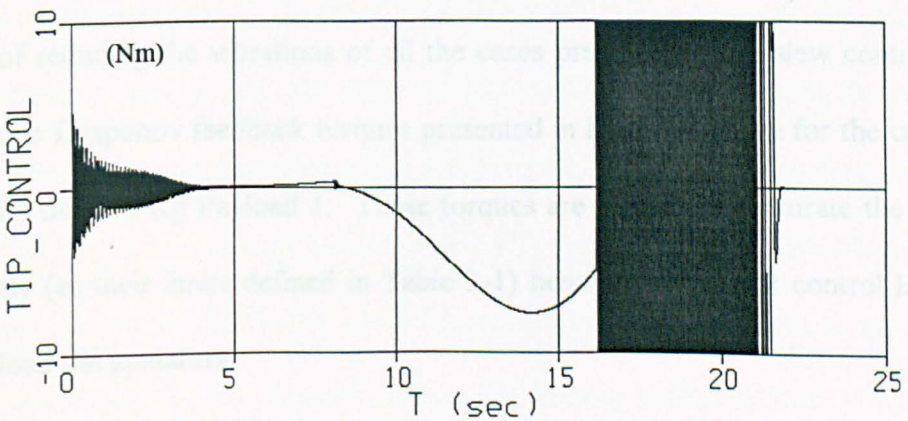

Figure 4.61: Lyapunov Feedback tip actuator torque time history for a 50° minimum-energy slew of an extending DRM with Payload 1

4.6.2.3 Complete Lyapunov Control Results

As has been shown in the two previous sections it is clear that the Lyapunov feedback control laws for the tip and root actuators reduce vibration levels considerably when acting separately. In this section results are shown where both feedback controllers are used together for an extending arm. It is also shown that the complete control system is robust to payload uncertainties.

Figure 4.63 shows the same results as in Figure 4.14, with the Lyapunov feedback control active. The results can be seen to be very good, the vibrations are completely reduced in a short time both throughout the manoeuvre and after its completion. Figure 4.62 shows the DRM manoeuvre with Payload 0 (of 50 Kg) and for comparison Figure 4.64 presents the same manoeuvre for Payload 3 (of 500 Kg). It must be reiterated that the last simulation with Payload 3 is included here for illustration purposes only, as has been noted earlier in this thesis, Section 2.5, the modal shape approximations do not reproduce the vibration frequencies correctly for the DRM plus such a large payload.

The Lyapunov control law, with no changes or gain adjustments can adapt and be capable of reducing the vibrations of all the cases presented. The slew control torque and the two Lyapunov feedback torques presented in Figure 4.65 are for the case of the DRM with the 200 Kg Payload 1. These torques are seen not to saturate the actuators excessively (as their limits defined in Table 3-1) hence the feedback control law would not overload the actuators.

The second set of results demonstrate the robustness requirements as stated earlier, the control system must be able to deal with payload mass uncertainties and reach the specified slew angle. Figure 4.66 shows a 50° for Payload 1 but the control system has

been given an overestimated mass of +15%, as required by the robustness requirement. Thus, the complete control system (Open loop slew torque and Lyapunov feedback torques) believe that they are trying to manoeuvre a 230 Kg payload when in fact the payload is only 200 Kg. This will have the effect of producing an incorrect open loop torque to drive the DRM using Equation (3.2.1), the torque will overshoot the desired slew angle (50°) as has been shown in Section 4.5. In this case the Lyapunov root feedback control law, Equation (3.5.24):

$$T_1 = -J_1\dot{\theta}_e - J_2\theta_e - J_3\int_0^a \rho_2(L_1+x)\left[(L_1+x)\ddot{\theta}_e + \ddot{y}_2\right]dx - J_3 I_{yy}\left(\ddot{\theta}_e + \ddot{y}_2'(a)\right) - J_3 M_p(L_1+a)\left[(L_1+a)\ddot{\theta}_e + \ddot{y}_2(a)\right]$$

$$J_1 = 3x10^4 \quad J_2 = 3x10^3 \quad J_3 = 2x10^{-4}$$

contains two correction terms involving θ_e and $\dot{\theta}_e$. These terms are defined as the difference between the desired angular position and velocity at every time step of the manoeuvre and the actual attained velocity and position during the manoeuvre as measured by the sensors on-board the DRM (angular encoder and tachometer for example). Therefore, due to the inclusion of these two feedback terms the feedback controller can correct deviations throughout the slew manoeuvre. In this specific case the velocity and position time histories will deviate from those expected, since the open loop torque will be calculated for a 230 Kg payload and the actual payload is only 200 Kg, the DRM angular velocity and position will overshoot during the execution of the manoeuvre, and the feedback root control law will have to compensate by counteracting the slew motor input. The control torques can be seen in Figure 4.68, where the plot scales have been slightly extended for the feedback control torques to more clearly show the amount of time the actuators spend at their limits, as can be appreciated it is not excessive. It is also worth noting that the overshoot, which without feedback reaches

56.21°, as shown in Figure 4.38, reaches 50.07° with the Lyapunov feedback controller in use, and it is quickly corrected to the desired 50°. To illustrate the robustness of this control strategy further, Figure 4.67 shows the results of having a large payload (Payload 3, of 500 Kg) and performing a minimum-energy slew with an error in its reported mass of −15%. From the slew angle plot it can be clearly seen that the slew angle is eventually reached as expected, and the tip vibrations are damped out.

These results confirm the stability and performance of this Lyapunov feedback control method. As a last set of results Figure 4.69 shows the tip vibration results of a minimum-time slew and Figure 4.70 for a minimum-energy slew with a certain amount of smoothing, $\varphi = 0.005$. It is clear, as shown in Section 4.2, that any amount of torque smoothing can reduce vibrations considerably so if the Lyapunov feedback control laws are applied together with the open loop torque smoothing the results are very good as can be seen when compared with the same simulations without feedback control as shown in Figure 4.17 and Figure 4.26.

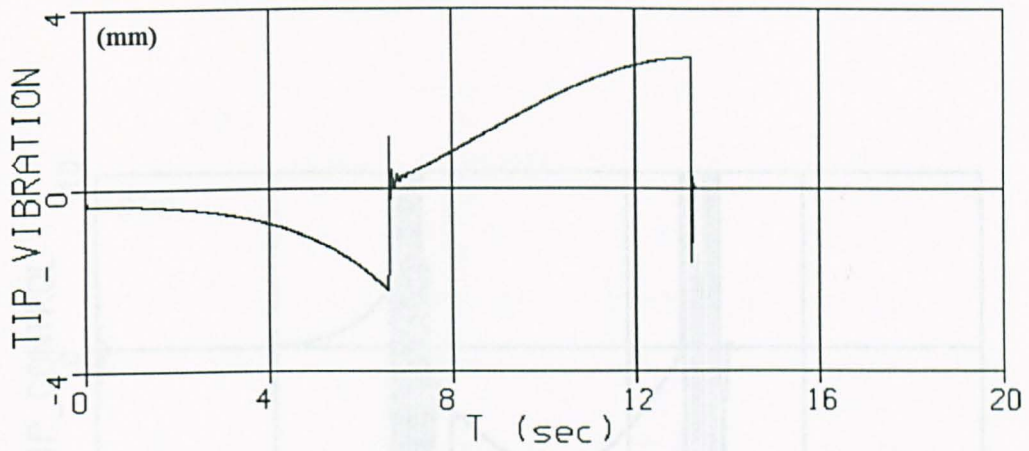

Figure 4.62: Lyapunov damped tip vibrations for a 50° minimum-time slew of an extending DRM with Payload 0

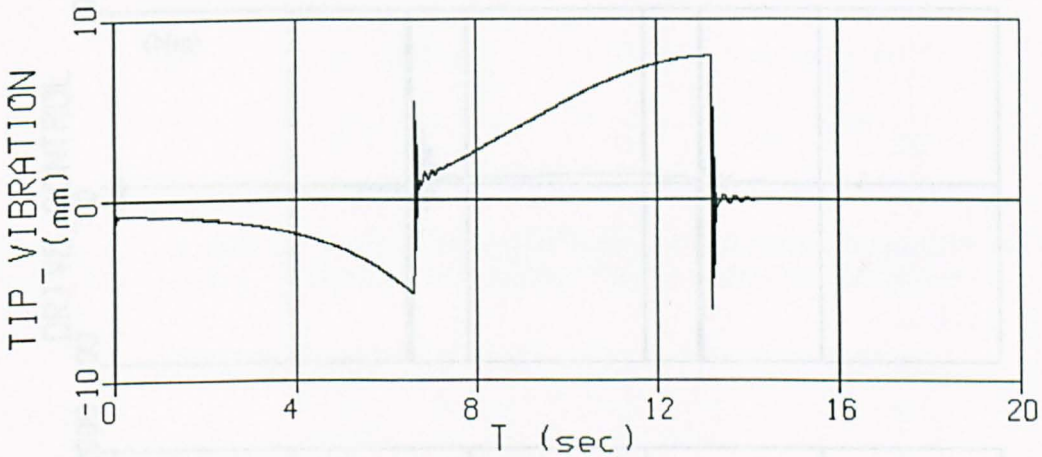

Figure 4.63: Lyapunov damped tip vibrations for a 50° minimum-time slew of an extending DRM with Payload 1

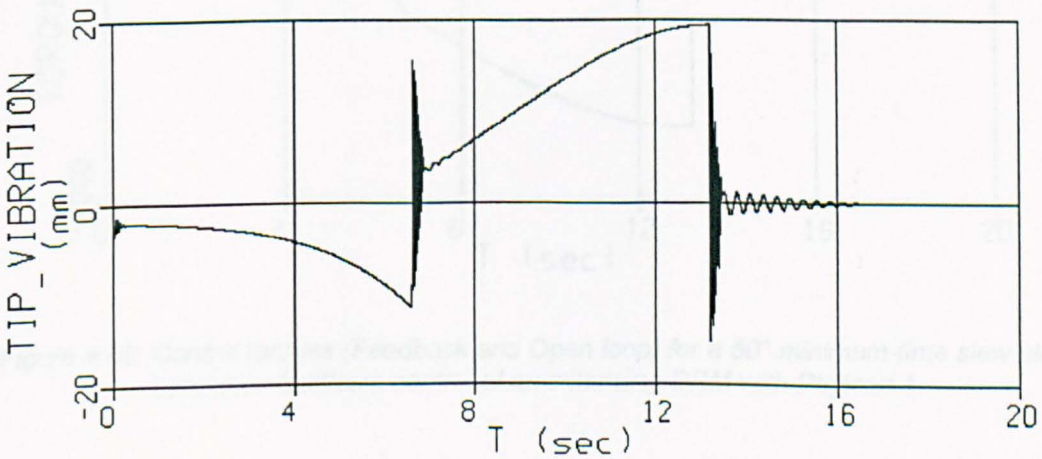

Figure 4.64: Lyapunov damped tip vibrations for a 50° minimum-time slew of an extending DRM with Payload 3

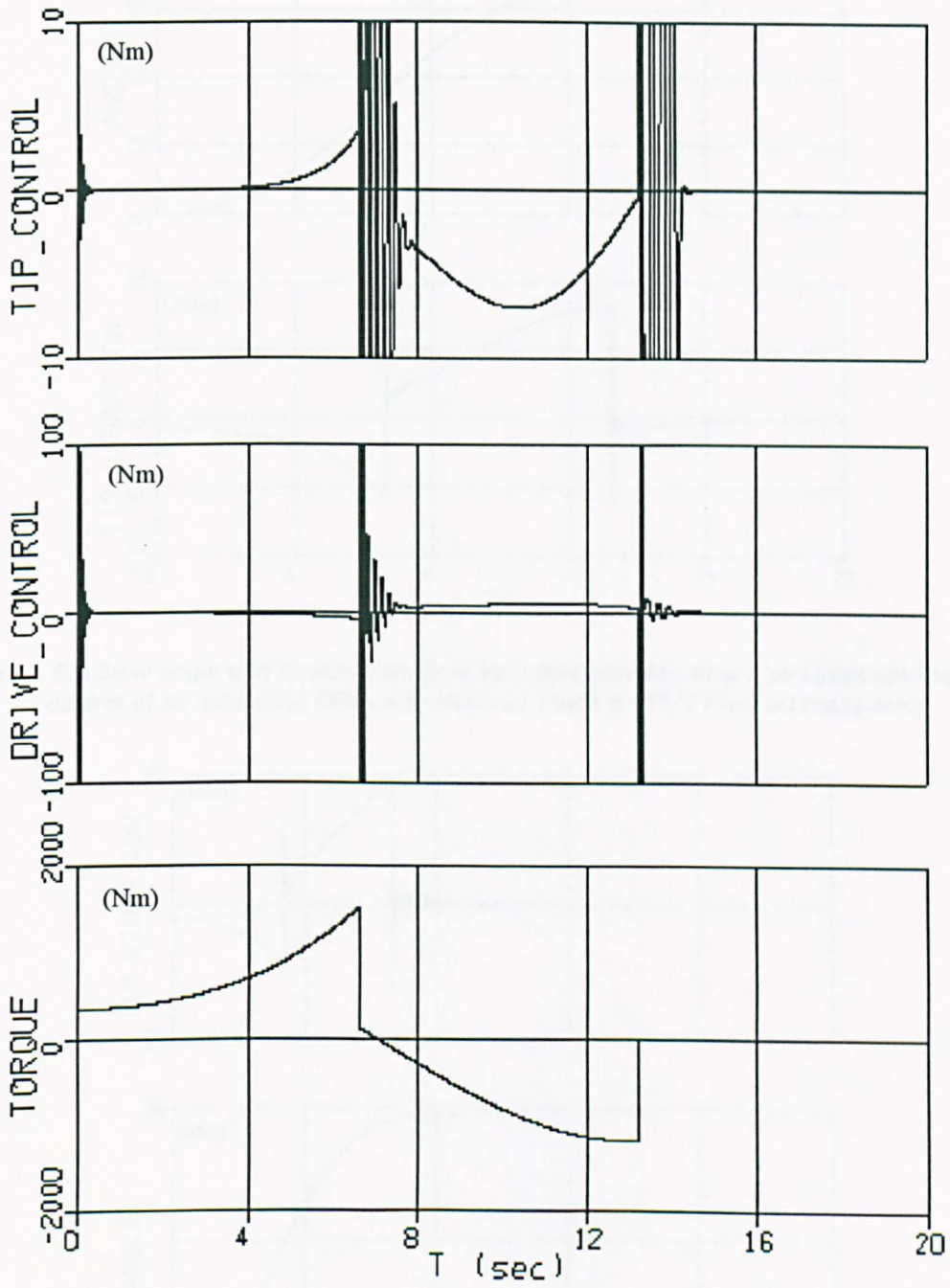

Figure 4.65: Control torques (Feedback and Open loop) for a 50° minimum-time slew plus Lyapunov feedback control of an extending DRM with Payload 1

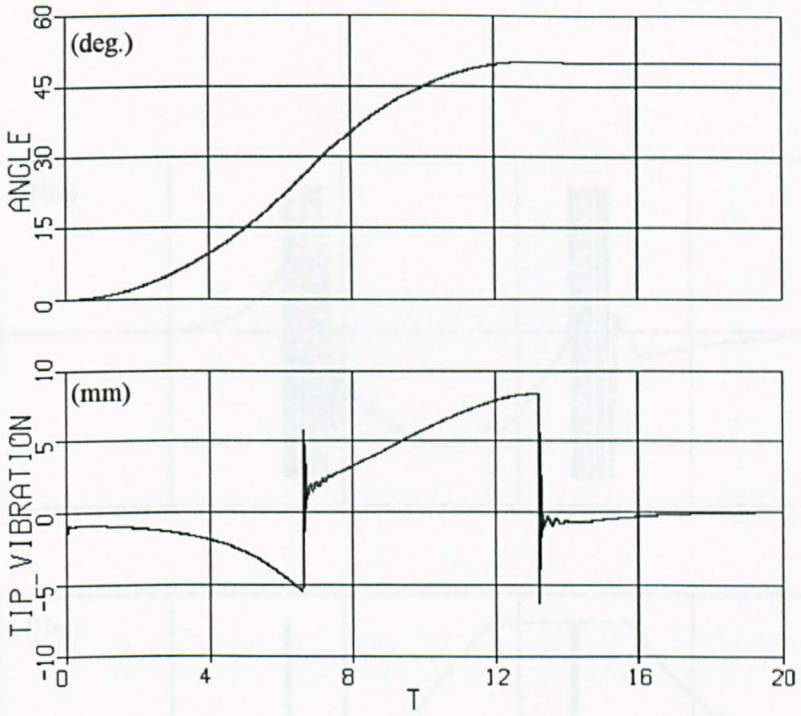

Figure 4.66: Slew angle and tip vibration for a 50° minimum-time slew plus Lyapunov feedback control of an extending DRM with Payload 1 with a +15% Payload mass error

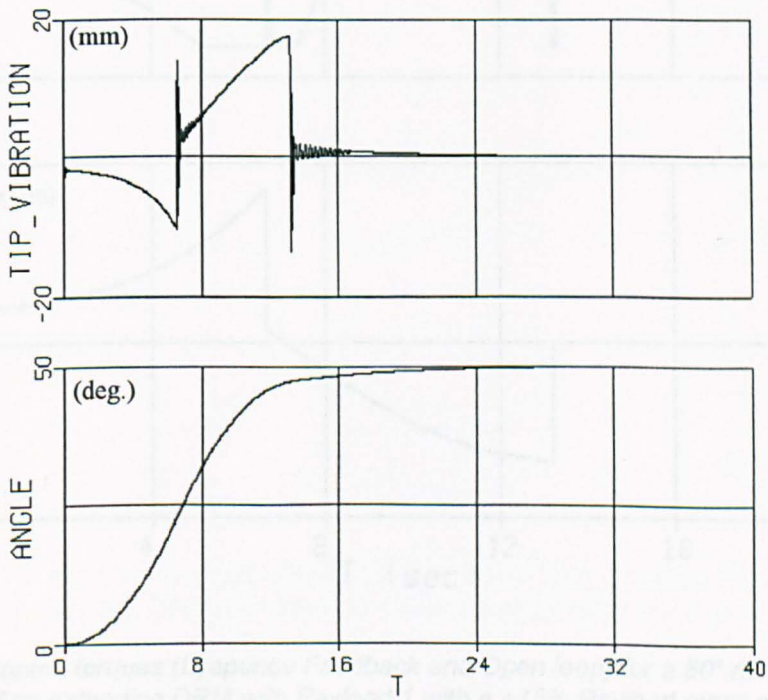

Figure 4.67: Slew angle and tip vibration for a 50° minimum-time slew plus Lyapunov feedback control of an extending DRM with Payload 3 with a -15% Payload mass error

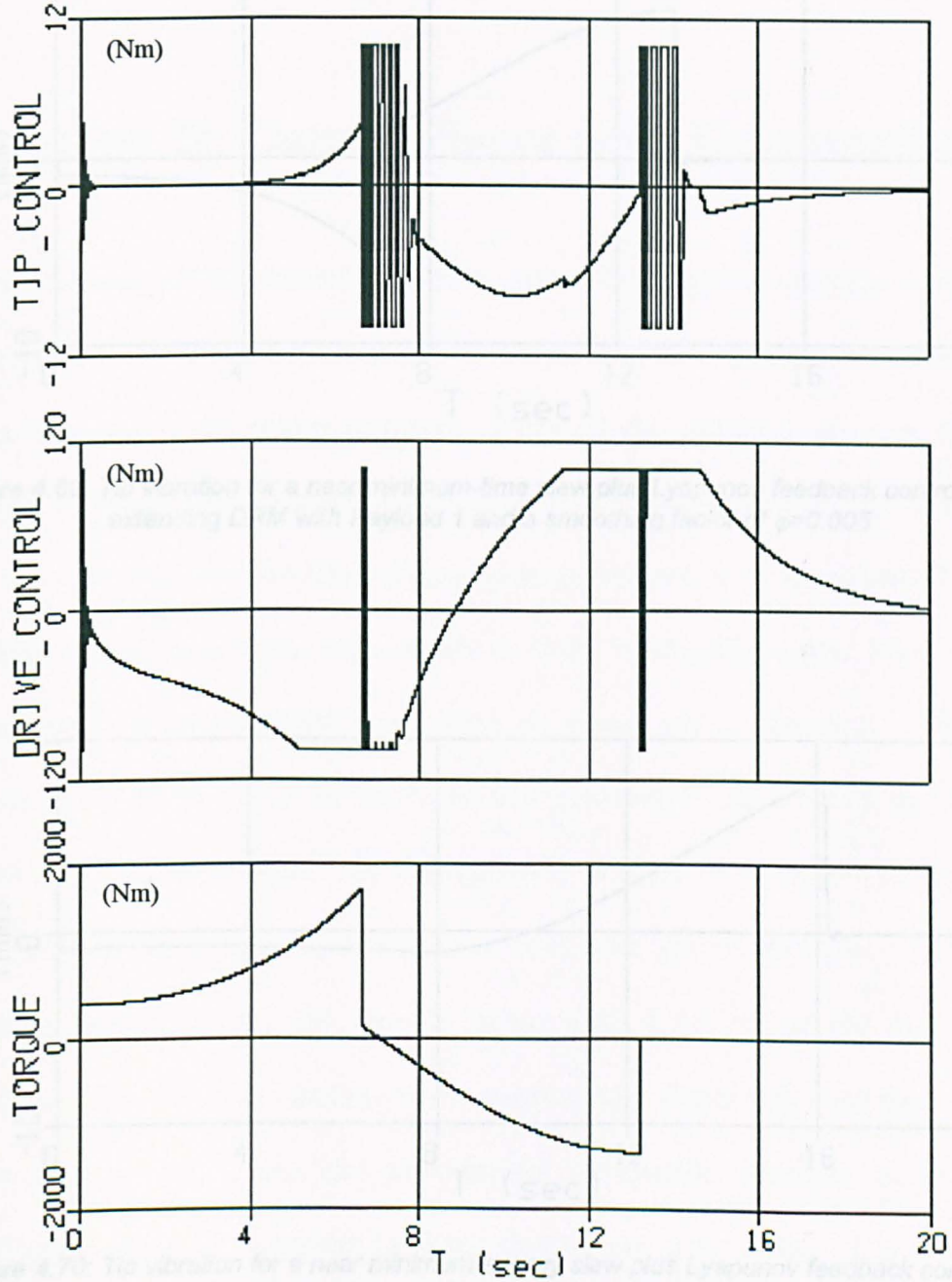

Figure 4.68: Control torques (Lyapunov Feedback and Open loop) for a 50° minimum-time slew of an extending DRM with Payload 1 with a +15% Payload mass error

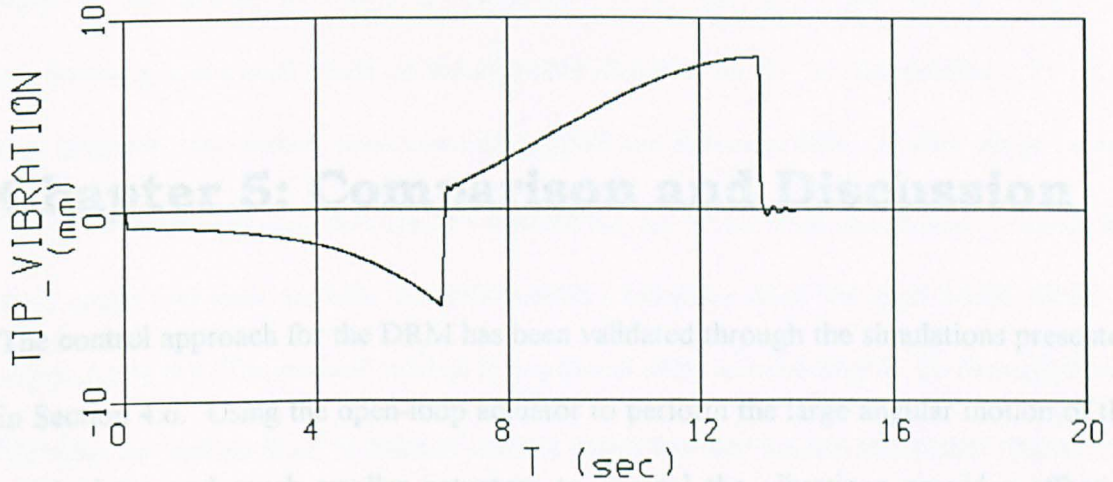

Figure 4.69: Tip vibration for a near minimum-time slew plus Lyapunov feedback control of an extending DRM with Payload 1 and a smoothing factor of φ=0.005

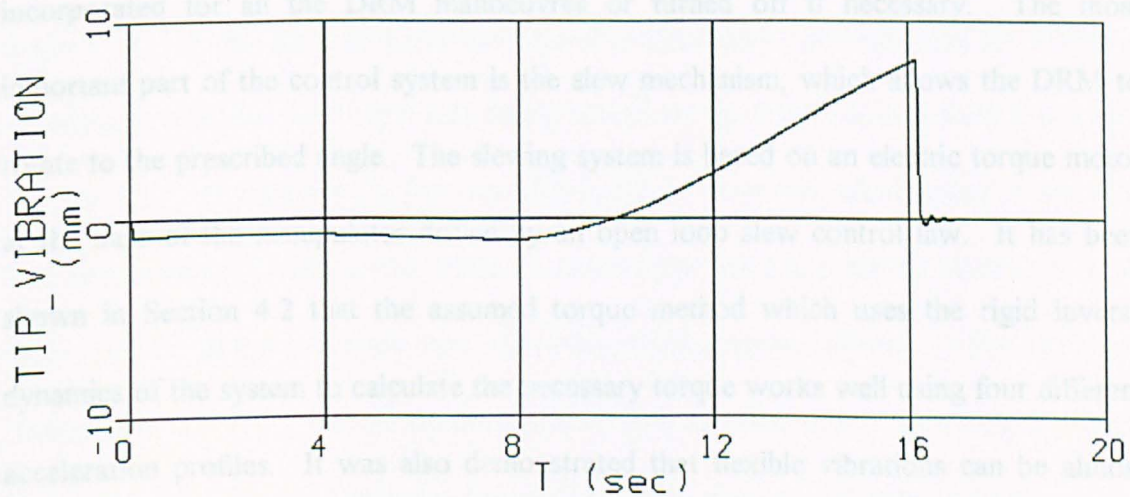

Figure 4.70: Tip vibration for a near minimum-energy slew plus Lyapunov feedback control of an extending DRM with Payload 1 and a smoothing factor of φ=0.005

Chapter 5: Comparison and Discussion

The control approach for the DRM has been validated through the simulations presented in Section 4.6. Using the open-loop actuator to perform the large angular motion of the manipulator and much smaller actuators to control the vibrations provides effective damping to reduce vibrations and it adds robustness. The manipulator can complete a slew correctly even when the mass of the payload is misreported or approximated.

The control system has been shown as three independent parts, which can be incorporated for all the DRM manoeuvres or turned off if necessary. The most important part of the control system is the slew mechanism, which allows the DRM to rotate to the prescribed angle. The slewing system is based on an electric torque motor at the base of the manipulator driven by an open loop slew control law. It has been shown in Section 4.2 that the assumed torque method which uses the rigid inverse dynamics of the system to calculate the necessary torque works well using four different acceleration profiles. It was also demonstrated that flexible vibrations can be almost completely avoided by smoothing the input slew torque to the DRM. This could be a valid slewing strategy if the level of complexity of the control system want to be kept to a minimum.

The second part of the control system involves the feedback actuators, in particular the root actuator. This actuator was introduced collocated with the slew motor at the base of the manipulator and it can introduce a reaction torque to the DRM by accelerating a reaction wheel in the opposite direction of the torque needed. To drive this actuator two control laws were developed and demonstrated. A very simple linear feedback control is demonstrated in Section 4.6.1.1 which only takes into account the slew angle and slew angular rate errors with respect to what the rigid DRM model is expected to do. The second control law is much more complicated in its derivation and formulation coming from Lyapunov's direct method of driving any dynamical system to a target state by always guaranteeing the value of the time derivative of the Lyapunov function is kept negative at all times, its results are shown in Section 4.6.2.1.

Inclusion of the root actuator in the control system can be seen to be fundamental for the robustness requirement, without it the DRM could not reach the correct slew angle if any of the payload's physical characteristics was incorrect. As for vibration damping, it provides very important inputs to reduce tip vibration, and from the results (Figure 4.40 and Figure 4.52, for example) it can be seen that when acting as the only feedback actuator the linear root feedback control law can damp out the vibrations faster than the Lyapunov control law, for the configuration shown. For different configurations and manoeuvre conditions, such as faster slew speed, larger payloads, etc it is very much expected that the Lyapunov control law would prove superior to the linear feedback control law. As discussed below simulations for these cases cannot be reliably performed for the existing DRM mathematical model and therefore it should be studied in an extension to this work.

The third part of the control system is the tip actuator, which even though is quite small is very important to reduce vibrations of the DRM during a slew manoeuvre. It is attached to the tip of the flexible link 2 of the DRM collocated with the grapple mechanism at the tip, for example. Results for slew manoeuvres using the tip actuator as the only mechanism for vibration damping (Figure 4.44, and Figure 4.58, for example) show very similar results for the linear and the Lyapunov feedback control laws, with the later being slightly faster at damping out tip vibrations than the former for the same configuration and manoeuvre.

Finally looking at the control system together, slew motor plus reaction wheel actuators, it can be seen from Figure 4.47 and Figure 4.63 that the vibration damping is equivalent whether the linear or the Lyapunov control laws are used. The latter provides slightly faster settling time but only by a few seconds. The robustness simulations show that the control system is able to adjust to reach the correct slew angle even in the presence of significant payload mass errors. Figure 4.66 and Figure 4.48 show the results from the two feedback control laws in the same configuration and the results are practically identical. In fact, given that the feedback actuators are bound and that the simulation model only permits the accurate simulations of small to medium payloads the choice of feedback control law becomes almost irrelevant and is only a matter of personal choice. Given a less constrained simulation model where, for example, large payloads could be simulated and the feedback actuators were unbound the Lyapunov control law would prove itself superior to the linear control law. This can be appreciated in the simulation results shown in the Figures on page 176. The simulation results are for a 3000 Kg payload so they are merely indicative, since the vibration response cannot be accurately represented with the simulation model programmed here, and the feedback

controllers are unbounded, thus the Lyapunov control law can be seen to provide almost instant damping. This goes to show that the Lyapunov feedback control law is mathematically superior to the linear feedback control law and can be applied to a much larger number of configurations in the day to day operations of the DRM, but in a pseudo-realistic simulation environment having limited the size of payloads that can be accurately represented there is not much difference in what closed loop control law is selected.

Finally other DRM operating conditions have been considered for study but not included in this research. The most important one is the movement of the base along the length of the in-orbit structure as has been considered before (Hokamoto et al, 1998), (Hokamoto et al, 1995), (Marom and Modi, 1993). This would be a basic feature of a robotic manipulator design following the DRM idea, since it has the disadvantage of not being able to reach the working space around its base. Motion of the base point of the DRM along the in-orbit structure is assumed by this researcher to take place in particular configurations, slowly, and with the slew brakes activated, so it falls outside the scope of this work. It is not considered likely that a slew manoeuvre would be attempted while moving the base along the structure. In this special case, the motion would become more complicated and the large slew torque motor may saturate as it tries to slew the manipulator while correcting for the base motion. It would be also possible to define the linear base motion as a control input of the DRM system as an interesting extension of this work.

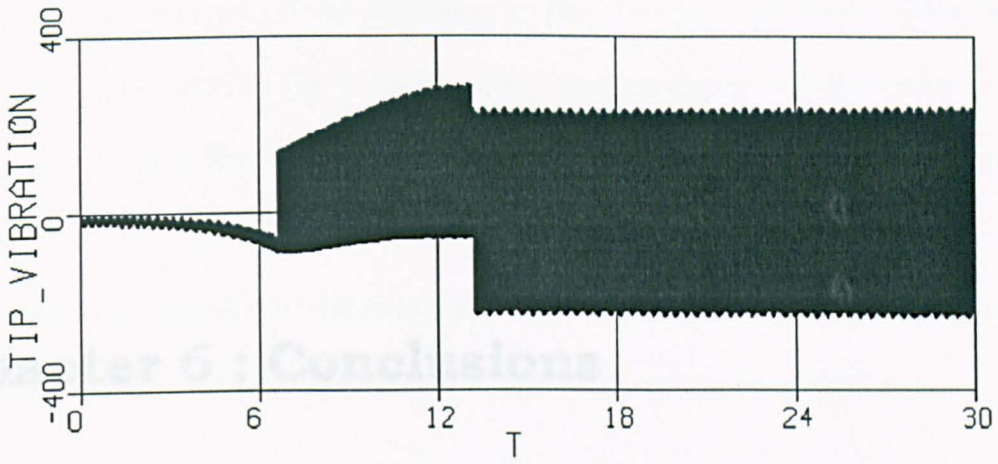

Figure 5.1: Undamped tip vibrations for a minimum-time slew of an extending DRM with a 3000Kg Payload

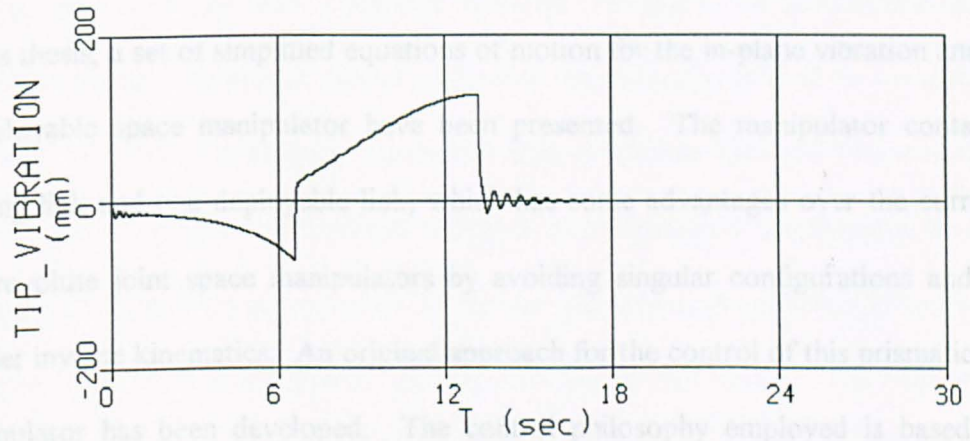

Figure 5.2: Linear feedback control tip vibrations for a minimum-time slew of an extending DRM with a 3000Kg Payload

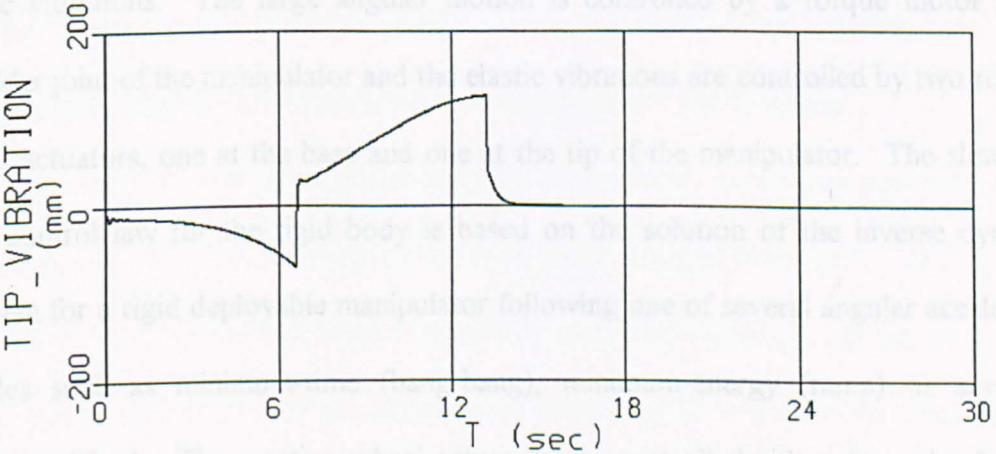

Figure 5.3: Lyapunov feedback tip vibrations for a minimum-time slew of an extending DRM with a 3000Kg Payload

Chapter 6 : Conclusions

6.1 Summary

In this thesis, a set of simplified equations of motion for the in-plane vibration analysis of a deployable space manipulator have been presented. The manipulator contains one slewing link and one deployable link, which has some advantages over the current two link revolute joint space manipulators by avoiding singular configurations and having simpler inverse kinematics. An original approach for the control of this prismatic-jointed manipulator has been developed. The control philosophy employed is based on the separation of the gross angular displacements of the rigid body and the damping of the elastic vibrations. The large angular motion is controlled by a torque motor at the shoulder joint of the manipulator and the elastic vibrations are controlled by two reaction wheel actuators, one at the base and one at the tip of the manipulator. The slew open loop control law for the rigid body is based on the solution of the inverse dynamics problem for a rigid deployable manipulator following one of several angular acceleration profiles such as minimum-time (bang-bang), minimum-energy (ramp) or smoothed versions of both. The reaction wheel actuators are controlled either by a simple linear position and velocity error feedback control law or by a more sophisticated control law

derived using Lyapunov's direct method to produce a robust and stable control law for this time-varying system. The feedback control laws are proven via simulations and they both show the capability to reduce the flexible vibrations produced by the open loop slew manoeuvre. It is also shown that either of the feedback control laws can ensure a successful slew manoeuvre even when the payload mass information is misreported to the control system, adding a certain degree of redundancy to the system.

6.2 Closing Remarks

The set of reduced order equations of motion developed for the DRM have shown that a simplified system can provide effective dynamic simulations to understand the behaviour of a complex system. Elsewhere it is sometimes assumed that one must use very complex mathematical simulation tools to provide high order dynamic simulations of arbitrarily complex systems when in the end the intended applications can be easily captured by a basic development such as the one in this thesis. The reduced order system must be understood and its limitations and simplifications must always be present so as not to push the capabilities of the formulations beyond the original assumptions. In the case of the DRM this has involved reducing the mass of the payloads that can be correctly simulated and avoiding large slew velocities and accelerations.

The control system developed in this thesis is versatile, since it can deal with a time-varying system, with different size payloads and with payload mass errors. It is also fast since it reacts to manipulator vibrations quickly and damps them out, as has been shown in the simulation results. It is convenient in that it relies only on output information, quantities which in principle can be easily measured so that the dynamical system's entire

state vector does not have to be estimated during the manoeuvre, this makes it a good candidate for real-time implementation where onboard processor power may be limited.

6.3 Future Research Direction

Further studies of the DRM dynamics are recommended, directions for future extension of this work have been indicated in the text when warranted. The main ones are that a new dynamical model could be developed to simulate correctly payloads that are orders of magnitude larger than the ones simulated in these pages and more critically including torsion to correctly model the full DRM response. The new dynamical model could be accomplished by using more sophisticated assumed functions for the flexible link deflection, or by using a more sophisticated discretization method such as the finite element method. The control system analysis could also be enhanced by the inclusion of the sensor and actuator dynamics, the reduction gear of the slew motor, and drive shaft flexibility.

References

AIAA, *Aerospace Design Engineers Guide*, Third Edition, AIAA, Washington DC, 1993.

Allen D.H., Haisler W.E., *Introduction to Aerospace Structural Analysis*, John Wiley & Sons, Inc., New York, New York, 1985.

Anderson B.D.O., Moore J.B., *Optimal Control - Linear Quadratic Methods*, Prentice Hall, Englewood Cliffs, New Jersey, 1989.

Ata A., Elkhoga S., Shalaby M., Asfour S., *Causal inverse dynamics of a flexible hub-arm system through Liapunov's second method*, Robotica, Cambridge University Press, Vol. 14, pp 381-389, 1996.

Banerjee A., Kane T., *Extrusion of a Beam from a Rotating Base*, Journal of Guidance, Control and Dynamics, Vol. 12, pp 140-146, 1989.

Bayo E., *A Finite-Element Approach to Control the End-Point Motion of a Single-Link Flexible Robot*, Journal of Robotic Systems, Vol. 4, No. 1, 1987.

Beards C.F., *Vibration Analysis and Control System Dynamics*, Ellis Horwood Ltd., Chichester, England, 1981.

Bhat R.B., *Nature of Stationarity of the Natural Frequencies at the Natural Modes in the Rayleigh-Ritz Method*, Journal of Sound and Vibration, Vol. 203, No. 2, pp 251-263, June 1997.

Blevins R.D., *Formulas for Natural Frequency and Mode Shape*, Robert E. Krieger Publishing Co., Malabar, Florida, 1979.

Book W.J., *Structural Flexibility of Motion Systems in the Space Environment*, IEEE Transactions on Robotics and Automation, Vol. 9, No. 5, October 1993.

Bryson A.E., Ho Y-H, *Applied Optimal Control*, Taylor & Francis, 1975.

Cetikunt S., Book W.J., *Flexibility Effects on the Control System Performance of Large Scale Robotic Manipulators*, The Journal of the Astronautical Sciences, Vol. 38, No 4, Special Issue on Robotics in Space, October-December 1990.

Chapnik B.V., Heppler G.R., Aplevich J.D. *Controlling the Impact Response of a One-Link Flexible Robotic Arm*, IEEE Transactions on Robotics and Automation, Vol. 9, No 3, June 1993.

Choura S., Jayasuriya S., Medick M.A., *On the Modeling, and Open-Loop Control of a Rotating Thin Flexible Beam*, Journal of Dynamic Systems, Measurement and Control, Vol. 113, pp 26-33, March 1991.

Dimarogonas A., *Vibration for Engineers*, Second Edition, Prentice Hall Inc., Upper Saddle River, New Jersey, 1996.

Franklin G.F., Powell J.D., Emami-Naeini A., *Feedback Control of Dynamic Systems*, Third Edition, Addison-Wesley Pub. Co., Reading, Massachusetts, 1994.

Gordaninejad F., Azhdari A., Chalhoub N., *Nonlinear Dynamic Modelling of a Revolute-Prismatic Flexible Composite-material Robot Arm*, Journal of Vibration and Acoustics, Vol. 113, pp 461-468, 1991.

Graham W.B., Singhal R.K., Kalaycioglu S., *Robotics Evaluation and Characterization (REACH) of the SSRMS Concept and Technical Issues*, AIAA Aerospace Design Conference, Irvine, California, February 1993.

Harris C.M., Crede C.E., *Shock and Vibration Handbook*, Second Edition, McGraw-Hill, New York, 1976.

Hedley D.J., *Design Characteristics and Design Feature Analysis of the Shuttle Remote Manipulator Arm*, Society of Automotive Engineers Transactions in Aerospace, Section 7, Vol. 95, 1986.

Hokamoto S., Kuwahara M., Modi V.J. and Misra A.K., *Formulation and Control of Space-Based Flexible Robots with Slewing-Deployable Links*, Acta Astronautica, Vol. 42, pp. 519-531, 1998.

Hokamoto S., Modi V.J., Misra, A.K., *Dynamics and Control of Mobile Flexible Manipulators with Slewing and Deployable Links*, AAS 95-322, AAS/AIAA Astrodynamics Specialist Conference, Halifax, Canada, 1995.

Huang J.-K., Yang L.-F., *Large Planar Maneuvers for Articulated Flexible Manipulators*, AIAA Guidance, Navigation and Control Conference, Minneapolis, Minnesota Canada, 1988.

Hyochoong, B., *Manoeuvre and vibrations control of flexible space structures by Lyapunov stability theory*, PhD dissertation, Texas A&M University, Texas, 1992.

Jacobsen L.S., Ayre R.S., *Engineering Vibrations*, McGraw-Hill, New York, 1958.

Jnifene A., Fahim A., *A Computed Torque/Time Delay Approach to the End-Point Control of a One-Link Flexible Manipulator*, Dynamics and Control, Vol. 7, pp. 171-189, 1997.

Juang J.-N., Horta L.G., Roberstshaw H.H., *A Slewing Control Experiment for Flexible Structures*, Journal of Guidance, Control, and Dynamics, Volume 9, Number 5, pp 599-607, Sept.-Oct. 1986.

Juang J.-N., Yang L.-F., Huang J.-K., *Lyapunov-Based Control Designs for Flexible-Link Manipulators*, AIAA 30th Structures, Structural Dynamics and Materials Conference, Mobile, Alabama, April 1989.

Junkins J.L. (Ed.), *Mechanics and Control of Large Flexible Structures*, Progress in Astronautics and Aeronautics, Volume 129, American Institute of Aeronautics and Astronautics, Washington DC, 1990.

Junkins J.L., Bang H., *Manoeuvre and Vibration Control of Hybrid Coordinate Systems Using Lyapunov Stability Theory*, Journal of Guidance, Dynamics and Control, Vol. 16, No 4, 1993.

Junkins J.L., Kim Y., *Introduction to Dynamics and Control of Flexible Structures*, AIAA Education Series, Washington DC, 1993.

Junkins J.L., Rahman Z., Bang H., *Near Minimum-Time Maneuvers of Flexible Vehicles: A Lyapunov Control Law Design Method*, AIAA-90-1222, AIAA Dynamics Specialist Conference, Long Beach, April 1990.

Junkins J.L., Turner J.D., *Optimal Spacecraft Rotational Maneuvers*, Studies in Astronautics 3, Elsevier Science Publishers, The Netherlands, 1986.

Kim Y-K., *Adaptive Control of a Robotic Manipulator with a Sliding Flexible Link*, PhD Thesis, Department of Mechanical Engineering, University of California-Los Angeles, 1988.

Kim Y-K., Gibson J.S., *A Variable-Order Adaptive Controller for a Manipulator with a Sliding Flexible Link*, IEEE Transactions on Robotics and Automation, Vol. 7, No. 6, pp 818-827, December 1991.

Kirk C.L., Doengi F.L., *Closed-Loop Vibration Control of Flexible Space Shuttle Manipulator*, Acta Astronautica, Vol. 32, No. 9, pp 561-576, 1994.

Kirk C.L., Doengi F.L., *Proof-Mass Actuator Control of Shuttle-Based Astromast*, Acta Astronautica, Vol. 32, No.7, pp 97-106, 1994.

Kirk D.E., *Optimal Control Theory an Introduction*, Prentice Hall Electrical Engineering Series, Prentice Hall Inc., Englewood Cliffs, New Jersey, 1970.

Kreyszig E., *Advanced Engineering Mathematics*, Seventh Edition, John Wiley & Sons, New York, 1993.

Leonard N.E., Levine W.S., *Using MATLAB® to Analyze and Design Control Systems*, Benjamin/Cummings Publishing Co. Inc., Redwood City, California, 1992.

Marion J.B., Hornyak W.F., *Principles of Physics*, Saunders College Publishing, New York, New York, 1984.

Marom I., *A Study of the Flexible Space Platform Based Deployable Manipulator*, PhD Thesis, Department of Mechanical Engineering, University of British Columbia, July 1993.

Marom I., Modi V.J., *On the dynamics and control of the manipulator with a deployable arm*, AAS 93-670, AAS/AIAA Astrodynamics Specialist Conference, Victoria, Canada, 1993.

MathWorks Inc., *The Student Edition of MATLAB® User's Guide*, Prentice Hall Inc., Englewood Cliffs, New Jersey, 1995.

Meirovitch, L., Elements of Vibration Analysis, 2nd Ed. Mc Graw-Hill Book Company, New York, NY, 1986.

MGA Software, *Advanced Continuous Simulation Language (ACSL) Reference Manual*, Version 11, MGA Software, Concord, Massachussets, 1995.

Oh H.-S., Vadali S.R., Junkins J.L., *Use of the Work-Energy Rate Principle for Designing Feedback Control Laws*, AIAA Journal of Guidance, Control, and Dynamics. Volume 15, Number 1, January-February 1992.

Pandey S., Agrawal S.K., *Path Planning of Free-Floating Prismatic-Jointed Manipulators*, Multibody System Dynamics, Vol. 1, No. 1, March 1997.

Papadopoulos E., Dubowsky S., *On the Dynamic Singularities in the Control of Free-Floating Space Manipulators*, Dynamics and Control of Multibody/Robotic Systems with Space Applications, American Society of Mechanical Engineers, New York, 1989.

Pun J., Semercigil S.E., *Joint Stiffness Control of a One-Link Flexible Arm*, Journal of Sound and Vibration, Vol. 203, No 2, pp 341-351, June 1997.

Scott M., Gilbert M., *Active Vibration Damping of the Space Shuttle Remote Manipulator System*, Journal of Guidance, Control and Dynamics, Vol. 16, No 2, pp 275-279, 1993.

Seto W., *Theory and Problems of Mechanical Vibrations*, Schaum's Outline Series, McGraw-Hill, New York, 1964.

Shahian B., Hassul M., *Control System Design using MATLAB®*, Prentice Hall Inc., Englewood Cliffs, New Jersey, 1993.

Skaar S.B. (Ed.), Ruoff C.F. (Ed.), *Teleoperation and Robotics in Space*, Progress in Astronautics and Aeronautics, Volume 161, American Institute of Aeronautics and Astronautics, Washington DC, 1994.

Slotine J.E., Li W., *Applied Nonlinear Control*, Prentice Hall Inc., Englewood Cliffs, New Jersey, 1991.

Tabarrok B., Leech C.M., Kim Y.I., *On the dynamics of axially moving beams*, Journal of the Franklin Institute, Vol. 297, No. 3, pp 201-220, 1974.

Theodore R.J., Arakeri J.H., Ghosal A., *The Modelling of Axially Translating Flexible Beams*, Journal of Sound and Vibration, Vol. 191, No. 3, pp 363-376, 1996.

Timoshenko S., *Vibration Problems in Engineering*, Second Edition, Constable and Company Ltd., London, 1937.

Timoshenko S., Young D.H., Weaver W., *Vibration Problems in Engineering*, Fourth Edition, John Wiley & Sons, New York, 1974.

Tokhi M.O., Azad A.K.M., *Modelling of a single link flexible manipulator system: theoretical and practical investigations*, Robotica, Vol. 14, pp 91-102, 1996.

Tokhi M.O., Azad A.K.M., *Real-time finite difference simulation of a single-link flexible manipulator system incorporating hub inertia and payload*, Proceedings of Institute of Mechanical Engineers, Vol. 209, pp 21-33, 1995.

Tokhi M.O., Poerwanto H., Azad A.K.M., *Dynamic Simulation of Flexible Manipulator Systems Incorporating Hub Inertia, Payload and Structural Damping*, Machine Vibration, Vol. 4, pp 106-124, 1995.

Van de Vegte J., *Feedback Control Systems*, Second Edition, Prentice Hall Inc., Englewood Cliffs, New Jersey, 1990.

Wang D., Vidyasagar M., *Passive Control of a Stiff Flexible Link*, The International Journal of Robotics Research, Vol. 11, No. 6, December 1992.

Wang P., Wei J-D., *Vibrations in a Moving Flexible Robot Arm*, Journal of Sound and Vibration, Vol. 116, pp 149-160, 1987.

Wie B., Hu A., Singh R., *Multibody Interaction Effects on Space Station Attitude Control and Momentum Management*, AIAA Journal of Guidance and Control, Vol. 13, No. 6, pp 993-999, November 1990.

Wolfram S., *MATHEMATICA: A System for Doing Mathematics by Computer*, Addison-Wesley Publishing Company, Wolfram Research, 1988.

Yuh J., Young T., *Dynamic Modelling of an Axially Moving Beam in Rotation: Simulation and Experiment*, Journal of Dynamic Systems, Measurement, and Control, Vol. 113, pp 34-40, March 1991.

Yüksel S., Gürgöze M., *On the Flexural Vibrations of Elastic Manipulators with Prismatic Joints*, Computers and Structures, Vol. 62, No. 5, pp 897-908, March 1997.

Appendix A: Characteristic Problem Coefficients

In section 2.3 of this thesis, the characteristic problem of the P-DRM is solved to find the exact natural frequencies of vibration. In that section a homogeneous system of algebraic equations has to be solved, Equation (2.3.22). The coefficients of the equations presented there, equations (2.3.19), (2.3.20) and (2.3.21) are given in this Appendix.

The coefficients of equation (2.3.19) can be written in expanded form as:

$$D_1 = -\sin(ak) - \frac{0.5c^2k^2L_pM_p\sin(ak) + c^2k^3I_{yy}\cos(ak)}{EI_2}$$

$$D_2 = \frac{c^2k^3I_{yy}\sin(ak) - 0.5c^2k^2L_pM_p\cos(ak)}{EI_2} - \cos(ak)$$

$$D_3 = \sinh(ak) - \frac{c^2k^3I_{yy}\cosh(ak) + 0.5c^2k^2L_pM_p\sinh(ak)}{EI_2}$$

$$D_4 = -\frac{0.5c^2k^2L_pM_p\cosh(ak) + c^2I_{yy}k^3\sinh(ak)}{EI_2} + \cosh(ak)$$

The coefficients of equation (2.3.20) can be written in expanded form as:

$$E_1 = \frac{c^2kM_p\sin(ak)}{EI_2} - \cos(ak) \quad ; \quad E_2 = \frac{c^2kM_p\cos(ak)}{EI_2} + \sin(ak)$$

$$E_3 = \frac{c^2kM_p\sinh(ak)}{EI_2} + \cosh(ak) \quad ; \quad E_4 = \frac{c^2kM_p\cosh(ak)}{EI_2} + \sinh(ak)$$

Finally, the F_i coefficients of (2.3.21) can be written in expanded form as:

$$F_0 = I_R - \frac{1}{2}L_p(a+L_1)M_p$$

$$F_1 = \frac{L_1\rho_2}{k} + kI_{yy}\cos(ak) - \frac{a\rho_2\cos(ak)}{k} - \frac{L_1\rho_2\cos(ak)}{k} + aM_p\sin(ak) + \frac{1}{2}L_pM_p\sin(ak) + L_1M_p\sin(ak) + \frac{\rho_2\sin(ak)}{k^2}$$

$$F_2 = -\frac{\rho_2}{k^2} + aM_p\cos(ak) + \frac{1}{2}L_pM_p\cos(ak) + L_1M_p\cos(ak) + \frac{\rho_2\cos(ak)}{k^2} - kI_{yy}\sin(ak) + \frac{1}{k}a\rho_2\sin(ak) + \frac{1}{k}L_1\rho_2\sin(ak)$$

$$F_3 = -\frac{L_1\rho_2}{k} + I_{yy}k\cosh(ak) + \frac{1}{k}a\rho_2\cosh(ak) + \frac{1}{k}L_1\rho_2\cosh(ak) + aM_p\sinh(ak) + \frac{1}{2}L_pM_p\sinh(ak) + L_1M_p\sinh(ak) - \frac{1}{k^2}\rho_2\sinh(ak)$$

$$F_4 = \frac{\rho_2}{k^2} + aM_p\cosh(ak) + \frac{1}{2}L_pM_p\cosh(ak) + L_1M_p\cosh(ak) - \frac{1}{k^2}\rho_2\cosh(ak) + kI_{yy}\sinh(ak) + \frac{1}{k}a\rho_2\sinh(ak) + \frac{1}{k}L_1\rho_2\sinh(ak)$$

Appendix B: Assumed Mode Method Examples

In Section 2.4.1 the assumed modes method was introduced as the discretization method for the DRM and here we investigate the accuracy of the assumed modes method applied to simple uniform beams. These examples will serve as a guide to validating the method as applied to the DRM.

- **Transverse vibrations of a cantilever beam**

The first consideration is that of the free transverse vibrations of a cantilever Euler-Bernoulli beam with constant mass density ρ and bending stiffness EI. The kinetic and strain energies are:

$$T = \frac{1}{2}\rho\int_0^L \left(\frac{dy}{dt}\right)^2 dx \tag{B.1}$$

$$V = \frac{1}{2}EI\int_0^L \left(\frac{\partial^2 y}{\partial x^2}\right)^2 dx \tag{B.2}$$

where the elastic deflection $y(x,t)$ is discretized, as described in Section 2.4.1, by the assumed modal summation:

$$y(x,t) = \sum_{i=1}^{n} q_i(t)\phi_i(x) \tag{B.3}$$

which on substituting into the energy expressions, above, give the approximated energies as:

$$T = \frac{1}{2}\rho\int_0^L \left[\sum_i^n \dot{q}_i(t)\phi_i(x)\right]\left[\sum_j^n \dot{q}_j(t)\phi_j(x)\right]dx \tag{B.4}$$

$$V = \frac{1}{2} EI \int_0^L \left[\sum_i^n q_i(t) \phi_i''(x) \right] \left[\sum_j^n q_j(t) \phi_j''(x) \right] dx \tag{B.5}$$

where $q_i(t)$ are the generalised coordinates of the system. Defining the Lagrangian as, $L = T - V$, and applying Lagrange's equation for zero external forces, $\frac{d}{dt}\left(\frac{\partial L}{\partial \dot{q}_i}\right) - \frac{\partial L}{\partial q_i} = 0$, the approximate equations of motion are:

$$\left[\sum_i^n \sum_j^n \int_0^L \rho \phi_i(x) \phi_j(x) dx \right] \ddot{\mathbf{q}} + \left[\sum_i^n \sum_j^n \int_0^L EI \phi_i''(x) \phi_j''(x) dx \right] \mathbf{q} = \mathbf{0} \tag{B.6}$$

so that for a particular set of n assumed functions we obtain all the elements of the mass and stiffness matrix for any selected $\phi(x)$. The number of assumed functions, n, can be changed and the results of an eigenvalue analysis compared as we increase the value of n. Precisely this has been conducted for three different assumed shapes, as follows:

$$\phi_i = \left(\frac{x}{L}\right)^{i+2} \tag{B.7}$$

$$\phi_i = (i+2)\left(\frac{x}{L}\right)^{i+1} - i\left(\frac{x}{L}\right)^{i+2} \tag{B.8}$$

$$\phi_i = 1 - \cos\left(\frac{i\pi x}{L}\right) + \frac{1}{2}(-1)^{i+1}\left(\frac{i\pi x}{L}\right)^2 \tag{B.9}$$

Function (B.9) is chosen from (Junkins and Kim, 1993), while Function (B.7) is a simple cubic curve and Function (B.8) is based on the static deflection curve of a cantilever beam carrying a point mass payload (Timoshenko, 1937).

The *geometric* and *natural* boundary conditions for the cantilever beam are found by inspection to be,

at x = 0: $\quad y(0) = 0, \quad \left.\frac{dy}{dx}\right|_{x=0} = 0 \quad$ (deflection and slope)

at x = L: $\left.\frac{d^2y}{dx^2}\right|_{x=L} = 0, \qquad \left.\frac{d^3y}{dx^3}\right|_{x=L} = 0$ (shear force and bending moment)

Analysing the proposed assumed functions above we can determine whether they are *admissible* or *comparison* functions for this example. For function (B.7) the four boundary conditions are as follows,

1. $\left. y(0) = \left(\frac{x}{L}\right)^{i+2} \right|_{x=0} = 0$

2. $\left.\frac{dy}{dx}\right|_{x=0} = (i+2)\left.\frac{x^{i+1}}{L^{i+2}}\right|_{x=0} = 0$

3. $\left.\frac{d^2y}{dx^2}\right|_{x=L} = (i+1)(i+2)\left.\frac{x^{i}}{L^{i+2}}\right|_{x=L} = (i+1)(i+2)\frac{1}{L^2}$

4. $\left.\frac{d^3y}{dx^3}\right|_{x=L} = i(i+2)(i+1)\left.\frac{x^{i-1}}{L^{i+2}}\right|_{x=L} = i(i+2)(i+1)\frac{1}{L^3}$

therefore function (B.7) is an *admissible* function as it satisfies the geometrical boundary conditions of this example but not the natural boundary conditions. For function (B.8) the boundary conditions are resolved as follows,

1. $\left. y(0) = (i+2)\left(\frac{x}{L}\right)^{i+1} - i\left(\frac{x}{L}\right)^{i+2} \right|_{x=0} = 0$

2. $\left.\frac{dy}{dx}\right|_{x=0} = (i+1)(i+2)\frac{x^{i}}{L^{i+1}} - i(i+2)\left.\frac{x^{i+1}}{L^{i+2}}\right|_{x=0} = 0$

3. $\left.\frac{d^2y}{dx^2}\right|_{x=L} = i(i+1)(i+2)\frac{x^{i-1}}{L^{i+1}} - i(i+1)(i+2)\left.\frac{x^{i}}{L^{i+2}}\right|_{x=L} = 0$

4. $\left.\frac{d^3y}{dx^3}\right|_{x=L} = i(i-1)(i+1)(i+2)\frac{x^{i-2}}{L^{i+1}} - i^2(i+1)(i+2)\left.\frac{x^{i-1}}{L^{i+2}}\right|_{x=L} =$

$$= \left[i(i-1)(i+1)(i+2) - i^2(i+1)(i+2)\right]\frac{1}{L^3}$$

so that this assumed function is also an *admissible* function since it satisfies both of the geometric boundary conditions and not all of the natural ones. It would be expected that function (B.8) would give better results for this example than function (B.7) since it satisfies one of the natural boundary conditions. A similar analysis as above for function (B.9) shows that it satisfies all of the boundary conditions for this example, so it is a *comparison* function.

The exact natural frequencies for the fixed-free cantilever were obtained from the standard eigenvalue problem, and are compared with the approximate results in Table B-3 for the three different assumed shapes and for an increasing number of retained functions. The results are produced using the function **beamnac2.m**, **beamnac3.m**, as found in Appendix D, for the program MATLAB, and the function beamasm (Junkins and Kim, 1993). An error analysis on the values of Table B-3 is presented in the companion Table B-1. The values on both tables are compared with the exact result obtained by an infinite dimensional analysis (Harris and Crede, 1976). The material properties are taken as one, that is EI=1, ρ=1, and L=1. These results show the characteristics of this approximate method. First that the frequencies of vibration calculated will be always higher or equal to the exact one, as Lord Raleigh showed in his treatise on the theory of sound (Jacobsen and Ayre, 1958). Secondly that the accuracy depends not only on a good selection of the assumed functions but also on retaining enough terms in the approximation.

Table B-1: Natural frequencies errors for an Assumed Mode discretization model of a Cantilever Beam

Exact Solution	Assumed Function $\phi_i = \left(\frac{x}{L}\right)^{i+2}$			Assumed Function $\phi_i = (i+2)\left(\frac{x}{L}\right)^{i+1} - i\left(\frac{x}{L}\right)^{i+2}$			Assumed Function $\phi_i = 1 - \cos\left(\frac{i\pi x}{L}\right) + \frac{1}{2}(-1)^{i+1}\left(\frac{i\pi x}{L}\right)^2$		
ω	n=1 % error	n=4 % error	n=16 % error	n=1 % error	n=4 % error	n=16 % error	n=1 % error	n=4 % error	n=16 % error
3.5160	160.7	9.03	1.42	1.63	0	0	0.75	0.03	0
22.0345		9.84	1.31		0.002	0		0.32	0.006
61.6972		25.7	1.36		3.42	0		1.24	0.02
120.9019		261.5	1.45		9.53	0		1.56	0.04

It can be seen from the results and from the error analysis in Table B-1 that there is a compromise between the number of terms to retain for the approximation and the assumed function to use. A sufficiently large number of terms retained for Function (B.7) would approximate the results well enough for simulation purposes, but it means dealing with a large number of equations which is not satisfactory from a computation-time point. For Functions (B.8) and (B.9) a much smaller number of retained terms would provide a good discretization and retain good correlation with the behaviour of the real system.

- **Vibrations of a cantilever beam with a tip point mass**

The second test case considers the transverse vibrations of a cantilevered Euler-Bernoulli beam with a tip point mass (M_p), as shown in Figure B.1. The kinetic and strain energies of the system are

$$T = \frac{1}{2}\rho\int_0^L \left(\frac{dy}{dt}\right)^2 dx + \frac{1}{2}M_p\left(\frac{dy(L)}{dt}\right)^2 \qquad \text{(B.10)}$$

$$V = \frac{1}{2} EI \int_0^L \left(\frac{\partial^2 y}{\partial x^2} \right)^2 dx \tag{B.11}$$

Substituting Equation (B.3) into (B.10) and (B.11) and applying Lagrange's equation gives the approximate equations of motion for the n degree of freedom model as:

$$\left[\sum_i^n \sum_j^n \int_0^L \rho \phi_i(x) \phi_j(x) dx + M_p \phi_i(L) \phi_j(L) \right] \ddot{\mathbf{q}} + \left[\sum_i^n \sum_j^n \int_0^L EI \phi_i''(x) \phi_j''(x) dx \right] \mathbf{q} = \mathbf{0} \tag{B.12}$$

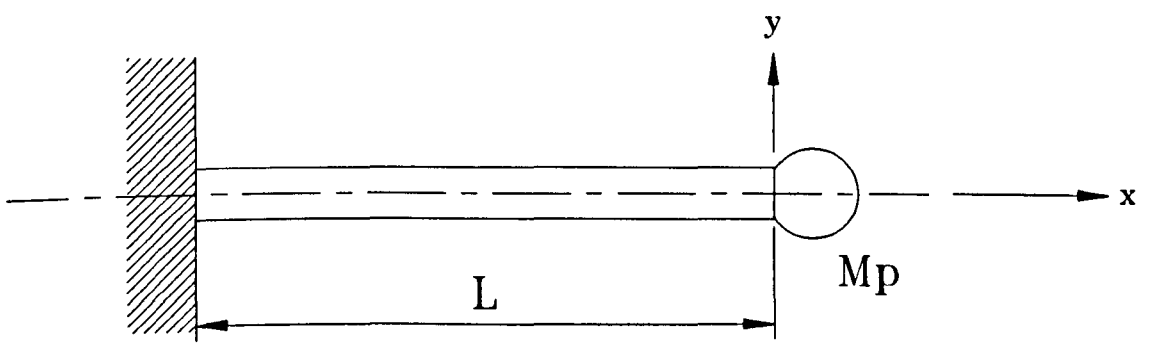

Figure B.1: Cantilever Euler-Bernoulli Beam with a Tip Point Mass.

For a particular assumed function using Equation (B.12) and increasing n we can compare the effect on the natural frequency calculations.

The geometric and natural boundary conditions can be found as the following:

at x=0: $y(0) = 0, \qquad \left. \frac{dy}{dx} \right|_0 = 0$

at x=L: $\left. \frac{d^2 y}{dx^2} \right|_{x=L} = 0, \qquad EI \left. \frac{d^3 y}{dx^3} \right|_{x=L} = M_p \ddot{y}(L)$

As for the previous example, at the attachment point (x = 0) the deflection has to be zero and the slope at that point must be zero. At the tip of the beam the bending moment is zero, since it is assumed that the tip mass has negligible mass moment of inertia. At the tip of the beam the shear force has to match the motion of the tip mass. The same

analysis as before can be done for these boundary conditions for the three different assumed functions (B.7), (B.8), and (B.9) and it can be easily seen that all of the functions are only *admissible* functions. These functions satisfy only the essential boundary conditions of this problem and are thus not accurate approximations of the eigenfunctions. Therefore, the functions do not inherently "know" that the model considered has a finite tip mass. Although the finite tip mass is correctly included in the kinetic energy of the system, Equation (B.10), the approximate equations of motion, Equation (B.12), will not approximate correctly all of the system's natural frequencies. The approximating function will still provide a reasonable approximation to the lower natural frequencies as is shown below.

Using the assumed functions above ((B.7), (B.8), and (B.9)) the natural frequencies have been calculated by doing an eigenvalue analysis with the mass and stiffness matrices of the equations of motion. Equation (B.12). The natural frequencies are compared in Table B-4 and an error analysis is presented in Table B-2. The results are produced using the function **massnac2.m**, **massnac3.m**, and **massasm.m** as found in Appendix D, for the program MATLAB. The material properties for the beam are taken as one, that is EI=1, ρ=1 and L=1, the tip mass is taken as M_p=100 Kg. A comparison to the exact first natural frequency (Harris and Crede, 1976) shows that the assumed modes method approximates the natural frequencies as expected by approaching the exact value from above. Thus, the approximated natural frequencies are all either greater than or equal to the predicted value. The rest of the 'exact solution' natural frequencies come from the infinite degree of freedom analysis by finding the zeros of the characteristic equation up to 16 significant figures (using the same procedure as presented for the DRM in Section 2.3.3, above).

Table B-2: Natural frequencies errors for an Assumed Mode discretization model of a Cantilever Beam with a 100 Kg tip mass

Exact Solution	Assumed Function $\phi_i = \left(\frac{x}{L}\right)^{i+2}$			Assumed Function $\phi_i = (i+2)\left(\frac{x}{L}\right)^{i+1} - i\left(\frac{x}{L}\right)^{i+2}$			Assumed Function $\phi_i = 1 - \cos\left(\frac{i\pi x}{L}\right) + \frac{1}{2}(-1)^{i+1}\left(\frac{i\pi x}{L}\right)^2$		
ω	n=1 % error	n=4 % error	n=16 % error	n=1 % error	n=4 % error	n=16 % error	n=1 % error	n=4 % error	n=16 % error
0.17300	100.1	6.60	0.913	0.0	0.0	0.0	0.63	0.06	0.0
15.42765		9.73	1.48		0.002	0.0		0.50	0.01
49.97488		15.82	2.77		1.25	0.0		3.37	0.05
104.2577		163.8	2.24		4.50	0.0		4.21	0.09

It is clear from the error analysis done in Table B-2, that the approximating function (B.8) provides the best results using the least number of functions and that as the number of functions increases it approaches the exact values faster than the other two assumed functions. What is not evident from the results presented is that as the number of assumed functions used in the approximation increases the mass matrix of the system became increasingly ill-conditioned. This was particularly true for functions (B.7), and (B.8), to the point where for n=30 the determinant of the mass matrix is zero for function (B.7) and -9.57×10^{-297} for function (B.8). On the other hand, function (B.9) did not produce ill-conditioned mass matrices for any of the cases tried and so it would prove to be the best choice if a large number of assumed functions was used.

In the analysis of the DRM, since the aim is to produce a simple but accurate dynamical model for vibration analysis function (B.9) has been discarded as being too complicated to be used. Function (B.7) requires too many retained functions to provide

reasonably accurate approximations to the frequencies of vibration so it is discarded since the equations would include too many degrees of freedom for the dynamic analysis. Function (B.8) will be used to discretize the flexible deflections of link 1 and link 2 of the DRM since it provides a relatively simple function to manipulate, and it approximates the natural frequencies reasonably well.

Table B-3: Natural Frequencies of Cantilever Beam

Exact Solution	Assumed Modes Method $\phi_i = \left(\frac{x}{L}\right)^{i+2}$				Assumed Modes Method $\phi_i = (i+2)\left(\frac{x}{L}\right)^{i+1} - i\left(\frac{x}{L}\right)^{i+2}$				Assumed Modes Method $\phi_i = 1 - \cos\left(\frac{i\pi x}{L}\right) + \frac{1}{2}(-1)^{i+1}\left(\frac{i\pi x}{L}\right)^2$			
ω^1 (rad/sec)	n=1	n=4	n=16	n=30	n=1	n=4	n=16	n=30	n=1	n=4	n=16	n=30
3.5160	9.1651	3.8336	3.5611	3.5584	3.5675	3.5160	3.5160	3.5160	3.5398	3.5170	3.5160	3.5160
22.0345		24.2027	22.3242	22.3075		22.0351	22.0345	22.0345		22.1055	22.0360	22.0347
61.6972		77.5239	62.5348	62.5002		63.8061	61.6972	61.6972		62.4631	61.7089	61.6990
120.9019		437.095	122.6614	122.5621		132.426	120.9019	120.9019		122.787	120.9461	120.9089
199.8595			203.2614	203.3541			199.8595	199.8595			199.9839	199.8788

1. Exact solution (Harris and Crede, 1976).

Table B-4: Natural Frequencies of Cantilever Beam with a tip point mass, M_p=100 kg

Exact Solution	Assumed Modes Method $\phi_i = \left(\frac{x}{L}\right)^{i+2}$				Assumed Modes Method $\phi_i = (i+2)\left(\frac{x}{L}\right)^{i+1} - i\left(\frac{x}{L}\right)^{i+2}$				Assumed Modes Method $\phi_i = 1 - \cos\left(\frac{i\pi x}{L}\right) + \frac{1}{2}(-1)^{i+1}\left(\frac{i\pi x}{L}\right)^2$			
ω (rad/sec)	n=1	n=4	n=16	n=30	n=1	n=4	n=16	n=30	n=1	n=4	n=16	n=30
0.17300[1]	0.34616	0.18442	0.17458	0.17472	0.17300	0.17300	0.17300	0.17300	0.17409	0.17312	0.17300	0.17300
15.42765[2]		16.9293	15.6568	15.6644		15.4279	15.4277	15.4277		15.5031	15.4295	15.4279
49.97488[2]		57.8808	51.3568	50.9288		50.5993	49.9748	49.9748		51.6587	49.9999	49.9786
104.2577[2]		275.0442	106.5984	106.4837		108.9536	104.2577	104.2577		108.6446	104.3502	104.2727
178.27973[2]			182.4653	182.3137			178.2799	178.2797			178.6054	178.3283

1. Exact solution (Harris and Crede, 1976).
2. Approximate solution (up to 16 digits) from an infinite degree of freedom analysis.

Appendix C: The DRM Approximate Dynamic Model.

Applying Lagrange's Equation to the Lagrangian on Section 2.5, for the rest of the discrete coordinates produces the following equations:

For α:

$$\frac{d}{dt}\left(\frac{\partial L_T}{\partial \dot{\alpha}}\right) = \left\{\begin{array}{l}\frac{11L_1^2\rho_1}{20} + a^2\rho_2 + 2aL_1\rho_2 + \frac{11L_1^2\rho_2}{20} - \frac{3(L_1-b)^4\rho_2}{4L_1^2} + \frac{(L_1-b)^5\rho_2}{5L_1^3} + \\ 2aM_p + L_pM_p + 2L_1M_p\end{array}\right\}\ddot{\theta} +$$

$$\left\{\begin{array}{l}\frac{33L_1\rho_1}{35} + 4a\rho_2 + \frac{33L_1\rho_2}{35} - \frac{9(L_1-b)^5\rho_2}{5L_1^4} + \frac{(L_1-b)^6\rho_2}{L_1^5} - \\ \frac{(L_1-b)^7\rho_2}{7L_1^6} + 4M_p\end{array}\right\}\ddot{\alpha} +$$

$$\left\{\frac{3a\rho_2}{2} + 4M_p + \frac{3L_pM_p}{a}\right\}\ddot{\beta} +$$

$$\left\{2a\dot{a}\rho_2 + 2\dot{a}L_1\rho_2 + \frac{3\dot{b}(L_1-b)^3\rho_2}{L_1^2} - \frac{\dot{b}(L_1-b)^4\rho_2}{L_1^3} + 2\dot{a}M_p\right\}\dot{\theta} +$$

$$\left\{4a\rho_2 + \frac{9b(L_1-b)^4\rho_2}{L_1^4} - \frac{6\dot{b}(L_1-b)^5\rho_2}{L_1^5} + \frac{\dot{b}(L_1-b)^6\rho_2}{L_1^6}\right\}\dot{\alpha} +$$

$$\left\{-\dot{a}\rho_2 - \frac{6\dot{a}L_pM_p}{a^2}\right\}\dot{\beta} + \left\{\frac{-5\ddot{a}\rho_2}{2} + \frac{6\dot{a}^2L_pM_p}{a^3} - \frac{3\ddot{a}L_pM_p}{a^2}\right\}\beta$$

$$\frac{\partial L_T}{\partial \alpha} = \left(\begin{array}{l} \frac{-2.4a^2\rho_2}{L_1} - 1.16L_1\rho_2 + \frac{6a^2(L_1-b)^3\rho_2}{L_1^4} + \frac{6(L_1-b)^3\rho_2}{L_1^2} - \frac{4.5a^2(L_1-b)^4\rho_2}{L_1^5} - \\ \frac{4.5(L_1-b)^4\rho_2}{L_1^3} + \frac{0.9a^2(L_1-b)^5\rho_2}{L_1^6} - \frac{2.7(L_1-b)^5\rho_2}{L_1^4} + \\ \frac{3(L_1-b)^6\rho_2}{L_1^5} - \frac{0.64(L_1-b)^7\rho_2}{L_1^6} - \frac{24M_p}{5} - \frac{24aM_p}{5L_1} + \frac{12a(L_1-b)^3M_p}{L_1^4} + \\ \frac{12(L_1-b)^3M_p}{L_1^3} - \frac{9a(L_1-b)^4M_p}{L_1^5} - \frac{9(L_1-b)^4M_p}{L_1^4} + - \frac{9a(L_1-b)^5M_p}{5L_1^6} + \\ \frac{9(L_1-b)^5M_p}{5L_1^5} \end{array} \right) \dot{\theta}^2\alpha$$

$$+ \left\{ \begin{array}{l} -\frac{12EI_1}{L_1^3} - \frac{12EI_2}{L_1^3} + \frac{36EI_2(L_1-b)}{L_1^4} - \frac{36EI_2(L_1-b)^2}{L_1^5} + \frac{12EI_2(L_1-b)^3}{L_1^6} + \\ \frac{3\ddot{a}\rho_2}{2} + \frac{24a\ddot{a}\rho_2}{5L_1} - \frac{12a\ddot{a}(L_1-b)^3\rho_2}{L_1^4} - \frac{12\ddot{a}(L_1-b)^3\rho_2}{L_1^3} + \frac{9a\ddot{a}(L_1-b)^4\rho_2}{L_1^5} + \\ \frac{18\ddot{a}(L_1-b)^4\rho_2}{L_1^4} - \frac{9a\ddot{a}(L_1-b)^5\rho_2}{5L_1^6} - \frac{9\ddot{a}(L_1-b)^5\rho_2}{L_1^5} + \frac{3\ddot{a}(L_1-b)^6\rho_2}{2L_1^6} + \\ \frac{24\ddot{a}M_p}{5L_1} - \frac{12\ddot{a}(L_1-b)^3M_p}{L_1^4} + \frac{9\ddot{a}(L_1-b)^4M_p}{L_1^5} - \frac{9\ddot{a}(L_1-b)^5M_p}{5L_1^6} \end{array} \right\} \alpha$$

For β:

$$\frac{d}{dt}\left(\frac{\partial L_T}{\partial \dot{\beta}}\right) = \left\{\frac{3I_p}{a} + \frac{11a^2\rho_2}{20} + \frac{3aL_1\rho_2}{4} + 2aM_p + \frac{3L_pM_p}{2} + 2L_1M_p + \frac{3L_pL_1M_p}{2a}\right\}\ddot{\theta} +$$

$$\left\{\frac{3a\rho_2}{2} + 4M_p + \frac{3L_pM_p}{a}\right\}\ddot{\alpha} +$$

$$\left\{\frac{9I_p}{a^2} + \frac{33a\rho_2}{35} + 4M_p + \frac{6L_pM_p}{a}\right\}\ddot{\beta} +$$

$$\left\{\frac{-3\dot{a}I_p}{a^2} + \frac{11a\dot{a}\rho_2}{10} + \frac{3\dot{a}L_1\rho_2}{4} + 2\dot{a}M_p + \frac{3\dot{a}L_pM_p}{2a} - \frac{3\dot{a}(L_1+a)L_pM_p}{2a^2}\right\}\dot{\theta} +$$

$$\left\{\frac{3}{2}\dot{a}\rho_2 - \frac{3\dot{a}L_pM_p}{a^2}\right\}\dot{\alpha} + \left\{\frac{-27\dot{a}I_p}{a^3} - \frac{41\dot{a}\rho_2}{70} - \frac{9\dot{a}L_pM_p}{a^2}\right\}\dot{\beta} +$$

$$\left\{\frac{27\dot{a}^2I_p}{a^4} - \frac{9\ddot{a}I_p}{a^3} - \frac{107\ddot{a}\rho_2}{70} + \frac{6\dot{a}^2L_pM_p}{a^3} - \frac{3\ddot{a}L_pM_p}{a^2}\right\}\beta$$

$$\frac{\partial L_T}{\partial \beta} = \left\{\frac{-3\dot{a}I_p}{a^2} - \frac{9a\dot{a}\rho_2}{10} - \frac{5\dot{a}L_1\rho_2}{4} - \frac{3\dot{a}L_p(L_1+a)M_p}{2a^2}\right\}\dot{\theta} + \left\{\frac{-5\dot{a}\rho_2}{2} - \frac{3\dot{a}L_pM_p}{a^2}\right\}\dot{\alpha} +$$

$$\left\{\frac{-9\dot{a}I_p}{a^3} - \frac{107\dot{a}\rho_2}{70} - \frac{3\dot{a}L_pM_p}{a^2}\right\}\dot{\beta} + \left\{\begin{array}{l} -\frac{12EI_2}{a^3} + \frac{9\dot{a}^2I_p}{a^4} + \frac{87\dot{a}^2\rho_2}{35a} + \frac{3\ddot{a}\rho_2}{2} + \frac{24\ddot{a}M_p}{5a} + \\ \left(-1.16a\rho_2 - \frac{24M_p}{5} - \frac{24L_1M_p}{5a}\right)\dot{\theta}^2 \end{array}\right\}\beta$$

As discussed in Section 2.5, the equations of motion for the discretized DRM can be represented in matrix form, Equation (2.5.6). The elements of those matrices are as follows:

$$M_{\theta\theta} = \left\{\begin{array}{l} I_p + \frac{L_1^3\rho_2}{3} + \frac{a^3\rho_2}{3} + L_1a^2\rho_2 + L_1^2a\rho_2 + \frac{L_1^3\rho_2}{3} - \frac{(L_1-b)^3\rho_2}{3} + \\ \frac{aL_pM_p}{2} + \frac{L_pL_1M_p}{2} + a(L_1+a)M_p + \frac{L_p(L_1+a)M_p}{2} + L_1(L_1+a)M_p + \\ \left\{\begin{array}{l} -1.16L_1\rho_2 + \frac{6(L_1-b)^3\rho_2}{L_1^2} - \frac{4.5(L_1-b)^4\rho_2}{L_1^3} - \frac{2.7(L_1-b)^5\rho_2}{L_1^4} + \\ \frac{3(L_1-b)^6\rho_2}{L_1^5} - \frac{0.65(L_1-b)^7\rho_2}{L_1^6} \end{array}\right\}\alpha^2 + \\ \left\{-1.16a\rho_2 - \frac{24M_p}{5} - \frac{24L_1M_p}{5a}\right\}\beta^2 \end{array}\right\}$$

$$M_{\theta\alpha} = \frac{11L_1^2\rho_1}{20} + a^2\rho_2 + 2aL_1\rho_2 + \frac{11L_1^2\rho_2}{20} - \frac{3(L_1-b)^4\rho_2}{4L_1^2} + \frac{(L_1-b)^5\rho_2}{5L_1^3} +$$
$$2aM_p + L_pM_p + 2L_1M_p$$

$$M_{\theta\beta} = \frac{3I_p}{a} + \frac{11a^2\rho_2}{20} + \frac{3aL_1\rho_2}{4} + 2aM_p + \frac{5L_pM_p}{2} + 2L_1M_p + \frac{3L_pL_1M_p}{2a}$$

$$M_{\alpha\alpha} = \frac{33L_1\rho_1}{35} + 4a\rho_2 + \frac{33L_1\rho_2}{35} - \frac{9(L_1-b)^5\rho_2}{5L_1^4} + \frac{(L_1-b)^6\rho_2}{L_1^5} - \frac{(L_1-b)^7\rho_2}{7L_1^6} + 4M_p$$

$$M_{\alpha\beta} = \frac{3a\rho_2}{2} + 4M_p + \frac{3L_pM_p}{a}$$

$$M_{\beta\beta} = \frac{9I_p}{a^2} + \frac{33a\rho_2}{35} + 4M_p + \frac{6L_pM_p}{a}$$

$$C_{\theta\theta} = a^2\dot{a}\rho_2 + 2a\dot{a}L_1\rho_2 + \dot{a}L_1^2\rho_2 + \dot{b}(L_1-b)^2\rho_2 + a\dot{a}M_p + \dot{a}L_pM_p + \dot{a}L_1M_p + \dot{a}(L_1+a)M_p$$

$$C_{\theta\alpha} = 2a\dot{a}\rho_2 + 2\dot{a}L_1\rho_2 + \frac{3\dot{b}(L_1-b)^3\rho_2}{L_1^2} - \frac{\dot{b}(L_1-b)^4\rho_2}{L_1^3} + 2\dot{a}M_p$$

$$C_{\theta\beta} = \frac{-6\dot{a}I_p}{a^2} + \frac{a\dot{a}\rho_2}{5} - \frac{\dot{a}L_1\rho_2}{2} + 2\dot{a}M_p - \frac{3\dot{a}L_pM_p}{2a} - \frac{3\dot{a}L_1L_pM_p}{a^2}$$

$$C_{\alpha\theta} = 2a\dot{a}\rho_2 + 2\dot{a}L_1\rho_2 + \frac{3b(L_1-b)^3\rho_2}{L_1^2} - \frac{\dot{b}(L_1-b)^4\rho_2}{L_1^3} + 2\dot{a}M_p$$

$$C_{\alpha\alpha} = 4a\rho_2 + \frac{9b(L_1-b)^4\rho_2}{L_1^4} - \frac{6\dot{b}(L_1-b)^5\rho_2}{L_1^5} + \frac{\dot{b}(L_1-b)^6\rho_2}{L_1^6}$$

$$C_{\alpha\beta} = -\dot{a}\rho_2 - \frac{6\dot{a}L_pM_p}{a^2}$$

$$C_{\beta\theta} = 2\dot{a}a\rho_2 + 2\dot{a}L_1\rho_2 + 2\dot{a}M_p + \frac{3\dot{a}L_p^2M_p}{2a}$$

$$C_{\beta\alpha} = 4\dot{a}\rho_2$$

$$C_{\beta\beta} = \frac{-18\dot{a}I_p}{a^3} + \frac{33\dot{a}\rho_2}{35} - \frac{6\dot{a}L_pM_p}{a^2}$$

$$K_{\theta\beta} = \frac{6\dot{a}^2I_p}{a^3} - \frac{3\ddot{a}I_p}{a^2} - \frac{9\dot{a}^2\rho_2}{10} - \frac{9a\ddot{a}\rho_2}{10} - \frac{5\ddot{a}L_1\rho_2}{4} + \frac{3\dot{a}^2L_pM_p}{2a^2} - \frac{3\ddot{a}L_pM_p}{2a} + \frac{3\dot{a}^2L_pL_1M_p}{a^3} - \frac{3\ddot{a}L_pL_1M_p}{2a^2}$$

$$K_{\alpha\alpha} = \frac{12EI_1}{L_1^3} + \frac{12EI_2}{L_1^3} - \frac{36EI_2(L_1-b)}{L_1^4} + \frac{36EI_2(L_1-b)^2}{L_1^5} - \frac{12EI_2(L_1-b)^3}{L_1^6} -$$
$$\frac{3a\rho}{2} + \frac{12\ddot{a}(L_1-b)^3\rho_2}{L_1^3} - \frac{18\ddot{a}(L_1-b)^4\rho_2}{L_1^4} + \frac{9\ddot{a}(L_1-b)^5\rho_2}{L_1^5} - \frac{3\ddot{a}(L_1-b)^6\rho_2}{2L_1^6} +$$
$$\left(1.16L_1\rho_2 - \frac{6(L_1-b)^3\rho_2}{L_1^2} + \frac{4.5(L_1-b)^4\rho_2}{L_1^3} + \frac{2.7(L_1-b)^5\rho_2}{L_1^4} - \frac{3(L_1-b)^6\rho_2}{L_1^5} + \frac{0.64(L_1-b)^7\rho_2}{L_1^6}\right)\dot{\theta}^2$$

$$K_{\alpha\beta} = \frac{-5\ddot{a}\rho_2}{2} + \frac{6\dot{a}^2L_pM_p}{a^3} - \frac{3\ddot{a}L_pM_p}{a^2}$$

$$K_{\beta\beta} = \frac{12EI_2}{a^3} + \frac{18\dot{a}^2I_p}{a^4} - \frac{9\ddot{a}I_p}{a^3} - \frac{87\dot{a}^2\rho_2}{35a} - \frac{106\ddot{a}\rho_2}{35} - \frac{24\ddot{a}M_p}{5a} + \frac{6\dot{a}^2L_pM_p}{a^3} - \frac{3\ddot{a}L_pM_p}{a^2} +$$
$$\left(1.16a\rho_2 + \frac{24M_p}{5} + \frac{24L_1M_p}{5a}\right)\dot{\theta}^2$$

Appendix D: Computer Programs

Included here are the computer programs used to generate most of the results presented in this thesis. These programs are referred to in bold text in the main body of the thesis when particular results have been presented. Each one presented is preceded by a short description of what it is used for. They are written for use with the following computer programs; Matlab, Mathematica, ACSL.

beamnac2.m

Purpose:

Mathematical model of a fixed-free uniform Euler-Bernoulli beam undergoing transverse vibration. This program computes the mass matrix M and stiffness matrix K for a beam (length, L;mass density, rho;elastic modulus, E;cross-sectional are moment of inertia I).Using the assumed function: $\phi_i = \left(\frac{x}{L}\right)^{i+2}$, n is the number of admissible functions retained in the approximation.

Matlab Code:

```
function [Mqq,Kqq]=beamnac2(n,rho,L,E,I)
% beamnac2  Euler-Bernoulli Beam: Assumed Mode Method (Fixed-Free)
%
%  [M,K]=beamnac2(n,rho,L,E,I)
%
%  Assumed mode function = (x^(i+2)/L^(i+2))
%
%  This subroutine returns the mass (M) and stifness (K) matrices
%  in the second order system of odes (using assumed modes method):
%
%  M xdd(t) + K x(t) = 0
```

```
%
%  Programmed by Nacho Romero
%              Department of Aerospace Science
%              Cranfield University
%
%  Revision dates: October 21, 1996
%  Material & geometric properties
%
EI=E*I;
%
%  Initializing Matrices to establish dimensions
%
Mqq=zeros(n,n); Kqq=zeros(n,n); phi=zeros(n,1);
%
%  Construct Mass and Stiffness Matrices
%
for i=1:n;
   for j=1:n;
      m=(L)/(i+j+5);
      Mqq(i,j)=rho*m;
      Kqq(i,j)=EI*(((i+2)*(i+1)*(j+2)*(j+1))/((i+j+1)*(L^3)));
end
end
```

beamnac3.m

Purpose:

Mathematical model of a fixed-free uniform Euler-Bernoulli beam undergoing transverse vibration. This program computes the mass matrix M and stiffness matrix K for a beam (length, L;mass density, rho;elastic modulus, E;cross-sectional are moment of inertia I).Using the assumed function: $\phi_i = (i+2)\left(\frac{x}{L}\right)^{i+1} - i\left(\frac{x}{L}\right)^{i+2}$, n is the number of admissible functions retained in the approximation.

Matlab Code:

```
function [Mqq,Kqq]=beamnac3(n,rho,L,E,I)
% beamnac2  Euler-Bernoulli Beam: Assumed Mode Method (Fixed-Free)
%  [M,K]=beamnac3(n,rho,L,E,I)
%
%  Assumed mode function = (i+2)*(x/L)^(i+1)-i*(x/L)^(i+2)
%  This subroutine returns the mass (M) and stifness (K) matrices
%  in the second order system of odes (using assumed modes method):
%           M xdd(t) + K x(t) = 0
%
%  Programmed by Nacho Romero
%           Department of Aerospace Science
%           Cranfield University
%  Revision dates: October 21, 1996
%
%  Material & geometric properties
EI=E*I;
%
%  Initializing Matrices to establish dimensions
Mqq=zeros(n,n); Kqq=zeros(n,n); phi=zeros(n,1);
%
%  Construct Mass and Stiffness Matrices
for i=1:n;
  for j=1:n;
    m1=((i+2)*(j+2))/(i+j+3);
    m2=(i*(j+2)+j*(i+2))/(i+j+4);
    m3=(i*j)/(i+j+5);
     m=L*((m1)-(m2)+(m3));
     Mqq(i,j)=rho*m;
     k1=((i+2)*(i+1)*i*j*(j+1)*(j+2))/(i+j-1);
     k2=(2*i*j*(i+2)*(i+1)*(j+2)*(j+1))/(i+j);
```

```
        k3=(i*j*(i+2)*(i+1)*(j+2)*(j+1))/(i+j+1);
        Kqq(i,j)=(EI/L/L/L)*(k1-k2+k3);
    end
end
```

massnac2.m

Purpose:

Mathematical model of a fixed-free uniform Euler-Bernoulli beam with a tip mass undergoing transverse vibration. This program computes the mass matrix M and stiffness matrix K for a beam and tip mass (length, L;mass density, rho;elastic modulus, E;cross-sectional are moment of inertia I;tip mass, Mp).Using the assumed function: $\phi_i = \left(\frac{x}{L}\right)^{i+2}$, n is the number of admissible functions retained in the approximation.

Matlab Code:

```
function [Mqq,Kqq]=massnac2(n,rho,L,E,I,Mp)
% massnac1   Euler-Bernoulli Beam + tip mass: Assumed Mode Method (Fixed-Free)
%
%  [M,K]=massnac2(n,rho,L,E,I,Mp)
%  n : No. of assumed modes
%  Assumed mode function = (x^(i+2)/L^(i+2))
%
%  This subroutine returns the mass (M) and stifness (K) matrices
%  in the second order system of odes (using assumed modes method):
%
%  M xdd(t) + K x(t) = 0
%
%  Programmed by Nacho Romero
%              Department of Aerospace Science
%              Cranfield University
%
%  Revision dates: October 21, 1996
%  Material & geometric properties
EI=E*I;
%
```

```
%  Initializing Matrices to establish dimensions
%
Mqq=zeros(n,n); Kqq=zeros(n,n); phi=zeros(n,1);
%
%  Construct Mass and Stiffness Matrices
%
for i=1:n;
   for j=1:n;
      m=(L)/(i+j+5);
      Mqq(i,j)=rho*m+Mp;
      Kqq(i,j)=EI*(((i+2)*(i+1)*(j+2)*(j+1))/((i+j+1)*(L^3)));
end
end
```

massnac3.m

Purpose:

Mathematical model of a fixed-free uniform Euler-Bernoulli beam with a tip mass undergoing transverse vibration. This program computes the mass matrix M and stiffness matrix K for a beam and tip mass (length, L;mass density, rho;elastic modulus, E;cross-sectional are moment of inertia I;tip mass, Mp).Using the assumed function: $\phi_i = (i+2)\left(\frac{x}{L}\right)^{i+1} - i\left(\frac{x}{L}\right)^{i+2}$, n is the number of admissible functions retained in the approximation.

Matlab Code:

```
function [Mqq,Kqq]=massnac3(n,rho,L,E,I,Mp)
% massnac3 Euler-Bernoulli Beam + tip mass: Assumed Mode Method (Fixed-Free)
%                  [M,K]=massnac3(n,rho,L,E,I,Mp)
%
%  Assumed mode function = (i+2)*(x/L)^(i+1)-i*(x/L)^(i+2)
%  This subroutine returns the mass (M) and stifness (K) matrices
%  in the second order system of odes (using assumed modes method):
%                  M xdd(t) + K x(t) = 0
%  Programmed by Nacho Romero
%            Department of Aerospace Science
%            Cranfield University
%
%  Revision dates: October 21, 1996
```

```
%
%  Material & geometric properties
EI=E*I;
%  Initializing Matrices to establish dimensions
Mqq=zeros(n,n); Kqq=zeros(n,n); phi=zeros(n,1);
%
%  Construct Mass and Stiffness Matrices
for i=1:n;
   for j=1:n;
      m1=((i+2)*(j+2))/(i+j+3);
     m2=(i*(j+2)+j*(i+2))/(i+j+4);
     m3=(i*j)/(i+j+5);
      m=L*((m1)-(m2)+(m3));
      Mqq(i,j)=rho*m+Mp*((i+2)*(j+2)-i*(j+2)-j*(i+2)+i*j);
      k1=((i+2)*(i+1)*i*j*(j+1)*(j+2))/(i+j-1);
      k2=(2*i*j*(i+2)*(i+1)*(j+2)*(j+1))/(i+j);
      k3=(i*j*(i+2)*(i+1)*(j+2)*(j+1))/(i+j+1);
      Kqq(i,j)=(EI/L/L/L)*(k1-k2+k3);
   end
end
```

massasm.m

Purpose:

Mathematical model of a fixed-free uniform Euler-Bernoulli beam with a tip mass undergoing transverse vibration. This program computes the mass matrix M and stiffness matrix K for a beam and tip mass (length, L;mass density, rho;elastic modulus, E;cross-sectional are moment of inertia I;tip mass, Mp).Using the assumed function: $\phi_i = 1 - \cos\left(\frac{i\pi x}{L}\right) + \frac{1}{2}(-1)^{i+1}\left(\frac{i\pi x}{L}\right)^2$, n is the number of admissible functions retained in the approximation.

Matlab Code:

```
function [M,K]=massasm(n,rho,L,E,I,Mp)
% massasm   Euler-Bernoulli Beam + tip mass: Assumed Mode Method (Fixed-Free)
%           [M,K]=massasm(n,rho,L,E,I,Mp)
```

```
%  This subroutine returns the mass (M) and stifness (K) matrices
%  in the second order system of odes (using assumed modes method):
%                M xdd(t) + K x(t) = 0
%
%  Programmed by  Nacho Romero
%                 Department of Aerospace Science
%                 Cranfield University
%  Revision dates: 22 October 1996
%
%  Material & geometric properties
EI=E*I;
%
%  Initializing Matrices to establish dimensions
Mqq=zeros(n,n); Kqq=zeros(n,n); phi=zeros(n,1);
%
%  Construct Mass and Stiffness Matrices
for i=1:n;
   phi=1-cos(i*pi)+(-1)^(i+1)*i*i*pi*pi/2;
   for j=1:n;
   phj=1-cos(j*pi)+(-1)^(j+1)*j*j*pi*pi/2;
      m1=1+(-1)^(i+j)*(i*i/j/j+j*j/i/i);
      m2=(-1)^(i+1)*i*i*pi*pi/6+(-1)^(j+1)*j*j*pi*pi/6;
      m3=(-1)^(i+j)*i*i*j*j*pi*pi*pi*pi/20;
      m=m1+m2+m3;
      k=(-1)^(i+j);
      if j == i; m=m+0.5; k=k+0.5; end
      M(i,j)=rho*L*m+Mp*phi*phj;
      K(i,j)=E*I*k*(i*i*j*j*pi*pi*pi*pi/L/L/L);
   end
end
```

drmnac3.m

Purpose:

Mathematical model of a partially flexible DRM where only link 2 is considered a flexible component of the structure. This program computes the mass matrix M and stiffness matrix K. Using the assumed function: $\phi_i = (i+2)\left(\frac{x}{L}\right)^{i+1} - i\left(\frac{x}{L}\right)^{i+2}$, n is the number of admissible functions retained in the approximation.

Matlab Code:

```
function [M,K]=drmnac3(n,m1,m2,L1,L2,Lp,Sp,a,E,I,Mp)
%
% drmnac3 DRM + long payload: Assumed Mode Method
%
%  [M,K]=drmnac3(n,m1,m2,L1,L2,Lp,Sp,a,E,I,Mp)
%  n : No. of assumed modes
%  Mp: payload mass
%  Lp: payload length
%  Sp: Payload width
%
%  Assumed mode function = (i+2)*(x/L)^(i+1)-i*(x/L)^(i+2)
%
%  This subroutine returns the mass (M) and stifness (K) matrices
%  in the second order system of odes (using assumed modes method):
%
%  M xdd(t) + K x(t) = 0
%
%  Programmed by Nacho Romero
%              Department of Aerospace Science
%              Cranfield University
%
%  Revision dates: November 27, 1996
%            April 19, 2000 (added Sp for the inertia)

%
%  Material properties for L2 - the flexible link
%
mp=Mp/Lp;
EI=E*I;
b=L2-a;
delta=0;
%
%  Initializing Matrices to establish dimensions
%
Mqq=zeros(n,n); Kqq=zeros(n,n); phi=zeros(n,1);Mtq=zeros(1,n);Mqt=zeros(n,1);
%
%  Construct Mass and Stiffness Matrices
%
Mtt=(1/3)*m1*L1^3+(1/3)*m2*(L1^3-(L1-b)^3)+(1/3)*m2*a^3+...
   m2*a^2*L1+m2*a*L1^2+(1/12)*Mp*(4*Lp^2+Sp^2)+mp*Lp^2*(L1+a)+...
   mp*Lp*(L1+a)^2;
for i=1:n;
     Mtq(i)=0.5*mp*Lp^2*2+0.5*mp*Lp^2*(L1+a)*(((i+2)*(i+1)-i*(i+2))/a)+ ...
          mp*(L1+a)*Lp*2+(1/12)*Mp*(4*Lp^2+Sp^2)*(((i+2)*(i+1)-i*(i+2))/a)+
...
```

```
            m2*((((i+2)*a^2)/(i+3))-(i*a^2/(i+4)))+m2*L1*(1-(i/(i+3)))*a;
        Mqt(i)=Mtq(i);
      for j=1:i;
        if j == i;
          delta=1;
        end
        w1=m2*(((i+2)*(j+2)/(i+j+3))-(i*(j+2)/(i+j+4))- ...
          (j*(i+2)/(i+j+4))+(i*j/(i+j+5)))*a;
        w2=(1/12)*Mp*(4*Lp^2+Sp^2)*((((i+2)*(i+1)-i*(i+2))*((j+2)*(j+1)-
j*(j+2)))/a^2);
        w3=mp*Lp*Lp*2*(((i+2)*(i+1)-i*(i+2))/a)*delta+ ...
          0.5*mp*Lp*Lp*(2*(((i+2)*(i+1)-i*(i+2))/a)+...
          (((j+2)*(j+1)-j*(j+2))/a)*2)*(1-delta);
        Mqq(i,j)=mp*Lp*4+w1+w2+w3;

        Kqq(i,j)=EI*(i*j*(i+2)*(i+1)*(j+2)*(j+1)*(2/((i+j)*(i+j+1)*(i+j-1)*a^3)));

        if j < i;
          Mqq(j,i)=Mqq(i,j);
          Kqq(j,i)=Kqq(i,j);
        end
    delta=0;
      end
    end
    M=[Mtt Mtq;Mqt Mqq];
    %M=[Mtt zeros(1,n);Mqt Mqq];
    %M=Mqq;
    K=[0 zeros(1,n);zeros(n,1) Kqq];
    %K=Kqq;
```

flexnac2.m

Purpose:

Mathematical model of a flexible DRM where link 1 and link 2 are considered flexible components of the structure. This program computes the mass matrix M and stiffness matrix K. Using the assumed function: $\phi_i = \left(\frac{x}{L}\right)^{i+2}$, n is the number of admissible functions retained in the approximation.

Matlab Code:

```
function [M,K]=flexnac2(n,m,m1,m2,mp,L1,L2,Lp,a,E1,I1,E2,I2)
%  flexible DRM + long payload: Assumed Mode Method
%
%  [M,K]=flexnac2(n,m,m1,m2,mp,L1,L2,Lp,a,E1,I1,E2,I2)
%  n : No. of assumed modes for Link 1 (length L1)
%  m : No. of assumed modes for Link 2 (Length a)
%  Assumed mode function = (x/L)^(i+2)  L : L1 and 'a'
%
%  This subroutine returns the mass (M) and stifness (K) matrices
%  in the second order system of odes (using assumed modes method):
%
%  M xdd(t) + K x(t) = 0
%
%  Programmed by Nacho Romero
%               Department of Aerospace Science
%               Cranfield University
%  Revision dates: January 23, 1997
%  Material properties for both flexible links
%
EI1=E1*I1;
EI2=E2*I2;
b=L2-a;
%   The Kronecker delta
delta=0;
%    Initializing Matrices to establish dimensions
%
Maa=zeros(n,n); Kaa=zeros(n,n);Mta=zeros(1,n);Mab=zeros(n,m);
Mbb=zeros(m,m); Kbb=zeros(m,m);Mtb=zeros(1,m);
%    Construct Mass and Stiffness Matrices
%
Mtt=(1/3)*m1*L1^3+(1/3)*m2*(L1^3-(L1-b)^3)+(1/3)*m2*a^3+ ...
```

```
  m2*(a^2)*L1+m2*a*L1^2+(1/3)*mp*Lp^3+mp*Lp^2*(L1+a)+ ...
  mp*Lp*((L1+a)^2);
for i=1:n;
    Mta(i)=m1*((L1^2)/(i+4))+ ...
        m2*((L1^2)/(i+4))-m2*(((L1-b)^(i+4))/((i+4)*L1^(i+2)))+ ...
        m2*L1*a+0.5*m2*a^2+mp*Lp*a+mp*L1*Lp+0.5*mp*Lp^2;
  for j=1:i;
    o1=m1*(L1/(i+j+5));
   o2=m2*(L1/(i+j+5));
    o3=m2*(((L1-b)^(i+j+5))/((i+j+5)*L1^(i+j+4)));
    Maa(i,j)=o1+o2-o3+m2*a+mp*Lp;
    Kaa(i,j)=EI1*(((i+2)*(i+1)*(j+2)*(j+1))/((i+j+1)*L1^3))+ ...
          EI2*(((i+2)*(i+1)*(j+2)*(j+1))/((i+j+1)*L1^3))- ...
       EI2*(((i+2)*(i+1)*(j+2)*(j+1)*(L1-b)^(i+j+1))/((i+j+1)*L1^(i+j+4)));
    if j < i;
      Maa(j,i)=Maa(i,j);
     Kaa(j,i)=Kaa(i,j);
    end
  end
end
for v=1:m;
    Mtb(v)=m2*L1*(a/(v+3))+m2*(a^2/(v+4))+mp*Lp*a+mp*L1*Lp+ ...
       0.5*mp*Lp^2+0.5*mp*a*Lp^2*((v+2)/a)+0.5*mp*L1*Lp^2*((v+2)/a)+ ...
        (1/3)*mp*Lp^3*((v+2)/a);
  for w=1:v;
        if w == v;
         delta=1;
        end
    oo1=m2*(a/(v+w+5))+mp*Lp;
   oo2=delta*mp*Lp^2*((w+2)/a)+ ...
      0.5*mp*Lp^2*(((w+2)/a)+((v+2)/a))*(1-delta);
    Mbb(v,w)=oo1+oo2+(1/3)*Lp^3*mp*((v+2)/a)*((w+2)/a);
    Kbb(v,w)=EI2*(((v+2)*(v+1)*(w+2)*(w+1))/((v+w+1)*a^3));
        if w < v;
          Mbb(w,v)=Mbb(v,w);
          Kbb(w,v)=Kbb(v,w);
        end
    delta=0;
  end
end
 for i=1:n;
  for v=1:m;
   Mab(i,v)=m2*(a/(v+3))+0.5*mp*Lp^2*((v+2)/a)+mp*Lp;
  end
 end
M=[Mtt Mta Mtb;Mta' Maa Mab;Mtb' Mab' Mbb];
K=[0 zeros(1,n) zeros(1,m);zeros(n,1) Kaa zeros(n,m);zeros(m,1) zeros(m,n) Kbb];
```

flexnac3.m

Purpose:

Mathematical model of a flexible DRM where link 1 and link 2 are considered flexible components of the structure. This program computes the mass matrix M and stiffness matrix K. Using the assumed function: $\phi_i = (i+2)\left(\frac{x}{L}\right)^{i+1} - i\left(\frac{x}{L}\right)^{i+2}$, n is the number of admissible functions retained in the approximation.

Matlab Code:

```
function [M,K]=flexnac3(n,m,m1,m2,mp,L1,L2,Lp,a,E1,I1,E2,I2)
%
%  flexible DRM + long payload: Assumed Mode Method
%
%  [M,K]=flexnac3(n,m,m1,m2,mp,L1,L2,Lp,a,E1,I1,E2,I2)
%  n : No. of assumed modes for Link 1 (length L1)
%  m : No. of assumed modes for Link 2 (Length a)
%  Assumed mode function = (i+2)*(x/L)^(i+1)-i*(x/L)^(i+2)
%
%                    L -> L1 and 'a'
%
%  This subroutine returns the mass (M) and stifness (K) matrices
%  in the second order system of odes (using assumed modes method):
%
%  M xdd(t) + K x(t) = 0
%
%  Programmed by Nacho Romero
%            Department of Aerospace Science
%            Cranfield University
%
%  Revision dates: January 28, 1997
%          February 17, 1997
%
%  Material properties for both flexible links
%
EI1=E1*I1;
EI2=E2*I2;
b=L2-a;
%  The Kronecker delta
delta=0;
%  Initializing Matrices to establish dimensions
Maa=zeros(n,n); Kaa=zeros(n,n);Mta=zeros(1,n);Mab=zeros(n,m);
```

```
Mbb=zeros(m,m); Kbb=zeros(m,m);Mtb=zeros(1,m);
%    Construct Mass and Stiffness Matrices
%
Mtt=(1/3)*m1*L1^3+(1/3)*m2*(L1^3-(L1-b)^3)+(1/3)*m2*a^3+ ...
   m2*(a^2)*L1+m2*a*L1^2+(1/3)*mp*Lp^3+mp*Lp^2*(L1+a)+ ...
   mp*Lp*((L1+a)^2);

 for i=1:n;
      Mta(i)=m1*L1^2*(((i+2)/(i+3))-(i/(i+4)))+ ...
           m2*((8 + 3*i)*L1^2/(12 + 7*i + i^2) - ...
            (1 - b/L1)^i*(-b + L1)^3*...
           (3*b*i + b*i^2 + 8*L1 + 3*i*L1)/...
           ((3 + i)*(4 + i)*L1^2))+ ...
           m2*L1*a*2+0.5*m2*a^2*2+mp*Lp*a*2+mp*L1*Lp*2+...
           0.5*mp*Lp^2*2;
   for j=1:i;
      o1=m1*L1*(((i+2)*(j+2)/(i+j+3))-(i*(j+2)/(i+j+4))- ...
        (j*(i+2)/(i+j+4))+(i*j/(i+j+5)));
     o2=m2*(2*(40 + 23*i + 3*i^2 + 23*j + 7*i*j + 3*j^2)*L1/...
        ((3+i+j)*(4+i+j)*(5+i+j))-...
        (1-b/L1)^(i+j)*((2+i)*(2+j)*(-b+L1)^3/((3+i+j)*L1^2)-...
        2*(i + j + i*j)*(-b + L1)^4/((4 + i + j)*L1^3) + ...
        i*j*(-b + L1)^5/((5 + i + j)*L1^4)));
      Maa(i,j)=o1+o2+m2*a*4+mp*Lp*4;

      Kaa(i,j)=EI1*(i*j*(i+2)*(i+1)*(j+2)*(j+1)*...
             (2/((i+j)*(i+j+1)*(i+j-1)*L1^3)))+ ...
            EI2*(2*i*(2 + 3*i + i^2)*j*(2 + 3*j + j^2)/...
           ((-1 + i + j)*(i + j)*(1 + i + j)*L1^3) - ...
            i*(2+3*i+i^2)*j*(2+3*j+j^2)*(1-b/L1)^(i+j)*...
           (b^2*i-b^2*i^2+b^2*j-2*b^2*i*j-b^2*j^2+2*b*L1 - ...
            2*b*i*L1 - 2*b*j*L1 - 2*L1^2)/...
           ((-1 + i + j)*(i + j)*(1 + i + j)*(b - L1)*L1^4));
     if j < i;
        Maa(j,i)=Maa(i,j);
       Kaa(j,i)=Kaa(i,j);
      end
   end
 end
 for v=1:m;
      Mtb(v)=m2*L1*(3*a/(3+v))+m2*((((v+2)*a^2)/(v+3))-(v*a^2/(v+4)))+...
           mp*Lp*a*2+mp*L1*Lp*2+ ...
           0.5*mp*Lp^2*2+(0.5*mp*a*Lp^2+0.5*mp*L1*Lp^2+ ...
           (1/3)*mp*Lp^3)*(((v+2)*(v+1)-v*(v+2))/a);
   for w=1:v;
         if w == v;
          delta=1;
```

```
            end
        oo1=m2*a*(((v+2)*(w+2)/(v+w+3))-(v*(w+2)/(v+w+4))- ...
          (w*(v+2)/(v+w+4))+(v*w/(v+w+5)))+mp*Lp*4;
        oo2=delta*mp*Lp^2*(2*(((w+2)*(w+1)-w*(w+2))/a))+ ...
           0.5*mp*Lp^2*(2*(((w+2)*(w+1)-w*(w+2))/a)+...
             2*(((v+2)*(v+1)-v*(v+2))/a))*(1-delta);
        Mbb(v,w)=oo1+oo2+(1/3)*Lp^3*mp*(((v+2)*(v+1)-...
              v*(v+2))/a)*(((w+2)*(w+1)-w*(w+2))/a);
        Kbb(v,w)=EI2*(v*w*(v+2)*(v+1)*(w+2)*(w+1)*...
              (2/((v+w)*(v+w+1)*(v+w-1)*a^3)));
           if w < v;
             Mbb(w,v)=Mbb(v,w);
             Kbb(w,v)=Kbb(v,w);
           end
       delta=0;
     end
   end

  for i=1:n;
   for v=1:m;
    Mab(i,v)=m2*2*(3*a/(v+3))+0.5*mp*Lp^2*2*(((v+2)*(v+1)-v*(v+2))/a)+...
           mp*Lp*2*2;
   end
  end
M=[Mtt Mta Mtb;Mta' Maa Mab;Mtb' Mab' Mbb];
K=[0 zeros(1,n) zeros(1,m);zeros(n,1) Kaa zeros(n,m);zeros(m,1) zeros(m,n) Kbb];
```

flexasm.m

Purpose:

Mathematical model of a flexible DRM where link 1 and link 2 are considered flexible components of the structure. This program computes the mass matrix M and stiffness matrix K. Using the assumed function: $\phi_i = 1 - \cos\left(\frac{i\pi x}{L}\right) + \frac{1}{2}(-1)^{i+1}\left(\frac{i\pi x}{L}\right)^2$, n is the number of admissible functions retained in the approximation.

Matlab Code:

```
function [M,K]=flexasm(n,m,m1,m2,mp,L1,L2,Lp,a,E1,I1,E2,I2)
%
%  flexible DRM + long payload: Assumed Mode Method
%
%  [M,K]=flexasm(n,m,m1,m2,mp,L1,L2,Lp,a,E1,I1,E2,I2)
%  n : No. of assumed modes for Link 1 (length L1)
%  m : No. of assumed modes for Link 2 (Length a)
%  Assumed mode function = as in Junkins and Kim book(Eq. 4.88)
%
%  This subroutine returns the mass (M) and stifness (K) matrices
%  in the second order system of odes (using assumed modes method):
%
%  M xdd(t) + K x(t) = 0
%
%  Programmed by Nacho Romero
%              Department of Aerospace Science
%              Cranfield University
%
%  Revision dates: February 11, 1997
%
%  Material properties for both flexible links
%
EI1=E1*I1;
EI2=E2*I2;
b=L2-a;
%   The Kronecker delta
delta=0;
%    Initializing Matrices to establish dimensions
%
Maa=zeros(n,n); Kaa=zeros(n,n);Mta=zeros(1,n);Mab=zeros(n,m);
Mbb=zeros(m,m); Kbb=zeros(m,m);Mtb=zeros(1,m);
%   Construct Mass and Stiffness Matrices
```

```
%
Mtt=(1/3)*m1*L1^3+(1/3)*m2*(L1^3-(L1-b)^3)+(1/3)*m2*a^3+ ...
   m2*(a^2)*L1+m2*a*L1^2+(1/3)*mp*Lp^3+mp*Lp^2*(L1+a)+ ...
   mp*Lp*((L1+a)^2);
 for i=1:n;
      Mta(i)=m1*(L1^2/(i^2*pi^2)+(4*L1^2+(-1)^(1+i)*i^2*L1^2*pi^2)/8-...
              L1^2*cos(i*pi)/(i^2*pi^2))+ ...
           m2*((4*L1^2 + (-1)^(1+i)*i^2*L1^2*pi^2)/8 -...
             (-b+L1)^2*(4*L1^2 +(-1)^(1+i)*i^2*(-b+L1)^2*pi^2)/(8*L1^2)-...
             L1^2*cos(i*pi)/(i^2*pi^2) + ...
             L1^2*cos(i*(-b + L1)*pi/L1)/(i^2*pi^2))+ ...
           m2*L1*a*(1-cos(i*pi)+0.5*(-1)^(i+1)*(i*pi)^2)+...
           0.5*m2*a*a*(1-cos(i*pi)+0.5*(-1)^(i+1)*(i*pi)^2)+...
           mp*Lp*a*(1-cos(i*pi)+0.5*(-1)^(i+1)*(i*pi)^2)+...
           mp*L1*Lp*(1-cos(i*pi)+0.5*(-1)^(i+1)*(i*pi)^2)+...
           0.5*mp*Lp^2*(1-cos(i*pi)+0.5*(-1)^(i+1)*(i*pi)^2);
   for j=1:i;
      o1=m1*(L1-...
          (-1)^i*L1*i^2*pi^2/6-...
          (-1)^j*L1*j^2*pi^2/6+ ...
          (-1)^(i+j)*L1*i*i*j*j*pi^4/20+...
          (-1)^i*i^2*L1*cos(j*pi)/j^2+ ...
          (-1)^j*L1*j^2*cos(i*pi)/i^2);
%    The Kronecker delta
      if j == i;
        o1=o1+.5*m1*L1;
      end
%
    o2=m2*(b - (-1)^i*b*i^2*pi^2/2 - (-1)^j*b*j^2*pi^2/2 - ...
      (-1)^i*b^3*i^2*pi^2/(6*L1^2) - ...
      (-1)^j*b^3*j^2*pi^2/(6*L1^2) + ...
      (-1)^i*b^2*i^2*pi^2/(2*L1) + ...
      (-1)^j*b^2*j^2*pi^2/(2*L1) + ...
      (-1)^(i + j)*b*i^2*j^2*pi^4/4 + ...
      (-1)^(i + j)*b^5*i^2*j^2*pi^4/(20*L1^4) - ...
      (-1)^(i + j)*b^4*i^2*j^2*pi^4/(4*L1^3) + ...
      (-1)^(i + j)*b^3*i^2*j^2*pi^4/(2*L1^2) - ...
      (-1)^(i + j)*b^2*i^2*j^2*pi^4/(2*L1) + ...
      (-1)^j*j^2*L1*cos(i*pi)/i^2 + ...
      (-1)^i*i^2*L1*cos(j*pi)/j^2 + ...
      (-1)^j*b*j^2*cos(i*(-b + L1)*pi/L1)/i^2 - ...
      (-1)^j*j^2*L1*cos(i*(-b + L1)*pi/L1)/i^2 + ...
      (-1)^i*b*i^2*cos(j*(-b + L1)*pi/L1)/j^2 - ...
      (-1)^i*i^2*L1*cos(j*(-b + L1)*pi/L1)/j^2 + ...
      L1*sin(i*(-b + L1)*pi/L1)/(i*pi) + ...
      (-1)^j*j^2*L1*sin(i*(-b + L1)*pi/L1)/(i^3*pi) + ...
      (-1)^j*b*j^2*pi*sin(i*(-b + L1)*pi/L1)/i - ...
```

```
    (-1)^j*b^2*j^2*pi*sin(i*(-b + L1)*pi/L1)/(2*i*L1) - ...
    (-1)^j*j^2*L1*pi*sin(i*(-b + L1)*pi/L1)/(2*i)  + ...
    (-1)^i*i^2*L1*sin(j*(-b + L1)*pi/L1)/(j^3*pi) + ...
    L1*sin(j*(-b + L1)*pi/L1)/(j*pi) + ...
    (-1)^i*b*i^2*pi*sin(j*(-b + L1)*pi/L1)/j - ...
    (-1)^i*b^2*i^2*pi*sin(j*(-b + L1)*pi/L1)/(2*j*L1) - ...
    (-1)^i*i^2*L1*pi*sin(j*(-b + L1)*pi/L1)/(2*j));
    if j == i;
      o2=o2-m2*L1*cos(j*(-b + L1)*pi/L1)*sin(i*(-b + L1)*pi/L1)/((i+j)*pi);
    else
     o2=o2- ...
       m2*(i*L1*cos(j*(-b + L1)*pi/L1)*sin(i*(-b + L1)*pi/L1))/((i*i-j*j)*pi)- ...
       m2*(j*L1*cos(i*(-b + L1)*pi/L1)*sin(j*(-b + L1)*pi/L1))/((j*j-i*i)*pi);
    end
%   The Kronecker delta
    if j == i;
      o2=o2+0.5*m2*b;
    end
    Maa(i,j)=o1+o2+a*m2*(1-cos(i*pi)+0.5*(-1)^(i+1)*(i*pi)^2)*...
          (1-cos(j*pi)+0.5*(-1)^(j+1)*(j*pi)^2)+...
         mp*Lp*(1-cos(i*pi)+0.5*(-1)^(i+1)*(i*pi)^2)*...
          (1-cos(j*pi)+0.5*(-1)^(j+1)*(j*pi)^2);
    e1=(-1)^(i+j);
    e2=(-1)^(i+j);
%   The Kronecker delta
    if j == i;
      e1=e1+0.5;
     e2=e2+0.5;
    end
  Kaa(i,j)=EI1*e1*(i^2*j^2*pi^4/L1^3)+ ...
    EI2*(e2*b*i^2*j^2*pi^4/L1^4 + ...
    (-1)^j*i*j^2*pi^3*sin(i*(-b + L1)*pi/L1)/L1^3 - ...
    i^2*j^2*pi^3*cos(j*(-b+L1)*pi/L1)*sin(i*(-b+L1)*pi/L1)/((i+j)*L1^3)+...
    (-1)^i*i^2*j*pi^3*sin(j*(-b + L1)*pi/L1)/(L1^3));

    if j < i;
      Maa(j,i)=Maa(i,j);
     Kaa(j,i)=Kaa(i,j);
    end
  end
end
for v=1:m;
    Mtb(v)=m2*L1*(a+(1/6)*a*v^2*pi^2*(-1)^(v+1))+...
        m2*(a^2/(pi^2*v^2)+(4*a^2+(-1)^(1+v)*a^2*pi^2*v^2)/8 -...
         a^2*cos(pi*v)/(pi^2*v^2))+...
        mp*Lp*a*(1-cos(v*pi)+0.5*(-1)^(v+1)*(v*pi)^2)+...
        mp*L1*Lp*(1-cos(v*pi)+0.5*(-1)^(v+1)*(v*pi)^2)+ ...
```

```
          0.5*mp*Lp*Lp*(1-cos(v*pi)+0.5*(-1)^(v+1)*(v*pi)^2)+...
          (0.5*mp*a*Lp*Lp+0.5*mp*L1*Lp*Lp+ ...
          mp*Lp*Lp*Lp/3)*((-1)^(v+1)*(v^2*pi^2/a));
  for w=1:v;
        if w == v;
         delta=1;
         end
     oo1=m2*(a-(-1)^v*a*pi^2*v^2/6 -...
       (-1)^w*a*pi^2*w^2/6 + ...
       (-1)^(v + w)*a*pi^4*v^2*w^2/20 + ...
       (-1)^w*a*w^2*cos(pi*v)/v^2 +...
       (-1)^v*a*v^2*cos(pi*w)/(w^2)+a*delta/2);
    oo2=delta*mp*Lp*Lp*(1-cos(v*pi)+0.5*(-1)^(v+1)*(v*pi)^2)*...
         (-1)^(w+1)*(w^2*pi^2/a)+ ...
        0.5*mp*Lp^2*((1-cos(v*pi)+0.5*(-1)^(v+1)*(v*pi)^2)*...
         (-1)^(w+1)*(w^2*pi^2/a)+(1-cos(w*pi)+0.5*(-1)^(w+1)*(w*pi)^2)*...
         (-1)^(v+1)*(v^2*pi^2/a))*(1-delta);
     Mbb(v,w)=oo1+oo2+...
        mp*Lp*((1-cos(v*pi)+0.5*(-1)^(v+1)*(v*pi)^2)*...
        (1-cos(w*pi)+0.5*(-1)^(w+1)*(w*pi)^2))+...
        (1/3)*Lp*Lp*Lp*mp*((-1)^(v+1)*(v^2*pi^2/a)*...
        (-1)^(w+1)*(w^2*pi^2/a));

     Kbb(v,w)=EI2*(((-1)^(v+w)+delta*.5)*pi^4*v^2*w^2/a/a/a);

        if w < v;
          Mbb(w,v)=Mbb(v,w);
          Kbb(w,v)=Kbb(v,w);
        end
%   Resetting the Kronecker delta for the next pass
%
     delta=0;
   end
 end
 for i=1:n;
  for v=1:m;
   Mab(i,v)=m2*((1-cos(i*pi)+0.5*(-1)^(i+1)*(i*pi)^2)*...
            (a+(1/6)*a*v^2*pi^2*(-1)^(v+1)))+...
        0.5*mp*Lp^2*((1-cos(i*pi)+0.5*(-1)^(i+1)*(i*pi)^2)*...
          ((-1)^(v+1)*(v^2*pi^2/a)))+...
        mp*Lp*((1-cos(i*pi)+0.5*(-1)^(i+1)*(i*pi)^2)*...
          (1-cos(v*pi)+0.5*(-1)^(v+1)*(v*pi)^2));
  end
 end
M=[Mtt Mta Mtb;Mta' Maa Mab;Mtb' Mab' Mbb];
K=[0 zeros(1,n) zeros(1,m);zeros(n,1) Kaa zeros(n,m);zeros(m,1) zeros(m,n) Kbb];
```

gensol.ma

Purpose:

This program finds the characteristic problem for the P-DRM and finds the solution graphically and numerically which represent the natural frequencies of the system. Once the characteristic problem solution is found the mode shapes can also be plotted.

Mathematica Code:

```
Clear[a,b,L1,L2,rho1,rho2,EI2,Mp,Lp,Sp,k,Iyy,Iii,c]
(* below is equation 3 of 27/06/97 page 1, which satisfies the bending moment *)
(* boundary condition for the partially flexible DRM *)

third:=-C1 Sin[k a] - C2 Cos[k a] + C3 Sinh[k a] + C4 Cosh[k a]-
    (Iyy/EI2) (k C1 Cos[k a] - k C2 Sin[k a]+
     k C3 Cosh[k a] + k C4 Sinh[k a]) -
    0.5 (Mp/EI2) Lp (C1 Sin[k a] +
      C2 Cos[k a] + C3 Sinh[k a] + C4 Cosh[k a])

(* below is equation 4 of 27/06/97 page 2, which satisfies the shear force *)
(* boundary condition for the partially flexible DRM *)

fourth:=-C1 Cos[k a]+C2 Sin[k a]+C3 Cosh[k a]+C4 Sinh[k a]+
      (Mp/EI2) ((L1+a) (k c^2 C0) + k c^2 (-C0 (L1+a) + C1 Sin[k a] +
       C2 Cos[k a] + C3 Sinh[k a] + C4 Cosh[k a]))

(* below is equation 5 of 30/06/97 page 2, which is the theta equation*)
(* of motion for the partially flexible DRM *)

fifth:=Iii C0 +
 Iyy (C0+(-C0+k C1 Cos[k a]-k C2 Sin[k a]+k C3 Cosh[k a]+k C4 Sinh[k a])) +
 Mp (L1+a) ((L1+a) C0+(-C0 (L1+a)+C1 Sin[k a]+C2 Cos[k a]+C3 Sinh[k a]+C4
Cosh[k a])) +
 0.5 Mp Lp (-C0 (L1+a)+C1 Sin[k a]+C2 Cos[k a]+C3 Sinh[k a]+C4 Cosh[k a]) +
 rho2 Integrate[(x+L1) ((x+L1) C0+(-C0 (L1+x)+C1 Sin[k x]+C2 Cos[k x]+C3
Sinh[k x]+
          C4 Cosh[k x])), {x,0,a}]
(* the linear velocity of the payload's cm due to the rate of change of the *)
(* slope of the tip of the DRM is being ignored below from 15/7/97 because  *)
(* Mathematica can't handle this (?) I have no idea why ...                  *)
(* + 0.5 Mp Lp (L1+a) (-C0+k C1 Cos[k a]-k C2 Sin[k a]+k C3 Cosh[k a]+k C4
Sinh[k a])*)

(* Collecting the terms in the above equations *)
```

```
big3:=Collect[third,{C0,C1,C2,C3,C4}]
big4:=Collect[fourth,{C0,C1,C2,C3,C4}]
big5:=Collect[fifth,{C0,C1,C2,C3,C4}]

(* The components of the coefficient matrix *)

D0:=Coefficient[big3,C0]
D1:=Coefficient[big3,C1]
D2:=Coefficient[big3,C2]
D3:=Coefficient[big3,C3]
D4:=Coefficient[big3,C4]

E0:=Coefficient[big4,C0]
E1:=Coefficient[big4,C1]
E2:=Coefficient[big4,C2]
E3:=Coefficient[big4,C3]
E4:=Coefficient[big4,C4]

F0:=Coefficient[big5,C0]
F1:=Coefficient[big5,C1]
F2:=Coefficient[big5,C2]
F3:=Coefficient[big5,C3]
F4:=Coefficient[big5,C4]

(* the coefficients' matrix *)

Sol:={{-L1, 0, 1, 0, 1},
    {-1, k, 0, k, 0},
    {D0, D1, D2, D3, D4},
    {E0, E1, E2, E3, E4},
    {F0, F1, F2, F3, F4}}

(* for the case of no slew equation *)

Sol2:={{0, 1, 0, 1},
     {k, 0, k, 0},
     {D1, D2, D3, D4},
     {E1, E2, E3, E4}}

determinant=Chop[Det[Sol]];
determinant2=Chop[Det[Sol2]];

Clear[k]
L1=7.;
L2=8.;
a=1.;
```

```
b=L2-a;
EI2=3. 10^6;
rho2=75/L2;
rho1=100/L1;
Mp=500.;
Lp=2.0;
Sp=1.0;
c=Sqrt[EI2/rho2];

Iyy:=(Mp (4 Lp^2 + Sp^2))/12;
Iii:=rho1 (L1^3)/3+rho2 ((L1^3)/3-((L1-b)^3)/3)+Mp Lp (L1+a);

Plot[Log[1+Abs[determinant]], {k, .001,2}]
Plot[Log[1+Abs[determinant2]], {k, .001,2}]

N[FindRoot[determinant == 0,{k,0.5}],16]
kk = 1 * k /. %;
k=kk;
(* the nat. freq. in Hz *)
N[(k^2 c)/(2 Pi), 16]

(* Plotting the shape of the modes *)
k=kk;
N[NullSpace[Chop[Sol]], 16];
Coeff = %
Plot[-Coeff[[1,1]] (L1+x) + Coeff[[1,2]] Sin[k x] + Coeff[[1,3]] Cos[k x] +
Coeff[[1,4]] Sinh [k x] + Coeff[[1,5]] Cosh[k x], {x, 0.00, 4.0}, PlotPoints -> 100,
AxesOrigin -> {0,0}, AspectRatio -> Automatic]
```

Written in ACSL/GM. It is an interpreted FORTRAN code generator to simulate dynamical systems. The picture below shows the screen shot for the complete DRM simulation as created for the research in this thesis.

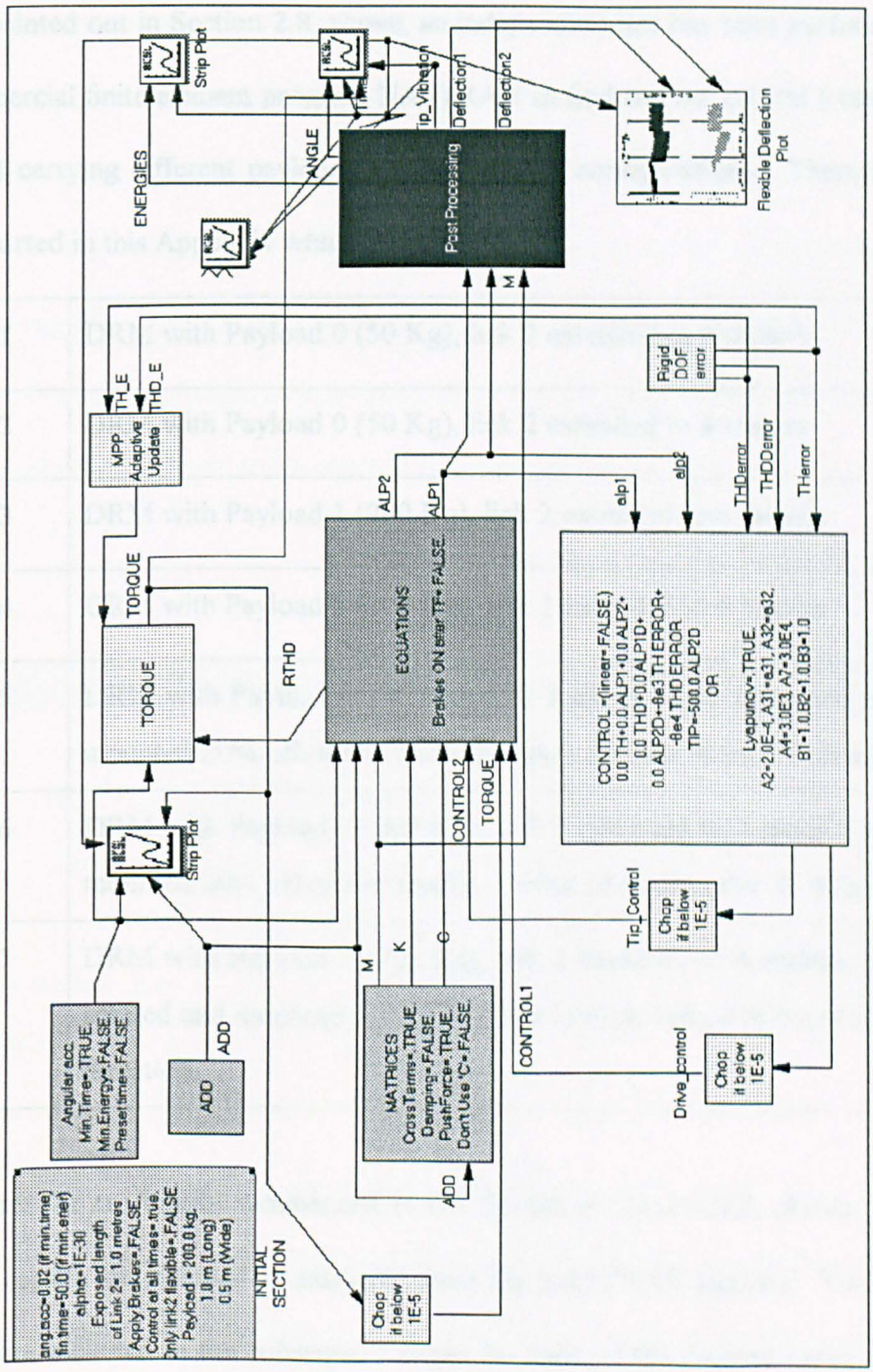

Figure D.1: The ACSL DRM dynamic simulation environment

Appendix E: The NASTRAN Finite Element Results

As pointed out in Section 2.8, above, an independent test has been performed using the commercial finite element program NASTRAN to find out the natural frequencies of the DRM carrying different payloads and in different configurations. There are seven cases reported in this Appendix which are as follows:

Case 1	DRM with Payload 0 (50 Kg), link 2 extended to 6 meters
Case 2	DRM with Payload 0 (50 Kg), link 2 extended to 8 meters
Case 3	DRM with Payload 1 (200 Kg), link 2 extended to 6 meters
Case 4	DRM with Payload 1 (200 Kg), link 2 extended to 8 meters
Case 5	DRM with Payload 0 (50 Kg), link 2 extended to 8 meters, payload mounted 20% off-centre from its centre of mass in the –Y direction.
Case 6	DRM with Payload 1 (200 Kg), link 2 extended to 8 meters, payload mounted 20% off-centre from its centre of mass in the –Z direction.
Case 7	DRM with Payload 1 (200 Kg), link 2 extended to 8 meters, payload rotated and mounted 20% off-centre from its centre of mass in the –Z direction.

The results are briefly summarised in the Tables in Section 2.8, above. Here the complete results are included as extracted from the NASTRAN analysis. Two tables of numbers are included in the subsequent pages for each of the defined cases. This first table (Eigenvalues) includes the first ten natural frequencies in radians and in Hz (cycles),

and the second indicates the maximum displacement for each of the natural frequencies in each of the six degrees of freedom; T1, T2, T3, R1, R2, or R3 (3 translation and 3 rotation). In the latter table and highlighted as bold text are indicated the in—plane bending natural frequencies under consideration in this study.

The model simulated in NASTRAN can be described as a three phase cantilever beam with a payload at its end. The three phases of the cantilever beam are as can be seen in Figure E.1, shown as lengths L_1, b and a. The pin joint was represented in NASTRAN as a constraint in the three translational degrees of freedom and in the rotation along the length of the DRM (T1,T2,T3, R1). This definition of the constraint best approximated the intended system since it is a symmetric tube, and therefore the bending in-plane is assumed to be equal to the bending out-of-plane.

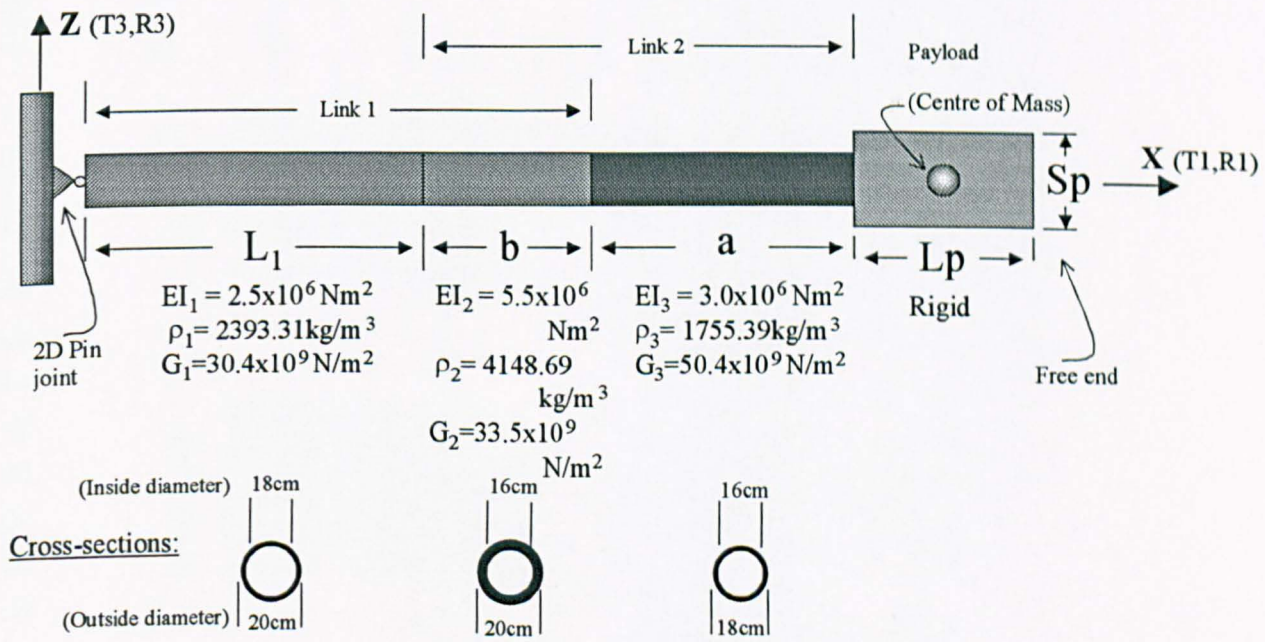

Figure E.1: The DRM NASTRAN model definition

In the results in the next pages it can be seen that the first two natural frequencies for each of the cases are very close to zero. They represent the free rotation mode, since

the DRM is able to perform slew rotations. The rest of the modes are all paired representing in-plane vibration modes (rotation around the Y axis in Figure E.1), of main interest in this research, and out-of-plane vibration modes (rotation around the Z axis in Figure E.1), which comes about due to the 3D nature of the NATRAN analysis. The torsional mode (rotation around the X axis in Figure E.1) can be seen in the result tables below in the results for the 200 Kg payload. As discussed above, in Section 2.8, the way this payload is grappled by the DRM affects the first torsional frequency since the mass moment of inertia around the X axis in Figure E.1 increases considerably as shown in Figure 2.12.

R E A L E I G E N V A L U E S; Case 1 (50 Kg Payload, link 2 extended 6 meters)

MODE NO.	EXTRACTION ORDER	EIGENVALUE	REAL EIGENVALUES RADIANS	CYCLES	GENERALIZED MASS	GENERALIZED STIFFNESS
1	1	-5.774200E-08	2.402956E-04	3.824424E-05	1.000000E+00	-5.774200E-08
2	2	-5.116453E-08	2.261958E-04	3.600018E-05	1.000000E+00	-5.116453E-08
3	3	9.974211E+02	3.158197E+01	**5.026427E+00**	1.000000E+00	9.974211E+02
4	4	9.975090E+02	3.158337E+01	5.026649E+00	1.000000E+00	9.975090E+02
5	5	1.404209E+04	1.184993E+02	**1.885975E+01**	1.000000E+00	1.404209E+04
6	6	1.404613E+04	1.185164E+02	1.886246E+01	1.000000E+00	1.404613E+04
7	7	7.750387E+04	2.783952E+02	**4.430797E+01**	1.000000E+00	7.750387E+04
8	8	7.757598E+04	2.785247E+02	4.432858E+01	1.000000E+00	7.757598E+04
9	9	2.104043E+05	4.586985E+02	**7.300413E+01**	1.000000E+00	2.104043E+05
10	10	2.106378E+05	4.589529E+02	7.304462E+01	1.000000E+00	2.106378E+05

MAXIMUM DISPLACEMENTS

	T1	T2	T3	R1	R2	R3
1	3.9260811E-15	9.4603024E-02	1.8501630E-03	2.1266963E-16	1.6088375E-04	8.2263499E-03
2	1.3980543E-14	1.8501680E-03	9.4602764E-02	9.5429246E-17	8.2263276E-03	1.6088417E-04
3	1.5095445E-14	6.4257585E-11	8.4180184E-02	6.9066643E-16	**3.3184703E-02**	2.5358561E-11
4	1.0639131E-14	8.4185302E-02	6.4215397E-11	1.2859892E-16	2.5324213E-11	3.3184748E-02
5	6.9957747E-15	6.3147404E-12	9.7801797E-02	8.3045896E-17	**5.9977092E-02**	3.8945553E-12
6	5.4521279E-15	9.7807527E-02	6.3226429E-12	6.4044383E-16	3.8821789E-12	5.9967186E-02
7	9.6766314E-17	5.1499905E-14	1.4171639E-01	2.0378412E-17	**1.0784797E-01**	3.8876525E-14
8	1.7289163E-16	1.4176737E-01	5.1113458E-14	1.3468176E-16	3.8796227E-14	1.0779797E-01
9	5.6166151E-16	1.2030997E-13	1.2661262E-01	4.8120016E-16	**1.2659460E-01**	1.1976711E-13
10	5.4424419E-16	1.2680995E-01	1.2074228E-13	6.6581072E-16	1.1825428E-13	1.2664844E-01

R E A L E I G E N V A L U E S; Case 2 (50 Kg Payload, link 2 extended 8 meters)

		REAL EIGENVALUES				
MODE NO.	EXTRACTION ORDER	EIGENVALUE	RADIANS	CYCLES	GENERALIZED MASS	GENERALIZED STIFFNESS
1	1	8.811185E-08	2.968364E-04	4.724298E-05	1.000000E+00	8.811185E-08
2	2	9.068754E-08	3.011437E-04	4.792851E-05	1.000000E+00	9.068754E-08
3	3	4.997174E+02	2.235436E+01	**3.557806E+00**	1.000000E+00	4.997174E+02
4	4	4.997478E+02	2.235504E+01	3.557915E+00	1.000000E+00	4.997478E+02
5	5	6.258640E+03	7.911156E+01	**1.259100E+01**	1.000000E+00	6.258640E+03
6	6	6.260031E+03	7.912035E+01	1.259239E+01	1.000000E+00	6.260031E+03
7	7	2.953188E+04	1.718484E+02	**2.735053E+01**	1.000000E+00	2.953188E+04
8	8	2.954295E+04	1.718806E+02	2.735565E+01	1.000000E+00	2.954295E+04
9	9	9.021397E+04	3.003564E+02	**4.780321E+01**	1.000000E+00	9.021397E+04
10	10	9.027540E+04	3.004586E+02	4.781948E+01	1.000000E+00	9.027540E+04

	MAXIMUM DISPLACEMENTS					
	T1	T2	T3	R1	R2	R3
1	9.8406309E-13	1.2346953E-03	1.0192819E-01	1.1578555E-13	6.5760124E-03	7.9657781E-05
2	5.7988732E-13	1.0192837E-01	1.2346931E-03	1.1467881E-13	7.9657635E-05	6.5760235E-03
3	1.6771867E-10	7.7422252E-10	9.7253874E-02	2.2849593E-13	**2.7587218E-02**	1.7187743E-09
4	4.1124279E-13	9.7256601E-02	2.5397137E-10	3.0068477E-14	7.4517198E-11	2.7587153E-02
5	4.9047241E-13	4.5321451E-12	1.1253458E-01	4.6658793E-14	**5.2716866E-02**	1.1161324E-11
6	3.3961787E-13	1.1254891E-01	2.2187456E-12	1.4734341E-14	5.3455153E-12	5.2713923E-02
7	8.7663421E-15	3.1474302E-13	1.0568494E-01	3.4387952E-16	**6.8451114E-02**	2.3606854E-13
8	2.6359977E-13	1.0571513E-01	2.1601334E-12	4.4799180E-14	4.8899179E-12	6.8436079E-02
9	7.1468703E-17	4.6044748E-14	1.1751664E-01	4.0039194E-16	**9.2257716E-02**	3.6539670E-14
10	2.3995297E-17	1.1753642E-01	4.6260505E-14	1.3484329E-17	3.5941099E-14	9.2225499E-02

R E A L E I G E N V A L U E S; Case 3 (200 Kg Payload, link 2 extended 6 meters)

R E A L E I G E N V A L U E S

MODE NO.	EXTRACTION ORDER	EIGENVALUE	RADIANS	CYCLES	GENERALIZED MASS	GENERALIZED STIFFNESS
1	1	-2.207162E-08	1.485652E-04	2.364489E-05	1.000000E+00	-2.207162E-08
2	2	-2.191155E-08	1.480255E-04	2.355899E-05	1.000000E+00	-2.191155E-08
3	3	6.573553E+02	2.563894E+01	**4.080564E+00**	1.000000E+00	6.573553E+02
4	4	6.573553E+02	2.563894E+01	4.080564E+00	1.000000E+00	6.573553E+02
5	5	1.065555E+04	1.032257E+02	**1.642888E+01**	1.000000E+00	1.065555E+04
6	6	1.065555E+04	1.032257E+02	1.642888E+01	1.000000E+00	1.065555E+04
7	7	2.324694E+04	1.524695E+02	2.426627E+01	1.000000E+00	2.324694E+04
8	8	4.128813E+04	2.031948E+02	**3.233946E+01**	1.000000E+00	4.128813E+04
9	9	4.128813E+04	2.031948E+02	3.233946E+01	1.000000E+00	4.128813E+04
10	10	1.387656E+05	3.725125E+02	**5.928721E+01**	1.000000E+00	1.387656E+05

MAXIMUM DISPLACEMENTS

	T1	T2	T3	R1	R2	R3
1	2.5890052E-17	6.8457339E-05	6.1809018E-02	9.1835524E-16	5.3746975E-03	5.9528124E-06
2	8.4017628E-18	6.1816458E-02	6.8449102E-05	4.8553548E-16	5.9520962E-06	5.3753443E-03
3	1.1936880E-17	8.5445885E-14	6.5607712E-02	7.1266737E-16	**2.4733128E-02**	3.2396974E-14
4	2.0282057E-17	6.5752335E-02	8.5071876E-14	1.9970453E-16	3.2604270E-14	2.4729073E-02
5	2.6318865E-17	3.2298508E-15	1.0278040E-01	4.6916493E-17	**5.3930987E-02**	1.7091575E-15
6	2.9833179E-17	1.0351289E-01	2.8337303E-15	7.4959742E-17	1.5015712E-15	5.4031778E-02
7	1.3781512E-18	2.8184460E-16	6.4556140E-16	1.2216944E-01	3.4462091E-16	9.8159472E-17
8	4.1919734E-13	2.1762960E-12	1.3859321E-01	6.1628443E-17	**1.0308360E-01**	4.7869942E-12
9	1.0261347E-11	1.4557032E-01	3.2185709E-11	8.1936078E-18	7.2092908E-11	1.0007060E-01
10	8.2947577E-10	4.2598041E-09	1.2011922E-01	5.6811565E-17	**1.2204675E-01**	8.9496792E-09

R E A L E I G E N V A L U E S; Case 4 (200 Kg Payload, link 2 extended 8 meters)

MODE NO.	EXTRACTION ORDER	EIGENVALUE	REAL EIGENVALUES RADIANS	CYCLES	GENERALIZED MASS	GENERALIZED STIFFNESS
1	1	-1.005901E-08	1.002946E-04	1.596239E-05	1.000000E+00	-1.005901E-08
2	2	-9.473297E-09	9.733086E-05	1.549069E-05	1.000000E+00	-9.473297E-09
3	3	3.805086E+02	1.950663E+01	**3.104577E+00**	1.000000E+00	3.805086E+02
4	4	3.805086E+02	1.950663E+01	3.104577E+00	1.000000E+00	3.805086E+02
5	5	4.920018E+03	7.014284E+01	**1.116358E+01**	1.000000E+00	4.920018E+03
6	6	4.920018E+03	7.014284E+01	1.116358E+01	1.000000E+00	4.920018E+03
7	7	1.435638E+04	1.198181E+02	1.906964E+01	1.000000E+00	1.435638E+04
8	8	2.174667E+04	1.474675E+02	**2.347018E+01**	1.000000E+00	2.174667E+04
9	9	2.174667E+04	1.474675E+02	2.347018E+01	1.000000E+00	2.174667E+04
10	10	5.915381E+04	2.432156E+02	**3.870896E+01**	1.000000E+00	5.915381E+04

MAXIMUM DISPLACEMENTS

	T1	T2	T3	R1	R2	R3
1	9.4241849E-16	1.0824160E-03	6.3713185E-02	9.6104299E-17	4.1105282E-03	6.9833295E-05
2	2.7693549E-16	6.3717671E-02	1.0823399E-03	2.1946425E-16	6.9928377E-05	4.1108173E-03
3	1.4144385E-15	2.2689194E-13	1.0172182E-01	2.4483429E-16	**2.2894830E-02**	5.6210384E-14
4	7.9067630E-16	1.0193643E-01	2.2665840E-13	2.4675203E-16	5.5860783E-14	2.2961399E-02
5	2.5408239E-17	1.0478575E-16	1.1478408E-01	2.8060623E-17	**4.6544828E-02**	1.4604801E-16
6	4.3372239E-17	1.1613105E-01	1.0180420E-16	6.4532694E-17	9.1549022E-17	4.6300519E-02
7	7.5717797E-17	4.3915763E-16	4.7223617E-16	1.2216944E-01	7.4980656E-16	5.3772960E-16
8	1.8532936E-13	6.8051142E-13	1.0523337E-01	9.5686599E-17	**6.6326939E-02**	1.3227139E-12
9	1.3032709E-13	1.0819609E-01	6.0915406E-13	1.1000097E-17	1.2227982E-12	6.7601971E-02
10	2.7533137E-10	1.1707331E-09	1.1539796E-01	1.3551496E-17	**8.6896904E-02**	2.1805118E-09

R E A L E I G E N V A L U E S; Case 5 (50 Kg Offset Payload, link 2 extended 8 m.)

MODE NO.	EXTRACTION ORDER	EIGENVALUE	REAL EIGENVALUES RADIANS	CYCLES	GENERALIZED MASS	GENERALIZED STIFFNESS
1	1	-4.915637E-08	2.217124E-04	3.528662E-05	1.000000E+00	-4.915637E-08
2	2	-4.147296E-08	2.036491E-04	3.241176E-05	1.000000E+00	-4.147296E-08
3	3	4.987702E+02	2.233316E+01	**3.554433E+00**	1.000000E+00	4.987702E+02
4	4	4.989872E+02	2.233802E+01	3.555206E+00	1.000000E+00	4.989872E+02
5	5	6.187882E+03	7.866309E+01	**1.251962E+01**	1.000000E+00	6.187882E+03
6	6	6.225001E+03	7.889867E+01	1.255711E+01	1.000000E+00	6.225001E+03
7	7	2.878930E+04	1.696741E+02	**2.700447E+01**	1.000000E+00	2.878930E+04
8	8	2.925445E+04	1.710393E+02	2.722175E+01	1.000000E+00	2.925445E+04
9	9	8.510656E+04	2.917303E+02	**4.643032E+01**	1.000000E+00	8.510656E+04
10	10	8.850202E+04	2.974929E+02	4.734746E+01	1.000000E+00	8.850202E+04

MAXIMUM DISPLACEMENTS

	T1	T2	T3	R1	R2	R3
1	9.4728119E-14	3.2519670E-03	1.0188378E-01	7.4809131E-13	6.5731471E-03	2.0980433E-04
2	1.7063885E-14	1.0187954E-01	3.2521021E-03	4.0684222E-14	2.0981304E-04	6.5728743E-03
3	7.5369303E-14	9.5489305E-10	9.7186580E-02	2.8156938E-03	**2.7523560E-02**	2.7118685E-10
4	3.6228121E-06	9.7188257E-02	9.5472541E-10	2.7415637E-11	2.7071256E-10	2.7588708E-02
5	5.1861296E-14	2.3264838E-12	1.1225925E-01	2.4473177E-02	**5.1661819E-02**	1.1233285E-12
6	8.7899316E-05	1.1218236E-01	2.2867689E-12	6.2705781E-13	1.1698356E-12	5.2784275E-02
7	2.4492650E-15	1.8828705E-13	1.0578261E-01	8.1067316E-02	**6.6774070E-02**	1.2326235E-13
8	5.7685550E-04	1.0501913E-01	1.9245063E-13	1.7411817E-13	1.3514816E-13	6.8789899E-02
9	9.2809144E-18	8.7938028E-17	1.1543450E-01	2.2063750E-01	**8.4788688E-02**	9.8585602E-17
10	2.8951922E-03	1.1666910E-01	9.9624288E-16	2.6992793E-16	1.0586756E-15	9.2820182E-02

R E A L E I G E N V A L U E S; Case7 (200 Kg Rotate + Offset Payload, link 2 extended 8 m.)

REAL EIGENVALUES

MODE NO.	EXTRACTION ORDER	EIGENVALUE	RADIANS	CYCLES	GENERALIZED MASS	GENERALIZED STIFFNESS
1	1	-8.166353E-09	9.036787E-05	1.438249E-05	1.000000E+00	-8.166353E-09
2	2	-3.816240E-09	6.177573E-05	9.831911E-06	1.000000E+00	-3.816240E-09
3	3	3.919448E+02	1.979760E+01	**3.150885E+00**	1.000000E+00	3.919448E+02
4	4	3.936949E+02	1.984175E+01	3.157912E+00	1.000000E+00	3.936949E+02
5	5	1.781554E+03	4.220846E+01	6.717685E+00	1.000000E+00	1.781554E+03
6	6	5.573858E+03	7.465827E+01	**1.188223E+01**	1.000000E+00	5.573858E+03
7	7	5.709270E+03	7.555971E+01	1.202570E+01	1.000000E+00	5.709270E+03
8	8	2.723621E+04	1.650340E+02	**2.626597E+01**	1.000000E+00	2.723621E+04
9	9	2.841995E+04	1.685822E+02	2.683068E+01	1.000000E+00	2.841995E+04
10	10	8.034176E+04	2.834462E+02	**4.511187E+01**	1.000000E+00	8.034176E+04

MAXIMUM DISPLACEMENTS

	T1	T2	T3	R1	R2	R3
1	8.3023951E-16	4.4793742E-05	6.3721284E-02	6.9083044E-16	4.1110506E-03	2.8899187E-06
2	4.3456620E-16	6.3726850E-02	4.4789831E-05	4.0517597E-14	2.8896666E-06	4.1114097E-03
3	4.7195354E-06	1.2570221E-13	1.0166997E-01	2.2079716E-15	**2.2878790E-02**	3.0283545E-14
4	1.0106738E-15	1.0189974E-01	1.2170194E-13	1.9912340E-03	2.8954862E-14	2.2945818E-02
5	5.3343455E-17	1.1425268E-02	4.0313848E-16	1.2193517E-01	3.3313917E-16	1.9449953E-03
6	1.4185747E-04	1.0981748E-15	1.1443332E-01	1.6208594E-16	**4.6594597E-02**	4.9043832E-16
7	2.4082553E-17	1.1601608E-01	1.1289502E-15	5.8462615E-03	5.0852290E-16	4.6395723E-02
8	1.1138661E-03	2.4105750E-13	1.0490842E-01	4.2246112E-16	**6.5890141E-02**	5.1849703E-13
9	1.1052108E-13	1.0816548E-01	3.1087735E-13	2.6805841E-03	5.9474935E-13	6.7603752E-02
10	7.9744626E-03	2.4106830E-10	1.1255300E-01	3.4263544E-15	**8.5497551E-02**	5.3459809E-10